AD 685151

FOREIGN TECHNOLOGY DIVISION

ATOMIZATION OF LIQUIDS
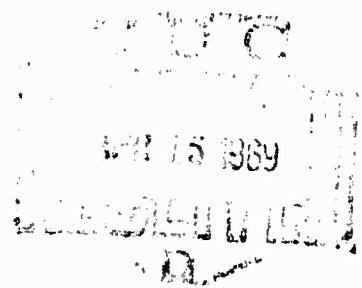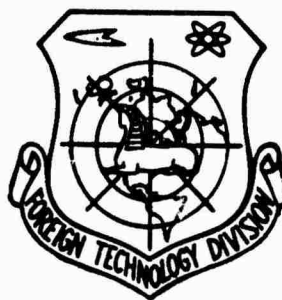
by

V. A. Borodin, Yu. F. Dityakin, et al.

EDITED MACHINE TRANSLATION

ATOMIZATION OF LIQUIDS

By: V. A. Borodin, Yu. F. Dityakin, et al.

English pages: 310

V. A. Borodin, Yu. F. Dityakin,
L. A. Klyachko, V. I. Yagodkin

RASPYLIVANIYE ZHIDKOSTEY

DATA HANDLING PAGE

ABSTRACT:
This book deals with the physical bases of the atomization of liquids. The principles of action of an atomizer are examined, data about the form of streams and films created by atomizers are given. Hydraulic theory and methods of designing swirlers, including adjustable swirlers, are given. The theory of disintegration of streams and films of liquid is developed. The influence of parameters of injectors and physical properties of liquid on the form of streams and films, and also on the size of the liquid drops is examined. Data on the distribution of liquid in the spray created by the atomizing devices is given. The method of experimental investigation of injectors is given.

The book is designed for scientific workers and technical engineers investigating devices for atomizing liquid (for combustion chambers in engines, furnaces, equipment used in the chemical and food industry, agriculture, etc.).

TABLE OF CONTENTS

This book deals with the physical bases
of the atomization of liquids. The principles
of action of an atomizer are examined, data
about the form of streams and films created
by atomizers are given. Hydraulic theory
and methods of·designing swirlers, including
adjustable swirlers, are given. The theory
of disintegration of streams and films of
liquid is developed. The influence of para-
meters of injectors and physical properties of
liquid on the form of streams and films, and
also on the size of the liquid drops is examined.
Data on the distribution of liquid in the spray
created by the atomizing devices is given.
The method of experimental investigation of
injectors is given.

The book is designed for scientific
workers and technical engineers investigating
devices for atomizing liquid (for combustion
chambers in engines, furnaces, equipment used
in the chemical and food industry, agriculture,
etc.).

PREFACE

As experiment was shown, the effectiveness of the burning of liquid fuel in the combustion chambers of engines and furnaces, just as the perfect development of a number of technological processes, frequently in considerable measure depends on the quality of the atomization of liquids. By this it is possible to explain the constant and ever-increasing interest toward the study of the atomization of liquids exhibited by a wide circle of engineers and scientists. A considerable number of articles has been published concerning this question in various journals. There are several monographs dedicated either to the technical aspects of the atomization of liquids in reference to any branch of technology, or dedicated to developing the theory of disintegration of streams.

This book is dedicated to the consideration of a problem which is very significant for contemporary technology — the atomization of liquid during continuous outflow from an injector. Just such a process takes place during the atomization of fuel in the combustion chambers of jet and rocket engines and in power furnaces, and also in a number of apparatuses used in the chemical and food industry, agriculture, etc.

An extensive class of repeating atomizers (for example, those used in internal combustion engines goes beyond the framework of this book. Nonetheless, certain general regularities of atomization during the continuous outflow of liquid which are given in this book can be used during the study of the mechanism of atomization

of injectors with periodic outflow of liquid.

Basic attention in the book is allotted to swirlers, which are very widely used in contemporary technology. Injectors and other types are examined also.

It is necessary to indicate that questions of the distribution of atomized liquid in gas flow are examined in the coming monograph of B. V. Raushenbakh, S. A. Belyy and others "Physical Bases of the Working Process in Combustion Chambers of Airbreathing Jet Engines," and therefore are not illustrated in this book.

This book expounds physical concepts about the mechanism of disintegration of streams, films and drops of liquid and makes an attempt to construct a single theory of these processes. Considerable attention is allotted to the theory and methods of hydraulic design of atomizers.

Along with materials in print, the book uses the results of investigations of the authors.

Chapters I and II are written by Yu. F. Dityakin, Chapters III and IV by L. A. Klyachko, Chapter V by V. I. Yagodkin, and V. A. Borodin, Chapter VI by Yu. F. Dityakin, V. A. Borodin and V. I. Yagodkin, Chapters VII and VIII by Yu. F. Dityakin, and L. A. Klyachko.

C H A P T E R   I

PRINCIPLES OF THE ACTION OF INJECTORS AND PHYSICAL
PROCESSES OCCURRING DURING THE
ATOMIZATION OF LIQUIDS

Devices for the atomization of liquids (injectors and atomizers) are widely used in contemporary technology. Injectors are of expecially great value in arrangement for the burning of fuels (in reciprocating engines and internal combustion turbines, in jet engines, in furnaces). Injectors are also widely used in equipment used in the chemical industry, in agriculture, construction industry and other branches of the national economy.

In spite of the great variety of designs, injectors can be classified by the principle of their action. Injectors are intended for the atomization of a stream of liquid into a great number drops and the distribution of these drops in space. Atomization of a stream of liquid is a complex physical process, depending on many external and internal causes. The basic external cause is the influence on the surface of a stream of aerodynamic forces, whose magnitude depends on the relative stream velocity and density of the surrounding gas. The aerodynamic forces tend to deform and tear the stream, and the forces of surface tension prevent this.

Internal causes of disintegration are various kinds of initial disturbances, caused by, for example, a breakdown of the cylindrical form of the stream when it leaves the nozzle, vibrations of nozzle, etc.

External causes in most cases are the determining ones for

atomization, therefore it is advisable when developing a classification of injectors to origninate from a method of creating displacement of the stream relative to gaseous medium.

The first method is bound up in the fact that liquid flows into a fixed gaseous environment, and in the second, it flows at low velocity into a moving gas flow. Thus in the first case the kinetic energy of the liquid is used for its atomization, and in the second — the kinetic energy of gas.

The second method of atomization of liquid is called the "gas" or pneumatic method. We can also imagine the combination of both methods of atomization.

Fig. 1. Scheme of classification of methods of atomization: 1 — cylindrical nozzle; 2 — slot nozzle; 3 — atomizer with coaxial fluid and gas flows; 4 and 5 — atomizers with feed of liquid at a right angle to the airflow; Г) gas; Ж) liquid.

Figure 1 gives the classification of methods of atomization of liquid and the scheme of corresponding injectors and atomizers. The simplest injector for the mechanical atomization of liquid is a jet injector, constituting a cylindrical nozzle from which flows a stream of liquid which disintegrates into drops and forms a spray of atomized

liquid with small vertex angle. If the nozzle is in the form of a narrow slot, then upon leaving the injector a flat liquid film will be formed, which then disintegrates into drops. One variety of jet injector is an injector with colliding streams. As a result of the collision of two streams, at a certain angle from the point of collision the liquid spreads radially, forming film which disintegrates into drops.

We will examine in greater detail the form of disintegration of a stream of liquid flowing from a cylindrical hole. Since these forms have been investigated well, it is sufficient to indicate only the basic conclusions of the investigations. When the values of stream velocity are low, at a certain distance from the nozzle the stream starts to be deformed. Amplitudes of axisymmetrical deformations grow, and the stream breaks up into separate large drops of equal diameters (Fig. 2) [6]. This form of stream disintegration is called axisymmetrical. As the stream velocity increases, the character of the deformations and disintegration changes: there appear wave-like deformations and the stream axis is distorted. These deformations are strengthened due to the influence of the gaseous medium and lead to "wave-like disintegration" (Fig. 3). Finally, when stream velocity increases still more, the wave-like deformations become very complicated. The length of the undecomposed section of the stream is sharply reduced, and the stream starts to disintegrate near the nozzle. Such a form of disintegration is called atomization (Fig. 4). The stream turns into a spray of atomized liquid, consisting of numerous small drops, dimensions of which change in great limits. During atomization drops are apparently formed because on the surface of the stream small waves appear (small as compared to the radius of a drop), and the ridges of these waves are detached from the stream. Such waves are very noticeable on the lateral surface of a stream flowing from a narrow slot (Fig. 5).
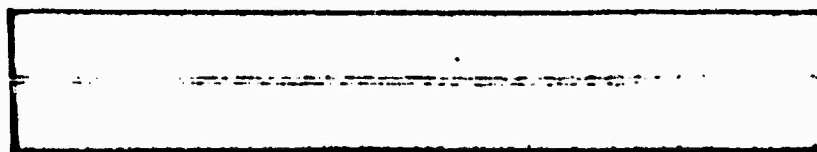
Fig. 2. Photograph of stream in conditions of axisymmetrical disintegration [6].
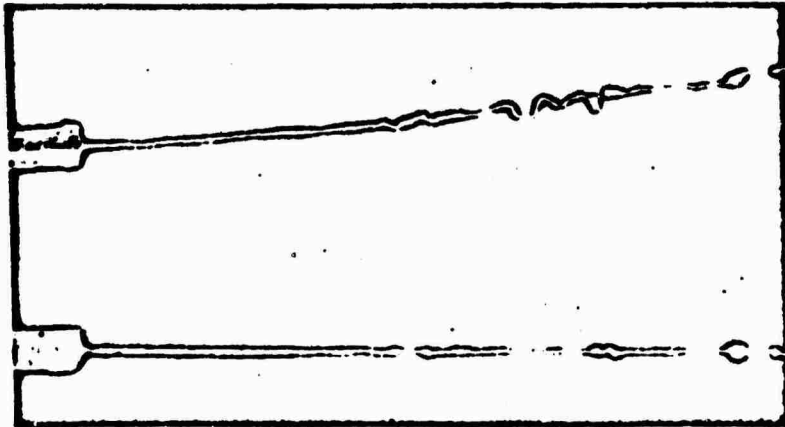
Fig. 3. Photograph of stream in conditions of wave-like disintegration.
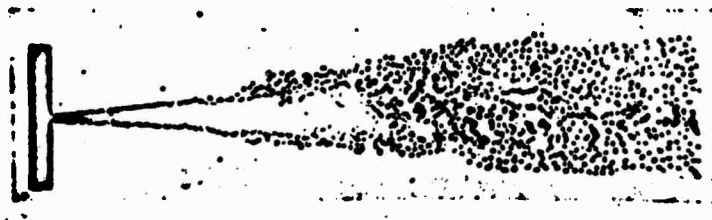
Fig. 4. Photograph of stream in conditions of atomization.

Fig. 5. Photography of a stream of liquid flowing from a narrow slot.

Fig. 6. Photograph of film forming upon the collision of streams.

Considering the disintegration of a film which forms upon the collision of two streams, when their velocity is sufficiently great (Fig. 6) on the surface of the film peripheral waves and radial folds are detected, which spread from the point of collision of the streams [3]. The folds, interacting with the peripheral waves, lead to the appearance of ridges from which after their breakaway drops will be formed. Furthermore, drops, as also in the case of moderate stream velocities, will be formed as a result of splitting of the edge of the film.

In widely used swirlers the liquid in front of the nozzle outlet is intensely rotated in the twisting chamber, where it proceeds through tangential channels. Upon leaving the nozzle, the liquid will form a tapering film, constituting a hollow cone. This film loses stability and disintegrates into drops.

5

The development of film deformation can be traced by photographs. At a low liquid exit velocity the film takes the form of a "bubble" (Fig. 7a). Outgoing liquid forms a continuous thin film, which again is contracted under the influence of the forces of surface tension. As exit velocity increases, the "bubble" passes into "tulip" form (Fig. 7b), and with a further increase of velocity, the length of the film is reduced and the site of drop formation shifts toward the nozzle until disintegration of the film begins practically right at the nozzle. Such a form of disintegration when a liquid spray is formed is called atomization (Fig. 7c). Photographing a disintegrating film at exposures of 10^{-5}-10^{-6} s reveals that its disintegration is preceeded by the rapid process of a buildup of disturbances; however, near the nozzle there is always a section of undisintegrated film. On its surface propagate waves, which with outflow intensively
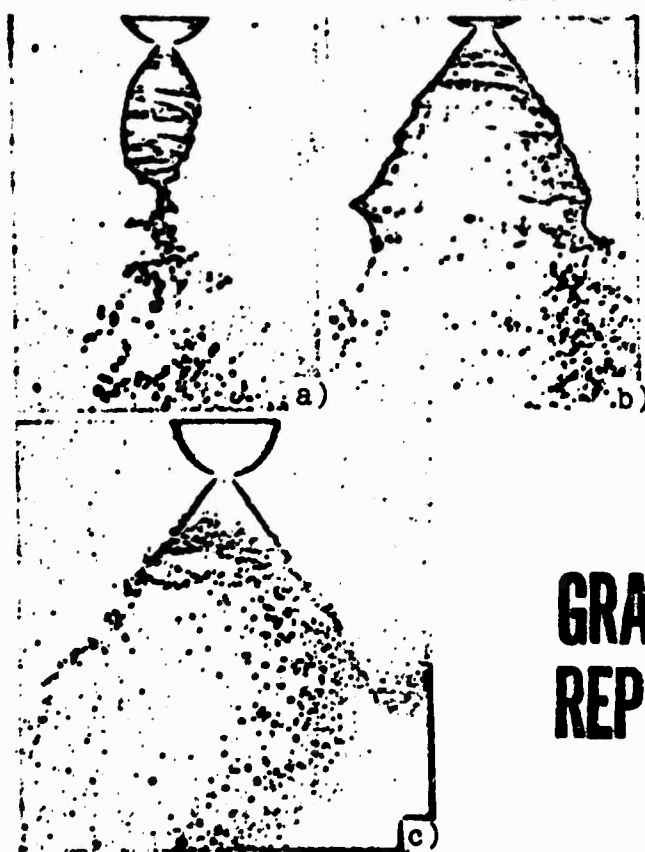
GRAPHIC NOT REPRODUCIBLE

Fig. 7. Photograph of disintegrating film: (a) "bubble" form; (b) "tulip" form; (c) atomization.

increase in amplitude (Fig. 8), which leads to the abrupt termination of their ridges. The separating liquid under the influence of surface tension turns into drops. Thickness of the film upon disintegration is very small. However, the drop diameters exceed the film thickness, since drops are formed from shapeless pieces of disintegrating film.

Let us consider further the method of gas atomization (Fig. 1). In gas injectors of the first type a stream or film of liquid is fed into a coaxial gas flow. On the gas-liquid interface appear unstable waves and the stream (film) breaks up into drops just as was described earlier. In a gas injector of the second type a stream or film of liquid is fed at a certain angle to the direction of gas flow. The stream is deformed by the flow and breaks up into drops.

Fig. 8. Photography of swirler film.

GRAPHIC NOT REPRODUCIBLE

Let us examine photographs of a disintegrating film of liquid flowing from a thin circular slot perpendicularly to the airflow (see Fig. 1) [4]. In the absence of airflow (Fig. 9a) the forming film is not deformed and disintegrates along the periphery, forming large drops. At a low air velocity (Fig. 9b), the film upon collision with the airflow does not break up immediately, but first is deformed into an "umbrella" shape, on the edge of which appears a thick unstable cylinder which disintegrates into drops. As air velocity increases, the liquid film disintegrates under the impact of disturbances and from its edge are detached smaller drops (Fig. 9c). At a high air velocity peripheral waves start to predominate, and from the surface of the film are detached short ridges, forming small drops (atomization) (Fig. 9d).

Fig. 9.   Photograph of films of liquid flowing from a circular slot
perpendicularly to the airflow: (a) in the absence of airflow, width
of slot, 265 µ; (b) air velocity, 7.6 m/s; thickness of film upon
collision with airflow, 58 µ; (c) velocity of airflow, 30.5 m/s;
thickness of film upon collision with airflow, 88 µ; (d) velocity of
airflow, 91.4 m/s; thickness of film upon collision with airflow,
88 µ.

     If the air flow around the film twists with respect to an axis
of the film, this will lead to expansion of the spray of atomized
liquid, an increase of the distribution drops in space and a decrease
in their size. When a stream of liquid is streamlined by a gas
flow normal to the stream axis, a number of peculiarities shows up,
distinguishing this disintegration from disintegration of a stream
in a wake flow [1]. Near the base of the stream appears a more or
less extended section (a few calibrations), where the stream is
insignificantly disturbed (Fig. 10). Further is a section where there
are great disturbances. Under the impact of the air flow, prior to
the moment of disintegration the stream seems to flatten, turning
into a unique film, which further disintegrates into drops.

     In an injector with rotating atomizer such liquid of the film
is created by the rotation of a disk or drum, into whose internal
cavity the liquid is fed. This film during runoff from the edges
of the disk or drum becomes unstable and breaks up into drops.

     Let us examine disintegration of a liquid film flowing from a
revolving drum. When the flow rate of the liquid is very low, on
the edge of the drum appears a liquid torus which under the impact

of centrifugal forces is deformed so that spherical nodes are formed
on it. Growth of these nodes leads to the breakaway of several drops
from the edge of the drum. With an increase of the flow rate of the
liquid, these spherical nodes on the torus turn into thin streams
and filaments flowing from the edge of the drum [5]. The number of
these filaments increases as the flow rate of the liquid increases,
and achieves a certain constant value, after which it remains
constant independently of the flow rate. The liquid filaments break
up into drops at a certain distance from the edge of the drum.

Fig. 10. Photograph of a stream
of liquid normally streamlined
by an airflow [1].

GRAPHIC NOT
REPRODUCIBLE

Upon further increase of the liquid flow rate, the filaments,
whose number remains constant, cannot transmit all the liquid from
the torus to the edge, and therefore the torus breaks away from the
edge and forms a film. This film in the beginning stretches to a
specific distance from the edge, and further breaks up into filaments
and large drops, which in turn are subjected to splitting due to the
action of aerodynamic forces. Similar stages of disintegration can
also be observed in the case of film flowing from the edge of a
revolving disk (Figs. 11 and 12) [2].

In ultrasonic atomizers liquid is "crushed" under the impact
of rapid vertical shifts of a plate, occurring at ultrasonic frequency.
On the surface of the layer of liquid fed to the vibrating plate of
the ultrasonic emitter appear standing waves, and from the ridges

9

of these waves break off drops, forming a spray.

In other schemes of ultrasonic injectors a stream or film of liquid flowing from a hole or slot is subjected to the action of ultrasonic air vibrations, created by a generator.

During electrical atomization of liquids (Fig. 1) the stream is in an electrical field. Under the action of this field on the surface of the stream appears a certain distribution of pressures, which deforms the stream and causes a loss of stability, disintegration and formation of drops.

Let us examine now the regions of application of different types of atomizers.
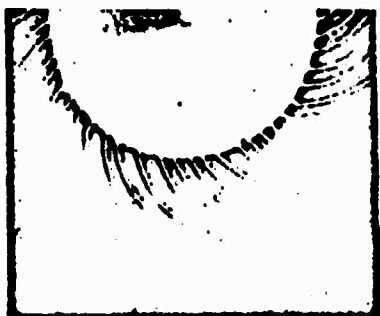
Fig. 11. Photograph of disintegration of a film flowing from a rotating disk (formation of filaments).

Jet and slot injectors are used in internal combustion engines. The necessity of a feed of liquid fuel under high pressure and the small root angle of the spray hamper the use of these injectors in gas turbine and jet engines. However, injectors with impinging jets sometimes are used in liquid-fuel jet engines; these injectors also are used in fire-fighting equipment.

Fig. 12. Photograph of disintegration of a film flowing from a rotating disk (disintegration of film upon overcrowding of disk).

Swirlers are widely used in the rational economy, in contemporary gas-turbine and liquid-fuel jet engines, different furnaces, chemical industrial equipment, etc. The wide use of swirlers is due to the simplicity of construction, reliability, sufficient effectiveness of atomization and simplicity of selecting the shape of the spray. Furthermore, in swirlers the discharge coefficient can be easily changed, i.e., adjustable swirlers can be created.

Injectors with rotating atomizers (disks, drums) are used mainly in the chemical industry for atomization of viscous liquids and suspensions.

Gas injectors are used in both internal-combustion engines (in carburetors and in jet engines) and different technological processes. However, satisfactory quality of fuel atomization in an engine requires a rather great quantity of air.

Ultrasonic atomizers are used mainly in different technological assemblies (reactors, desiccators, etc.).

Systems of electrical atomization of liquids have also been used in technological processes (painting by atomization, drying, etc.).

Circuit analysis of the classification of methods of the atomization of liquids permits making the following general conclusions.

1. The flow of liquid before atomization should be converted into forms (stream, film) which possess the greatest surface energy and therefore are unstable and disintegrate rapidly.

2. All examined methods of the atomization of liquid are caused by a loss of flow stability in streams or films due to the appearance of unstable waves on the liquid-gas interface.

Literature

1. Raushenbakh B. V. i dr. Fizicheskiye osnovy rabochego protsessa v kamerakh sgoraniya vozdushno-reaktivnykh dvigateley (Physical bases of the working process in the combustion chambers of air breathing jet engines). M., Izd-vo "Mashinostroyeniye." 1964.

11

2. Freyzer. Raspylivaniye zhidkogo topliva (Atomization of liquid fuel). In the collection. "Voprosy goreniya raketnykh topliv". M., Izd-vo inostr. lit., 1959.

3. Dombrowski N., Hooper P. A study of the spray formed by impinging jets in laminar and turbulent flow. Journal of Fluid Mechanics, Vol. 18, Pt. 3, 1964.

4. Fraser R., Dowbrowski N., Routley J. The mechanism of disintegration of liquid sheets in cross-current air streams. Applied Scientific Research. Sec. A, V. 12, No. 2, 1963.

5. Hinze J., Milborn H. Atomization of liquids by means of rotating cup. Journal of Applied Mechanics, V. 17, No. 2, 1950.

6. Littaye G. Contribution a l'etude des jets liquides. Publication Scientifique et technique du Secretariat d'etat a l'aviation. Paris, 1942.

12

C H A P T E R II

FORM OF STREAMS AND FILMS CREATED BY ATOMIZERS

§ 1. Jet Injectors

Jet injector nozzles are usually cylindrical, while on the side of the nozzle entrance the edges are beveled or round to decrease liquid breakaway from the walls. As the liquid approaches the nozzle opening, the trajectories of the moving particles are deflected from straight lines; in the stream appear centrifugal forces, under whose influence it narrows, attaining the least dimension a certain distance from the cut of the nozzle. The contraction factor of the stream ε is the ratio of the area of the narrowed section of the stream to the nozzle area.

Volumetric flow rate of the liquid Q is connected with pressure drop on the injector Δp by the following relationship:

$$Q = \frac{\varepsilon}{\sqrt{1+\varphi}} f \sqrt{\frac{2\Delta p}{\rho}} = \mu f \sqrt{\frac{2\Delta p}{\rho}}.$$

where $\frac{\varepsilon}{\sqrt{1+\varphi}} = \mu$ — discharge coefficient of liquid; φ — coefficient of exit velocity — relative kinetic energy losses; f — nozzle opening ρ — density of liquid.

Discharge coefficient μ is determined experimentally; it depends on pressure drop Δp, on counterpressure, on temperature and properties of liquid, and also on geometric dimensions of the nozzle. Usually on the basis of experimental results the dependence of discharge coefficient on the square root of the Reynolds number is constructed (Fig. 13). The curve consists of three sections. The

13

first section corresponds to streamline conditions; here the discharge coefficient changes linearly with respect to $\sqrt{Re}$. The second section corresponds to transition operating conditions, where the discharge coefficient passes through its maximum. On the third section, referred to conditions of turbulence, the discharge coefficient can be accepted as constant. All three sections can be seen on the curve shown on Fig. 14, which represents the results of determination of the discharge coefficient for nozzles having different ratios of length of cylindrical part to nozzle diameter [7]. Figure 15 is a similar graph for nozzles of other design [7].
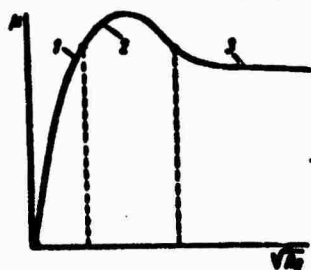
Fig. 13.
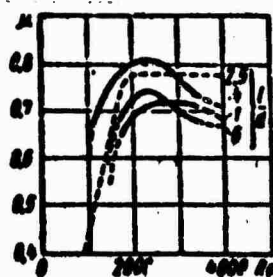
Fig. 14.

Fig. 13. Change of discharge coefficient from square root of Reynolds number: 1 — section of streamline conditions: 2 — section of transition operating conditions; 3 — section of conditions of turbulence.

Fig. 14. Dependence of discharge coefficient on Reynolds number for different values of the ratio of length of nozzle opening to its diameter py(l/d).
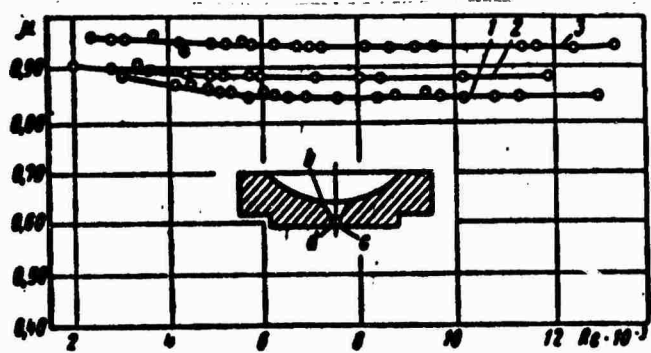
Fig. 15. Dependence of discharge coefficient on Reynolds number: 1 — dependence for case of entrance face at 60°; angles b, c, and d — acute, l/d = 1; 2 — dependence for case of entrance face at 60°; angle b slightly rounded, c and d — polished, l/d = 1; 3 — entrance face at 60°; angles b, c and d slightly rounded, l/d = 1; o — experimental points.

14

§ 2.   Injector with Colliding Streams

Let us examine the problem of liquid flow obtained as a result of the collision of two streams of inviscid and incompressible liquid [3]. On Figure 16 are shown two streams of equal diameter d, colliding at angle 2α. From the point of intersection liquid will spread radially, forming a film lying in the plane of symmetry. Since both streams spread symmetrically, it is possible to limit ourselves to the consideration of one stream, considering the plane of symmetry as impenetrable (Fig. 17).
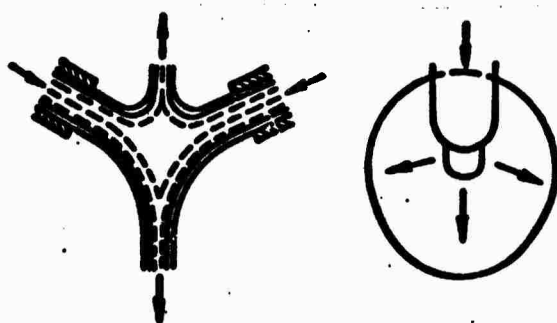
Fig. 16. Diagram of collision of streams.

We introduce system of coordinates r, φ, and place the origin of coordinates at point O, where the flow is completely stagnated. Let us designate by v, ρ the velocity and density of the liquid. Let us assume that there are no tangential flows of liquid, i.e., that $\frac{\partial v}{\partial \varphi} = 0$.

At a sufficiently great distance r from the point of collision of streams the distortion of flow lines in the film may be disregarded and liquid pressure along the length of the film may be considered constant and equal to the ambient pressure. Then from Bernoulli's equation it follows that velocities in stream and film must be identical (at constancy of ambient pressure). Let us write the expression for liquid discharge in a sector element with angle Δφ:

$$\Delta G_\varphi = \rho v h_\varphi r \Delta \varphi.$$

where h_φ — variable thickness of film in the examined section of a cylindrical surface of radius r.

15

From the last relationship it follows that at constant velocity film thickness changes with the radius by hyperbolic law. From conditions of maintaining flow rate and momentum we will obtain the following relationships:

$$\int_0^{2\pi} h_0 d\varphi = \frac{\pi d^2}{4v}$$ (1)

and

$$\int_0^{2\pi} h_0 \cos\varphi d\varphi = \frac{\pi d^2}{4v} \sin\alpha;$$

$$\int_0^{2\pi} h_0 \sin\varphi d\varphi = 0,$$ (2)

where d — stream diameter.

Using these equations we can find the law of change of film thickness in the selected section. We will look for this law as the particular solution of system of equations (1) and (2) in the following form:

$$h_0 = \frac{h_1}{1 - \sin^n\alpha \sin\varphi},$$ (3)

where h_1, n — functions of angle α which must be determined.
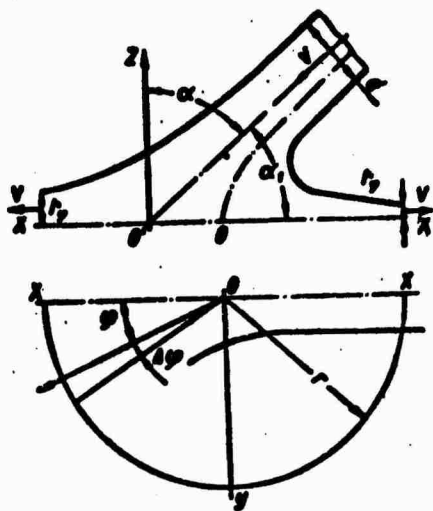
Fig. 17. Working diagram of colliding streams.

16

Substituting the value of equation (3) into equations (1) and (2) and making the necessary transformations, we obtain

$$h_\varphi = \frac{h_0 \cos^2 \alpha}{1 + \sin^2 \alpha - 2 \sin \alpha \cos \varphi},$$ (4)

where

$$h_0 = \frac{d^2}{8r}.$$

From formula (4) it follows that the film thickness in any section of a cylindrical surface does not depend on the flow rate of the liquid, but is a function of d and of the angle of collision of streams $\alpha = \frac{\pi}{2} - \alpha_1$. Film thickness will be maximum at $\phi = 0$:

$$h_{max} = \frac{h_0 \cos^2 \alpha}{1 + \sin^2 \alpha - 2 \sin \alpha}.$$

Relative thickness of film

$$\bar{h}_\varphi = \frac{h_\varphi}{h_{max}} = \frac{1 + \sin^2 \alpha - 2 \sin \alpha}{1 + \sin^2 \alpha - 2 \sin \alpha \cos \varphi}.$$ (5)

Upon collision of two streams the film thickness, calculated by formulas (4) or (5), is doubled. An experimental check of formula (5), carried out in [3], showed the necessity of introducing a correction which considers the effect of tangential flows. Taking into account the correction, formula (5) should be written in the form

$$\bar{h}_{\varphi_0} = \frac{1 + \sin^2 \alpha - 2 \sin \alpha}{1 + \sin^2 \alpha - 2 \sin \alpha \cos (a\varphi)},$$ (6)

where $a = \cos^{1/4} \alpha$ — the experimental coefficient.

Formula (6) is valid at $0 \leq \alpha \leq 60°$.

From formula (4) can be obtained the equation of film contour in a horizontal plane. Solving equation (4) with respect to r, we obtain the equation of an ellipse in polar coordinates:

$$r = \frac{p}{1 - \varepsilon \cos \varphi},$$

where

$$p = \frac{d^2}{8h_\varphi} \cdot \frac{\cos^2 \alpha}{1 + \sin^2 \alpha}; \quad \varepsilon = \frac{2 \sin \alpha}{1 + \sin^2 \alpha}.$$

17

Indeed, photographs of film (Fig. 18) show that its contour in a horizontal plane constitutes an ellipse.

Fig. 18. Photograph of the liquid film forming upon the collision of two streams [3]: (a) angle between streams, 50°; (b) angle between streams, 80°; flow rate of streams 7.3 m/s.

§ 3. Centrifugal Injector

As was shown in the first chapter, the film of liquid flowing from a swirler appears due to the "twisting" of the liquid in the chamber. Such a film can be especially distinctly examined by observing the outflow of liquid at low feed pressures or in a gaseous environment with density lower than atmospheric.

In order to obtain the equation describing the form of the liquid film, we will examine the condition of equilibrium of forces acting on the film [1, 6]. On Fig. 19 is represented the diagram of a circular film element of width dx. This element rotates due to the "twisting" of the liquid in the swirler and at a distance r from the axis of rotation has peripheral velocity $v_t(r)$ (Fig. 20). Let us designate by dV = rdφδ(r)dx volume of element; δ(r) — width of ring in radial direction, dφ — angle element. On the surfaces of the element act forces caused by surface tension and designated by P_1 and P_2. For external surface force we have

$$2\sigma dx \sin \frac{d\varphi}{2} \approx 2\sigma dx \frac{1}{2} d\varphi = \sigma dx d\varphi = P_1 dx. \tag{7}$$

Pressure determined by force P_1 will be

18

$$p_1 = \frac{P_1 dx}{dF_1} = \frac{\sigma d\varphi dx}{\left[r + \frac{1}{2}\delta(r)\right]d\varphi dx} = \frac{\sigma}{r + \frac{1}{2}\delta(r)}. \tag{8}$$

For the internal surface of the element we obtain

$$p_2 = -\frac{\sigma}{r - \frac{1}{2}\delta(r)}. \tag{9}$$
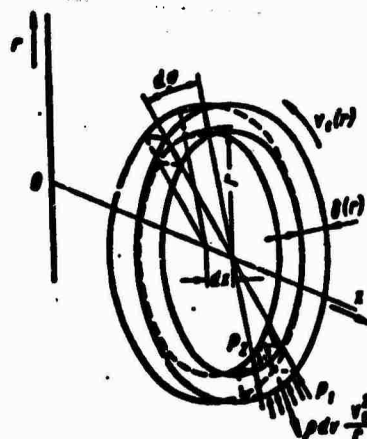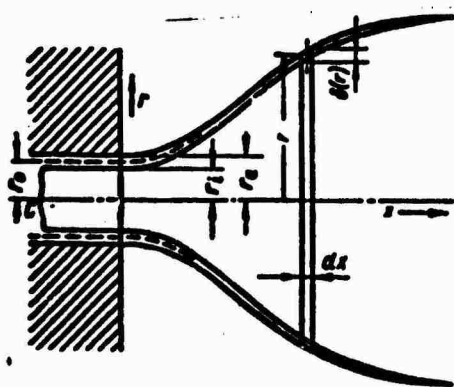
Fig. 19. Diagram of liquid film flowing from swirler.

Fig. 20. Circular film element.

On an element, besides pressures p_1 and p_2, caused by surface tension, centrifugal force $\rho dV \frac{v_t^2}{r}$ acts. The condition of equilibrium of an element will have the form

$$\rho dV \left(\ddot{r} - \frac{v_t^2}{r}\right) = -(p_1 dF_1 - p_2 dF_2). \tag{10}$$

where $\ddot{r} = \frac{d^2 r}{dt^2}$ — acceleration in radial direction. But area elements can be written as

$$dF_1 = \left[r + \frac{1}{2}\delta(r)\right]d\varphi dx; \tag{11}$$

$$dF_2 = \left[r - \frac{1}{2}\delta(r)\right]d\varphi dx. \tag{12}$$

Substituting in equation (10) the values of p_1, p_2 from expressions (8) and (9), and also the values of dF_1 and dF_2 from

expressions (11) and (12), we obtain

$$\rho \, dV\left(\ddot{r} - \frac{v_t^2}{r}\right) = -2\sigma \, d\varphi \, dx = -2\sigma \frac{dV}{r\delta(r)}. \tag{13}$$

From equation (13) we obtain the equation of motion of liquid particles in the radial direction

$$\ddot{r} = \frac{v_t^2(r)}{r} - \frac{2\sigma}{\rho r \delta(r)}. \tag{14}$$

Let us designate by $r_0 = \frac{r_0 + r_i}{2}$ the mean radius of the liquid film in the nozzle exit section. Then from the condition of constancy of angular momentum we obtain

$$v_t = \frac{K}{r}, \tag{15}$$

where $K = v_{t0}r_0$, v_{t0} – peripheral velocity of liquid inside torsion chamber of injector. We consider approximately that axial velocity of the liquid v_x is constant and is equal to axial velocity v_{x0} in the nozzle exit section. Then from continuity equation

$$\pi(r_0^2 - r_i^2)v_{x0} \approx 2\pi r_0 \delta_0 v_{x0} = 2\pi r \delta(r) v_{x0}$$

we obtain the width of the film

$$\delta(r) = \frac{r\delta_0}{r_0}. \tag{16}$$

where δ_0 – width of film in nozzle exit section. Substituting the values of equations (15) and (16) into (14), we obtain

$$\ddot{r} = \frac{K^2}{r^3} - \frac{2\sigma}{\rho r^2 \delta_0} = -K^2\left(\frac{1}{r_g^2} - \frac{1}{r^3}\right). \tag{17}$$

where $r_{\text{Д}}$ – the radius, determined from the relationship corresponds to the condition

$$r_g = \sqrt[3]{\frac{K^2 \rho r_0 \delta_0}{2\sigma}} = r_0 \sqrt[3]{\frac{v_{t0}^2 \rho \delta_0}{2\sigma}} = r_0 W^{\frac{1}{3}}. \tag{18}$$

corresponds to the condition $\ddot{r} = \dot{v}_r = 0$, i.e., equilibrium in the radial direction $\left(v_r = \frac{dv_r}{dt} \right)$. The dimensionless quantity is called Weber's criterion:

$$W = \frac{r_0^2 v_0}{2\sigma}.$$ (19)

In equation (17) acceleration $\ddot{r} = f[r(t)]$, but

$$\dot{r} = \frac{dr}{dt} = v_r[r(t)]$$ (20)

and

$$\ddot{r} = \frac{dv_r}{dt} = \frac{dv_r}{dr}\dot{r} = \frac{d}{dr}\left(\frac{v_r^2}{2}\right).$$ (21)

Substituting the value of equation (21) into expression (17), we have

$$\ddot{r} = \frac{d\left(\frac{v_r^2}{2}\right)}{dr} = K^2\left(\frac{1}{r^2} - \frac{1}{r_0^3}\right).$$ (22)

After integrating expression (22) we obtain

$$v_r^2 = 2K^2\left(-\frac{1}{2r^2} - \frac{r}{r_0^3}\right) + C.$$ (23)

Constant C is found from the condition $v_{ro} = 0$ at $r = r_0$

$$C = K^2\left(\frac{1}{r_0^2} + \frac{2r_0}{r_0^3}\right).$$ (24)

Then

$$v_r^2 = \frac{dr}{dt} = \pm K\left[\frac{1}{r_0^2} - \frac{1}{r^2} - \frac{2}{r_0^3}(r - r_0)\right]^{1/2}.$$ (25)

We will consider that the total velocity of liquid particles v in the film is constant, i.e., that

21

$$v^2 = v_x^2 + v_t^2 + v_r^2 = \text{const.} \qquad (26)$$

Substituting into equation (26) the values of v_t and v_r^2 from conditions (15) and (25), we obtain

$$v_x = \left[v^2 - v_{t_0}^2 + \frac{2K^2}{r_0^2}(r - r_0) \right]^{v_x}. \qquad (27)$$

But in the nozzle exit section $v_{r0} = 0$ and $v^2 - v_{t0}^2 = v_{x0}^2$. Then from equation (27) we have

$$v_x = \left[v_{x0}^2 + 2\frac{K^2}{r_0^2}(r - r_0) \right]^{v_x}. \qquad (28)$$

Dividing the left and right sides of expression (25) by the left and right sides of equation (28) respectively, we obtain

$$\frac{dr}{dx} = \frac{v_r}{v_x} = \pm \left[\frac{1}{r_0^2} - \frac{1}{r^2} - \frac{1}{r_0^2}(r - r_0) \right]^{\frac{1}{2}} \left[v_{x0}^2 + \right. $$
$$\left. + 2\frac{K^2}{r_0^2}(r - r_0) \right]^{-\frac{1}{2}}. \qquad (29)$$

or after transformations

$$\frac{dr}{dx} = \pm \left[1 - \frac{r_0^2}{r^2} - \frac{2r_0^2}{r_0^2}(r - r_0) \right]^{\frac{1}{2}} \times \left[\left(\frac{v_{x0}}{v_0} \right)^2 + 2\frac{r_0^2}{r_0^2}(r - r_0) \right]^{-\frac{1}{2}}. \qquad (30)$$

After introducing dimensionless parameters

$$m = \frac{r_0}{r_a}; \quad n = \frac{r_a}{r_0} W^{-\frac{1}{3}} = \frac{W^{-\frac{1}{3}}}{m}; \qquad (31)$$

$$X = \frac{x}{r_a}; \quad R = \frac{r}{r_a};$$

$$\frac{v_{x0}}{v_0} = m \frac{\sqrt{2m(1 - m)}}{(1 - 2m)^2} \qquad (32)$$

and integrating equation (30), we obtain the equation of the liquid film surface

$$X = \int_0^R \frac{(AR^2 + BR)\,dR}{\sqrt{CR^4 + DR^3 + ER^2 + FR + L}}. \qquad (33)$$

22

where

$$
\begin{aligned}
A &= 2m^3n^2; \\
B &= \frac{2m^3(1-m) - 2m^4n^2(1-2m)^4}{(1-2m)^4}; \\
C &= -4m^4n^2; \\
D &= 2m^2n^3\left[1 - \frac{2m^2(1-m)}{(1-2m)^4} + 4m^2n^3\right]; \\
E &= (2m^4n^2 + 1)\left[\frac{2m^2(1-m)}{(1-2m)^4} - 2m^2n^3\right]; \\
F &= -2m^4n^2; \\
L &= -m^2\left[\frac{2m^2(1-m)}{(1-2m)^4} - 2m^2n^3\right].
\end{aligned}
\tag{34}
$$

The integral in formula (33) in general is elliptic and can be expressed through normal elliptic integrals of the first, second and third kinds.

To bring the integral in formula (33) to canonical form it is necessary to find the zeros of the fourth degree polynomial under the radical. This polynomial can be expanded in the following way:

$$
\begin{aligned}
CR^4 + DR^3 + ER^2 + FR + L = \\
-4m^4n^2(R-R_1)(R-R_2)(R-R_3)(R-R_4).
\end{aligned}
\tag{35}
$$

Here

$$
\begin{aligned}
R_1 &= m > 0; \\
R_2 &= \frac{1 + \sqrt{1 + 4m^4n^2}}{4m^4n^2} > 0; \\
R_3 &= \frac{1 - \sqrt{1 + 4m^4n^2}}{4m^4n^2}; \\
R_4 &= m\left[1 - \frac{1-m}{m^2(1-2m)^4}\right].
\end{aligned}
\tag{36}
$$

To study the forms of the liquid film we will examine the behavior of the roots of polynomial (36) in the region of parameters m and n. On Fig. 21 is given the partition of the plane of parameters m and n into regions corresponding to different distributions of the polynomial roots on a numerical straight line. The range of change of parameters m and n is selected so that it embraces the

23

case in which we are interested. The boundaries of these domains are obtained as the result of solving the equations

$$R_1 = R_2; \; R_2 = R_3; \; R_3 = R_4; \; R_1 = R_4.$$

The case $R_1 = R_3$ corresponds to the origin of coordinates. Boundary curve $R_2 = R_3$ lies in the negative part of the plane of parameters and therefore does not have physical meaning.

Let us consider forms of liquid film corresponding to the values of parameters lying on these boundary curves for which the integral in formula (33) degenerates into a pseudoelliptic integral. It turns out that only that part of the plane lying under boundary curve $R_1 = R_2$ has physical meaning. In the part located above curve $R_1 = R_2$, the integral in formula (33) becomes imaginary. This occurs because on the boundary curve $R_1 = R_2$ itself criterion $W = 1$, i.e., the forces of inertia are balanced by the forces of surface tension and liquid does not flow from the nozzle. In particular, $m = n = 1$ the integral in formula (33) gives the equation of the meniscus.
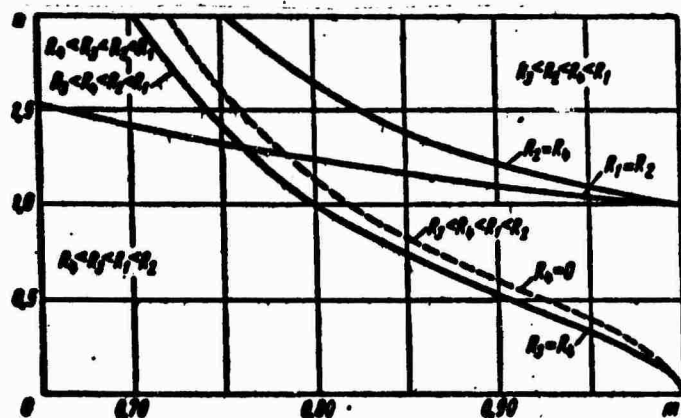
Fig. 21. Partition of plane of parameters m and n into regions corresponding to different distributions of the polynomial roots.

On section of curve $R_3 = R_4$, where criterion W changes from 1 to ∞, the integral in formula (33) is taken in quadratures

$$X = -\sqrt{-R^2 + (R_1 + R_2)R + R_1 R_2} + \\ + \frac{R_1 + R_2}{2}\left(\frac{3\pi}{4} - \arcsin\frac{R_1 + R_2 - 2R}{R_1 - R_2}\right). \quad (37)$$

24

Taking into account periods of the arc sine in expression (37), we obtain periodic curves of the film contour (Fig. 22) for various values of criterion W. The period of these curves is

$$X_0 = \pi (R_1 + R_2). \tag{38}$$

The axis of abscissas on Fig. 21 corresponds to the case $W = \infty$, when formula (33) gives the equation of a hyperboloid of rotation:

$$X = \frac{m \sqrt{2m(1-m)}}{(1-2m)^2} \sqrt{R^2 - m^2}. \tag{39}$$

In regions lying along both sides of curve $R_3 = R_4$, the integral in formula (33) is expressed through normal elliptic integrals of all three kinds.

Let us investigate the effect of criterion W on the form of the film, for which we will use a particular form of surface equation (37). On Fig. 22 are depicted film contours for different values of criterion W. The greater W is, the bigger the root angle, maximum radius and
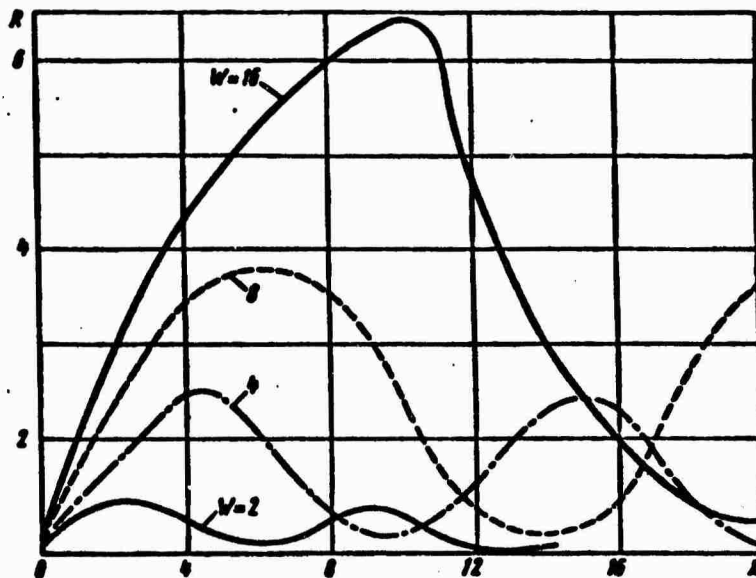
Fig. 22. Curves of film contour for different values of criterion W.

period of surface X_0. Knowing the film contours, one can determine
its thickness at different distances from the nozzle. From the
continuity equation we obtain the dependence of film thickness $\delta(r)$
and its radius

$$\frac{\delta(r)}{\delta_0} = \frac{r_0}{r} \tag{40}$$

or in dimensionless coordinates

$$\delta^0 = \frac{\delta(r)\, m}{\delta_0 R}. \tag{41}$$

Using the curves shown on Fig. 23 and formula (41), it is
possible to construct the dependences of film thickness on distances
to nozzle for different values of criterion W. After a sharp drop
of δ^0 near the nozzle, the curve also takes a periodic character,
wherein the period increases as criterion W becomes larger. On
Fig. 7 are shown photographs characterizing the change of forms of
the film with an increase of the pressure drop on the injector (or
accordingly criterion W). At small values the film of liquid obtains
a "bubble" form (it bursts at the beginning of the second wave).
As criterion W increases the place where the film breaks shifts
nearer to the nozzle; then the "tulip" shape will be formed: the
film breaks up throughout the first wave. Finally, with a further
increase of criterion W the place where the film breaks comes close
to the nozzle: liquid will form drop fog. Comparison of forms of
film with theoretical data (Fig. 22) shows that the above theory
qualitatively predicts correctly the appearance and replacement of
film shapes as criterion W changes.
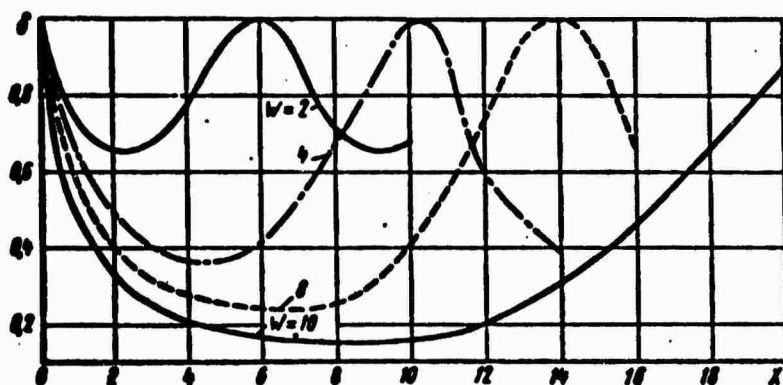
Fig. 23. Dependence
of dimensionless thick-
ness of film on distance
to nozzle.

Along with the above theoretical works we should still note the work of Valdenazzi [2], in which an equation of the film surface created by a swirler also is obtained. However, this work used the condition of static equilibrium of a film element, as a result of which this theory could not reveal the periodic character of the film or explain the appearance of such a film shapes as the "bubble" and the "tulip." Further, we should note work which examines the equilibrium of a twisted ring-shaped film taking into account pressure drop Δp between the internal and external surfaces [6]. In this case film equilibrium depends not only on Weber criterion W, but also on Euler criterion Eu = $\frac{\Delta p}{\rho w_a^2}$. However, for liquid streams Δp is insignificantly small and therefore criterion Eu need not be taken into account.

As was shown above, during the hydraulic calculation of swirlers, conducted to determine injector dimensions and root angle of the spray of atomized liquid, there is no necessity to take into account the action of surface tension forces. Considering the wide use of swirlers in technology, the following chapters are dedicated to their hydraulic calculation for injectors of different types.

§ 4. Injectors with Rotating Atomizers [Rotating Drums and Disks]

As was shown earlier, in injectors with rotating atomizers the liquid film is created by rotating a drum or disk.
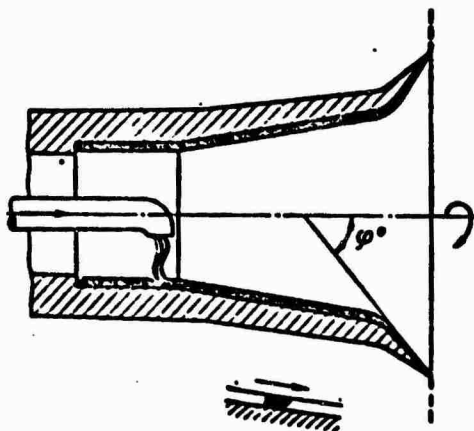
Fig. 24. Diagram of liquid flow inside revolving drum.

Let us consider the pattern of flow and formation of a film in rotating drum inside which liquid is fed (Fig. 24). During the study of liquid flow inside a drum Kinsey and Milborn considered that the thickness of the layer of viscous liquid is small as compared to the dimensions of the drum, and that the flow of liquid is axisymmetrical. Under these assumptions the static pressure is constant in the layer and velocity component v_ϕ is small as compared to component v_ξ along the drum generatrix; component v_θ is small as compared to component v_ξ. It is also assumed that the path of a particle of liquid is linear and the particle moves along the radius; it is considered that there is no liquid sliding relative to the drum surface. Then the equation of motion takes the form

$$\frac{\partial^2 v_\xi}{\xi^2 \partial \psi^2} + \frac{\rho \omega^2 \xi}{\mu} \sin^2 \varphi_0 = 0. \tag{42}$$

Boundary conditions:

$$\text{on wall } (\psi = 0) \ v_\xi = 0;$$
$$\text{on free surface } (\psi = \psi_1) \qquad\qquad \tag{43}$$
$$\frac{\partial v_\xi}{\xi \partial \psi} = 0.$$

The solution of equation (42) with boundary conditions (43) is written in the following way:

$$v_\xi = \frac{\rho \omega^2}{\mu} \sin^2 \varphi_0 \left(\xi_1^3 \psi_1 \psi - \xi^3 \frac{\psi^2}{2} \right).$$

where ρ — density of liquid; ω — angular velocity of rotation of drum; μ — coefficient of viscosity; ξ_1 — value of ξ on free surface.

The quantity ψ_1 is determined from condition that the overall discharge of liquid in the layer equals the discharge of liquid Q, fed into the drum. Then

$$Q = \int_0^{\psi_1} 2\pi r' v_\xi d\psi = \frac{2\pi \rho \omega^2 \xi_1^5 \sin^3 \varphi_0 \psi_1^3}{3\mu}.$$

Designating $\delta = \xi_1 \psi_1$ and $r = \xi_1 \sin \phi_0$, we obtain

$$Q = \frac{2\pi \rho \omega^2 r^2 \delta^3 \sin \varphi_0}{3\mu}. \tag{44}$$

From formula (44) we obtain the thickness of the layer of liquid film:

28

$$\delta = \left(\frac{3\mu Q}{2\pi\rho\omega^2 r^3 \sin\varphi_0}\right)^{\gamma_0}. \tag{45}$$

The above simplifying assumptions mean that $\psi_1 \ll 1$ or $\frac{\delta}{\xi_1} \ll 1$, i.e.,

$$\left(\frac{\mu Q \sin^2\varphi_1}{\rho\omega^2 r^6}\right)^{\gamma_0} \ll 1. \tag{46}$$

Earlier it was assumed that a particle of liquid moves radially with respect to the drum. However, for a fixed observer the trajectory of a particle constitutes a spiral whose differential equation has the form

$$\frac{d\xi}{r\,d\theta} = \frac{v_\xi}{\omega r}.$$

The value of v_ξ we connect with maximum peripheral velocity:

$$v_\xi = k v_{\xi\,max}, $$

where $0 \le k \le 1$ and

$$v_{\xi\,max} = \left(\frac{9\rho\omega^2 \sin\varphi_V Q^2}{32\mu\pi^2 r}\right)^{\gamma_0}. \tag{47}$$

Then differential equation (47) takes the form

$$\frac{d\xi}{d\theta} = A\xi^{-\frac{1}{3}}, \tag{48}$$

where

$$A = k\left(\frac{9\rho Q^2}{32\pi^3\mu\omega}\right)^{\frac{3}{4}}.$$

After integration of equation (48) we obtain the equation of the spiral

$$\xi = \left(\frac{4}{3} A\theta\right)^{\frac{3}{4}}, \tag{49}$$

where the constant of integration is taken equal to zero. From equation (49) can be obtained the expression for the distance between

two adjacent turns:

$$\Delta\xi = \left(\frac{8\pi A}{3}\right)^{\frac{3}{4}} - \left(h^3 \frac{16\pi\eta Q^2}{3\mu\omega}\right)^{\frac{1}{4}}. \tag{50}$$

From consideration of the last formula it may be concluded that $\Delta\xi$ does not depend on the angle of taper of the drum ϕ_0 and on ξ, but is a constant from the point of liquid feed to the edge of the drum.
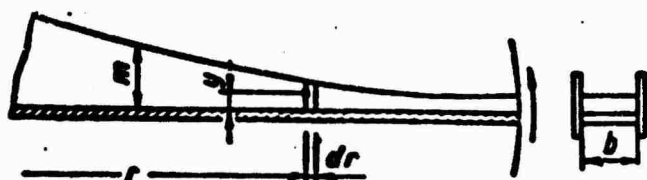
Fig. 25. Diagram of revolving disk element.

Thus, the thickness of the film of liquid formed using a rotating drum, necessary to calculate dimensions of the drops, may be determined by formula (50).

Let us examine the flow and formation of a film on a rotating disk [8]. On Fig. 25 is shown the diagram of an element of a rotating disk. Usually to prevent liquid slide with respect to the disk, blades are placed on its surface.

We will consider that the liquid is supplied in the center of the disk. If we disregard sliding of liquid with respect to the disk within limits of the distance between blades, and do not consider viscous friction, the time required for the liquid to move over the periphery of the disk t can be determined from the relationship

$$\omega t = N_\theta = \arcsin r \cdot r_0. \tag{51}$$

where ω — angular velocity of disk; N_θ — number of radians passable by a particle of liquid up to the periphery of the disk; r — radial coordinate; r_0 — radial coordinate corresponding to the point where the film has constant thickness.

Equation (51) is approximate and shows that the theoretical trajectory of a particle of liquid on a disk constitutes a hyperbola.

If we consider sliding and viscous friction of the liquid, then for the case of laminar flow the following system of joint nonlinear differential equations can be obtained, describing the movement of a particle of liquid on a disk [8]:

$$\frac{d^2r}{dt^2} + \frac{3\mu}{\rho}\left(\frac{2\pi r}{Q}\right)^2\left(\frac{dr}{dt}\right)^3 - r\frac{d\theta}{dt} = 0;$$ (52)

$$\frac{d}{dt}\left(r\frac{d\theta}{dt}\right) - \frac{12\mu\pi r^3}{\rho Q^2}\left(\omega - \frac{d\theta}{dt}\right)\left(\frac{dr}{dt}\right)^2 = 0,$$ (53)

where Q — volumetric flow rate of liquid; θ — angle of rotation of particle; μ, ρ — viscosity and density of liquid.

In the absence of sliding equation (53 drops out, since $\omega = \frac{d\theta}{dt}$ and $\frac{d}{dt}\left(r\frac{d\theta}{dt}\right) = 0$. If, furthermore, we disregard viscous friction, then equation (52) is simplified and reduces to an equation whose integral is relationship (51).

When the disk has radial blades, considering viscous friction and disregarding sliding, it is possible to a compose differential equation for the radial velocity of the liquid, proceeding from equilibrium of forces in an element (Fig. 25):

$$mb\rho\omega^2 r \, dr - \mu b\left(\frac{dV_r}{dy}\right)_{y=0} dr = mb\rho\frac{d(V_r)_{cp}}{dt} = 0,$$ (54)

where m — thickness of film of liquid normal to plane of blade; b — width of channel; y — vertical coordinate.

The velocity gradient on the liquid-blade interface in the case of a parabolic velocity profile is equal to

$$\left(\frac{dV_r}{dy}\right)_{y=0} = \frac{3(V_r)_{cp}}{m},$$ (55)

where $(V_r)_{cp}$ – average velocity of liquid on radius r.

Subsequently the index "cp" will be dropped, understanding by V_r its mean value on given radius r.

Substituting the value of m from continuity equation m = Q/bV_r into equations (55) and (54), we obtain a nonlinear differential equation describing laminar flow of liquid along a disk with blades:

$$V_r\left(\frac{dV_r}{dr}\right) + \frac{3\mu b^4}{\rho q^2}V_r^3 - \omega^2 r = 0,$$ (56)

where q – volumetric flow rate of liquid in one channel.

The corresponding equation for turbulent flow can be written as:

$$V_r\left(\frac{dV_r}{dr}\right) + \left(\frac{fb}{2q}\right)V_r^3 - \omega^2 r = 0,$$ (57)

where f – coefficient of friction in turbulent flow.

Equations (56) and (57) can be written in general form:

$$V_r\frac{dV_r}{dr} + AV_r^3 - \omega^2 r = 0.$$ (58)

where A depends only on viscosity, properties of liquid and velocity gradient in the liquid film. Equation (53) was solved by Marshall [8] for different values of A and r_0 (where r_0 – radius on which liquid is introduced onto the disk). Results of calculations are represented on Figs. 26 and 27. The effect of r_0 on the radial velocity is shown on Fig. 26. Figure 27 shows the effect of A on
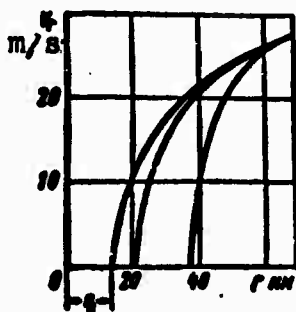
Fig. 26. Change of radial velocity along radius of rotating disk for different values of r_0 [8]:
A = $25.8 \cdot 10^{-3}$ s/m^2;
ω^2 = $21.6 \cdot 10^6$ 1/s^2.

32
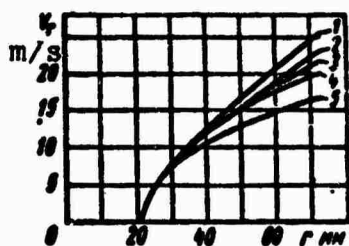
Fig. 27. Influence of viscosity of liquid on radial velocity of liquid [8]: 1 — A = 0; 2 — A = $3 \cdot 10^{-3}$ s/m^2; 3 — A = $6 \cdot 10^{-3}$ s/m^2; 4 — A = $10 \cdot 10^{-3}$ s/m^2; 5 — A = $25.8 \cdot 10^{-3}$ s/m^2.

radial velocity.

When the radius is larger, radial velocity of the liquid can be calculated by equation (56), which in this case turns into a cubic equation. It may be solved approximately with help of series expansion

$$z = x^{\prime\prime} - \frac{1}{9x} - \frac{1}{27x^{\prime\prime}} - \frac{62}{218x^{\prime\prime}},$$

where

$$x = r \cdot \overline{A\omega};\ z = V_r \sqrt{A/\omega}.$$

The work of A. M. Lastovtsev [4] gives a more grounded derivation of the differential equation of turbulent movement of liquid in radial channels of a rotating atomizer disk. Equation (58) in this case takes the form

$$V_r \frac{dV_r}{dr} + A V_r^{2.55} - \omega^2 r = 0. \tag{59}$$

while coefficient A equals $0.105 v^{0.25} b^{0.25} q^{-0.5}$,
where v — kinematic vescosity of liquid; b — width of channel; q — volumetric flow rate of liquid passing through channel.

As a result of numerical integration of equation (59) a formula is obtained for calculation of the radial velocity of a liquid V_r on exit from an atomizer with radial channels:

$$V_r = \frac{\omega^{0.6} R^{0.4}}{B^{0.4}} \left(1 - \frac{0.35}{B^{0.52} \omega^{0.42} R^{1.43}} \right)^{0.4}. \tag{60}$$

where $B = 0.09 r_z^{0.35} v^{0.25} n^{0.5} Q^{-0.5}$ (for round channels); $B = 0.105 b^{0.25} v^{0.25} n^{0.5} Q^{-0.5}$ (for rectangular channels); r_K — radius of channel: Q — volumetric flow rate in m^3/s; n — number of channels in atomizer; R — radius of disk.

33

Formula (59) was experimentally checked by Lastovtsev [4]. This formula should be used in the determination of the dimensions of drops of liquid atomized by a rotating disk.

Literature

1. Borodin V. A., i Dityakin Yu. F. O forme zhidkoy plenki, sozdavayemoy tsentrobezhnoy forsunkoy (The form of the liquid film created by a swirler). "Izv. AN SSSR. OTN. Mekhanika i mashinostroyeniye" No. 2, 1960.

2. Val'denatstsi O forme zhidkoy plenki tsentrobezhnoy forsunki (The form of the liquid film of a swirler). "Voprosy raketnoy tekhniki," 1957. No. 3.

3. Panevin I. G. O raspredelenii zhidkosti v fakele forsunki so stalkivayushchimisya struyami (The distribution of liquid in the spray of an injector with impinging jets). V sb. "Rabochiye protsessy v teplovykh dvigatel'nykh ustanovkakh." M., Oborongiz, 1960 (Trudy MAI. Vyp. 119).

4. Lastovtsev A. M. Gidrodinamicheskiy raschet vrashchayushchegosya raspylitelya (Hydrodynamic design of a rotating atomizer). M., 1957. (Trudy MIKhM. t. II).

5. Euteneuer G. Einfluss der Oberflächespannung auf die Ausbildung von Flüssigkeits—Hohlstrahlen. Forschung auf dem Gebiete des Ingenieurwesens, Bd. 22, No. 4, 1956.
6. Euteneuer G. Das Schwingungsverhalten drallbehafteter Hohlstrahlen unter der Wirkung von Qruckkräften. Ingenieur Archiv, Bd. 33, Heft 3, 1964.
7. Marshall W. Atomization and spray drying. Chemical Engineering Progress Monography Series, No. 2, 1954

C H A P T E R   III

THE HYDRAULICS OF THE CENTRIFUGAL INJECTOR

§ 1. Theory of the Centrifugal
Injector for an Ideal Liquid

The basic difference between swirlers and other injectors is
that the liquid flowing through the swirler obtains in it angular
momentum with respect to the axis of the nozzle.

Liquid is fed into the injector swirl chamber along tangential
channels whose axis is shifted with respect to the nozzle axis (Fig.
28). In the swirl chamber liquid goes into intense rotation and
proceeds to the nozzle. Trajectories of liquid particles in the
swirl chamber can be obtained by combining the drain with the

Fig. 28. Swirler.

35
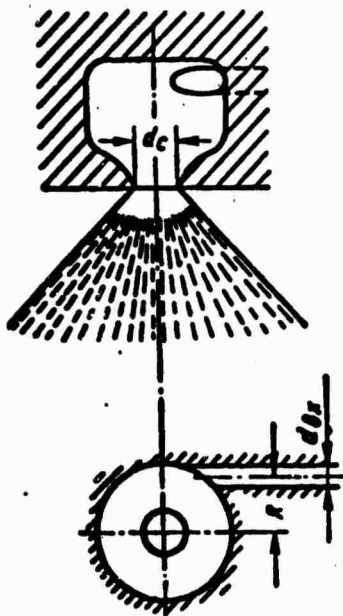
potential vortex, and in the cylindrical part of the nozzle — the forward flow with the potential vortex.

On leaving the injector nozzle, the liquid particles, on which the action of centripetal forces cease, scatter along linear trajectories, forming a spray.

The liquid flow in a swirler is characterized by features caused by the action of angular momentum of the liquid particles (with respect to the nozzle axis). These features show up first of all in the fact that the discharge coefficient and root angle of the spray in the case of swirlers essentially differ from those for jet injectors. It is especially important that these parameters be regulated in a wide range depending upon the relationship between dimensions of nozzle, swirl chamber, and entrance channels.

Let us examine the simplest case — the flow of an ideal incompressible liquid in a swirler. The theory of a swirler for an ideal liquid, based on the principle of maximum flow rate, has been developed by G. N. Abramovich [1, 2]. Somewhat later L. A. Klyachko [11], G. Taylor [31] and Bammert [22] arrived at similar results.

For the flow of an ideal liquid the law of conservation of momentum and the law of preservation of mechanical energy are accurate. The angular momentum of any liquid particle (with respect to the axis of the nozzle) maintains a constant value equal to the initial moment on entrance into the swirl chamber.

$$ur = V_{ax}R.$$ (61)

where u — tangential component of velocity in nozzle; r — distance from axis of nozzle to particle of liquid in nozzle; V_{ax} — velocity in entrance channels; R — distance from axis of nozzle to particle of liquid in entrance channels.

From an analysis of formula (61) it follows that on the approach to the nozzle axis the tangential component of velocity increases. However, the flow remains irrotational.[1]

36

For an ideal incompressible liquid the law of conservation of energy will be written in Bernoulli equation form:

$$p + \frac{\rho}{2}(u^2 + w^2) = p_T.$$ (62)

where p — pressure in flow; ρ — density of liquid; p_T — pressure of stagnated flow (pressure in reservoir from which the outflow comes); w — axial component of velocity in nozzle.

The action of gravity is disregarded, which is fully permissible for the feed pressure used usually.

From equations (61) and (62) it follows that near the nozzle axis of the injector (r → 0) the tangential component of flow rate should have an infintely large positive value, and pressure — an infinitely large negative value, which physically is impossible. In reality near the nozzle axis velocity will increase, and pressure will drop, but only as long as pressure does not equal atmospheric pressure or the pressure of the medium into which the liquid is injected.

The liquid pressure cannot fall below atmospheric, since through the nozzle the injector is connected with the atmosphere. Consequently, the central part of the nozzle is filled not with liquid, but with air; in this part is the air vortex, in which excess pressure is zero ($p_m = 0$).

Flow in the nozzle occurs through a ring-shaped section whose internal radius is equal to the radius of the air vortex r_m, and whose external radius equals nozzle radius r_c.

Area of annular section

$$F = \pi(r_c^2 - r_m^2) = \varphi \pi r_c^2.$$ (63)

where ϕ — space factor of nozzle;

$$\varphi = 1 - \frac{r_m^2}{r_c^2}.$$ (64)

We will find the pressure distribution over the nozzle section.

37

For this we use the condition of dynamic possibility of liquid motion with rotational (circulatory) velocity.

Let us separate a liquid element on radius r, of thickness dr, length $dl = rd\theta$ and height equal to unity (Fig. 29).
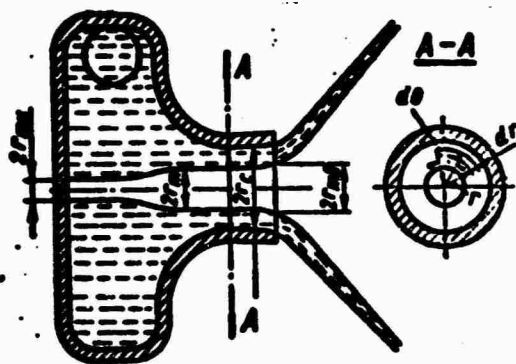
Fig. 29. Diagram of liquid flow in swirler.

The difference of pressures on lateral surfaces of the element should balance centrifugal force

$$dl\,dp = \frac{u^2}{r}\,dm.$$

Mass of element

$$dm = \rho\,dl\,dr.$$

According to the law of preservation of angular momentum

$$u = \frac{u_m r_m}{r}.$$

Substituting expressions for dm and u, we obtain

$$dp = \rho u_m^2 r_m^2 \frac{dr}{r^3}.$$

whence, by integrating we find

$$p = -\frac{\rho}{2} u_m^2 r_m^2 \frac{1}{r^2} + \text{const.}$$

The constant of integration is determined from the condition that on the boundary of the air vortex (at $r = r_m$) excess pressure $p_m = 0$. Thus, pressure distribution in the nozzle cross section is determined by the expression

$$p = \frac{\rho}{2}(u_m^2 - u^2). \tag{65}$$

Substituting expression (65) for pressure into equation (62), we

conclude that the axial (forward) velocity component in the nozzle remains constant across the flow cross section:

$$w = \sqrt{\frac{2}{\rho} p_T - u_m^2} = \text{const.} \tag{66}$$

Then the expression for volumetric flow rate of liquid through the nozzle can be written in the form

$$Q = \pi r_c^2 \varphi w. \tag{67}$$

Let us convert the expression for w. For this we will use the law of conservation of momentum

$$u_m = \frac{V_{ex} R}{r_m},$$

expressing V_{ex} through volumetric flow rate

$$V_{ex} = \frac{Q}{n \pi r_{ex}^2},$$

where n is the number of entrance channels.

Putting u_m into expression (66), we obtain

$$w = \sqrt{\frac{2}{\rho} p_T - \frac{R^2 Q^2}{n^2 \pi^2 r_{ex}^2 r_m^2}}.$$

But from expression (67)

$$w = \frac{Q}{\pi r_c^2 \varphi}.$$

Equating the right side of both expressions for w, we find

$$Q = \frac{\pi r_c^2}{\sqrt{\frac{A^2}{1-\varphi} + \frac{1}{\varphi^2}}} \sqrt{2 \frac{p_T}{\rho}}. \tag{68}$$

In formula (68) A designates a dimensionless quantity — the geometric characteristic of the injector

$$A = \frac{R r_c}{n r_{ex}^2}, \tag{69}$$

which plays an important role in the theory of swirlers.

39

From formula (68) it follows that the discharge coefficient of a swirler is determined by the expression

$$\mu = \frac{1}{\sqrt{\frac{A^2}{1-\varphi} + \frac{1}{\varphi^2}}} \qquad (70)$$

and depends on two parameters: geometric characteristics of injector and the nozzle space factor.

As ϕ increases, discharge coefficient μ changes nonmonotonically and passes through maximum.

When the values of space factor are small, the area of the useful flow cross section is small, and for great values of ϕ (small radii of vortex) energy is expended on the creation of great tangential velocities in points close to the nozzle axis, which leads to small values of the axial velocity component. Thus, in both cases the discharge coefficient is small.

As G. N. Abramovich assumed [1, 2], in the swirler nozzle an air vortex is setup of such radius with which the discharge coefficient at a given pressure takes its maximum value and just these vortex dimensions correspond to stable flow conditions. This assumption, which will be examined below in greater detail, obtained the name of the principle of maximum flow rate.

Let us find the space factor corresponding to the maximum of discharge coefficient. Differentiating expression (70) with respect to ϕ and considering $\frac{d\mu}{d\varphi} = 0$, we obtain the following relationship between space factor and geometric characteristics of the injector:

$$A = \frac{(1-\varphi)\sqrt{2}}{\varphi\sqrt{\varphi}}. \qquad (71)$$

Dependence of ϕ on A by formula (71) is represented on Fig. 30.

Putting the obtained expression in equation (70), we find the expression for the swirler discharge coefficient:

$$\mu = \sqrt{\frac{\varphi}{2-\varphi}}. \tag{72}$$

With the help of formulas (71) and (72) it is easy to construct the dependence of discharge coefficient on geometric characteristics of the injector (Fig. 30). When the geometric characteristic of the injector changes from A = 0 to A = ∞ the discharge coefficient decreases from one to zero.
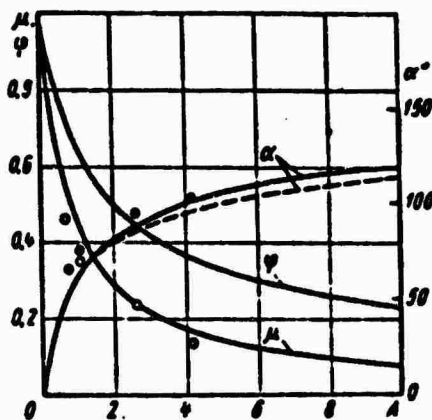
Fig. 30. Dependences of discharge coefficient μ, nozzle space factor φ and spray angle α on the geometric characteristic of the injector A; ○ and ● — experimental points.

For round tangential channels the geometric characteristic is determined by formula (69). When the cross section of the entrance channels differs from a circle, and their direction is not perpendicular to axis of the nozzle, it is easy to show that the expression for geometric characteristic is of the form

$$A = \frac{R r_c \pi}{n f_{ex}} \sin \beta, \tag{73}$$

where f_{ex} — area of cross section of entrance channel; β — angle between direction of entrance channel and axis of nozzle.

Mass flow per second of liquid through an injector with discharge coefficient μ is found by the formula

$$G = \pi r_c^2 \mu \sqrt{2 \rho p_T}. \tag{74}$$

Before crossing to determination of the root angle of the spray, let us note the following circumstance, which was first studied by V. I. Skobelkin. On the nozzle section of the injector liquid pressure should be constant over the whole flow cross section and

41

equal to ambient pressure (correction for pressure of surface tension can be neglected as small). Consequently, in a cylindrical nozzle of an injector occurs a transformation of excess centrifugal pressure into impact pressure. This transformation leads to an increase of the axial velocity component and its nonuniform distribution over the cross section of the liquid ring: near the nozzle wall it becomes larger than on the air vortex boundary. The radius of air vortex on the nozzle section is larger than in the depth of the swirl chamber. Actually, in the flow of incompressible liquid in a cylindrical nozzle, the axial velocity component can increase only when the useful cross section of flow decreases, i.e., when the radius of the air vortex increases.

The discharge coefficient is naturally not affected by the transformation of pressure into impact pressure since the continuity equation still holds.

As the author has shown, the distribution of axial velocity component and radius of the air vortex in the nozzle exit section can be found in the following way.

Since on the nozzle section of the injector excess pressure is equal to zero over the whole cross section, from equation (62) we have[2]

$$w^2 + u^2 = \frac{2p_T}{\rho}. \tag{75}$$

According to the law of preservation of angular momentum $u = \frac{RV_{ax}}{r}$. Expressing V_{ax} through the volumetric flow rate, we obtain

$$u = A \frac{r_{cH}}{r} \sqrt{\frac{2}{\rho} p_T}. \tag{76}$$

Substituting u into equation (75), we find the unknown distribution of axial velocity component on the nozzle section:

$$w = \sqrt{1 - \frac{R^2 A^2 r_c^2}{r^4}} \sqrt{\frac{2}{\rho} p_T}. \tag{77}$$

Hence it is clear that w increases with an increase of the distance from the nozzle axis. The least value of w is on the air

42

vortex boundary, the biggest – near the nozzle wall.

The air vortex radius on leaving the nozzle r_{mu} is determined by expressing the volumetric flow rate in the form of the integral of the flow rate elements (on the nozzle section):

$$Q = \int_{r_{mo}}^{r_c} w 2\pi r\, dr = \pi r_c^2 \mu \sqrt{\frac{2}{\rho} p_T}.$$

Substituting w from expression (77) and integrating, we obtain the transcendental equation for finding r_{mo}:

$$\mu = \sqrt{1 - \mu^2 A^2} - S\sqrt{S^2 - \mu^2 A^2} - $$
$$ - \mu^2 A^2 \ln \frac{1 + \sqrt{1 - \mu^2 A^2}}{S + \sqrt{S^2 - \mu^2 A^2}}, \tag{78}$$

where $S = \frac{r_{mo}}{r_c}$ – dimensionless radius of vortex on nozzle section.

The connection between μ and A is determined from formulas (71) and (72) or curve on Fig. 30.

Solving graphically equation (78), we find the dependence of the dimensionless air vortex radius on the nozzle section on the geometric characteristic of the injector. On Fig. 31 this dependence is shown; in the same place is given the graph for the dimensionless radius of the vortex at the beginning of the nozzle. As we would have expected, curve $\frac{r_{mo}}{r_c}$ passes above curve $\frac{r_m}{r_c}$, since the radius of the air vortex at the beginning of the nozzle is less than on the exit. Still less is the radius of the air vortex on the rear wall of the swirl chamber.
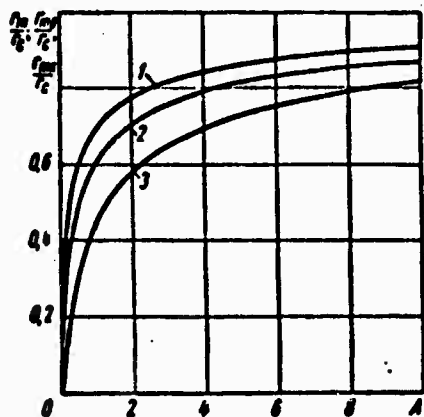
Fig. 31. Dependence of dimensionless radius of air vortex on geometric characteristic of injector: 1 – radius of vortex on leaving nozzle; 2 – radius of vortex in depth of nozzle; 3 – radius of vortex on rear wall of swirl chamber.

43

The spray angle is determined by the ratio of tangential and axial velocity components. This ratio changes over the nozzle cross section. Streams adjacent to the air vortex flow out at the greatest angle, and those adjacent to the nozzle wall at the least angle. Therefore the angle of the swirler spray should be characterized by a certain mean value of the ratio $\frac{\overline{u}}{\overline{w}}$:

$$tg\frac{a}{2} = \frac{\overline{u}}{\overline{w}}.$$

Let us take as mean values $\overline{u}$ and $\overline{w}$ the values of these quantities calculated for $\overline{r} = \frac{(r_s + r_{ex})}{2} = \frac{r_0(1+S)}{2}$.

From expressions (76) and (77) we find the mean values:

$$\overline{u} = \frac{2\mu A}{1+S}\sqrt{\frac{2}{\rho}p_T}; \qquad \overline{w} = \sqrt{1 - \frac{4\mu^2 A^2}{(1+S)^2}}\sqrt{\frac{2}{\rho}p_T}.$$

Then the expression for the tangent of half the spray angle takes the form

$$tg\frac{a}{2} = \frac{2\mu A}{\sqrt{(1+S)^2 - 4\mu^2 A^2}}. \tag{79}$$

Figure 30 shows the dependence of the spray angle on the geometric characteristic of the injector. If A = 0 (flow is not twisted), then the spray angle is zero. When the geometric characteristic increases, the spray angle increases and under an unlimited increase of A it tends to 180°. Moreover, as was already noted, the discharge coefficient decreases from one to zero.

In the work of L. V. Kulagin [15] a definitized formula is obtained for the spray angle, considering the interaction of elemental circular streams of liquid, flowing from the nozzle at different angles (averaging is over the stream momentum). The formula obtained in this work has the form

$$tg\frac{a}{2} = \frac{2\mu A\left(\sqrt{1-\mu^2 A^2} + \sqrt{S^2-\mu^2 A^2}\right)}{1-S^2 + 2\mu^2 A^2 \ln S} - \frac{2\mu A\left[\mu A\left(\arccos \mu A - \arccos \frac{\mu A}{S}\right)\right]}{1-S^2 + 2\mu^2 A^2 \ln S}. \tag{80}$$

44

Dependence of spray angle on the geometric characteristic of injector by formula (80) is given on Fig. 30 by the broken curve.

As we see, the difference between values of the spray angle obtained with calculation by formulas (79) and (80) does not exceed 4-5%.

Hydraulic parameters of the swirler (discharge coefficient and spray angle) for an ideal liquid are simply determined by the geometric characteristic. Consequently, the geometric characteristic is the criterion of the hydraulic similarity of swirlers during a flow of inviscid liquid.

To check the basic positions of swirler theory experiments were conducted with an enlarged model (R = 15.9 mm; d_c = 10.8 and 16.8 mm; n = 1; d_{ex} = 11.4 and 23 mm), having a transparent rear wall which permitted observing the flow of liquid in the swirl chamber and nozzle [1].

It was shown that on the axis of the injector is an air-filled cavity (air vortex), one base resting against the rear wall of the swirl chamber, and the other in contact with the atmosphere. Liquid flow in the injector nozzle is through a circular section between the nozzle wall and the air vortex.

The air vortex has on the rear wall of the swirl chamber minimum diameter; as the nozzle is approached, the vortex diameter gradually increases. In the cylindrical part of the nozzle the diameter of the air vortex is constant and only on leaving the nozzle does the vortex expand, passing into the internal surface of a liquid sheet. A diagram of the air vortex is shown on Fig. 29.

The air vortex diameter on the rear wall of the swirl chamber decreases because on the wall the axial velocity component of the flow (normal to wall) turns into zero. But since on the surface of the air vortex pressure is constant, from the energy equation it follows that the smaller the axial velocity component the greater the

45

peripheral component and consequently, the less the radius of the air vortex.

An enlarged injector model was tested for four values of the geometric characteristic: A = 0.65, A = 1.01, A = 2.64, A = 4.11 (water was fed into the injector). Corresponding experimental values of the discharge coefficient and spray angle are shown in Fig. 30. As we see, for an enlarged injector model experimental data satisfactorily agree with theoretical data.

This theory is confirmed in tests of working swirlers.

In Table 1 are given experimental and computed values of discharge coefficient and root angle of the spray for two swirlers of a turbojet engine with round tangential channels (investigated on kerosene at Δp = 4-50 kgf/cm^2); the basic dimensions of atomizers of these injectors are also given.

Table 1.

Injectors	d_c in mm	d_{oc} in mm	R in mm	n	A	μ_{sc}	μ_{mexp}	a_{sc}	a_{mexp}
OP-20	0.78	0.81	1.6	5	0.76	0.475	0.50	53°	56°
OP-500	1.3	1.1	2.0	3	1.43	0.41	0.36	78°	71°

We see that for these injectors calculation according to the theory of swirlers for an ideal liquid gives satisfactory results.

However, in a number of cases essential deviations of theoretical data from experimental data are revealed.

Before passing to an analysis of the causes of these deviations we will examine the physical content of the principle of maximum flow rate, which was formulated above.

46

§ 2. Principle of Maximum Flow Rate

Flow in the swirler is accompanied by the formation of a free surface — the surface of the air vertex on which is established constant atmospheric pressure. Such flows (widespread in nature and technology) include the flows of trickling liquids in open channels (flows in rivers, flumes, spillways, etc.); their study is the subject of numerous works. In contrast to these flows, in which a free surface is formed under the action of gravity, in the nozzle of a swirler it is formed under the action of centrifugal force.

The motion of liquid in a cylindrical injector nozzle of constant radius is similar to the flow of a heavy liquid along a horizontal channel of constant depth h. For the last case N. Ye. Zhukovskiy [9] showed that during a steady flow the flow rate cannot exceed $c = \sqrt{gh}$, equal to the propagation velocity of long waves on a liquid surface.

A similar position is also valid with respect to a swirler: the forward velocity of liquid in a nozzle in steady-state conditions should equal the velocity of waves propagating along the free surface of a liquid in a centrifugal force field. As will be shown below, flow rate through an injector at a given pressure has a maximum value.

The application of such an interpretation of the principle of maximum flow rate was first proposed by I. I. Novikov and then developed by G. N. Abramovich and V. I. Skobelkin.

A similar approach to a foundation of the principle of maximum flow rate is contained in the works of foreign authors [23, 24].

Following G. N. Abramovich and V. I. Skobelkin, we will prove that at maximum flow rate the forward velocity of a flow of liquid in an injector nozzle is equal to the propagation velocity of waves along the surface of the air vortex.

First of all let us find the expression for propagation velocity of waves on a free surface of liquid in a centrifugal force field.

47

We will examine the pattern of liquid flow in a cylindrical nozzle of constant radius (Fig. 32). Let us introduce a cylindrical system of coordinates, where we direct the x-axis along the axis of the nozzle. The radius of undisturbed surface of the air vortex is designated by r_m; ζ designates radial deviation of profile of free surface of wave from the equilibrium position. Obviously, ζ is a function of coordinate x and time t.

Fig. 32. Diagram of liquid flow in a cylindrical nozzle.

Flow in the nozzle possesses axial symmetry, and therefore the Euler equation of motion in cylindrical coordinates will be written in the following form:

$$\frac{dV_r}{dt} = \frac{V_\phi^2}{r} - \frac{1}{\rho} \cdot \frac{\partial p}{\partial r}; \tag{81}$$

$$\frac{dV_x}{dt} = -\frac{1}{\rho} \cdot \frac{\partial p}{\partial x}. \tag{82}$$

where V_r — radial component of velocity; V_ϕ — tangential component of velocity; V_x — axial component of velocity.

We assume that except for centrifugal force, other mass forces do not act on the liquid.[3] Centrifugal acceleration is equal to $\frac{V_\phi^2}{r}$ and is directed along the radius from the nozzle axis.

Let us make the following assumption about the character of the wave process, usually made in the theory of long waves [13].

1. The radial velocity of particles changes very slowly. Consequently, radial acceleration of particles may be disregarded, i.e., we can set

$$\frac{dV_r}{dt} = 0.$$

48

2. The amplitude of oscillations of liquid particles is small as compared to the air vortex radius and the thickness of the liquid sheet in the injector nozzle.

Then equation (81) takes the form

$$\frac{V_\varphi^2}{r} - \frac{1}{\rho} \cdot \frac{\partial p}{\partial r} = 0. \tag{83}$$

The tangential component of velocity is determined from the law of conservation of momentum

$$V_\varphi = \frac{V_{ar}R}{r}.$$

Integrating equation (83), we find the dependence of pressure on radius

$$p = -\frac{\rho}{2} \frac{V_{ar}^2 R^2}{r^2} + f(x, t).$$

where $f(x, t)$ is an arbitrary function of x and t.

On the free boundary at $r = r_m + \zeta$ pressure is constant and equals atmospheric ($p = p_0$):

$$p_0 = -\frac{\rho}{2} \cdot \frac{V_{ar}^2 R^2}{(r_m + \zeta)^2} + f(x, t).$$

Calculating difference $p - p_0$, we obtain

$$p - p_0 = \frac{\rho}{2} V_{ar}^2 R^2 \left[\frac{1}{(r_m + \zeta)^2} - \frac{1}{r^2} \right] \tag{84}$$

and

$$\frac{\partial p}{\partial x} = -\rho \frac{V_{ar}^2 R^2}{(r_m + \zeta)^3} \cdot \frac{\partial \zeta}{\partial x}. \tag{85}$$

From expression (84) it follows that pressure distribution along the radius is the same as in expression (65) in the absence of wave motion. This should have been expected, since in both cases it is assumed that radial acceleration is absent.

Let us turn to an analysis of equation (82). First of all it

49

follows from it that acceleration in the axial direction $\frac{dV_s}{dt}$ does not depend on the radius. Consequently, uniformity of the distribution of the axial velocity component over the cross section of the liquid ring existing in the case of undistrubed flow in the nozzle will hold even in the presence of oscillations. Thus, V_x is a function only of x and t; therefore

$$\frac{dV_s}{dt} = \frac{\partial V_s}{\partial t} + V_s \frac{\partial V_s}{\partial x}.$$

But the last term, as was shown in the book of N. Ye. Kochin and others [13], may be disregarded; then

$$\frac{dV_s}{dt} = \frac{\partial V_s}{\partial t}.$$

Therefore equation (82) after substitution of $\frac{\partial p}{\partial x}$ from equation (85) will take the form

$$\frac{\partial V_s}{\partial t} = \frac{V_{as}^2 R^2}{(r_m + \zeta)^2} \cdot \frac{\partial \zeta}{\partial x}.$$

In force of the second assumption, disregarding ζ in comparison with r_m, we obtain finally

$$\frac{\partial V_s}{\partial t} = \frac{V_{as}^2 R^2}{r_m^2} \cdot \frac{\partial \zeta}{\partial x}. \tag{86}$$

Let us turn to a derivation of the equation of inseparability. Let us consider the volume of liquid between two planes AB and A'B', perpendicular to the nozzle axis and located at distance dx from each other. The volume of liquid passing during time dt through plane AB will be expressed as:

$$\{V_s \pi [r_e^2 - (r_m + \zeta)^2]\}_s \, dt.$$

The volume of liquid passing through plane A'B' in the same interval of time is:

$$\{V_s \pi [r_e^2 - (r_m + \zeta)^2]\}_{s+ds} \, dt.$$

The volume of liquid between the shown planes during the time dt will change, consequently, by a magnitude equal to

$$\frac{\partial \{V_s \pi [r_e^2 - (r_m + \zeta^2)]\}}{\partial x} \, dx \, dt. \tag{87}$$

50

But for an incompressible liquid this change of volume can occur only due to an increase or decrease of the level of liquid between AB and A'B'. During the time dt the level changes by $\frac{\partial \zeta}{\partial t} dt$, and the volume of liquid between AB and A'B' increases by

$$2\pi r_m \frac{\partial \zeta}{\partial t} dx dt. \qquad (88)$$

Equating expressions (87) and (88), we find

$$\frac{\partial \zeta}{\partial t} = \frac{1}{2r_m} \cdot \frac{\partial \{V_x [r_e^2 - (r_m + \zeta)^2]\}}{\partial x} =$$

$$= \frac{r_e^2 - (r_m + \zeta)^2}{2r_m} \cdot \frac{\partial V_x}{\partial x} - \frac{r_m + \zeta}{r_m} V_x \frac{\partial \zeta}{\partial x}.$$

The last term of the right side can be rejected as a magnitude of the second order of smallness [13]. Then, disregarding ζ as compared to r_m, we obtain a continuity equation for the examined case in the form

$$\frac{\partial \zeta}{\partial t} = \frac{r_e^2 - r_m^2}{2r_m} \cdot \frac{\partial V_x}{\partial x}. \qquad (89)$$

We exclude from equations (86) and (89) the quantity V_x. For this we preliminarily differentiate the first equation with respect to x, and the second with respect to t, and equate the expressions for mixed derivative $\frac{\partial^2 V_x}{\partial t \partial x}$. This gives

$$\frac{\partial^2 \zeta}{\partial t^2} = \frac{V_{ax}^2 R^2 (r_e^2 - r_m^2)}{2r_m^4} \cdot \frac{\partial^2 \zeta}{\partial x^2}. \qquad (90)$$

As is known, the general solution of the obtained wave equation has the form

$$\zeta = \Phi_1(x - ct) + \Phi_2(x + ct),$$

where

$$c = \frac{V_{ax} R}{r_m^2} \sqrt{\frac{r_e^2 - r_m^2}{2}}. \qquad (91)$$

Expression (91) and is the unknown propagation velocity of waves on the surface of liquid in a field of centrifugal force (Φ_1, Φ_2 are arbitrary functions).

51

After the expression for propagation velocity of waves in the injector nozzle is found, it is easy to show that the forward velocity of the liquid at maximum flow rate coincides with the propagation velocity of waves. Actually, from equation (67) we have

$$w = \frac{Q}{\pi r_c^2 \varphi}.$$

Expressing volumetric flow rate through velocity in the entrance channels $(Q = n \pi r_{ex}^2 V_{ex})$, we obtain

$$w = \frac{\pi_{ex}^2 V_{ex}}{r_c^2 \eta} = \frac{V_{ex} R}{A \varphi r_c}.$$

But at maximum flow rate the space factor is connected with the geometric characteristic by relationship (71).

Substituting this expression into the preceding formula, we obtain

$$w = \frac{V_{ex} R}{r_m^2} \sqrt{\frac{r_c^2 - r_m^2}{2}}. \tag{92}$$

Expressions (91) and (92) are identical. It follows from this that when forward velocity of liquid and the propagation velocity of waves are equal, the flow rate takes the maximum value.

Thus, the principle of maximum flow rate through a swirler is the result of the equality of forward velocity of flow in nozzle and propagation velocity of waves on the free surface of the air vortex in a field of centrifugal force. When this equality is fulfilled, motion of the liquid in an injector will be stable.

The same condition should be the starting point when establishing the connection between geometric characteristic and hydraulic parameters of a swirler (space factor, discharge coefficient, spray angle). This connection is expressed by formulas (71), (72), and (79).

52

§ 3. Analysis of Other Theories of a Centrifugal Injector for an Ideal Liquid

Along with the above theory of a swirler, based on the principle of maximum flow rate, in literature attempts have been made to create theories of a swirler for an ideal liquid, in which for closing the system of equations describing flow in an injector, assumptions other than the principle of maximum flow rate are introduced.

In the work of Feifel [28], dedicated to the theory of cyclones, the question on the carrying capacity of a cyclone in the presence of a flow of incompressible liquid, which is equivalent to the problem of flow rate of a liquid through a swirler is examined.

In solving the problem the author originates from the following assumptions:

1. Radius of air vortex is constant from rear wall of swirl chamber to cut of nozzle:

$$r_m = r_{mx} = \text{const.}$$

2. Rotational (tangential) velocity component is determined from the relationship

$$u_T = r_m \sqrt{\frac{2p_T}{\rho}}. \tag{93}$$

3. On the nozzle section pressure across the flow cross section is completely equal.

In these assumptions the connection of discharge coefficient and radii of air vortex with the geometric characteristic of the injector is given by the expressions:

$$\mu = \sqrt{1 - \left(\frac{r_m}{r_c}\right)^2} - \left(\frac{r_m}{r_c}\right)^2 \ln\left[\frac{r_c}{r_m} - \sqrt{\left(\frac{r_c}{r_m}\right)^2 - 1}\right]; \tag{94}$$

$$\mu A = \frac{r_m}{r_c}. \tag{95}$$

Comparison of the dependences of nozzle discharge coefficient

and space factor on the geometric characteristic of the injector, calculated according to Feifel and according to the theory of G. N. Abramovich, is represented on Fig. 33.
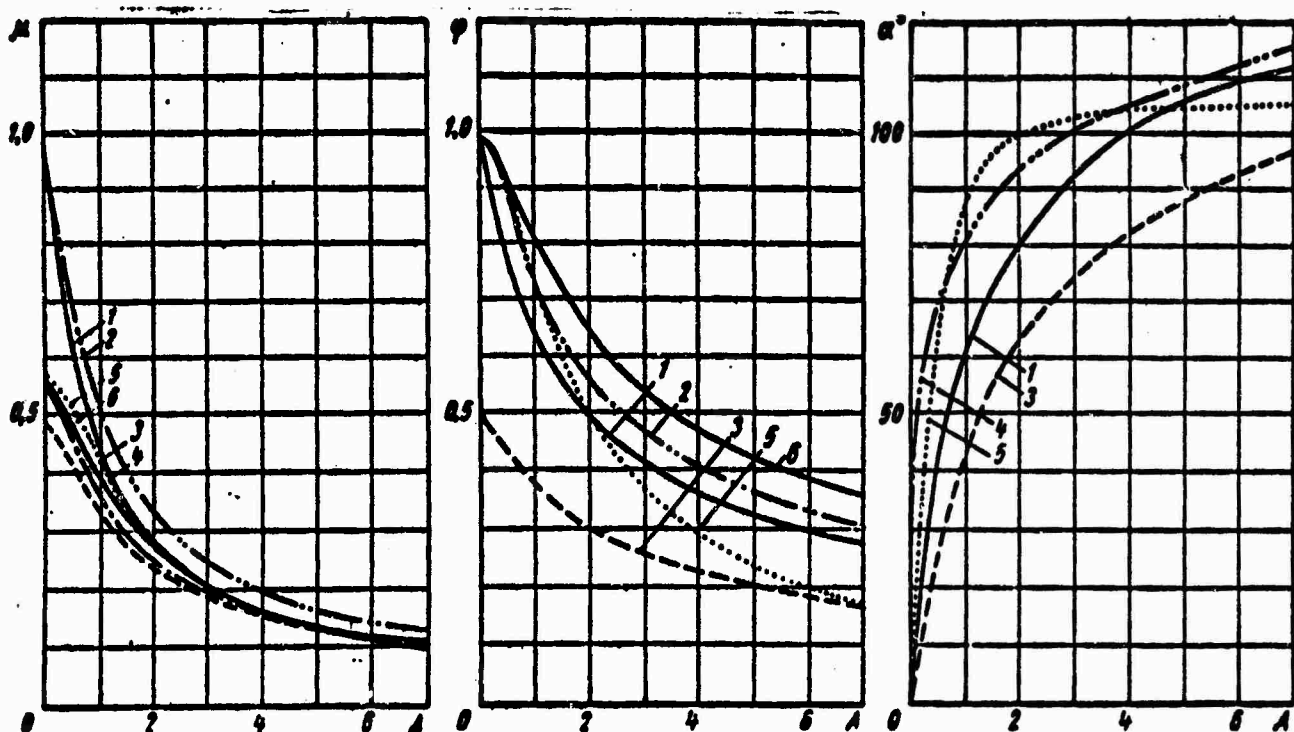
Fig. 33. Dependence of μ, ϕ, and α on A: 1) according to G. N. Abramovich [for α by definitized formula (79)]; 2) according to Ye. Feifel; 3) according to V. V. Talakvadze; 4) according to A. M. Prakhov (at $\frac{r_e}{R_s} = \frac{1}{9}$ and $\theta = 60°$); 5) according to V. B. Tikhonov; 6) according to M. A. Gol'dshtik and others.

As we see, according to both theories at $A = 0$ $\mu = \phi = 1$ and at $A = \infty$ $\mu = \phi = 0$. At the same time for intermediate values of the geometric characteristic a noticeable divergence in discharge coefficient is observed, attaining 22% at $A = 0.5$.

The cause of this divergence is the incorrectness of the first two assumptions introduced by Feifel.

In reality, the radius of the air vortex in the injector nozzle is more than on the rear wall of the swirl chamber (at $A = 0.5$ the ratio of vortex radius in the nozzle to vortex radius on the rear wall is 1.6).

54

The forward velocity component of the flow of liquid in a nozzle on the boundary of the air vortex is by no means zero, as follows from the second assumption of Feifel, but, as was shown above, in the initial section of the nozzle remains constant (this assumption leads to oversized values of the spray angle).

Let us note that Lawrence [29] found the same formula for discharge coefficient as Feifel.

While constructing the theory of a swirler for an ideal liquid, in a number of works the authors try to use the equation of momentum instead of the principle of maximum flow rate.

If Ye. Zenger [30] examines only the case of a completely opened injector (diameter of nozzle equals diameter of swirl chamber), then in the works of A. M. Prakhov [18], V. V. Talakvadze [20] and V. B. Tikhonov [21] the theory of an injector is developed for the general case.

Let us analyze the results of these works, limiting ourselves here to consideration of the flow of an ideal liquid [11].

Comparison of dependences of μ, ϕ, and α on the geometric characteristic of an injector according to theories of G. N. Abramovich and V. V. Talakvadze [20], represented on Fig. 33, shows that the greatest deviation in values of discharge coefficient and space factor of a nozzle calculated according to both theories occurs at $A = 0$. If, according to the theory of G. N. Abramovich, at $A = 0$ $\mu = \phi = 1$, then according to the theory of V. V. Talakvadze at $A = 0$ $\mu = \phi = 0.5$. For large values of the geometric characteristic this deviation decreases, and at $A > 5$ it becomes negligible.

As was noted, the work of V. V. Talakvadze uses instead of the principle of maximum flow rate the equation of momentum, which is written in the form

$$\int_{r_{me}}^{r_e} p_1 2\pi r\,dr = \int_{r_{me}}^{r_e} p_{11} 2\pi r\,dr + G w_{e}. \tag{96}$$

55

where p_I, p_{II} — excess pressure in sections I and II (Fig. 34); r_{ms} and r_{ms} — radius of air vortex in sections I and II; G — mass flow per second of liquid through injector; w_a — axial component of velocity in section II.
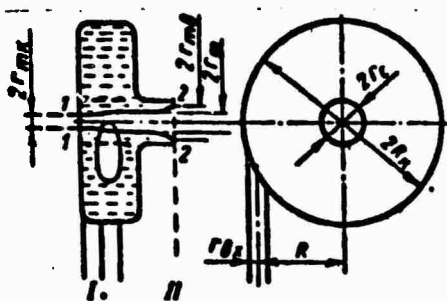
Fig. 34. Control surface for the integration of equation (96).

The control surface is the surface limited by planes I and II, the surface of the air vortex and the cylindrical surface with generatrix 1-2.

Thus, equation (96) does not consider momentum, introduced by the liquid through the cylindrical surface.

For small values of the geometric characteristic of the injector the component of momentum cannot be disregarded, since this leads to gross error in determination of liquid exit velocity.

Actually, we will apply the equation of momentum in the form of equation (96) to the case of a discharge of liquid without swirling through a nozzle from a vessel of great volume. Let us designate pressure in the vessel p_T, and outlet pressure from the nozzle p_a. Then from equation (96) we obtain

$$p_T \pi r_c^2 = p_a \pi r_c^2 + G w_a. \tag{97}$$

Substituting

$$G = \rho w_a \pi r_c^2.$$

where ρ — density of liquid, we find

$$w_a = \sqrt{\frac{p_T - p_a}{\rho}}. \tag{98}$$

56

In fact, as follows from the Bernoulli equation, exit velocity from the nozzle in this case is determined by the expression

$$w_s = \sqrt{\frac{2(p_T - p_s)}{\rho}}. \tag{99}$$

Consequently, application of the equation of momentum in the form employed in the work of V. V. Talakvadze gives at A = 0 a value of exit velocity $\sqrt{2}$ smaller, and as a result, an incorrect discharge coefficient. As the geometric characteristic increases, the error appearing when the equation of momentum is used in the form of equation (96), drops, since the value of the axial velocity component in the swirl chamber of the injector decreases.

Thus, in the region of small values of the geometric characteristic of an injector, application of the equation of momentum in the form used by V. V. Talakvadze [20] leads to essential error, which explains the deviation of values of nozzle discharge coefficient and space factor obtained in this work from real values, found by using the principle of maximum flow rate.

A. M. Prakhov [18] during integration of the equation of momentum used as the control surface the surface bounded by the walls of the swirl chamber and the nozzle, the plane passing through the nozzle section, and the surface of the air vortex.

Such selection of the control surface in considerable degree helped overcome difficulties appearing in the calculation of momentum of the liquid flowing through this surface.

However, there appear new difficulties connected with determining the pulse of pressure forces acting on the liquid in swirl chamber of the injector.

Trying to overcome these difficulties, A. M. Prakhov replaces true flow in the injector by a certain schematized flow, consisting of rotation of the liquid around the injector axis and drain into the nozzle. It is assumed that the drain of the liquid into the nozzle

occurs evenly through the surface of a spherical segment.

In order to estimate the error inserted with such a method of determining the rate of drain, we will proceed similarly to the preceding, i.e., we will examine the outflow from a jet injector in which liquid moves through the lateral wall with angular momentum relative to the nozzle axis equal to zero, and zero component of momentum along this axis (Fig. 35).
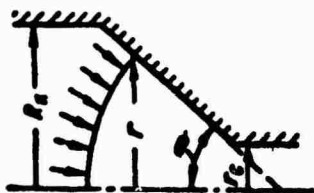
Fig. 35. Liquid flow in the nozzle of an injector; used in the derivation of formula (102).

The rate of drain is determined from the continuity equation:

$$w_{cm} = \frac{G}{\rho 2 \pi r^2}(1 + \cos\theta). \tag{100}$$

Pressure of liquid on the rear end wall is equal to p_T, and on the front $p_T - \frac{\rho w_{cm}^2}{2}$. Then the equation of momentum will be written in the form

$$\pi R_u^2 p_T - \pi(R_u^2 - r_c^2)p_T + \\ + \frac{G^2}{8\pi\rho}(1+\cos\theta)^2\left(\frac{1}{r_c^2} - \frac{1}{R_u^2}\right) - \pi r_c^2 p_a = \rho\pi r_c^2 w_a^2. \tag{101}$$

Substituting in equation (101) $G = \rho w_a \pi r_c^2$, we obtain after simple transformations the expression for exit velocity of liquid:[4]

$$w_a = \sqrt{\frac{p_T - p_a}{\rho\left[1 - \frac{(1+\cos\theta)^2}{8}\left(1 - \frac{r_c^2}{R_u^2}\right)\right]}}. \tag{102}$$

It is easy to see that when $\theta > 0$ and $\frac{r_c}{R_u} > 0$

$$\frac{1}{1 - \frac{(1+\cos\theta)^2}{8}\left(1 - \frac{r_c^2}{R_u^2}\right)} < 2$$

and, consequently, calculation by A. M. Prakhov's method gives a

58

decreased value of exit velocity. Besides, the greater θ is, the greater the error in determination of exit velocity.

Thus, A. M. Prakhov's [17] proposed method of calculation leads to essential errors in determination of the discharge coefficient for a jet injector (A = 0). As the geometric characteristic of the injector increases, naturally error drops since the value of the rate of drain of liquid into nozzle decreases. In connection with this in the region of large values of the geometric characteristic of an injector (A > 4) dependence μ = f(A) calculated by the method of A. M. Prakhov approaches the dependence obtained by G. N. Abramovich (see Fig. 33).

A feature of the work of V. B. Tikhonov [21] is that the equation of momentum is composed in differential form for flow of a liquid in an injector nozzle (Fig. 36). Section I is selected where the radius of the air vortex in the injector nozzle still has not begun to change, and section II — at distance dx downwards along the flow.
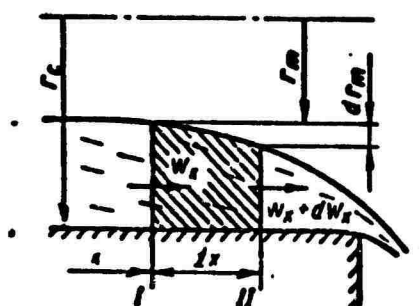
Fig. 36. Pattern of liquid flow in injector nozzle.

Then the equation of momentum will be written in the form

$$- dP_x = G dw_x. \qquad (103)$$

where P_x — pulses per minute of pressure forces in section x; w_x — axial component of velocity in this section.

The axial velocity component of liquid flow in an injector nozzle can be expressed through volumetric flow rate Q and space factor of the nozzle φ (see § 1, this chapter):

59

$$w_s = \frac{Q}{\pi r_e^2},$$

and, consequently,

$$dw_s = -\frac{Q}{\pi r_e^2} \cdot \frac{dr_e}{r_e^2}. \tag{104}$$

The guage pressure acting on the liquid in section x is determined by the formula

$$p = \frac{\rho}{2} V_{ax}^2 R^2 \left(\frac{1}{r_m^2} - \frac{1}{r^2} \right). \tag{105}$$

where $V_{ax} = \frac{Q}{\pi r_{ax}^2}$ — velocity in entrance (tangential) channels of injector.

Formula (105) is easy to obtain from equation (65), taking into account expression (61). Integrating formula (105), we find

$$P_x = \int_{r_m}^{r_e} p \, 2\pi r \, dr = \rho \pi V_{ax}^2 R^2 \left[\frac{1}{2} \left(\frac{r_e^2}{r_m^2} - 1 \right) + \ln \frac{r_m}{r_e} \right].$$

Hence

$$dP_x = \rho \pi V_{ax}^2 R^2 \left(-\frac{r_e^2 dr_m}{r_m^3} + d \ln \frac{r_m}{r_e} \right). \tag{106}$$

V. B. Tikhonov, assuming that in expression (106) $r_m \approx r_e$ (and, consequently, $\ln \frac{r_m}{r_e} = 0$), converts equation (103):

$$\pi V_{ax}^2 R^2 \frac{dr_m}{r_m} = Q \, dw_s \tag{107}$$

By replacing V_{ax}, w_s and r_m by volumetric flow rate Q and space factor ϕ, Tikhonov obtains the connection between geometric characteristic and space factor of nozzle

$$A = \frac{\sqrt{2(1-\varphi)}}{\varphi} \tag{108}$$

and further, substituting this expression in equation (70), he finds

$$\mu = \frac{\varphi}{\sqrt{3}}. \tag{109}$$

The dependences of μ and ϕ on A, calculated by the formulas (108)

and (109), are represented on Fig. 33. At $A = 0$ $\phi = 1$ and $\mu = \frac{1}{\sqrt{3}}$, i.e., liquid fills the entire nozzle cross section and at the same time the discharge coefficient, in spite of the absence of energy losses (ideal liquid), is less than one.

This result is undoubtedly erroneous and is connected with Tikhonov's assumption that $r_m \approx r_c$, which for small values of the geometric characteristic becomes absolutely unacceptable.[5] However, this assumption is not necessary.

Let us consider, the form to which the equation of momentum will be converted if we reject this unjustified assumption. Substituting in equation (106) $r_m = r_c \sqrt{1 - \phi}$ and differentiating, we obtain after simple transformations

$$dP_z = \rho \pi V_{ax}^2 R^2 \frac{\phi d\phi}{(1 - \phi)^2}. \tag{110}$$

Then equation (103) will take the form

$$- \pi V_{ax}^2 R^2 \frac{\phi d\phi}{(1 - \phi)^2} = Q dw_x. \tag{111}$$

Replacing dw_x and V_{ax} by their expressions, we obtain finally the unknown connection between the geometric characteristic of the injector A and the nozzle space factor ϕ.

Comparison of the obtained formula and formula (71) shows their full identity.

Thus, if the equation of momentum is used in the form proposed by V. B. Tikhonov, the connection between A and ϕ, obtained both with the use of this equation and on the basis of the principle of maximum flow rate, has an absolutely identical form and consequently the dependences of hydraulic parameters of an injector (μ, ϕ, and α) on its geometric characteristic coincide.

In conclusion we will examine the work of M. A. Gol'dshtik and others [8], in which the authors, instead of using the principle of maximum flow rate, introduce another extreme principle, namely, the

hypothesis of the minimum of the kinetic energy flow in the outlet section of the swirl chamber (for a completely opened injector) or of the injector nozzle.

The flow of kinetic energy has the following form:

$$T = 2\pi\rho \int_{r_m}^{r_s} r w \left(\frac{u^2}{2} + \frac{w^2}{2}\right) dr \tag{112}$$

or taking into account formulas (61) and (67):

$$T = \rho \frac{R^2}{a^3 f_c^2 r_c^2} Q^3 \left[\frac{1}{2A^2\varphi^2} - \frac{\ln(1-\varphi)}{2\varphi}\right]. \tag{113}$$

Further, from the condition $\frac{dT}{d\varphi} = 0$ the connection between the nozzle space factor and the geometric characteristic of the injector is determined in the form

$$A^2 = \frac{2(1-\varphi)}{\varphi^2 + \varphi(1-\varphi)\ln(1-\varphi)}. \tag{114}$$

With the help of formula (114) it is simple, using formula (70), to find the dependence of discharge coefficient on the geometric characteristic of the injector. Corresponding curves are represented on Fig. 33.

At $A = 0$ $\phi = 1$ and $\mu = \frac{1}{\sqrt{3}}$, which, as already has been noted, during the analysis of V. B. Tikhonov's work [21], is physically impossible.

In the theory which they developed, the authors of work [8] apparently allow two errors. The first error is that expression (113) for the flow of kinetic energy on leaving the injector neglects the transition of excess centrifugal pressure into impact pressure, and the second error is that in differentiating T with respect to ϕ the derivative was taken only of the expression in brackets, whereas flow rate Q also depends on ϕ.

In reality, on leaving the injector, if we disregard the radial component of velocity,

$$\frac{\rho}{2}(u^2 + w^2) = \text{const} = p_T.$$

62

where p_T — pressure of stagnated flow (guage feed pressure), consequently, the flow of kinetic energy is expressed in the form

$$T = Q p_T.$$

Thus, for a fixed value of p_T the extremum (not minimum but maximum) of the flow of kinetic energy depending upon ϕ coincides with the extremum of flow rate and the hypothesis of the authors of work [8] does not differ from the principle of maximum flow rate.

§ 4. Theory of a Swirler for a Real (Viscous) Liquid

As has already been indicated, the basic difference of swirlers from injectors of other types is that liquid flowing through the injector possesses angular momentum with respect to the nozzle axis. Just this influence of angular momentum of liquid particles conditions the appearance of a number of features in the operation of a swirler: formation of an air vortex, small discharge coefficient and large spray angle.

In the case of an ideal liquid the moment of external forces acting on the liquid in the swirl chamber is equal to zero and the flow obeys the law of conservation of momentum. Approaching the nozzle axis, the peripheral component of velocity increases in inverse proportion to the radius.

Due to viscosity of the liquid on the wall there appear frictional forces directed against the flow velocity. The moment of forces of friction causes angular momentum to decrease, which on the nozzle entrance turns out to be smaller than on the swirl chamber entrance. Moreover the radius of the air vortex decreases, the discharge coefficient increases and the spray angle decreases.

Thus, in a swirler friction on the swirl chamber wall leads to a somewhat unexpected result: the flow rate of real liquid through the injector exceeds the flow rate of an ideal liquid.

Let us examine the flow of real liquid in a swirl chamber of constant height.

63

We break down flow velocity V in the swirl chamber into tangential V_u and radial V_m components (Fig. 37). Let us separate a liquid element of height δ, equal to the height of the swirl chamber,
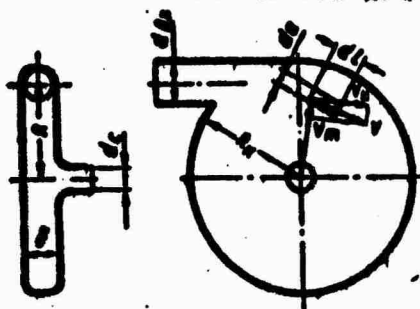
Fig. 37. Breakdown of the velocity of a flow of liquid in the swirl chamber into components.

length dl and width da. The mass of this element

$$dm = \rho\delta dl\,da$$

and the angular momentum

$$M' = rV_u\,dm.$$

On the lateral surface of the element touching the walls of the chamber $(df = 2dl\,da)$, acts frictional force

$$dF_{mp} = \tau_n df.$$

where τ_n — stress of friction on wall, expressed through coefficient of friction λ and velocity head

$$\tau_n = \frac{\lambda}{4} \cdot \frac{\rho V^2}{2}.$$

Moment of frictional force

$$N' = -\frac{\lambda}{4}\rho VV_u r\,dl\,da.$$

The change of angular momentum is equal to the moment of external force

$$\frac{dM'}{dt} = \frac{dM'}{dr} \cdot \frac{dr}{dt} = N'.$$

Substituting the expression for M' and N' and noticing that $\frac{dr}{dt} = -V_m,$ we obtain

$$d(rV_u) = -\frac{\lambda VV_u r\,dr}{4\delta V_m}.$$ (115)

64

Let us designate the angular momentum of a volume unit of liquid by M (liquid is considered incompressible):

$$M = \rho r V_e.$$ (116)

Expressing from the continuity equation V_m through volumetric flow rate Q

$$V_m = \frac{Q}{2\pi r \delta}$$ (117)

and substituting $V = \sqrt{V_e^2 + V_m^2}$, we obtain the differential equation determining change of angular mometum in the swirl chamber during a flow of viscous liquid:

$$\frac{dM}{M\sqrt{M^2 + \theta^2}} = \frac{\lambda \pi}{2\rho Q} dr,$$ (118)

where

$$\theta = \frac{\rho Q}{2\pi \delta}.$$

Integrating the left side of equation (118) within limits from M_0 to M and the right side within limits from R to r_c, we find

$$\ln \frac{M\left(\theta + \sqrt{M_0^2 + \theta^2}\right)}{M_0\left(\theta + \sqrt{M^2 + \theta^2}\right)} = -\frac{\lambda}{4\delta}(R - r_c).$$

Solving this equation with respect to M, we obtain

$$M = \frac{M_0}{\text{ch}\,\xi + \text{sh}\,\xi \sqrt{\frac{M_0^2}{\theta^2} + 1}}.$$ (119)

where

$$\xi = \frac{\lambda}{4\delta}(R - r_c).$$ (120)

From an analysis of this expression it follows that under the influence of friction angular momentum decreases as the nozzle is approached.

At $\lambda = 0$ (ideal liquid) we obtain the law of conservation of momentum ($M = M_0$).

We will consider that the height of the swirl chamber is equal to

65

the diameter of the inlet $(b = 2r_{ex})$, the number of entrance openings is n and the swirling arm is R.

Since the initial angular momentum (when liquid enters the swirl chamber)

$$M_\phi = \rho V_{ex} R = \frac{\rho Q R}{n \pi r_{ex}^2}.$$ (121)

then expression (119) takes the form

$$M = \frac{M_0}{ch\xi + sh\xi \sqrt{16 \frac{B^2}{n^2} + 1}}.$$ (122)

where

(123)

Formula (122) can be essentially simplified if we expand $sh\xi$ and $ch\xi$ in series and reject all terms except the first, i.e., assume that $sh\xi = \xi$, $ch\xi = 1$. Then

$$M = \frac{M_0}{1 + \xi \sqrt{16 \frac{B^2}{n^2} + 1}}.$$ (124)

The relative error allowed here does not exceed 3%, if $B \leq 16$ and $\lambda \leq 0.2$, i.e., the range embracing all practically encountered values of B and λ. Usually this error is a fraction of a percent.

When $\frac{B}{n} > 1$, it is possible to disregard one as compared to $16 \frac{B^2}{n^2}$, and then formula (124) appears as

$$M = \frac{M_0}{1 + \frac{\lambda}{2} \left(\frac{B^2}{n} - A \right)}.$$ (125)

The error inserted here does not exceed 1%.

Thus, relative error during calculation of angular momentum by formula (125) does not exceed 4% as compared to results of calculation by exact formula (122), if $\frac{B}{n} > 1$, $B \leq 16$ and $\lambda \leq 0.2$.

It is simple to show that when $\frac{B}{n} < 1$, then if formula (124) is

66

replaced by formula (125) error also is small and does not exceed 1-2% if $n \leq 6$ (a greater number of entrance channels is not used for practical purposes).

This analysis shows that in injector theory for real liquid formula (125) is sufficiently accurate. Angular momentum, according to this formula, decreases as the coefficient of friction λ and the complex $\frac{B^a}{a} - A$ increase.

We note that formula (125) can be obtained directly from equation (118), if we disregard in it θ^2 as compared to M^2 or, which is the same, V_m^2 as compared to V_u^2.

Friction of liquid on the swirl chamber wall causes, besides a decrease of angular momentum, also losses of energy.

On element of liquid dm (Fig. 37) acts force dF_{mp}. The work of this force on path ds will be

$$dA = dF_{mp}ds.$$

Then the loss of energy for a volume unit of liquid will be written in the form

$$dE = \frac{\lambda}{4b}\rho V^2 ds.$$

But ds is easily expressed through dr:

$$ds = -\frac{V}{V_m} dr.$$

Substituting V_m from equation (117), we will obtain the differential equation for determination of energy losses in the swirl chamber:

$$dE = -\frac{\lambda\pi}{2Q}\rho V^3 r dr. \tag{126}$$

To simplify formulas during integration of this equation, we will disregard V_m^2 as compared to V_u^2, i.e., let us assume $V \approx V_u$.

The current value of V_u from the expression similar to expression (125) is easy to represent in the form

67

$$V_a = \frac{RQ}{a w_{ax}^2 \left[1 + \frac{\lambda}{2}\left(\frac{R^2}{a} - \frac{R}{a r_{ax}^2}r\right)\right]}. \tag{127}$$

Substituting in equation (126), we obtain

$$dE = \frac{4\pi Q^2}{\lambda^2 a r^2} \cdot \frac{dr}{r^2 (r - x)^2}. \tag{128}$$

where

$$r = R + \frac{2}{\lambda} \cdot \frac{w_{ax}}{R}.$$

The full loss of energy in the swirl chamber is

$$\Delta E = \frac{4\pi Q^2}{\lambda^2 a r^4} \int_R^{r_a} \frac{dr}{r^2 (r - x)^2}. \tag{129}$$

Taking the integral, we find after simple transformations:

$$\Delta E = \frac{\rho Q^2}{2\pi^2 r_a^4} \Delta, \tag{130}$$

where

$$\Delta = \frac{\lambda}{a^2}\left\{\frac{1}{e}\left(1 - \frac{1}{C}\right) + \lambda\left[\left(\frac{A}{2} - \frac{1}{2a - \lambda}\right)\left(\frac{2}{e} + \frac{A}{2} + \frac{1}{2a - \lambda}\right) + \right. \right.$$
$$\left. \left. + \frac{3}{2a^2} \ln \frac{(2a - \lambda) A C}{2}\right]\right\};$$
$$a = \frac{1}{A} + \frac{\lambda}{2} C; \tag{131}$$
$$C = \frac{R}{r_a}.$$

The possibility of the above consideration of flow of a viscous liquid in a hydraulic formulation of the problem finds substantiation in the work of G. Taylor [32], which shows that the main part of the liquid is in the boundary layer. Let us note that Taylor also arrives at a conclusion about the increase of the discharge coefficient and the decrease of the spray angle for viscous liquid as compared to ideal.

Let us use obtained formulas for the calculation of discharge coefficient and spray angle during the flow of viscous liquid through an injector.

68

Due to friction on the swirl chamber wall, angular momentum and total pressure on the nozzle entrance of the injector is less than the initial.

But in the section of the nozzle (between r_c and r_m) the laws of conservation of momentum and energy hold.

As before designating, through u the peripheral velocity component in the entrance section of the nozzle, we have from expression (125) taking into account expression (121):

$$u = \frac{RQ}{m \pi r_{ex}^2 \left[1 + \frac{\lambda}{2}\left(\frac{B^2}{a} - A\right)\right]}.$$ (132)

On the air vortex boundary gauge pressure is equal to zero. Therefore the equation of energy is written in the form

$$p_T = \Delta E + \frac{\rho}{2}(u_m^2 + w^2).$$ (133)

Now, repeating the computations made in § 1 of this chapter in the derivation of the discharge coefficient formula we find that for a viscous liquid

$$\mu = \frac{1}{\sqrt{\frac{A_9^2}{1-\varphi} + \frac{1}{\varphi^2} + \Delta}}.$$ (134)

where

$$A_9 = \frac{A}{1 + \frac{\lambda}{2}\left(\frac{B^2}{a} - A\right)}.$$ (135)

In order to find the connection between ϕ and A_9, we use the principle of maximum flow rate, valid also for a viscous liquid.[6]

Then we obtain (Δ does not depend on ϕ):

$$A_9 = \frac{(1-\varphi)\sqrt{2}}{\varphi\sqrt{\varphi}}.$$ (136)

Thus, the functional connection between ϕ and A_9 remains the same as and between ϕ and A.

Consequently, the discharge coefficient formula taking into account friction differs from the corresponding formula for an ideal liquid by the replacement of A by A_B and the appearance of the term Δ.

As more detailed analysis shows, energy losses from friction on the swirl chamber wall are relatively small and in engineering calculations they may be disregarded, which leads to essential simplification of formulas for discharge coefficient and spray angle.

If we take approximately $\Delta = 0$, then formula (134) will take the form

$$\mu = \frac{1}{\sqrt{\frac{A^2}{1-\varphi} + \frac{1}{\varphi^2}}}.$$ (137)

Formula (137) differs from the corresponding formula for ideal liquid only by the replacement of A by A_B.[7] Hence it is clear that for determination of the discharge coefficient and in the case of real liquid, it is possible to use the curve given on Fig. 30, plotting along the x-axis instead of A the value of A_B.

The quantity A_B, replacing for viscous liquid the geometric characteristic, we shall call the equivalent characteristic of the injector.

In the case of entrance channels of noncircular cross section and not perpendicular to the nozzle axis it is easy to show that the formula for the equivalent characteristic of an injector acquires the form

$$A_b = \frac{A}{1 + \frac{\lambda}{2}\left(\frac{B^2}{a} \sin\beta - A\right)}.$$ (138)

where A is determined by formula (73); $B^2 = \frac{R r_{sx}}{f_{sx}}$ (f_{sx} is the area of the entrance channel); β — angle of inclination of entrance channel to axis of nozzle.

From analysis of expression (135) or (138) it follows that the

70

equivalent characteristic is less than the geometric.[*] But since as
A decreases the discharge coefficient increases, we arrive at an
important conclusion that during the transition for ideal liquid to
viscous liquid the discharge coefficient of the swirler increases,
and increases more strongly the greater the coefficient of friction
and the complex $\frac{\beta}{\alpha}-A$.

Comparing expressions (125) and (135), we see that

$$\frac{A_9}{A} = \frac{M}{M_9}.$$

The ratio of the equivalent characteristic to the geometric equals
the ratio of angular momentum of the liquid in front of the nozzle to
angular momentum on the entrance to the swirl chamber. The equivalent
characteristic reflects thus the decrease of angular momentum in the
swirl chamber.

If we disregard energy losses it is easy to show that the formula
for determination of the spray angle for a flow of viscous liquid has
the same form as for an ideal liquid, differing only by the fact that
in it the geometric characteristic of the injector is replaced by its
equivalent expression, i.e.,

$$\text{tg}\frac{\alpha}{2} = \frac{2\varphi A_9}{\sqrt{(1+\text{sy}-4\mu^2 A_9^2)}}. \tag{139}$$

Consequently, for a viscous liquid the root angle of the spray
also is determined by the curve shown on Fig. 63, with the only
difference that the values of the equivalent characteristic must be
plotted along the x-axis.

Since the equivalent characteristic is less than the geometric,
the spray angle for a viscous liquid is less than for an ideal liquid.

Thus, the hydraulic parameters of a swirler during a flow of
viscous liquid are determined by the equivalent characteristic.

Let us investigate how the equivalent characteristic of an
injector changes as the swirl arm and the diameter of entrance channels

are changed. The nozzle radius is considered constant (usually during calculations of an injector flow rate, feed pressure and spray angle are given; with these data the nozzle radius is determined simply).

Let us write the expression of the equivalent characteristic in the form

$$A_e = \frac{Rr_i}{nr_{ex}^2 + \frac{\lambda}{2}R(R-r_e)}. \tag{140}$$

We will examine two special cases: first — R increases without limit for constant r_c, r_{ex}, n, and λ and second — r_{ex} tends to zero at constant r_c, R, n, and λ.

In both cases the geometric characteristic of the injector increases ad infinitum, which for an ideal liquid leads to a decrease of the discharge coefficient to zero and increase of the spray angle to 180°. For a real liquid the position is significantly changed. During a monotonic increase of the swirl chamber the equivalent characteristic, as can be seen from consideration of formula (140), at first increases, and then, passing through maximum, decreases and when R → ∞ tends to zero. A_e has maximum at the following value of R:

$$R^* = r_{ex}\sqrt{\frac{2n}{\lambda}}.$$

Placing R^* in expression (140), we find the maximum equivalent characteristic:

$$A_m = \frac{r_i\sqrt{\frac{2}{\lambda n}}}{2r_{ex} - r_e\sqrt{\frac{\lambda}{2n}}} = \frac{D\sqrt{\frac{2}{\lambda n}}}{2 - D\sqrt{\frac{\lambda}{2n}}}, \tag{141}$$

where

$$D = \frac{r_c}{r_{ex}}.$$

In the second case when the diameter of entrance channels is decreased, the equivalent characteristic monotonically increases, but

remains bounded, and when $r_{as} \to 0$ approaches the value

$$A_{ae} = \frac{2r_c}{\lambda(R-r_c)} = \frac{2}{\lambda(C-1)}. \qquad \cdot(142)$$

where

$$C = \frac{R}{r_c}.$$

Consequently, for a real liquid when the geometric characteristic increases infinitely, the equivalent characteristic remains finite. The maximum value of the equivalent characteristic depends on how the geometric characteristic increases: due to growth of the swirl arm or due to a decrease of the diameter of entrance channels.

A unique "viscous barrier" is obtained: for a real liquid as the geometric characteristic increases the discharge coefficient cannot become smaller, nor the spray angle greater than certain values of μ^* and α^*, corresponding to the maximum equivalent characteristic of the injector.

When for a viscous liquid it is necessary to obtain small values of the discharge coefficient (large values of spray angle), one should select the geometric dimensions of the injector atomizer such that the influence of friction is minimum.

From an analysis of expression (140), it is clear that when the swirl arm equals the nozzle radius ($R = r_c$), the equivalent characteristic is equal to the geometric at any λ ("path of friction" is reduced to zero). Moreover,

$$A_s = \frac{r_c^2}{n r_{as}^2}.$$

By decreasing the radius of the entrance channels, arbitrarily large values of A_9 can be obtained, and thus the "viscous barrier" can be overcome.

If for an ideal liquid the hydraulic parameters of the injector are determined by the geometric characteristic, then for a real liquid they depend on two dimensionless geometric criteria $A = \frac{R r_c}{n r_{as}^2}$ and $B = \frac{R}{r_{as}}$

73

and on the coefficient of friction, i.e., on viscosity of the liquid and conditions of flow.

On Fig. 38 are given the dependences of the ratio of experimental values of discharge coefficient μ_{wx} to those calculated according to the theory of an injector for an ideal liquid μ_{wo} from pressure (during tests for kerosene) for injectors with approximately identical values of geometric characteristic A and various values of characteristic B. The diagram of the experimental injectors is depicted on Fig. 39. Injectors have one tangential channel of round cross section; height of the swirl chamber is equal to the diameter of the entrance channel.
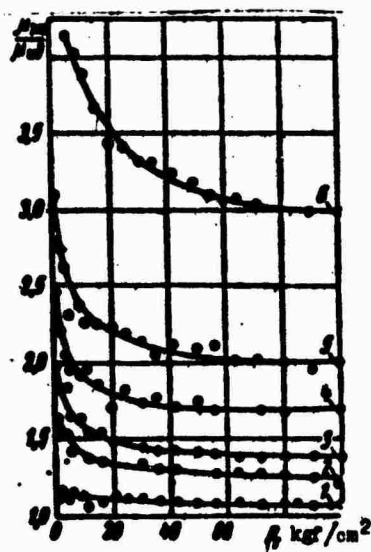
Fig. 38. Dependence of relative discharge coefficient on feed pressure for injectors with different values of B: 1 — A = = 5.11, B = 3.29; 2 — A = = 4.39, B = 4.39; 3 — A = = 4.62, B = 5.28; 4 — A = = 4.58, B = 6.88; 5 — A = = 4.46, B = 9.16; 6 — A = = 4.36, B = 14.75.
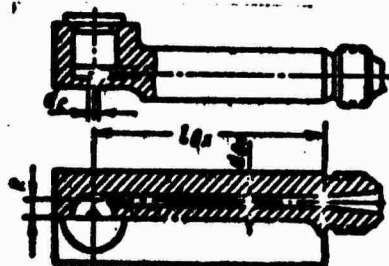
Fig. 39. Diagram of experimental injectors.

As we see, with an increase of characteristic B (and consequently, of the complex $\frac{f_{BX}}{R} - A$) the ratio $\frac{\mu_{wx}}{\mu_{wo}}$ increases and for large values of B considerably exceeds one (for an ideal liquid this ratio should

74

equal one independently of B). Furthermore, it is shown that the discharge coefficient decreases as pressure grows, which testifies to the dependence of the coefficient of friction on the flow rate of fuel through the injector.

Since the coefficient of friction depends on viscosity, then the hydraulic parameters of the injector also depend on fuel viscosity: the more the viscosity, the greater the discharge coefficient and the less the spray angle. Curves on Fig. 40, showing the dependence of $\frac{\mu}{\mu_{\text{м.н}}}$ on pressure for one of the experimental injectors during tests for gasoline, kerosene and turbine oil (corresponding values of coefficient of kinematic viscosity are $0.83 \cdot 10^{-6}$, $2.2 \cdot 10^{-6}$ and $24.9 \cdot 10^{-6}$ m^2/s), confirm this conclusion.
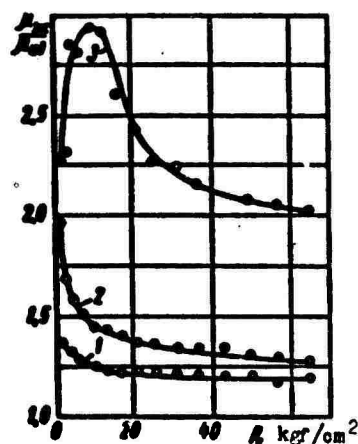
Fig. 40. Dependence of relative discharge coefficient on pressure for various liquids (A = = 2.42, B = 5.04): 1 — gasoline; 2 — kerosene; 3 — turbine oil.

For turbine oil even at small values of characteristic B the discharge coefficient essentially exceeds $\mu_{\text{м.н}}$.

A certain distinction in the character of the curve for turbine oil is explained, as experiments show, by a sharp decrease of the hydraulic discharge coefficient of the nozzle, i.e., the discharge coefficient of the nozzle when the flow through it undergoes no twisting (at small values of Re number).

As was shown, for real liquid hydraulic parameters of the injector depend on the equivalent characteristic, calculation of which requires, besides geometric data for the atomizer, knowledge of the coefficient

of friction. By determining by experimental values the discharge coefficient corresponding to the equivalent characteristic, the law of friction in a swirler can be found.

The dependence of the coefficient of friction on Re number, depicted on Fig. 41 in logarithmic coordinates, is obtained as a result of tests for gasoline, kerosene and turbine oil of experimental injectors whose height of the swirl chamber equals the diameter of the entrance channel (Fig. 39). Geometric characteristic A changed within limits from 1.13 to 7.74, and characteristic B went from 3.11 to 15.0.
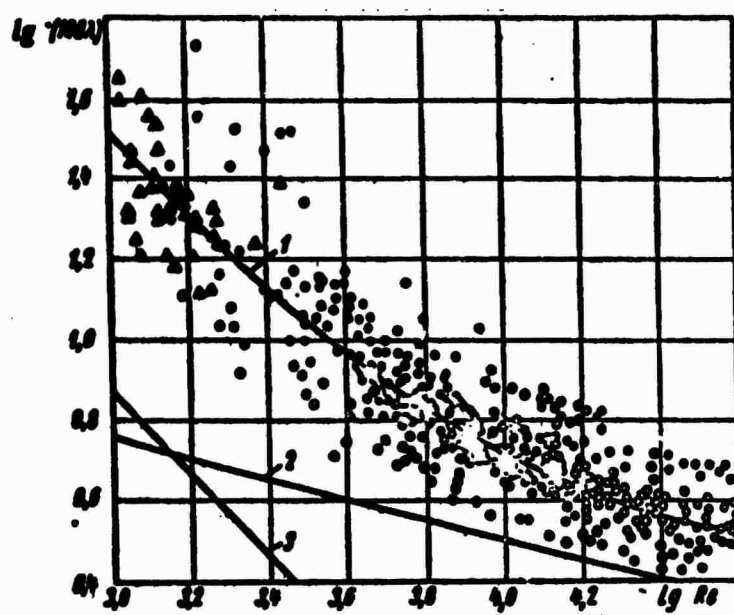
Fig. 41. Dependence of coefficient of friction on Reynolds number: 1 — average curve; 2 — according to the Blasius law; 3 — according to Poiseille law; O — gasoline; ● — kerosene; Δ — turbine oil.

In spite of the great spread of points, it is distinctly clear that as the Re number grows, the coefficient of friction decreases. Experimental points for gasoline, kerosene and turbine oil are well packed in one band. This confirms that for the flow in a swirler the Re number is a characteristic criterion.

The scattering of points is caused by the difference in the

76

hydraulic discharge coefficient for separate injectors (in connection with inaccuracy of manufacture of inlet edges of nozzle).

Re number for a swirler is determined by conditions on the swirl chamber entrance:

$$Re = \frac{V_{ex} d}{\nu}.$$

Moreover, as the characteristic dimension the diameter of the hole, whose area is equal to the total area of entrance channels is selected, i.e.,

$$d = \sqrt{n} d_{ex}.$$

where d_{ex} — diameter of entrance channel.

Expressing V_{ex} according to the continuity equation through mass flow rate G, we obtain the calculation formula for determination of the Re number:

$$Re = \frac{4G}{\pi \rho \nu \sqrt{n} d_{ex}}. \tag{143}$$

With such a selection of the characteristic dimension, the change of the number of entrance channels (with constant total area) does not influence the value of the Re number.

The curve represented accurately by the equation (in the interval $10^3 \leqslant Re \leqslant 10^5$)

$$\lg \lambda = \frac{25.8}{(\lg Re)^{2.58}} - 2. \tag{144}$$

is averaged over experimental points.

On Fig. 41 the straight lines expressing the law of friction for flow in smooth pipes during laminar and turbulent conditions are plotted for comparison. As we see, the coefficient of friction in swirlers considerably exceeds that in smooth pipes.

The last circumstance is connected with the fact that in a swirler the boundary layer will be formed under conditions of a large

77

transverse pressure gradient, causing the appearance of transverse (radial) currents in the boundary layer directed from a region with small values of peripheral velocity (on periphery of swirl chamber) to a region with great peripheral velocity (near nozzle).[9]

After the dependence of the coefficient of friction on Re number is established, calculation of the hydraulic parameters of a swirler for real liquid does not present difficulties and reduces to determination of the equivalent characteristic and — in more precise calculations — losses of energy,

For a real liquid, as was already noted, the monotonic increase of the geometric characteristic of an injector does not always correspond to the monotonic decrease of the discharge coefficient and growth of the spray angle, as is encountered in the case of an ideal liquid. Under certain conditions in the case of a real liquid the phenomenon of the "viscous barrier" shows up.

On Fig. 42 are given experimental values of the discharge coefficient and spray angle for injectors with different geometric characteristic. All injectors have an identical nozzle of diameter d_c = 1.21 mm with conical entrance and two tangential square channels 1.01 × 1.01 mm.

The geometric characteristic is changed by increasing the swirl arm within limits from R = 0 (when fuel is fed without swirling) to R = 15 mm. Accordingly the geometric characteristic changes within limits from A = 0 to A = 14.0.

Experimental points are obtained for Reynolds number $Re = 6 \cdot 10^3$ (on kerosene).

As we see, when the geometric characteristic grows, the discharge coefficient at first decreases and then increases, as follows from the theory of an injector for viscous liquid. The spray angle, conversely, at first increases and then, passing through maximum, decreases. Curves for an ideal liquid are drawn as thin lines.[10]

78
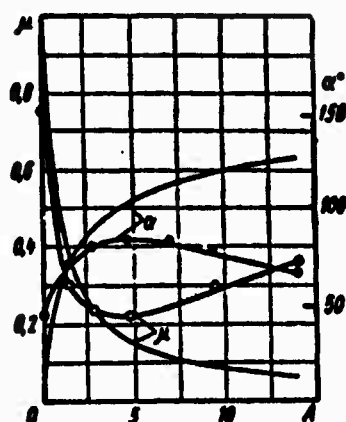
Fig. 42. Dependence of discharge coefficient and spray angle on A for injectors with various magnitude of swirl arm R.

Thus, obtaining for a real liquid small values of the discharge coefficient (large values of spray angle) presents specific difficulties, which are overcome by neglecting the dimensions of the injector atomizer such that the influence of friction on the swirl chamber wall is minimized.

Let us note that at A = 0 (flow without swirling) the experimental value of the discharge coefficient is less than one, and the spray angle is more than zero, whereas according to the theory of an injector at A = 0 μ = 1 and α = 0. The fact is that theory does not consider either the difference of the hydraulic discharge coefficient of the nozzle from one, or the expansion of the spray, which was observed in the case of jet injectors.

Examples of the starting and main jets of a gas turbine engine, whose hydraulic parameters are essentially influenced by fuel viscosity, are given in Table 2. We see that if the value of the experimentally measured discharge coefficient $\mu_{\text{экс}}$ considerably exceeds the computed value for an ideal liquid $\mu_{\text{ид}}$, then the computed value for a real liquid μ_p is close to $\mu_{\text{экс}}$.

To check the above theory of a swirler for a real liquid the experimental data given in works of Doble [25, 26] were used. Injectors with a varying number of inlets (from one to four) of round or rectangular shape were tested. Below data on injectors with round inlets are used, for the characteristic $C = \dfrac{R}{r_c} \geqslant 2.5$ and length of entrance channels exceed one calibration. The working fluid was water.

79

Table 2.

Injectors	d_c in mm	d_{s1} in mm	R in mm	n	α	A	B in deg-1	G_{20} in g/s	$\frac{\lambda_{3KC}}{\lambda_{3T}}$	$\frac{\alpha_{3KC}}{\alpha_{3T}}$
Starting injector FR-45	0,85	0,4	1,4	2	90°	7,43	17,07	2,95	1,59	0,99
First stage of two-stage injector FG-3	2,02	0,65	3,68	1	90°	35,2	92,4	12,1	2,66	0,97
First step of two-nozzle injector FR-3	1,20	0,515	2,36	2	61°30'	9,5	28,1	8,5	1,62	1,02

Note. G_{20} is the mass flow rate at $p_T = 20$ kgf/cm^2 (for kerosene).

Tests were conducted with a pressure in front of the injector from 2.1 to 4.9 kgf/cm^2. Parameters of injectors were changed within limits of $0.28 \leqslant A \leqslant 32.1$; $3.0 \leqslant B \leqslant 12.0$ (results of tests on 75 injectors were treated).

Results of the treatment are represented on Fig. 43. We see that for large values of the complex $\frac{B}{a} - A$ calculation according to the theory for ideal liquid gives sharply decreased values of the
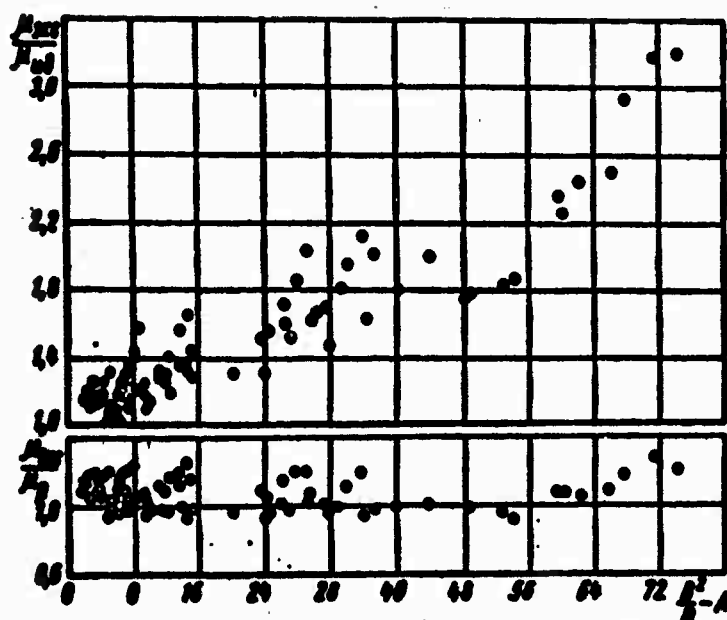
Fig. 43. Dependence of $\frac{\lambda_{3KC}}{\lambda_{3T}}$ and $\frac{\alpha_{3KC}}{\alpha_{3T}}$ on the complex $\frac{B}{a} - A$ [25].

80

discharge coefficient, whereas μ_p is close to μ_{nn} throughout the range of change of the complex $\frac{B^2}{R} - A$.

Experimental confirmation of the theory for real liquid is contained also in the work of L. V. Kulagin [15], which gives results of measurement of the spray angle during tests of a number of swirlers on diesel fuel $(0.8 \leqslant A \leqslant 7.0; \ 5 \leqslant p_T \leqslant 55$ kgf/cm$^2)$. On the basis of numerous experiments L. V. Kulagin [15] concludes that the root angle of the spray is simply determined by the value of the equivalent characteristic of the injector irrespective of the dependence on change of the quantities in it.

Calculation of the influence of friction is essentially valuable for injectors having a large complex $\frac{B^2}{R} - A$ (large swirl arm, small diameter of entrance channels) when the Re number is small (low flow rates, viscous liquid).

Such conditions are realized in the operation of starting jets and the first stages of adjustable injectors in a gas turbine engine.

At the same time in certain cases the influence of liquid viscosity on hydraulic parameters of a swirler is insignificant.

Let us determine analytically the conditions with which we can calculate the discharge coefficient and the spray angle, disregarding the influence of friction, according to the theory of an injector for an ideal liquid.

For an ideal liquid hydraulic parameters of the injector are determined by the geometric characteristic, and for a viscous liquid — by the equivalent characteristic where the form of the functional dependence in both cases is identical.

Dependence of the discharge coefficient on A (correspondingly on A_3) can be approximated by the expression

$$\mu = kA^{-n} \tag{145}$$

81

(in the interval $0.75 \leqslant A \leqslant 7.5$; $k = 0.44$ and $m = 0.65$; at $A > 7.5$ up to $A = 40$ $k = 0.67$ and $m = 0.905$).

Then the ratio of the discharge coefficient, calculated taking into account friction μ_p, to the discharge coefficient for an ideal liquid μ_{ui} is written in the form

$$\frac{\mu_p}{\mu_{ui}} = \frac{A_c}{A^m} = \left[1 + \frac{\lambda}{2} \left(\frac{R^2}{a} - A \right) \right]^m . \tag{146}$$

Hence it is distinctly clear that the smaller the complex $\frac{R^2}{a} - A$ and the smaller λ (i.e., the greater the Re number) then the nearer μ_p is to μ_{ui} and, consequently, the greater the accuracy with which it is possible to calculate according to the theory of an injector for an ideal liquid.

From formula (146) we have

$$\frac{R^2}{a} - A = \frac{2}{\lambda} \left[\left(\frac{\mu_p}{\mu_{ui}} \right)^{\frac{1}{m}} - 1 \right] . \tag{147}$$

Assigning accuracy of calculation of the discharge coefficient, we obtain from expression (147) the conditions under which calculation of the hydraulic parameters of an injector is possible according to the theory of an injector for ideal liquid.

In the interval $0.75 \leqslant A \leqslant 7.5$ $m = 0.67$ and formula (147) will take the form

$$\frac{R^2}{a} - A = \frac{2}{\lambda} \left[\left(\frac{\mu_p}{\mu_{ui}} \right)^{1.5} - 1 \right] . \tag{148}$$

Let us assume that, for example, the required accuracy of calculation is 10%, i.e., $\frac{\mu_p}{\mu_{ui}} = 1.1$, and let us assume that $\lambda = 0.05$ (Re = 10,000). Then from formula (148) we find that $\frac{R^2}{a} - A \leqslant 6.2$ the injector can be calculated with the indicated degree of accuracy, disregarding friction of liquid on the wall of the swirl chamber.

If μ exceeds μ_{ui} by not more than 10-15%, there is no necessity to consider a correction for the effect of friction, since there always causes leading to a decrease of the discharge coefficient.

In contrast to the above theory of a swirler for a real liquid, a number of researchers [3, 4, 27] have considered empirically the effect of friction on the swirl chamber wall.

Doumas and Laster [27], studying the flow of water in swirlers, introduce instead of the geometric characteristic the quantity

$$A' = A\left(\frac{r_c}{R}\right)^{0.6},$$

on which hydraulic parameters depend just as on A in the theory of G. N. Abramovich [2].

More justifiably they approach the generalization of experimental data of A. G. Blokh and Ye. S. Kichkin [3, 4], who investigated the atomization of liquids with different physical properties (water, aqueous solutions of glycerine, gas, oil, and kerosene) by swirlers with two tangential channels. Parameters were changed in the following limits: coefficient of dynamic viscosity $\eta = 1 \cdot 10^{-4} - 2.9 \cdot 10^{-4}$ kgf·s/m^2, density $\rho = 820 - 1190$ kg/m^3, gauge pressure $p_T = 5-30$ at, A = 1.72-9.51, ratio of diameter of swirl chamber to diameter of nozzle $\frac{D_k}{d_c} = 3.22 - 10$, Reynolds number Re = $1 \cdot 10^3 - 2.5 \cdot 10^4$.

Reynolds number was determined by conditions of flow in nozzle of injector Re = $\frac{v_c d_c}{v}$ (where $v_c = \frac{Q}{\pi r_c^2}$).

A. G. Blokh and Ye. S. Kichkin generalized results of their experiments for Re number $\ll 1.6 \cdot 10^4$ by the formula

$$\mu = 12.9 \mu_{id}\left(\frac{D_k}{d_c}\right)^{0.6} Re^{-\frac{1}{3}}. \tag{149}$$

In the region $1.6 \cdot 10^4 \ll Re \ll 2.5 \cdot 10^4$ the discharge coefficient is expressed by the formula

$$\mu = \mu_{id}\left(\frac{D_k}{d_c}\right)^{0.2} \tag{150}$$

and does not depend on the Reynolds number.

In spite of the fact that formulas (149) and (150) in a number

of cases will agree well with experimental data, they contain the inherent deficiencies of any purely empirical formulas. Thus, for example, it follows from them that as the diameter of the swirl chamber increases, the discharge coefficient continuously decreases, whereas in reality μ, attaining minimum value, increases as D_{K} grows ("viscous barrier").

§ 5. Influence of Structural Factors on the Hydraulics of a Centrifugal Injector

The preceding section examined an injector whose height of the swirl chamber was equal to the diameter of the entrance hole. Theoretical propositions referred to these injectors are accurate also when the height of the swirl chamber insignificantly exceeds the diameter of the entrance channel.[11]

Thus, for example, in experiments of Doumas and Laster [27] when $\frac{L_{K}}{D_{c}}$ changed from 0.66 to 1.67 (L_{K} — length, D_{K} — diameter of swirl chamber) the flow rate of liquid through the injector remained practically constant.

If the height of the swirl chamber considerably exceeds the diameter of the entrance channel, this theory can no longer be used, since there appear new circumstances which considerably complicate the phenomenon. In the swirl chamber liquid-filled cavities will be formed which, as a result of interaction with the main flow go into rotary-circulatory motion. Angular momentum of the main active flow decreases more strongly the greater the height of the swirl chamber. Therefore as the height of the chamber increases, the discharge coefficient increases, and the spray angle decreases.

Thus, when the height of the swirl chamber is great, the hydraulic parameters of the injector for real liquid (even for a small value of the complex $\frac{\mu}{a} - A$) essentially differ from the hydraulic parameters for ideal liquid.

Attempts known in literature to theoretically analyze the effect of chamber length of an injector on its hydraulic parameters have not

been convincing, so that this question still awaits exhausting investigation.

In the cylindrical part of the injector nozzle friction of liquid moving along helical trajectories on the nozzle wall leads to a further drop of angular momentum and, as a result, to a decrease of the spray angle as the nozzle length becomes greater.

As was already noted, the discharge coefficient is determined by conditions in the entrance section of the cylindrical part of the nozzle and therefore does not depend on its length.

On Fig. 44 are represented the dependences of the root angle of the spray and the discharge coefficient on nozzle length expressed in gauges, for experimental injectors with constant value of characteristics $A \approx 4.45$, $B \approx 4.44$ during tests for kerosene. As the
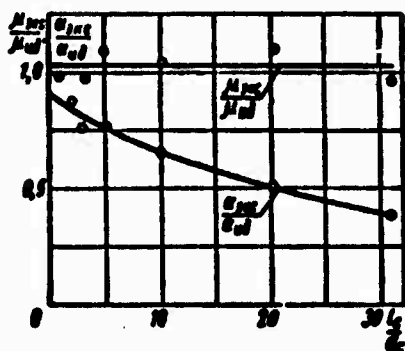
Fig. 44. Dependence of $\frac{\theta_{root}}{\theta_{id}}$ and $\frac{\mu_{c}}{\mu_{id}}$ on relative length of nozzle.

nozzle length increases the root angle of the spray decreases, whereas the discharge coefficient is practically independent of the nozzle length.

Friction of liquid on the nozzle wall for a given length has an effect which is stronger the larger the ratio of the circumferential velocity component to the axial (on entrance into nozzle), i.e., the greater the equivalent characteristic of the injector and the greater the coefficient of friction (small Re numbers). In the case of injectors with large values of the equivalent characteristic when Re numbers are small, even a small lengthening of the cylindrical part

of the nozzle leads to a noticeable decrease of the root angle of the
spray. In injectors having a long cylindrical part of the nozzle the
one-to-one correspondence between discharge coefficient and spray
angle is disturbed.

The hydraulic discharge coefficient of the nozzle,[12] as is known,
strongly depends on the shape of the nozzle entrance. It is always
smaller than one basically due to the narrowing of the stream in the
nozzle (cross section of stream is less than the cross section of the
nozzle).

When a swirling flow travels through a nozzle, under the action
of centrifugal forces liquid is thrown against the walls, so that the
effect of stream narrowing is weakened. However, even in this case in
the flow around sharp edges the separation of flow from wall is
inevitable (otherwise there would have had to be infinitely large
acceleration, which physically is impossible).

On Fig. 45 are represented sketches of nozzles with various
angles of entrance cone. Tests of nozzles conducted by S. A. Kosberg
showed that the smaller the cone angle on the entrance into the nozzle,
the bigger the discharge coefficient.[13] The curve shown in Fig. 45

Fig. 45. Dependence of relative
discharge coefficient on angle of
cone on entrance into nozzle.

Param-	No. nozzle (Fig. 45)					
eters	1	2	3	4	5	6
6°	· 120	90	60	45	30	15
Δ in mm	2.05	2.7	3.6	4.0	7.0	10.0

86

depicts the change of the ratio $\frac{f_{as}}{f_{ad}}$ depending upon the cone angle.
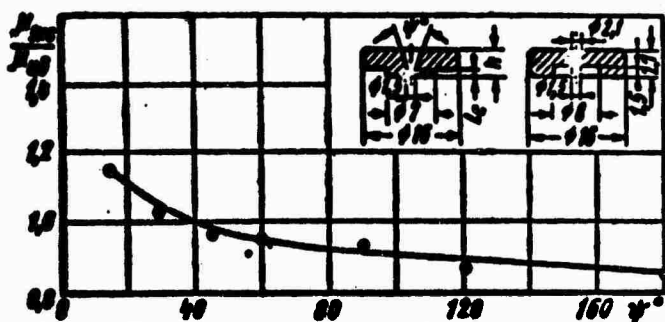Such character of the curve is explained on the one hand by a weakening
of the effect of stream narrowing in the nozzle as the cone angle
decreases on the nozzle entrance, and on the other hand by the increase
of the moistened nozzle surface which causes an additional decrease of
the angular momentum of liquid particles in the entrance section of
the cylindrical part. A decrease of the angular momentum, as was
shown above, is connected with growth of the discharge coefficient.

It is necessary, of course, to consider that at $\psi = 0$ the discharge
coefficient has the same value as at $\psi = 180^{\circ}$, i.e., in the interval
$0 \leqslant \psi \leqslant 15^{\circ}$ the curve passes through maximum.

Let us consider more specifically the conditions of flow on the
swirl chamber entrance of the injector.

Above it was assumed that liquid flow in the entrance channels
takes a direction coinciding with the axis of the channel. However,
for the flow to take the direction of the channel, a certain channel
length is required. If the channel length is insufficient, the flow
cannot assume the assigned direction and is deflected to the axis of
the swirl chamber, as is schematically shown on Fig. 46. The initial
angular momentum of the liquid on chamber entrance turns out to be
less than expected, which involves an increase of the discharge
coefficient and a decrease of the root angle of the spray. Naturally,
the value is not the absolute length of the entrance channel, but the
ratio of the length of the channel to its diameter or, in the case of
rectangular channels, to its width.

On Fig. 47 is shown the change of relative discharge coefficient
and root angle of spray depending upon length of entrance (tangential)
channels. If the channel length exceeds two calibrations, the
hydraulic parameters of the injector remain constant. If, however,
the channel length is less than two calibrations, then a growth of
the discharge coefficient and a decrease of the root angle of the
spray are observed.
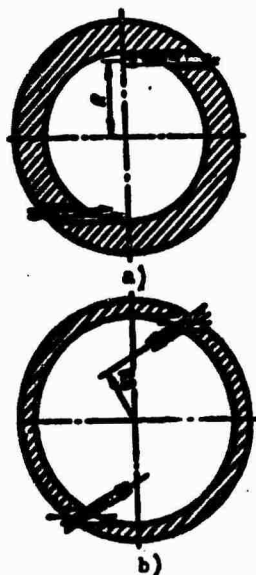
Fig. 46. Diagram of liquid flow in entrance channels: a) flow assumes direction of channel; b) flow is deflected to swirl chamber axis.
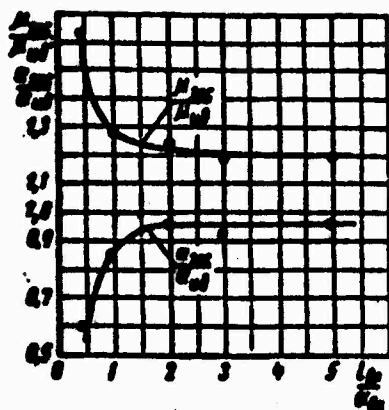
Fig. 47. Dependence of $\frac{v_{ox}}{v_{o}}$ and $\frac{\varphi_{ox}}{\varphi_{o}}$ on relative length of entrance channels.

Consequently, for the flow to take a tangential direction, the length of entrance channels should be not less than one and a half to two gauges. In the opposite case flow will be deflected to the swirl chamber axis and angular momentum imparted to the liquid will be less than that required — the injector will lose its centrifugal properties.

If the entrance channel has a smooth entrance, so that the flow wholly fills the cross section of the channel, the mean flow velocity is determined from the equation

$$V_{ox} = \frac{Q}{n f_{ox}}.$$ (151)

If during the flow around the inlet edges of the channel the flow narrows, then at the same volumetric flow rate the mean flow velocity

88

in the entrance channel increases:

$$V_{ax} = \frac{Q}{\varepsilon n f_{ax}}.$$ (152)

where ε — coefficient of contraction of flow in entrance channel.

Consequently, in this case the real angular momentum on the entrance of the swirl chamber will exceed that calculated with respect to the full area of the entrance channels. An increase of angular momentum should lead to a decrease of the discharge coefficient and growth of the root angle of the spray.

The coefficient of contraction of the flow in the hole depends basically on the shape of inlet edges and changes within limits from 0.6 to 0.95.

However, the values of coefficient of contraction, obtained for discharge from holes, cannot be directly used during calculation of flow in the entrance channels.[14] Apparently, upon passage into the swirl chamber the flow somewhat expands, so that its cross section becomes equal to 0.85-0.9 of the cross section of the entrance channel independently of the shape of the channel — round or rectangular.

In calculating the hydraulic parameters of a swirler the effect of narrowing of the flow in the entrance channels can be considered by introducing the expression of the active characteristic of the injector $A_\bullet$. In the case of ideal liquid the active characteristic is constructed just as the geometric, by replacing the area of the channel entrances by the area of the flow cross section in these channels, i.e.,

$$A_0 = \frac{R r_c \pi}{\varepsilon f_{ax}} = \frac{A}{\varepsilon}.$$ (153)

Dependence of discharge coefficient and root angle of spray on $A_\bullet$ remains the same as on A.

As is easy to show, in the case of real liquid the equivalent active characteristic of the injector is determined by the formula

89

$$A_{\omega} = \frac{A_y}{1 + \frac{\lambda}{2}\left(\frac{B^2}{\omega^2} - A_y\right)}. \qquad (154)$$

It is possible to take the value of the coefficient of contraction ε = 0.85-0.90 (at a sharp change of cross section of entrance to the tangential channel). During continuous flow in the entrance channels ε = 1.

Let us examine one more phenomenon which appears when a flow proceeds from entrance channels into the swirl chamber. For simplicity we consider that in the entrance channel there is no narrowing of the flow and the flow assumes the direction of the channel.

In the swirl chamber near the edge of the entrance channel two flows are encountered: one moves from the entrance channel, and the other flows along the swirl chamber wall (Fig. 48a). At point of
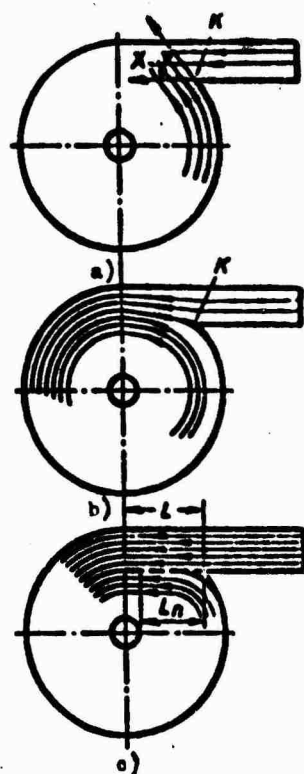
Fig. 48. Diagram of interaction of flows in entrance channels and swirl chamber.

merging к the directions of flow form angle χ, which is determined from the equation

$$\cos \chi = \frac{R - r_{ex}}{R + r_{ex}} = \frac{B - 1}{B + 1}. \tag{155}$$

However, in reality flow velocity cannot have in the same point different directions. Both flows, interacting with each other, are deflected so that the flow velocity will be changed continuously both in direction, and in terms of magnitude.

The cross section of the flow proceeding from the entrance channel will decrease, and the swirl arm will increase in its average size. The flow entering in the swirl chamber experiences a certain compression (Fig. 48b) which is greater the larger angle χ (the smaller the characteristic $B = \frac{R}{r_{ex}}$). Such deformation of flow on the swirl chamber entrance leads to a decrease of the discharge coefficient and an increase of the root angle of the spray as compared to computed values, calculated assuming no flow compression.

Compression of the flow in the swirl chamber was revealed during visual observations of a flow of water in an enlarged swirler model with transparent walls, having nozzle diameter 6 mm, swirl arm 15 mm, one rectangular entrance channel with sides of 10.4 and 9.5 mm, and height of swirl chamber equal to the height of the entrance channel.

To give the flow visibility chlorobenzene was added to the water, a drop of which formed in the water a sufficiently stable emulsion. Simultaneously on the same injector model the flow rate of water at a feed pressure p = 0.9 at was measured. Conditions of flow discharge from the entrance channel were changed by placing in the swirl chamber a thin diaphragm of variable thickness (from foil 0.2 mm thick) serving as a continuation of the entrance channel wall and partitioning partially the swirl chamber (Fig. 48b). The partition prevented flow compression and lead to an increase of the flow rate through the injector. Below are described the experimental data characterizing the interaction of flows in the entrance channels and swirl chamber:

Length of partition $\frac{L_n}{L}$ 0 0.25 0.5 1.0

Relative flow rate $\frac{G_{out}}{G_{uf}}$

$(G_{uf} = 130 \text{ g/s})$ ...... 0.8 1.09 1.22 1.31.

In the absence of a partition the flow rate was less than that calculated for an ideal liquid due to flow compression on the swirl chamber entrance. An increase of the partition length (L_n) leads to an increase of the flow rate, since the effect of flow compression is reduced (angle of incidence of the two flows χ tends to zero).

Apparently, an increase of the flow rate at values $L_n > 0.25 L$ as compared to theoretical is explained by the decrease of angular momentum of the flow in connection with the formation of a stagnant region (under the partition).

Flow compression thus leads to a decrease of the discharge coefficient (increase of spray angle) and appears at small values of the characteristic $B = \dfrac{R}{r_{ex}}$.

At present there still is no method of calculating flow compression in the swirl chamber.

Besides energy losses connected with friction on the chamber wall, in the injector there appear still hydraulic losses when liquid flows into the entrance channels, which in machine building practice usually have a sharp edge.

When impact pressure in entrance channels is small as compared to feed pressure, hydraulic losses do not essentially influence the operation of the injector. If, however, impact pressure is comparable w'th feed pressure, then under the influence of energy losses the flow rate of liquid through the injector can noticeably decrease.

The influence of energy losses in the entrance channels increases for swirlers with an opened nozzle or, as they are called, opened injectors, i.e., with a decrease of the ratio of swirler arm to nozzle radius $C = \dfrac{R}{r_{e}}$ $(C_{min} = 0.5)$, when, conversely, energy losses in the swirl chamber play an ever smaller role.

B. V. Novikov examined the effect of opening the swirler on its hydraulic parameters.[15]

92

Pressure drop in the entrance channels can be represented in the form

$$\Delta p_{ax} = \zeta_{ax} \frac{w_{ax}^2}{2}. \tag{156}$$

where ζ_{ax} — drag coefficient of entrance channels, depending on shape of edges and Reynolds number.

If we disregard energy losses in the swirl chamber, instead of equation (62) we obtain

$$p + \frac{\rho}{2}(u^2 + w^2 + \zeta_{ax} V_{ax}^2) = p_T. \tag{157}$$

If we also do not consider change of angular momentum, then, repeating the derivation given in § 1 of this chapter, after simple transformations we reach the following expression for discharge coefficient of the swirler considering the effect of hydraulic losses in the entrance channels:

$$\mu = \frac{1}{\sqrt{\dfrac{1}{\varphi^2} + \dfrac{A^2}{1-\varphi} + \Delta_{ax}}}. \tag{158}$$

where

$$\Delta_{ax} = \zeta_{ax} \frac{A^2}{C^2}.$$

Since Δ_{ax} does not depend on φ, then, using the principle of maximum flow rate, we obtain the former dependence of the nozzle space factor on the geometric characteristic of the injector; the dependence of root angle of spray on A remains constant.

Let us find now the ratio of μ to μ_{ad}. From expressions (70) and (158) we have

$$\frac{\mu}{\mu_{ad}} = \frac{1}{\sqrt{1 + \zeta_{ax} \dfrac{(\mu_{ad} A)^2}{C^2}}}. \tag{159}$$

At a given value of the geometric characteristic this ratio decreases with a decrease of C, i.e., as the injector nozzle opens.

93

At a given value of C there is a considerably weaker dependence of $\frac{\mu}{\mu_{wc}}$ on the geometric characteristic of the injector A. As A increases, discharge coefficient μ_{wc} decreases.

For large values of C hydraulic losses in the entrance channels no longer essentially influence the discharge coefficient of the swirler.

The drag coefficient was determined experimentally for holes simulating those entrance channels of swirlers most frequently encountered in practice. Dependence of drag coefficient on Reynolds number of entrance channels $(Re_{ex} = V_{ex}d_{ex}/\nu)$ is represented on Fig. 49.
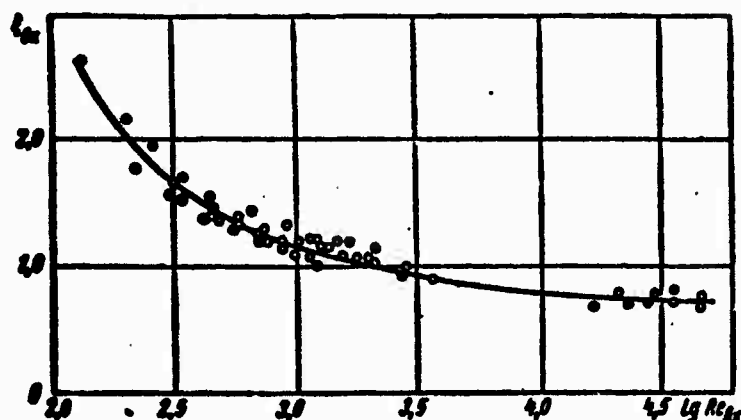
Fig. 49. Dependence of drag coefficient of entrance channels on Reynolds number.

Let us turn now to results of experimental investigation of injectors with different values of characteristic C maintaining the remaining injector dimensions constant.

On Fig. 50 are plotted experimental points showing the dependence of $\frac{\mu_{wc}}{\mu_{wc}}$ on C. As C decreases the ratio $\frac{\mu_{wc}}{\mu_{wc}}$ becomes less than one.

On the same figure the broken lines show the calculated dependences by formula (159) for different values of geometric characteristic A and drag coefficient $\xi_{ex} = 0.9$, corresponding to the range of changes of parameters of investigated injectors and the test conditions.
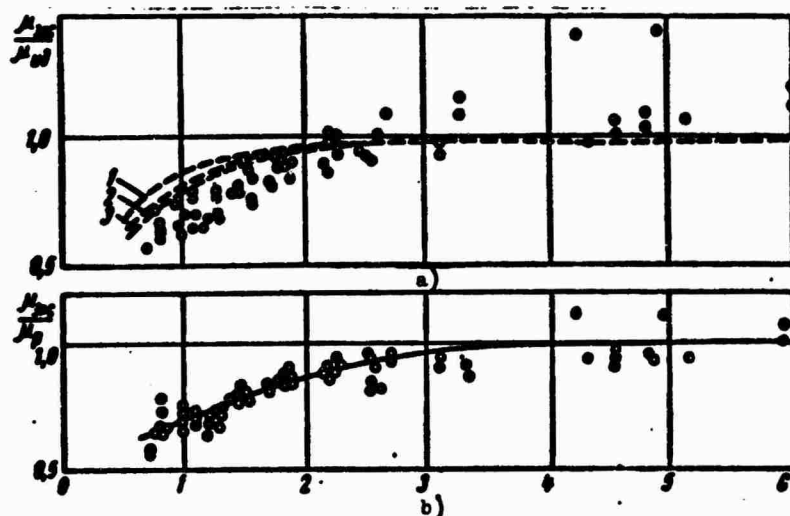
Fig. 50. Dependence of relative discharge
coefficient on characteristic $C = \frac{R}{r_c}$: a)
ratio $\frac{\mu_{exc}}{\mu_{ad}}$; broken lines — analytic curves
according to formula (159); 1 — A = 2;
2 — A = 4; 3 — A = 6; b) ratio $\frac{\mu_{exc}}{\mu_p}$: solid
line — averaged curve.

Comparison of calculated and experimental dependences shows that
they coincide with sufficient accuracy. Deviation at large values of
C is connected with the effect of friction in the swirl chamber.

A somewhat smaller spread of points is obtained (Fig. 50b) if we
refer experimental values of the discharge coefficient to those
calculated according to the equivalent characteristic of the injector,
i.e., taking into account viscosity of fuel.[16]

Thus, if the ratio of swirl arm to nozzle hole radius is less
than three (C < 3), then in calculating the discharge coefficient it
is necessary to introduce a correction, using the averaging curve
shown on Fig. 50b.

Besides the above-examined energy losses (in entrance channels
and in swirl chamber) there exist other sources of energy losses in
an injector: losses during flow in body of injector, losses on turn
of flow in injectors with swirl vane (worm) and others. The magnitude
of these losses in great degree depends on the construction of the
injector, and its design in general is difficult.

95

The investigation of the effect of pressure losses on the hydraulic characteristics of swirlers with different atomizer design is the subject of a work by Z. I. Geller, M. Ya. Moroshkin and others [5, 6, 7, 17].

Consideration of the features of liquid flow in a swirler shows that there exists a series of factors causing a deviation between the theory of an injector for an ideal liquid and experimental data.

Liquid friction on the swirl chamber wall, increase of the chamber height, deflection of flow in entrance channels to the axis of the swirl chamber lead to an increase of the discharge coefficient and a decrease of the root angle of the spray (as compared to $\mu_{и}$ and $\alpha_{и}$), whereas a narrowing of the flow in entrance channels and its compression upon entering the swirl chamber lead to a reverse action (decrease of μ and increase of α).

Energy losses in the entrance channels, obtaining an essential value when the injector nozzle is opened, and narrowing the flow in the nozzle cause a decrease of the discharge coefficient and do not influence the root angle of the atomization spray.

Increasing the nozzle length is connected with a decrease of the root angle of the spray.

§ 6. Selection of Rational Dimensions of Atomizer and the Design of Simple Centrifugal Injectors (Swirlers)

A swirler should give the atomized liquid a given root angle of the spray and ensure therein the required flow rate of liquid at a selected feed pressure.

It is desirable also to minimize energy losses, since as losses increase the exit velocity of liquid from the injector drops off and the quality of atomization deteriorates.

When swirlers with a large discharge coefficient and small root angle of spray (60-70°) are made, no essential angle difficulties are encountered.

The development of injectors with low discharge coefficient presents certain difficulties (especially with low flow rates of viscous liquid), connected basically with the effect of friction on the hydraulic parameters of the swirler.

Overcoming (at least partial) these difficulties first of all requires that the effect of friction on these hydraulic parameters be diminished as much as possible.

Complex $\frac{B}{a} - A$ should not, as a rule, exceed values of 5-10. This requirement means that characteristic B is less than 4-5 (when the work of injector works on water or kerosene). One should not, however, select values of B too small, since the absolute dimensions of the atomizer decrease excessively, and, consequently, technology is complicated and the precision of injector manufacture decreases.

An increase of the height of the swirl chamber leads to a decrease of the root angle of the spray and growth of discharge coefficient. Therefore in designing injectors the height of the chamber should be selected close to the diameter of the inlets (for rectangular channels — the height of the channel). From technological considerations the height of the chamber, however, should somewhat exceed the diameter of the inlets.

The cylindrical part of the injector nozzle should be short (not longer than 1-2 calibrations); an increase of nozzle length is undesirable, since it leads to a decrease of the root angle of the spray.

If the equivalent characteristic of the injector does not exceed 4-5, then nozzle length l_c may be from 0.5 to 1.0 d_c. When $A_{\bullet} > 4-5$ one should use shorter nozzles $[l_c = (0.25 - 0.5)d_c]$.

It is recommended that the cone angle on the nozzle entrance be within limits from 60 to 120°. Smaller cone angles are unadvisable, since the discharge coefficient increases, the root angle of the spray decreases and technology of manufacture is complicated. When the cone

angles are large, the turn of the flow when passing from swirl chamber into nozzle is too sharp and treatment of the inlet edge of the nozzle hole is hampered.

If entrance channels are insufficiently long, the flow cannot assume a tangential direction and is deflected to the axis of the swirl chamber, which leads to a decrease of the root angle of the spray and growth of the discharge coefficient. Therefore, the length of the entrance channels should be not less than 1.5 calibrations.[17] However, it must not exceed 3-4 gauges, since excessive lengthening of the channel results in an increase of friction losses and an increase of the dimensions of the injector.

Changing the number of entrance channels while maintaining a constant total area weakly affects the hydraulic parameters of the injector. As will be shown below, for "closed" injectors two-three channels are sufficient to obtain a symmetrical spray angle with equal distribution of fuel around its axis. When the number of channels is large, essential improvement of the uniformity of fuel distribution in the spray is not observed, but difficulties in manufacture considerably increase (precision of manufacture drops off). Therefore in designing swirlers the number of entrance channels should be from two to four.

The above recommendations on selection of rational dimensions of an atomizer refer first of all to the injectors of aircraft gas turbine engines.

Hydraulic design of a simple swirler consists in determination of the dimensions of nozzle, swirl chamber and entrance channels which guarantee obtaining rated values of productivity and the root angle of the spray.

Initial data for calculation are root angle of spray, flow rate per second of liquid, pressure in front of injector, density and coefficient of viscosity.

It is advisable to calculate on the basis of the theory of an injector for an ideal liquid with subsequent consideration of the effect of friction and different structural factors.

According to the rated value of the root angle of the spray, using the curve shown on Fig. 30, we determine the geometric characteristic of the injector A, by which we find the value of the discharge coefficient. Further, from the flow rate equation we find the diameter of the nozzle hole

$$d_c = \sqrt{\frac{4Q}{\pi \mu \sqrt{\frac{2 \Delta p_T}{\rho}}}}.$$ (160)

To determine the remaining dimensions of the atomizer we employ the equation of the geometric characteristic

$$A = \frac{R r_c}{n r_{ax}^2}.$$

Since this equation has three unknowns (R, n, r_{ax}), then two of them must be found. The most convenient to find is the number of entrance channels and the magnitude of the swirl arm. The number of entrance channels should be selected from 2 to 4. The magnitude of the swirl arm should be determined (for an ideal liquid) by proceeding from the assigned dimensions of the injector.

After the number of entrance channels and the magnitude of the swirl arm selected, we determine the diameter of the entrance channels[18]

$$d_{ax} = 2 \sqrt{\frac{R r_c}{i \mu A}}.$$ (161)

This finishes elementary calculation of the injector for an ideal liquid.

Further it is necessary to estimate the effect of friction and different structural factors on hydraulic parameters of the injector and to introduce into calculation necessary corrections, examining the calculation for an ideal liquid as a first approximation.

99

Let us determine the Re number of the swirl chamber entrance:

$$Re = \frac{4G}{\rho_r \sqrt{n z d_{ex}}}.$$ (162)

Here d_{ex} is taken from calculation for an ideal liquid.

By the Re number we find the coefficient of friction λ_1 (Fig. 44). Then we determine the equivalent characteristic

$$A_{s1} = \frac{Rr_i}{n r_{ex}^2 + \frac{\lambda_1}{2} R(R - r_i)}.$$ (163)

It is obvious that $A_{s1} < A$. If the difference between A_{s1} and A is small, i.e., if values of the discharge coefficient and root angle of spray corresponding to A_{s1} and A coincide with sufficient degree of accuracy (deviation does not exceed 5-10%), then we should limit ourselves to the first approximation. This will happen when friction has little affect on hydraulic parameters of the injector (at small values of λ and complex $\frac{R r_i}{n} - A$).

If the difference between A_{s1} and A is great, it is necessary to calculate the following approximation.

Assuming that the coefficient of friction is λ_1, and solving equation (163) with respect to r_{ex}, we find the new value of the inlet diameters [taking in equation (163) $A_{s1} = A$]

$$d_{ex}' = 2\sqrt{\frac{R r_i}{nA} - \frac{\lambda_1}{2n} R(R - r_i)}.$$ (164)

Then we determine the Re number and the value of the coefficient of friction λ_2, with respect to which we calculate equivalent characteristic A_{s2}, corresponding to entrance channels having diameter d_{ex}':

$$A_{s2} = \frac{Rr_i}{n r_{ex}'^2 + \frac{\lambda_2}{2} R(R - r_i)}.$$

Again we compare A_{s2} with A, and if the difference exceeds that permissible, we calculate the following approximation.

100

Usually two-three approximations are sufficient.[19]

In the case of a real liquid, when the magnitude of the swirl arm is selected one should consider that to overcome the "viscous barrier" it is necessary to decrease the swirl arm and simultaneously decrease the diameter of the entrance channels: the greater A is (i.e., the greater the assigned root angle of spray), the less R should be.

It is necessary to note that the less the flow rate of fuel and the greater its viscosity, the smaller the swirl arm should be.

Since in the entrance channels the flow narrows, a correction for the contraction factor should be introduced. For this the diameter of the entrance channels is calculated not with respect to A and A_s but with respect to the active characteristic of the injector A_s and A_{so} from formulas (153) and .(154).

We obtain for the first approximation

$$d_{ss}=2\sqrt{\frac{Rr_s}{\epsilon n A_0}}.$$ (165)

We select the value of the contraction factor within the limits $\epsilon = 0.85 - 0.90.$

After the diameter of the entrance channels is found, we determine remaining dimensions of the atomizer.

Diameter of the swirl chamber is calculated from the relationship

$$D_s = 2(R + r_{ss})$$

and the technical tolerance is added.

The height of the cylindrical part of the swirl chamber, nozzle length and length of the entrance channels is selected in accordance with recommendations given above $(\delta \approx d_{ss}; \frac{l_s}{d_s} = 0.25 - 1.0; \frac{l_{ss}}{d_{ss}} = 1.5 - 3.0).$

The angle of the cone on the nozzle entrance is selected within

101

limits from 60 to 120°.

For injectors with strong nozzle "opening" $(C = \frac{R}{r_c} < 2.5)$ and when the cone angles on the nozzle entrance, additional corrections must be introduced for losses in entrance channels and narrowing of the flow in the nozzle.

We will not discuss the design of injectors with whose entrance channels are not round, or whose channels are inclined to the axis of the swirl chamber, since in it does not entail new fundamental questions.

Let us explain the progression design by two examples.

Example 1. Design an injector with spray angle $\alpha = 60^O$ on flow rate G = 40 g/s under pressure p_T = 35 kgf/cm^2. Fuel — kerosene (ρ = 830 kg/m^3, ν = 2.2·10^{-6} m^2/s).

Root angle of spray $\alpha = 60^O$ corresponds to geometric characteristic A = 0.90 and discharge coefficient μ = 0.462.

From expression (160) we find nozzle diameter $d_c \approx 1.20$ mm.

We set the number of inlets n = 3 and magnitude of swirl arm R = 4r$_c$ = 2.4 mm (a greater value is unadvisable due to the excessive increase in dimensions of the injector).

We calculate diameter of the inlets by formula (161): d_{ex} = 1.46 mm and Re number = 11,080.

From the curve on Fig. 74, we determine the coefficient of friction λ = 0.051.

We calculate A_{e1} by formula (163): A_{e1} = 0.843.

Corresponding values of discharge coefficient and root angle of spray are μ_1 = 0.478, α_1 = 58°. Then $\frac{\mu_1}{\mu}$ = 1.035 and $\frac{\alpha_1}{\alpha}$ = 0.968.

102

The obtained values are close to the assigned and therefore we can limit ourselves to the first approximation.

Taking the flow contraction factor in the inlets as 0.9, we determine their real diameter by formula (165): $d_{ex} \approx 1.55$ mm.

We determine remaining dimensions of the injector atomizer: diameter of swirl chamber $D_c = 2(R + r_{ex}) = 6.35$ mm. Height of cylindrical part of swirl chamber is selected somewhat greater than diameter of inlets: $a = 1.8 - 1.9$ mm. Angle on nozzle entrance $\psi = 90°$. Length of nozzle $l_c = 0.5 \, d_c = 0.6$ mm; length of entrance channels $l_{ex} = 2 \, d_{ex} = 3.1$ mm.

Example 2. Design an injector with spray angle $\alpha = 120°$ on flow rate G = 6 g/s under pressure $p_T = 4$ kgf/cm^2. Fuel — kerosene ($\rho = 830$ kg/m^3, $\nu = 2.2 \cdot 10^{-6}$ m^2/s).

The value $\alpha = 120°$ corresponds to A = 10.0 and $\mu = 0.082$. We find diameter of nozzle hole $d_c = 1.91 \approx 1.90$ mm. We set the number of inlets n = 2 and magnitude of swirl arm R = 2.5 $r_c = 2.38 \approx 2.40$ mm.

We calculate diameter of inlets $d_{ex} = 0.676$ mm and determine the Re number. It is equal to 4400. From the curve on Fig. 74, we determine the coefficient of friction: $\lambda_1 = 0.084$.

Further we calculate A_{ex} by formula (163). We obtain $A_{ex} = 6.1$. This value of equivalent characteristic corresponds to $\mu_1 = 0.125$ and $\alpha_1 = 110°$. Then $\frac{\mu_1}{\mu} = 1.52$ and $\frac{\alpha_1}{\alpha} = 0.916$.

The deviation between μ_1 and μ is so great that it is necessary to calculate the following approximation. Putting in formula (164) the value of λ_1, we find diameter of inlet $d_{ex}' = 0.404$ mm. This inlet diameter corresponds to Re number = 7360 and $\lambda_2 = 0.062$.

We calculate the new value of the equivalent characteristic: $A_{ex} = 12.0$, for which $\mu_2 = 0.07$, $\alpha_2 = 123°$, $\frac{\mu_2}{\mu} = 0.843$, $\frac{\alpha_2}{\alpha} = 1.025$.

Since the deviation between μ_2 and μ is still great, we will

calculate the third approximation. We obtain $d_{ei}^{''} = 0.49$ mm and further Re number = 6050, $\lambda_3 = 0.069$ and $A_{e4} = 9.5$.

The value of equivalent characteristic $A_{e4} = 9.5$ corresponds to: $\mu_3 = 0.0855$ and $\alpha_3 = 119°$, $\frac{\mu_3}{\mu} = 1.045$, $\frac{\alpha_3}{\alpha} = 0.99$.

We can limit ourselves to the third approximation. Taking for the flow contraction factor in the inlets $\varepsilon = 0.9$, we determine the actual diameter of these holes. This gives $d_{ei} = 0.516$ mm. Since $\mu_3 > \mu$ the value of d_{ei} is rounded down: $d_{ei} = 0.51$ mm.

We determine remaining dimensions of the atomizer:

$D_s = 5.4$; $\delta = 0.6 - 0.65$ mm; $l_c = 0.25\ d_c = 0.5$ mm; $l_{ei} = 2\ d_{ei} = 1.0$ mm. Angle on nozzle entrance $\psi = 90°$.

Let us note that if for a given injector we select a large number of inlets, setting, for example, n = 4, then the diameter of these holes will be so small (near 0.35 mm) that manufacture of the atomizer will elicit certain technological difficulties.

§ 7. Manufacturing Precision of Centrifugal Injectors (Swirlers)

In a number of cases in the exploitation of swirlers (in gas turbine engines and installations) the requirements for accuracy of coincidence of their hydraulic and discharge characteristics are increased.

Certainly, it is impossible to prepare a set of injectors, which would have absolutely identical discharge characteristics. However, proceeding from required accuracy of coincidence of the discharge characteristics of separate injectors, the permissible tolerances in the dimensions of the atomizer for which established requirements will still be fulfilled can be found.

Discharge through injector is determined from the equation

$$G = \frac{\pi}{4}\, d_{ci}^2 \mu \sqrt{2 g \rho p_T}.$$

104

In this equation the product $d_c^2 \mu$ depends on accuracy of manufacture.

The relative change of discharge through an injector induced by a difference in the dimensions of the atomizer will be

$$\frac{\Delta Q}{Q} = \frac{\Delta(d_c^2\mu)}{d_c^2\mu} = \frac{\Delta\mu}{\mu} + 2\frac{\Delta d_c}{d_c}. \tag{166}$$

In order to find the change of the ratio $\frac{\Delta Q}{Q}$ depending upon manufacturing precision of the injector, i.e., on precision of preparing the nozzle, entrance channels and swirl chamber, we will express the discharge coefficient through the geometric characteristic of the injector (we will examine an ideal flow). This is done most simply by approximating the dependence of μ on A with the help of formula (145).

Substituting the expression for μ from formula (145) into expression (166) and replacing A by $\frac{2 d_c R}{n d_{ex}^2}$, we obtain after simple transformations:

$$\frac{\Delta Q}{Q} = (2 - m)\frac{\Delta d_c}{d_c} + \frac{2m\sum_{i=1}^{i=n}\Delta_i d_{ex}}{n d_{ex}} - \frac{m}{nR}\sum_{i=1}^{i=n}\Delta_i R. \tag{167}$$

where d_c — rated nozzle diameter; d_{ex} — rated diameter of inlets; R — rated size of swirl arm: Δd_c — real deviation for d_c; $\Delta_i d_{ex}$ — real deviation for d_{ex}; $\Delta_i R$ — real deviation for R.[20]

Expression (167) is called the equation of manufacturing precision of the injector. From consideration of this equation it follows that the precision of achieving dimensions d_c, d_{ex}, and R affects the relative change of discharge differently. Whereas with an increase of d_c and d_{ex} ($\Delta d_c > 0$; $\Delta d_{ex} > 0$) discharge increases as compared to the rated value, an increase of R ($\Delta_i R > 0$) conversely leads to a decrease of the discharge.

Equation (167) within the assigned accuracy of preparing the individual dimensions of the atomizer (d_c, d_{ex}, and R) permits determining deviation in flow rate or, conversely, within the assigned

maximum permissible deviation in flow rate and tolerances for preparing two dimensions (for example, d_c and d_{ez}), it permits determining the tolerance for the third dimension (for example, R) which ensures preservation of the assigned deviation in flow rate.

In the interval $0.75 < A < 7.5$ the exponent $m = 0.67$. Then equation (167) takes the form

$$\frac{\Delta G}{G} = 1.33\frac{\Delta d_c}{d_c} + \frac{1.34}{n}\frac{\sum_{i=1}^{i=n}\Delta_i d_{ez}}{d_{ez}} - \frac{0.67}{n}\frac{\sum_{i=1}^{i=n}\Delta_i R}{R}. \tag{168}$$

From consideration of equation (168) it follows that relative change of d_c and d_{ez} renders an identical influence on change of discharge (corresponding quantities have approximately identical coefficients), whereas the relative change of R has an affect half as strong (coefficient is half as large).

For nozzle and entrance channels tolerances are set in the system of the hole. In this case deviation will be positive. For the swirl arm the deviation can be both positive and negative. The radius of the swirl chamber (rated dimension) should be[21]

$$R_z = R + \Delta R + \frac{d_{ez} + \Delta d_{ez}}{2}.$$

where ΔR and Δd_{ez} — upper deviations for dimension of swirl arm and diameter of inlets.

Maximum relative deviation in discharge in the selected system of tolerances will be determined from the equation

$$\left(\frac{\Delta G}{G}\right)_{max} = 1.33\frac{\Delta d_c}{d_c} + 1.34\frac{\Delta d_{ez}}{d_{ez}} + 1.34\frac{\Delta R}{R}. \tag{169}$$

where Δd_c, Δd_{ez} and ΔR — absolute values of upper deviations for d_c, d_{ez} and R.

Even if for the size of the swirl arm a deviation of only one place is set, for example, negative (in this case the rated size of the swirl chamber radius should be selected as $R_z = R + \frac{d_{ez} + \Delta d_{ez}}{2}$), then the equation of maximum relative deviation of flow rate will take the form

106

$$\left(\frac{\Delta G}{G}\right)_{max} = 1.33\frac{\Delta d_c}{d_c} + 1.34\frac{\Delta d_{ex}}{d_{ex}} + 0.67\frac{\Delta R}{R}. \qquad (170)$$

Equations (169) and (170) permit determining the greatest possible deviation in flow rate with respect to assigned deviations of $d_c, d_{ex},$ and R or with respect to assigned deviations in flow rate, and in two dimensions (for example, d_c and d_{ex}) finding the most permissible deflection in the third dimension (for example, R).

Calculations show that, for example, under the condition $\left(\frac{\Delta G}{G}\right)_{max} < 0.03$ dimensions $d_c, d_{ex},$ and R must be held in the first class of accuracy. The smaller the absolute dimensions of the atomizer, the greater the precision in fulfilling them should be.

L. V. Kulagin [14] showed for a real (viscous) liquid requirements for manufacturing precision of injectors are somewhat lower.

Calculation of hydraulic characteristics of injectors, carried out not with respect to values of maximum deviations in the primary dimensions of the atomizer (within limits of field of tolerance), but with respect to values of probable deviations, naturally shows that in this case tolerances on the basic dimensions can be assigned more freely [14].

The problem of improving the construction of injectors should be in particular one safeguarding the technological possibility of manufacturing an atomizer with minimum tolerances.

Accuracy of fulfilling the remaining dimensions of the atomizer (height of swirl chamber, nozzle length, length of entrance channels) does not greatly effect the discharge characteristic of the injector. However, even these dimensions should be kept identical as possible for all injectors.

The problem of unequal flow rate of fuel through individual adjustable injectors, and also the problem of the effect of manufacturing precision for injectors on distribution of fuel in the spray will be examined below.

107

§ 8. Hydraulics of a Centrifugal Injector (Swirler) in a Feed of Superheated Liquid

In preceding sections during the analysis of the work of a swirler it was assumed that pressure of liquid vapors in the injector is small as compared to pressure of the medium, into which liquid is introduced.

When liquid is heated to the temperature at which its vapor pressure does not exceed the pressure of the medium into which the discharge occurs, a change in the work of the injector occurs only because of the effect of temperature on density and viscosity of liquid.

Upon further heating of the liquid, when its vapor pressure exceeds ambient pressure, a decrease of discharge through the injector is observed.

This question was first investigated by K. N. Yerastov and Ye. G. Nikolayev, who proposed the following formula for calculating the discharge coefficient of superheated liquid:

$$\mu_t = \mu \sqrt{\frac{p_\phi - p_u}{p_\phi - p_a}}, \tag{171}$$

where μ — discharge coefficient during discharge of cold liquid; p_ϕ — absolute pressure of liquid in front of injector; p_u — vapor pressure of liquid at temperature t; p_a — absolute pressure of medium.

Formula (171) has meaning when $p_u \geqslant p_a$ (when $p_u < p_a \; \mu_t = \mu$).

From formula (171) it follows that as vapor pressure of the liquid in the gas vortex increases, the discharge coefficient decreases as if the liquid discharge occurred not into a medium with pressure p_a, but into a medium whose pressure equals the liquid vapor pressure p_u.

Comparison of results of calculation by formula (171) with experimental data of the authors themselves shows that calculation

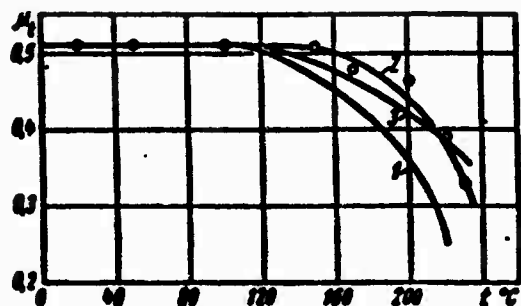gives a decreased value of the discharge coefficient (Fig. 51).

Fig. 51. Dependence of discharge coefficient on temperature of liquid (injector of engine BMW-003, liquid — water; pressure in front of injector $p_0 = 30$ kgf/cm^2): O — experimental points; 1 — analytic curve according to formula (171); 2 — analytic curve according to formula (173); 3 — analytic curve according to the method expounded in the work of Makhin and others [16].

The cause of this deviation is that in connection with the discharge of liquid vapor from the injector the pressure in the gas vortex on leaving the nozzle is lower than the pressure of the saturated vapor, which corresponds to the liquid temperature.

The work of V. A. Makhin and others [16] developed a theory of the discharge of superheated (boiling) liquid from a swirler taking into account the difference of pressure in the gas vortex from saturated vapor pressure of liquid. It is assumed that discharge occurs in thermodynamic equilibrium; discharge of liquid vapor and change of the liquid temperature are considered.

However, as calculation shows, if the liquid temperature is less than that which corresponds to vapor pressure (equal to pressure in front of injector), then vapor discharge can be disregarded. In the first approximation it is also permissible to assume that the temperature of liquid during the outflow is constant.

Thus, the problem leads to determination of pressure in the gas vortex on the injector nozzle exit. Pressure in the gas vortex on the injector nozzle exit differs from ambient pressure only during supercritical flow of liquid vapor. In this case

$$p_c = p_0 \left(\frac{2}{k+1} \right)^{\frac{k}{k-1}}. \tag{172}$$

where p_c — pressure in gas vortex (on nozzle exit); k — adiabatic vapor index.

109

Then the expression for discharge coefficient of superheated liquid will be written in the form

$$\mu_t = \mu \sqrt{\frac{p_0 - p_c}{p_0 - p_a}}.$$ (173)

Formula (173) is applicable if $p_c \geqslant p_a$ (at $p_c < p_a$ $\mu_t = \mu$). Let us note that during calculation of μ one should consider the change of density and viscosity of liquid depending upon its temperature.

Results of calculation of the discharge coefficient by formulas (172) and (173) are represented on Fig. 51 (in interval of temperatures $100^{\circ} < t < 250^{\circ}C$ for water vapor the mean value of adiabatic index $k = 1.30$ is accepted). On the same figure is given the analytic curve obtained taking into account vapor flow and change of liquid temperature [16].

As we see, both calculated dependences are close to each other and with a satisfactory degree of accuracy will agree with experimental data of K. N. Yerastov and Ye. G. Nikolayev.

The flow of gas in a swirler is not examined in this book. This question is analyzed in literature on cyclones and also to the Rank-Kilsh [Editor's Note: exact translation of names has not been found] effect.

Literature

1. Abramovich G. N. Teoriya tsentrobezhnoy forsunki (Theory of a swirler). In the collection "Promyshlennaya aerodinamika." M., izd. BNT TSAGI, 1944.

2. Abramovich G. N. Prikladnaya gazovaya dinamika (Applied gas dynamics). M., Gostakhizdat, 1951.

3. Blokh A.G. i Kichkina Ye. S. Raspylivaniye zhidkogo topliva mekhanicheskimi forsunkami tsentrobezhnogo tipa (Atomization of liquid fuel by mechanical injectors of centrifugal type). In the collection "Voprosy aerodinamiki i teploperedachi v kotel'no-topochnykh protsessakh." M., Gosenergoizdat, 1958.

4. Blokh A. G. i Kichkina Ye. S. O koeffitsiyentakh raskhoda i uglakh konusnosti fakela (Discharge coefficients and cone angles of spray). "Teploenergetika." 1957, No.10.

5. Geller Z. I., Ashikhmin V. I. i Shevchenko N. V. Ispol'zovaniye raspolagayemogo napora v tsentrobezhnykh forsunkakh (Use of available pressure in swirlers). "Teploenergetika." 1964, No. 4.

6. Geller Z. I. i Moroshkin M. Ya. Metodika rascheta i konstruktsiya tsentrobezhnykh forsunok dlya raspylivaniya topochnykh mazutov (Method of design and construction of swirlers for atomization of furnace mazuts). "Teploenergetika." 1963, No. 4.

7. Geller Z. I. i Moroshkin M. Ya. Gidravlicheskiye kharakteristiki tsentrobezhnykh forsunok (Hydraulic characteristics of swirlers). "Izvestiya vuzov. Energetika." 1960, No. 3.

8. Gol'dshtik M. A., Leont'yev A. K. i Paleyev I. I. Aerodinamika vikhrevoy kamery (Aerodynamics of an atomizer chamber). "Teploenergetika." 1961, No. 2.

9. Zhukovskiy N. Ye. Analogiya mezhdu dvizheniyem tyazheloy zhidkosti v uzkom kanale i dvizheniyem gaza v trube s bol'shoy skorost'yu (Anology between movement of a heavy liquid in a narrow channel and movement of gas in a pipe at high speed). T. VII. M., ONTI, 1937.

10. Karpukhovich D. T. O vybore naivygodneyshego diametra kamery zavikhreniya tsentrobezhnoy forsunki (Selection of optimum diameter of the swirl chamber for a centrifugal spray nozzle). "Teploenergetika." 1960, No. 11.

11. Klyachko L. A. K teorii tsentrobezhnoy forsunki (The theory of a centrifugal injector). "Teploenergetika." 1962, No. 3.

12. Klyachko L. S. Metod teoreticheskogo opredeleniya propusknoy sposobnosti apparatov s vrashchayushchimsya osesimmetrichnym techeniyem zhidkosti (Method of theoretical determination of carrying capacity of apparatuses with rotating axisymmetrical flow of liquid). In the collection "Teoriya i praktika obespylivayushchey ventilyatsii." Kn. 5. M., Profizdat, 1952.

13. Kochin N. Ye., Kibel' I. A. i Roze N. V. Teoreticheskaya gidromekhanika (Theoretical hydromechanics). T. I. M., Ogiz, 1948.

14. Kulagin L. V. Opredeleniye dopuskov na osnovnyye razmery tsentrobezhnykh forsunok (Determination of tolerances in basic dimensions of swirlers). M., Transzheldorizdat, 1960. (Trudy Vsesoyuznogo nauchno-issledovatel'skogo instituta zheleznodorozhnogo transporta. Vyp. 187).

15. Kulagin L. V. Opredeleniye ugla fakela pri istechenii topliva iz tsentrobezhnykh forsunok (Determination of spray angle in the flow of fuel from swirlers). "Vestnik Vsesoyuznogo nauchno-issledovatel'skogo instituta zheleznodorozhnogo transporta." 1959, No. 2.

16. Makhin V. A., Prisnyakov V. F. i Tokar' I. F. Teoriya istecheyiya kipyashchey zhidkosti cherez tsentrobezhnuyu forsunku

(Theory of the flow of boiling liquid through a swirler). "Izvestiya
vuzov. Aviatsionnaya tekhnika." 1962, No. 3.

17. Moroshkin M. Ya. Vliyaniye poter' napora na rabotu
tsentrobezhnykh forsunok (The effect of pressure losses on the operation
of swirlers). "Izvestiya vuzov. Energetika." 1960, No. 12.

18. Prakhov A. M. Issledovaniye i raschet tsentrobezhnoy
forsunki (Investigation and design of swirlers). In the collection
"Avtomaticheskoye regulirovaniye aviadvigateley." Vyp. I. M.,
Oborongiz, 1959.

19. Pfleyderer K. Tsentrobezhnyye i propellernyye nasosy
(Centrifugal and propeller pumps). M.-L., ONTI, 1937.

20. Talakvadze V. V. Teoriya i raschet tsentrobezhnoy forsunki
(Theory and design of swirlers). "Teploenergetika." 1961, No. 2.

21. Tikhonov V. B. K raschetu tsentrobezhnoy forsunki (Swirler
design). "Izvestiya vuzov. Aviatsionnaya tekhnika." 1958, No. 3.

22. Bammert K. Die Kern—Abmessungen in kreisenden Strömungen.
Zeitschrift VDI, Bd. 92, No. 26, 1950.
23. Binnie A. The passage of a perfect fluid through a critical cross—
section or «throat». Proceedings of the Royal Society, Ser. A, V. 197, No. 1051,
1949.
24. Binnie A. The theory of waves travelling on the core in swirling liquid.
Proceedings of the Royal Society, Ser. A, V. 205, No. 1083, 1951.
25. Doble S. Design of spray nozzles. Engineering, V. 159, No. 4122, 1945.
26. Doble S. Design of centrifugal spray nozzles. Engineering, V. 157,
No. 27, 1947.
27. Doumaa M., Laster R. Liquid—film properties for centrifugal spray
nozzles. Chemical Engineering Progress, V. 49, No. 10, 1953.
28. Feifel E. Zyklonentstaubung. Forschung auf dem Gebiete des ingeni-
eurwesens, Bd. 9, 1936.
29. Lawrence O. Communication on centrifugal spray nozzles. Procee-
dings of the Institution of Mechanical Engineers, V. 1957, No. 27, 1947.
30. Singer E. Theorie der Gemischaufbereitung in stationären Feuerun-
gen. Brennstoff—Chemie, Bd. 32, No. 1—2, 1951.
31. Taylor G. The mechanism of swirl atomizers. Proceedings 7-th Inter-
national Congress for Applied Mechanics, V. 1, London, 1948.
32. Taylor G. The boundary layer in the converging nozzle of a swirl
atomizer. The Quarterly Journal of Mechanics and Applied Mathematics, V. 3,
Pt. 2, 1950.

Footnotes

[1]The term "swirl chamber" is more correct than the term "vortex
chamber," which sometimes appears in literature.

[2]The radial velocity component is disregarded.

[3]Gravity may be disregarded. Calculation shows that acceleration
due to gravity even at pressures $P = 1$ kgf/cm^2 is in all only
hundredths of the centrifugal acceleration in the injector nozzle.

[4]In the derivation of equation (102) it was assumed, as was done
in the work of A. M. Prakhov [18], that there is no external compression
of the stream in the injector nozzle.

[5]This assumption is not stipulated in evident form in the work of V. B. Tikhonov [21].

[6]Propagation velocity of long waves for viscous and ideal liquid is identical [13].

[7]Calculations show that for injectors used practically $(0 < A < 7, \lambda < 0.1)$ the error appearing when formula (137) is used instead of formula (134) does not exceed 10%, and is usually considerably less.

In research calculations, and also for very viscous liquids it is necessary to use formula (134).

[8]Equality occurs only at $\lambda = 0$, i.e., for ideal liquid, or at $r_c = R$ (in this case $A = \frac{B^2}{a}$). But the latter case (and also when $r_c > R$, which gives $A_* > A$) should be excluded from consideration because in these cases formula (125) cannot be used, since its derivation assumed that liquid moves in the swirl chamber between two end walls.

[9]A similar phenomenon appears during the flow of liquid in a guiding device without blades (ring). Here raised values of the coefficient of friction also are obtained, changing within limits from 0.03 to 0.06 [19].

[10]The same character of dependence $\mu = f(A)$ as the swirl arm increases is experimentally established in the work of D. T. Karpukhovich [10].

[11]In practice injectors with variable height of swirl chamber frequently are encountered: on the periphery the height of the chamber is less than in the center (for example, in the presence of a cone on the entrance into the nozzle).

If on the periphery the height of the chamber is close to the diameter of the entrance channel and as the center is approached the height increases smoothly, then with sufficient degree of accuracy we can use the theory developed in the preceding section.

[12]The hydraulic discharge coefficient of the nozzle is called the discharge coefficient when liquid flows without swirling.

[13]All nozzles were tested with the same swirl vane, having four tangential rectangular channels ($a = 1.01, b = 0.53$ mm) and swirl arm $R = 2.2$ mm $(A = 2.44; \frac{B^2}{a} - A = 4.17)$.

[14]This is verified by results of the treatment of experimental data for injectors with various inlet edges of tangential channels.

[15]The decrease of discharge coefficient as the injector is opened has been experimentally established by the author. The possibility of explaining this decrease by hydraulic losses in the entrance channels was first shown by V. V. Talakvadze [20].

[16]When $\frac{B^2}{a} - A < 0$, the formula for A is used purely formally; we obtain $A_* > A$.

[17]Length of rectangular channel in calibrations is equal to the ratio of the length of the channel to its width.

[18]In the case of rectangular channels we determine consecutively their area, width, and height.

[19]It is simple to prove that successive approximations indeed converge to A. Convergence is disturbed only under the condition that $A > \frac{y_\iota}{\lambda_1(R-r_\iota)}$, since in this case equation (164) loses meaning. This indicates that the first approximation is too rough. Therefore it is necessary either to decrease the magnitude of the selected swirl arm, or during calculation of the second approximation to place in equation (164) not the value of λ_1 but a quantity which is 2-3 times smaller, so that the subradical expression becomes positive.

[20]By $\Delta_c R$ is understood total deviation for swirler arm, induced both by a shift of the axis of the entrance hole and by its nontangentiality.

[21]We consider that the tolerance on the diameter of the chamber is also given in the system of the hole, i.e., R_s real is equal to or more than R_s rated.

C H A P T E R IV

ADJUSTABLE AND TWO-COMPONENT CENTRIFUGAL
INJECTORS (SWIRLERS)

§ 1. <u>Principles of Adjustable Centrifugal</u>
<u>Injectors (Swirlers)</u>

In the combustion chambers of gas turbine plants and jet engines a wide range of change of fuel consumption must be ensured.

Thus, for example, when a air-breathing jet engine passes from conditions of maximum thrust near the ground to conditions of strong throttling at high altitudes the fuel consumption decreases 20-30 times.

In a simple swirler fuel consumption changes in approximately direct proportion to square root of pressure drop, so that an increase of fuel consumption of 30 times requires an increase of pressure drop of 900 times.

Presently used fuel pumps ensure a maximum pressure in front of injectors approximately equal to 75-80 kgf/cm^2. This pressure cannot be essentially increased without considerable complication and loading of fuel equipment and a decrease of its reliability.

If maximum feed pressure is 75-80 kgf/cm^2, then a decrease of consumption by 30 times requires a pressure reduction to 0.08-0.09 kgf/cm^2. But at such a low pressure the fuel stream from the injector does not break up into drops, forming a "bubble."

Satisfactory quality of atomization is attained with the use of kerosene only when gauge pressure in front of the injector is 3-4 kgf/cm^2; for gasoline this pressure is lower, but still composes 1-2 kgf/cm^2.

It is obvious that simple (unregulatable) swirlers in the interval of pressure from 3-4 kgf/cm^2 to 75-80 kgf/cm^2 cannot ensure the required range of change of fuel consumption (at satisfactory quality of atomization on low consumption).

Consequently, it becomes necessary to develop adjustable swirlers, i.e., such for which the flow rate with an increase of pressure increases faster than is proportional to the square root of pressure drop, so that the required range of change of flow rate will be attained in a comparatively narrow interval of feed pressure (from 3-4 kgf/cm^2 to 75-80 kgf/cm^2).

From the equation of flow rate

$$G = f \mu \sqrt{2g \rho}$$

it is clear that the flow rate of liquid of a given density is determined (besides by pressure) by the area of the nozzle hole and the discharge coefficient. In accordance with this, increasing with growth of pressure the nozzle area or the discharge coefficient (that or another) it is possible to achieve a flow rate faster than $\sqrt{p}$, and thus, to decide the problem at hand.

Adjustable injectors are of two types: an injector with variable area of nozzle hole and an injector with variable discharge coefficients.

Changes of nozzle hole area can be achieved by introducing into the nozzle a spring-loaded profiled needle; as pressure increases the needle rises and the area of the useful stream cross section is increased. However, realization of such method of adjustment of the nozzle hole area is connected with certain structural and

116

technological difficulties caused by the manufacture and operating conditions of the moving ground components.

The injector is complex in manufacture and unreliable in operation. Selection of injectors with identical discharge characteristic is hampered also. In connection with the shown deficiencies injectors with a needle did not find wide application.

Another way of developing injectors with variable area of nozzle hole involves one injector of two or several swirlers with concentrically located nozzles and separate swirl chambers (two-nozzle injectors).

In adjustable injectors of the second type a change of the discharge coefficient is determined by the flow velocity on the swirl chamber entrance, i.e., initial angular momentum.

Depending upon what method was used to change the flow velocity on the swirl chamber entrance, or, more exactly, to change the relationship of flow velocity on swirl chamber entrance and exit velocity from injector nozzle, we distinguish the following basic types of injectors with adjustable discharge coefficient:

1) injector with plunger (valve);

2) two-stage injector;

3) injector with fuel bypass.

In a swirler with a plunger the flow velocity on the swirl chamber entrance changes in connection with the change of the area of the tangential channels as the plunger moves.

In a two-stage injector this change of velocity is attained by choking the flow of fuel going into the swirl chamber through channels of the second stage.

117

In an injector with fuel bypass the flow velocity on the swirl chamber entrance is changed by controlling the quantity of fuel passing through.

It is also possible to develop combined adjustable injectors, combining elements of the enumerated structural types (for example, combination of two-stage injector and injector with fuel bypass or a two-nozzle injector and an injector with fuel bypass).

Below the principle of action, advantages and deficiencies of the basic types of adjustable swirlers are examined, and the method of calculating the hydraulic parameters of such injectors is also set forth.[1]

§ 2. Two-Nozzle Adjustable Injector

In two-nozzle injectors fuel consumption is regulated by changing the cross section area of the nozzle hole and partially choking the flow of fuel before the second stage.

Changing the area of the nozzle hole cross section in injectors of this type achieves a great range of flow rate, which can be still expanded due to the distinction in discharge coefficients of internal and external nozzles. The ratio of maximum and minimum flow rates is determined by the formula

$$\frac{G_{max}}{G_{min}} = \frac{f_1\mu_1 + f_2\mu_2}{f_2\mu_2}\sqrt{\frac{p_\kappa}{p_\mu}}. \tag{174}$$

where f_1 and f_2 — cross section areas of holes of internal and external nozzles; μ_1 and μ_2 — discharge coefficients of internal and external nozzles; p_κ and p_H — maximum and minimum gauge pressure before injector.

On Fig. 52 is given the schematic diagram of a two-nozzle injector. The swirl chambers of the first and second stages are divided and feed two independent concentrically located nozzles.
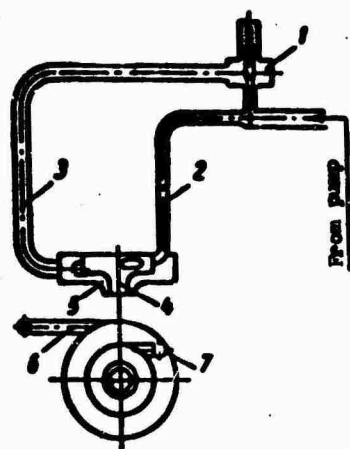
Fig. 52. Schematic diagram of two-nozzle injector: 1 — control valve; 2 and 3 — pipelines of first and second stages; 4 — interior nozzle (first stage); 5 — exterior nozzle (second stage); 6 and 7 — tangential channels of stages.

The interior nozzle is the nozzle of the first stage, the exterior — the nozzle of the second stage.

When feed pressures are low (small flow rates) fuel moves only through the interior nozzle. As pressure increases, the control valve is opened, and fuel has access to the swirl chamber and to the nozzle of the second stage. Circular streams of fuel emanating from interior and exterior nozzles form a common spray when they interact with each other.

Since both stages have separate nozzles, the fuel feed in the second stage starts when gauge pressure is close to zero and gradually increases as the valve opens. Therefore when the second stage cuts in, the quality of atomization deteriorates.

Figure 53 is the structural diagram of a working two-nozzle injector of a gas turbine engine.

Fuel is fed to two pipe connections located on the flange which is joined with the injector by tubes 1 and 2 and serves to fasten the injector to the combustion chamber. Through tube 1 the fuel moves into the central cavity of the injector and further into the internal nozzle (first stage), and through tube 2 it moves into the circular space and the external nozzle of the injector (second stage). The atomizer of the first stage consists of conical plug 3, on whose surface are cut helical grooves, and internal nozzle

119

Parameters	First stage	Second stage
Diameter of nozzle d_c in mm	1.3	2.0
Reduced diameter of inlet d_{es} in mm	0.586	0.91
Swirl arm R in mm	2.13	2.8
Number of inlets n	2	6
Geometric characteristic A	8.07	2.26

Fig. 53. Schematic of a two-nozzle injector on a gas turbine.
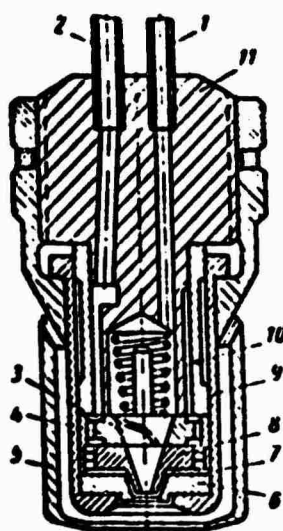
8. Plug 3 is pressed to the valve seat by spring 10. From the circular cavity of the second stage fuel passes through the hole in liner 4 and body of internal nozzle 8 and enters tangential cuts of plate 7 and further external nozzle 6.

Onto housing 11 of the injector is screwed container 5, tightening liner 9 and housing 11. This container has 12 holes through which air passes to the radial clearance between container 5 and liner 9 (for removal of carbon).

On Fig. 54 are given the characteristics of the flow rate of a two-nozzle injector when fuel is fed separately to each of the stages and simultaneously to both stages with identical pressure. It is easy to check that the sums of flow rates of fuel through both stages under identical feed pressure coincide with the total flow rate (difference does not exceed 1-2%). Such a result was also obtained in tests of other two-nozzle injectors with different mutual (in height) location of nozzles.

It follows from this that the flow rate through every stage of a two-nozzle injector is determined by the pressure of fuel in front of a given stage independently of the mutual location of nozzles.
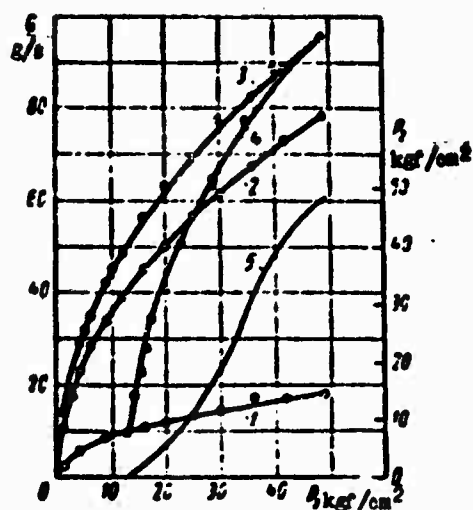
Fig. 54. Characteristics of the flow rate of a two-nozzle injector: 1 — for the first stage; 2 — for the second stage; 3 — for both stages (at identical pressure in front of stages); 4 — for transition operating conditions; 5 — dependence of pressure in front of second stage on pressure in front of first stage; O — experimental points.

Thus, the flow rate through each stage can be calculated independently by the method shown in Chapter III.

Since the first stage works at low flow rates of fuel and, consequently, at small Re number, and since for this stage the complex (B^2/n) - A usually is great (in connection with small diameter of inlets), then this stage of a two-nozzle injector should be designed according to injector theory for a real liquid.

Hydraulics of the second stage, working at considerably large Re numbers and smaller values of the complex (B^2/n) - A, as a rule are not essentially influenced by the fuel viscosity.

Here we must keep in mind that the second stage of a two-nozzle injector may be designed according to the usual method of swirler design only when the diameter of the air vortex in the nozzle of this stage exceeds the external diameter of the nozzle of the first stage, i.e., the internal nozzle does not go beyond the limits of the air vortex of the external nozzle.

If the external diameter of the internal nozzle exceeds the diameter of the air vortex on the nozzle exit of the second stage, then the discharge coefficient of this stage can be found from equation

121

(78), in which $S = S_w = \frac{r_a}{r_c}$, where r_w — the external radius of central nozzle — is a known quantity, but the discharge coefficient is unknown.

Solving graphically this equation, we find the dependence $\mu = f(A, S_w)$.

On Fig. 55 are given the dependences of discharge coefficient on S_w for different values of the geometric characteristic.
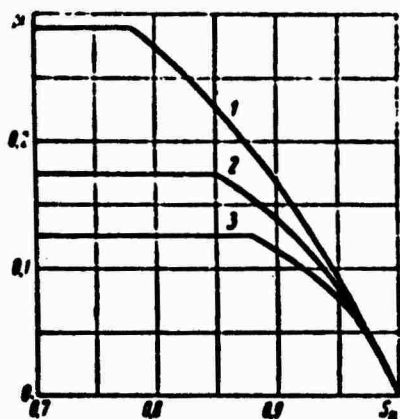

Fig. 55. Dependence of discharge coefficient μ on S_w: 1 — A = 2; 2 — A = 4; 3 — A = 6.

So we see, as S_w increases the discharge coefficient, referred to the full nozzle area of the second stage, decreases. Experimental data given in the work of L. V. Kulagin [5] confirm this conclusion.

Let us consider characteristics of the flow rate of a two-nozzle injector when both nozzles work together (both stages), but with different pressures in front of them.

On Fig. 54 are plotted the experimental points characterizing dependence of flow rate on pressure during joint operation of both stages and during choking of fuel in front of second stage (we will call this the transition mode). On the same figure is given the curve of pressure change in front of the second stage depending upon pressure in front of the first stage, corresponding to the selected transition mode. Every dependence $p_2 = f(p_1)$ corresponds to a defined characteristic of the control valve.

122

Above it was noted that in a two-nozzle injector flow rates through the separate stages do not depend upon each other. From this follows a simple method for constructing characteristic curves of the flow rate of a two-nozzle injector during the joint operation of both stages according to the characteristics of these stages separately and according to the relationship of pressures set by the control valve. For this it is sufficient to find according to the discharge characteristics of the stages the flow rate through every stage, corresponding to the given relationship of pressures, i.e., pressure p_1 in front of first stage and p_2 — in front of the second stage, and to combine the obtained flow rate values. In such a way the characteristic curve shown in Fig. 54 is constructed. As we see, fully satisfactory coincidence of the analytic curve with experimental points is obtained.

When the second stage of a two-nozzle injector is cut in, as already was noted, gauge pressure in front of this stage is close to zero and therefore comparable with the difference of hydrostatic pressures, and proportional to weight of the fuel column in the injector manifold in a vertical position (as it is located on the engine). Therefore under low fuel pressures in front of the second stage irregularity appears in the flow rate for injectors located in the upper and lower halves of the manifold.

If the characteristic curves of stages are known, it is simple to calculate the degree of flow rate irregularity of the injectors.

When the diameter of the fuel manifold is 1000 mm the degree of irregularity at the time of switching in the second stage reaches 15-20%. As pressure increases in front of the second stage the irregularity sharply drops.

Experiment shows that in a number of cases and when the manifold is in a horizontal location considerable irregularity is observed in flow rate through separate injectors at pressures somewhat exceeding pressure at which the second stage is cut in.

This irregularity apparently is because at small pressure drops
the flow rate through the external nozzle sharply changes for a small
change of pressure, induced by the difference in the drag of the fuel
duct of the second stage in the injectors. Actually, from the
equation of flow rate through the external nozzle we have

$$\frac{dG_2}{G_2} = \frac{1}{2} \cdot \frac{dp_2}{p_2}.$$ (175)

where G_2 — flow rate through second stage of injector; p_2 — gauge
pressure in front of second stage.

From equation (175) it follows that when p_2 is close to zero,
small changes of this pressure cause considerable irregularity
in the flow rate through the external nozzle.

The less the flow rate through the internal nozzle, at which
the external nozzle is cut in, the more sharp the irregularity in
flow rate will be.

Irregularity in the fuel flow rate is an essential deficiency
of two-nozzle injectors.

The root angle of the spray for two-nozzle injectors in a mode
of joint operation of both nozzles depends on both the spray root
angle of both stages and also on the mutual location of the nozzles.

If the ends of nozzles of both stages are located in one plane
and the spray root angle of the first stage exceeds the spray root
angle of the second stage, the total spray root angle of a two-nozzle
injector α_Σ is determined by expression [5]

$$\cos \frac{\alpha_\Sigma}{2} = \frac{w_1 G_1 \cos \frac{\alpha_1}{2} + w_2 G_2 \cos \frac{\alpha_2}{2}}{w_1 G_1 + w_2 G_2}.$$ (176)

where w_1, w_2, G_1, G_2, α_1, α_2 are exit velocity, flow rate and
angle of spray respectively for the first and second stages.

124

Experiments show that calculation data obtained by formula
(176) satisfactorily coincide with results of experiments.

At the same time special experiments conducted with a two-nozzle
injector, whose construction permits a sufficiently easy change of
the mutual location of nozzles in height (by means spacers) show
that the spray angle in conditions of joint operation of both
nozzles depends on their mutual location. Corresponding curves are
shown in Fig. 56. Depending upon the relative position of the nozzle
ends curve $\alpha = f(p)$ on the transition mode has a different appearance.
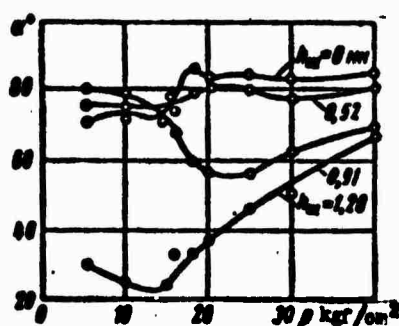

Fig. 56. Change of spray
angle depending upon
pressure in the operation
of a two-nozzle injector
on the transition mode
and with different mutual
location of nozzles.

Thus, by changing the location of the nozzles, it is possible to
influence the character of dependence $\alpha = f(p)$.

Moreover the mutual location of the nozzles influences mainly
the root angle of the spray in the first stage. As the thickness of
the liner is increased, the root angle of the spray decreases, since
the fuel stream hits against the wall of the external nozzle.

It is interesting to note that by means of corresponding
selection of the mutual location of nozzles, the root angle of the
spray can be made to remain almost constant during a change of fuel
pressure on the transition mode (Fig. 56, curve for $h_w = 0.52$ mm).

Advantages of two-nozzle injectors are:

a) no overflowing of fuel in injectors connected in parallel
(on manifold), observed, for example, in two-stage injectors and
leading to irregularity in fuel flow rate;

b) wide range of change of fuel flow rate (wider than for two-stage injectors and injectors with a plunger); the root angle of the spray in the whole range of change of flow rate, in contrast to the root angle of the spray in the case of adjustable injectors with variable discharge coefficient, can be maintained (with corresponding selection of mutual location of nozzles and root angles of the spray of both stages) practically constant.

Along with these advantages in a two-nozzle injector the switching in of the external nozzle is accompanied by impairment of the quality of atomization (at pressures close to the pressure of switching in the external nozzle). The quality of atomization is impaired because the external nozzle starts to work at gauge pressures close to zero, so that the exit velocity at these pressures is comparatively low.

Furthermore, when the second stage of two-nozzle injectors is switched in, there appears great irregularity in the fuel flow rates, especially through injectors located in different (in height) places of the fuel manifold.

§ 3. Adjustable Injector with Plunger

Such injectors are used in stationary and ship gas turbine plants.

A schematic diagram of an adjustable injector with a plunger is shown in Fig. 57. In the cylindrical swirl chamber a spring-loaded plunger (valve) can shift back and forth. The spring passes the plunger forward so that when the injector does not work one tangential hole (or the first row of them) remains open. As feed pressure increases, the plunger starts to open gradually following the tangential holes. The cavity above the plunger, in which the spring is located, is drained from a hole in the plunger, leading into the swirl chamber.

The structural diagram of an experimental injector with a plunger is given on Fig. 58.
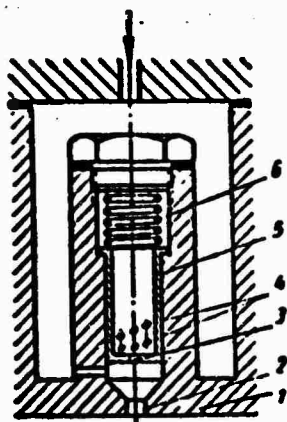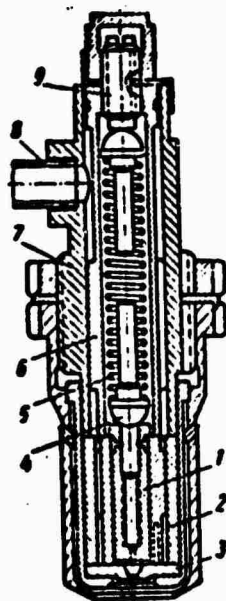
Fig. 57.

Fig. 58.

Fig. 57. Schematic diagram of injector with plunger: 1 — atomizer; 2 — nozzle hole; 3 — draining holes; 4 — tangential channels; 5 — plunger; 6 — spring.

Fig. 58. Diagram of experimental injector with plunger:

Diameter of nozzle d_c in mm...............	1.8
Number of entrance grooves n............	4
Limits of change of area of entrance grooves f_{aa} in mm.....	0.16-2.7
Swirl arm R in mm....	3.1
Diameter of plunger $d_{n.s}$ in mm............	7
Limits of change of geometric character- istic A..............	0.8-13.3

The injector consists of plunger 1, case 2 with tangential entrance grooves, nozzle plate 3, spring 5, hemispherical support 4 and screw 9, used to adjust the spring tension.

Fuel enters the injector along tube 8, welded to housing 7, and along channels cut into parts 6 and 2, and further through tangential grooves of case 2 enters the swirl chamber.

A characteristic peculiarity of the injector is insignificant preliminary spring tension great length and low rigidity. This makes it possible to secure a stable characteristic curve of the flow rate throughout its change.

For an ideal liquid the hydraulic parameters of the swirler are determined by its geometric characteristic $\left(A = \frac{R r_c}{n f_{aa}^2} \right)$. As the tangential holes open, the geometric characteristic decreases (in connection with the increase of n), which, as is shown in § 1 Chapter III, leads to growth of the discharge coefficient and decrease of the spray root angle. Consequently, with an increase of pressure

127

the flow rate will increase faster than $\sqrt{p_T}$ (p_T - full pressure in front of injector).

The geometric characteristic of an injector with a plunger changes within limits from $A_u = \dfrac{R r_c}{n_u r_{os}^2}$ to $A_u = \dfrac{R r_c}{n_u r_{os}^2}$, where n_u and n_u are respectively the number of open tangential holes at extreme positions of the plunger. For simplicity it is accepted that all tangential holes have identical diameter. According to these values of the geometric characteristic one can determine the range of change of the discharge coefficient and the root angle of the spray.

To determine the dependence of the hydraulic parameters of the injector on pressure (at intermediate positions of plunger) it is necessary to find the fuel pressure on the plunger. Using the equations of continuity, conservation of energy and preservation of angular momentum,[2] after transformations we obtain the expression for calculation of pressure distribution in the swirl chamber:

$$p = p_T \left[1 - \frac{\mu^2 r_c^4}{n^2 r_{os}^2} \left(\frac{1}{16} + \frac{R^4}{r_{os}^2} \right) \frac{1}{r^4} \right]. \tag{177}$$

Setting in formula (177) $p = 0$, we will find the radius of the air vortex on the rear face wall of the swirl chamber:

$$r_{os} = \mu r_c A \sqrt{1 + \frac{r_{os}^2}{16 R^2}}. \tag{178}$$

Since $r_{os} < R$, then $1 < \sqrt{1 + \frac{r_{os}^2}{16 R^2}} < 1.03$, i.e., it is fully permissible to set

$$\sqrt{1 + \frac{r_{os}^2}{16 R^2}} = 1.$$

Then

$$\frac{r_{os}}{r_c} = \mu A. \tag{179}$$

The curve expressing the dependence of r_{os} on A is given on Fig. 31.

128

The formula for pressure distribution in the swirl chamber
takes the form

$$p = p_T\left(1 - \frac{r_{mK}^2}{r^2}\right).$$

(180)

At $r = r_{mK}$ gauge pressure is equal to zero. With growth of r
pressure is increased, and when r = R differs from p_T by the
magnitude of impact pressure in the inlets. Pressure is increased
very sharply and already at $r = 2r_{mK}$ attains 75% of full pressure.

The expression for pressure distribution in the swirl chamber
permits determining the force on the plunger:

$$F = \int_{r_{mK}}^{R_K} p2\pi r\, dr,$$

where R_K— radius of swirl chamber.

Substituting expression for p from formula (180) and integrating,
we obtain

$$F = \Omega p_T.$$

(181)

where

$$\Omega = 2\pi\left[\frac{1}{2}(R_K^2 - r_{mK}^2) - r_{mK}^2 \ln\frac{R_K}{r_{mK}}\right].$$

The quantity Ω depends on feed pressure of fuel (in connection
with change of r_{mK}). However, as calculation shows, the change is
small. Therefore one may assume that the force of pressure on the
plunger is directly proportional to pressure p_T. This force is
balanced by the counteraction of the spring. Up to certain pressure
p_{TK} the spring holds the plunger in the extreme lower position (one
tangential hole is open). With further increase of pressure the
plunger starts to move away such that at $p_T = p_{TK}$ all n_K holes
are open.

The force of pressure on the plunger at $p_T = p_{T\kappa}$ will be determined from expression (181):

$$F_{\kappa} = p_{T\kappa} \Omega_{\kappa}.$$

The spring force counteracting this pressure

$$F_{\kappa} = t(l_0 - l_\kappa) = t\Delta, \tag{182}$$

where t — spring force; l_0 — length of free (uncompressed) spring; l_{κ} — initial length of spring in injector; Δ — initial tensor on spring.

With an increase of p_T the force of pressure on the plunger grows. Simultaneously, as the plunger shifts, the resisting force of the spring increases. At $p_T = p_{T\kappa}$ the force of pressure is

$$F_{\kappa} = p_{T\kappa} \Omega_{\kappa}.$$

and the balancing force of the spring

$$F_{\kappa} = t(l_0 - l_\kappa).$$

If, as is accepted above, tangential holes are located directly above one another,

$$l_{\kappa} = l_{\kappa} - (n_{\kappa} - 1) d_{o\kappa}.$$

and the expression for F_{κ} will take the form

$$F_{\kappa} = t[\Delta + (n_{\kappa} - 1) d_{o\kappa}]. \tag{183}$$

From equations (182) and (183) we find:

$$t = \frac{F_{\kappa} - F_{\kappa}}{(n_{\kappa} - 1) d_{o\kappa}}; \tag{184}$$

$$\Delta = \frac{F_{\kappa}(n_{\kappa} - 1) d_{o\kappa}}{F_{\kappa} - F_{\kappa}}. \tag{185}$$

130

Obtained expressions permit calculating spring force t and its initial tension Δ.

For values of pressure in the interval between $p_{Tн}$ and $p_{Tк}$ the movement of the plunger will be determined from the equation

$$l_к - l = \Delta + \frac{p_T \Omega}{t}. \tag{186}$$

Knowing the position of the plunger, it is simple to calculate the geometric characteristics of the injector for any p_T and to find the change of the discharge coefficient and root angle of the spray depending upon pressure.

When pressure in front of the injector is less than $p_{Tн}$, the injector works as a nonadjustable injector with discharge coefficient $\mu_н$. Upon further increase of pressure the discharge coefficient increases and at $p_T = p_{Tк}$ attains the value $\mu_к$, where $\mu_к > \mu_н$. Then the injector again starts to work as a nonadjustable injector, but with discharge coefficient $\mu_к$.

For a real liquid it is necessary to consider the influence of friction on the work of the injector with a plunger. In this case the hydraulic parameters are determined by the equivalent characteristic of the injector.

An especially strong influence is rendered by friction at low feed pressures, when a small number of inlets is open. Due to this the initial value of the discharge coefficient turns out to be considerably larger than for an ideal liquid, which leads to a narrowing of the flow rate range.

Comparison of experimental and computed values of the discharge coefficient for an experimental injector of the plunger type (Fig. 58) is shown in Fig. 59. At low pressures $\mu_{эф}$ considerably exceeds $\mu_{ид}$. Taking into account the influence of friction we obtain satisfactory agreement of theoretical and experimental data.

131

An adjustable injector with a plunger possesses a number of deficiencies which limit the possibility of its application.

The basic deficiency is the complexity of manufacturing a plunger pair and its insufficient reliability in operation. Due to jamming of the plunger instability in the flow rate of the injector is observed[3] and a considerable irregularity in the flow rate of the separate injectors of the fuel manifold. These deficiencies can be partially removed by the introduction of hemispherical supports under the spring and by decreasing the initial tension of the spring. However, decreasing the initial tension of the spring leads to a reduction of the flow rate range. For experimental injector shown on Fig. 58 when pressure increases from 3 to 60 kgf/cm^2 the flow rate changes by 12 times, while the minimum flow rate is approximately 10 g/s.
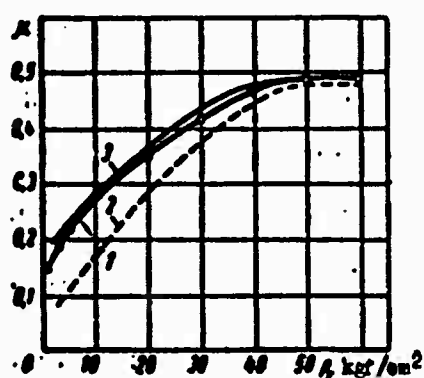

Fig. 59. Dependence of discharge coefficient on pressure of fuel (kerosene) for an experimental injector with a plunger: 1 — experimental curve; 2 — analytic curve for ideal liquid; 3 — analytic curve for real liquid.

§ 4.   Two-Stage Adjustable Injector

Adjustable two-stage injectors are used in the combustion chambers of many contemporary gas turbine engines. They find application also in other regions of technology.

A schematic diagram of a two-stage injector is shown in Fig. 60. At low feed pressures fuel enters tangential channels of the small section (first stage). With an increase of pressure the distributing valve opens, and fuel obtains access to tangential channels of the second stage, having a greater cross section (as compared to channels of the first stage). Streams coming from the entrance channels of both stages are mixed in the swirl chamber and then go to the injector nozzle.
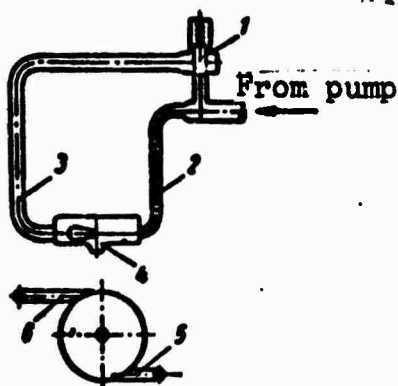
132

Fig. 60. Schematic diagram of a two-stage injector: 1 — control valve; 2, 3 — pipelines of first and second stages; 4 — nozzle; 5 and 6 — tangential channels of stages.

In a low flow rate mode the injector works as a nonadjustable injector with small discharge coefficient. Thanks to this, pressure in front of the injector is sufficient for good atomization.

When the control valve is opened, the discharge coefficient increases with pressure increase and reaches maximum when the valve is completely open. Moreover, to the maximum flow rate of fuel corresponds a considerably lower pressure than for an injector with constant initial discharge coefficient. After the control valve is completely open, a further increase in the flow rate again occurs for a constant — but considerably greater than for the first stage — discharge coefficient.

A structural diagram of a working two-stage injector in a gas turbine engine is represented on Fig. 61.

Fuel enters the injector through tubes 1 and 2. Through tube 2 fuel is fed into the central cavity of injector housings, feeding the first stage; through tube 1 it goes to the circular space feeding the second stage of the injector.

From the central cavity fuel along three spiral grooves cut on taper stop 5 enters the swirl chamber and further enters the nozzle, drilled in nozzle plate 6. Taper stop 5 is pressed to the seat by spring 8.

From the circular space of the second stage fuel enters tangential cuts of plate 7, is swirled in the chamber and emerges through nozzle 6.

133
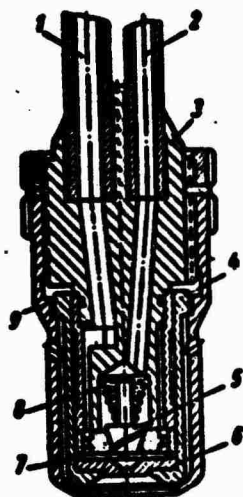
Parameters	First stage	Second stage
Diameter of nozzle d_0 in mm	1.8	
Reduced diameter of inlet d_{s5} in mm....................	0.588	0.906
Swirl arm R in mm..........	2.13	2.60
Number of inlets n.........	2	6
Geometric characteristic A.	9.55	2.0

Fig. 61. Schematic diagram of two-stage injector of a gas turbine.

Onto injector housing 3 is screwed container 9, tightening liner 4 with the housing. The container has 12 holes through which air is fed into the circular space between the container and liner 4 to remove the carbon on the injector nozzle.

Let us consider the flow of liquid in a two-stage injector.

First we consider an ideal liquid. The problem of the effect of friction on the work of a two-stage injector is examined later. The swirl arm for both stages is assumed to be identical. When the control valve is closed ($p_T \leqslant p_{TH}$) discharge coefficient μ_H and the root angle of the spray α_H are determined by the geometric characteristic of the first stage:

$$A_H = \frac{Rr_0}{n_1 r_{1H}^2}.$$ (187)

When the valve is completely open (if its drag decreases to zero), the geometric characteristic of the injector will be determined by the expression

$$A_H = \frac{Rr_0}{n_1 r_{1H}^2 + n_2 r_{2H}^2}.$$ (188)

where r_{1H} and r_{2H} — radii of entrance channels of first and second stages; n_1 and n_2 — number of entrance channels of first and second stages.

134

Since $A_\pi < A_\omega$, when the distribution valve is open discharge coefficient μ_π is larger and the root angle of the spray is less than when it is closed.

Let us consider the work of an injector in the interval of adjustment, when the control valve is open partially. We will consider that flow friction of the fuel pipes of both stages is not equal to zero. The friction of the fuel pipe of the first stage is constant, and that of the fuel pipe of the second stage, including the friction of the control valve, decreases with an increase of pressure (as the valve is opened).

Let us record the equation of energy for fuel pipes of each stage:

for the first stage

$$p_T = p_{1ex} + \frac{\rho V_{1ex}^2}{2}(1 + \xi_1); \tag{189}$$

for the second stage

$$p_T = p_{2ex} + \frac{\rho V_{2ex}^2}{2}(1 + \xi_2). \tag{190}$$

Here drag coefficients ξ_1 and ξ_2 are referred to impact pressure in entrance channels of stages (ξ_1 = const, ξ_2 changes from $\xi_2 = \infty$ for a closed valve and to $\xi_2 = 0$ for a completely open valve).

Since the entrance channels of both stages lead into the common swirl chamber, the static pressure from the channels should be identical:

$$p_{1ex} = p_{2ex} = p_{ex}.$$

Then from equations (189) and (190) we obtain

$$V_{2ex} = V_{1ex} \sqrt{\frac{1 + \xi_1}{1 + \xi_2}}. \tag{191}$$

135

Consequently, in the interval of adjustment fuel enters the swirl chamber at varying velocities; the velocity of the fuel stream in the entrance channels of the second stage is less than in the channels of the first stage. When the control valve is open ξ_2 drops off and the difference of velocities decreases.

Flows entering the swirl chamber from the entrance channels of both stages will form in the chamber a common flow whose resultant angular momentum will be determined from the equation of preservation of angular momentum:

$$V_{ar}RG_\phi = V_{1a,r}RG_1 + V_{2a,r}RG_2.$$

where V_{ar} is the resultant velocity of flow in the swirl chamber (on radius R); G_ϕ, G_1, G_2 — flow rates through injector and through each stage separately.

Hence,

$$V_{ar} = \frac{V_{1ar}G_1 + V_{2ar}G_2}{G_\phi}. \tag{192}$$

By the continuity equation

$$G_\phi = G_1 + G_2 = \pi\rho\left(n_1 r_{1ar}^2 V_{1ar} + n_2 r_{2ar}^2 V_{2ar}\right).$$

Substituting V_{2ar} from formula (191) and designating

$$\bar{r}_{ar} = \sqrt{n_1 r_{1ar}^2\left(1 + x\sqrt{\frac{1+\xi_1}{1+\xi_2}}\right)}. \tag{193}$$

where

$$x = \frac{n_2 r_{2ar}^2}{n_1 r_{1ar}^2} \tag{194}$$

is the ratio of areas of the entrance channels for the stages, we obtain

$$G_\phi = \rho\pi\bar{r}_{ar}^2 V_{1ar}. \tag{195}$$

136

Formula (192) is transformed and we obtain

$$V_{ex} = V_{1ex} \frac{1 + \varkappa \frac{1 + \xi_1}{1 + \xi_0}}{1 + \varkappa \sqrt{\frac{1 + \xi_1}{1 + \xi_0}}}.$$ (196)

Let us designate

$$\bar{R} = R \frac{1 + \varkappa \frac{1 + \xi_1}{1 + \xi_0}}{1 + \varkappa \sqrt{\frac{1 + \xi_1}{1 + \xi_0}}}.$$ (197)

Then the expression for angular momentum of a volume unit of liquid in the swirl chamber is written in the form

$$M = \rho R V_{ex} = \rho \bar{R} V_{1ex}.$$ (198)

Proceeding from equations (195) and (198) and repeating the derivation of the dependence of hydraulic parameters of a swirler (for ideal liquid) on the geometric characteristic (see § 1 Chapter III), we conclude that for a two-stage injector the role of geometric characteristic is played by $\bar{A}$:

$$\bar{A} = \frac{\bar{R}r_e}{\bar{r}_{ex}^2}.$$ (199)

Moreover the connection of discharge coefficient and root angle of spray with $\bar{A}$ remains the same as for a nonadjustable swirler. Energy losses in the control valve and swirl chamber are disregarded. These losses will be determined below.

Substituting in formula (199) the expressions for $\bar{R}$ and $\bar{r}_{ex}$, we obtain

$$\bar{A} = \varepsilon A_{II},$$ (200)

where

$$\sigma = \frac{1 + \varkappa \dfrac{1 + \xi_1}{1 + \xi_2}}{\left(1 + \varkappa \sqrt{\dfrac{1 + \xi_1}{1 + \xi_2}}\right)^2}.\tag{201}$$

Formula (200) expresses the dependence of hydraulic parameters of a two-stage injector on friction in the distribution valve (in the interval of adjustment). When the control valve is closed $\xi_2 = \infty$, then $\overline{A} = A_{\text{ж}}$; if for a completely open valve $\xi_2 = 0$, then $A = A_{\text{к}}$ (we consider that $\xi_1 = 0$).

If the entrance channels of the first stage are inclined toward the axis of the nozzle, as is done in a number of designs, the formula for determination of σ takes the form

$$\sigma = \frac{\sin\beta + \varkappa \dfrac{1 + \xi_1}{1 + \xi_2}}{\left(1 + \varkappa \sqrt{\dfrac{1 + \xi_1}{1 + \xi_2}}\right)^2}.\tag{202}$$

Moreover,

$$A_{\text{к}} = \frac{Rr_c}{n r_{\text{кн}}^2}\sin\beta,$$

where β is the angle between the direction of the entrance channel and the nozzle axis.

With the opening of the control valve its drag decreases and simultaneously characteristic $\overline{A}$ decreases; this, as was shown above, leads to an increase of the discharge coefficient and a decrease of the root angle of the spray.

Adjustment of the discharge coefficient (and as a result, the root angle of the spray) occurs in a two-stage injector as a result of a change in the relationship of flow velocities of fuel in the entrance channels of both stages (when $p_T \leqslant p_{T\text{н}}$, $\dfrac{V_{\text{вн}}}{V_{\text{нар}}} = \infty$; when $p_T \geqslant p_{T\text{н}}$ $\dfrac{V_{\text{вн}}}{V_{\text{нар}}} \approx 1$).

Finding the overall flow rate through the injector, it is simple to determine the flow rate through each stage separately:

$$G_1 = \frac{G_\phi}{1 + \varkappa \sqrt{\frac{1+\xi_1}{1+\xi_2}}}.$$

(203)

and

$$G_2 = \frac{\varkappa \sqrt{\frac{1+\xi_1}{1+\xi_2}}}{1 + \varkappa \sqrt{\frac{1+\xi_1}{1+\xi_2}}} G_\phi.$$

(204)

During the design of a two-stage injector energy losses are disregarded. Now let us turn to a determination of their magnitude.

Total energy losses specific for a two-stage injector are composed of the two components of losses in the control valve and losses when the streams of both stages mix in the swirl chamber.

The loss of energy in the control valve per second composes

$$\Delta E_\varkappa = G_1 \xi_{k2} \frac{v_{2\varkappa}^2}{2}.$$

(205)

Let us refer $\Delta E_\varkappa$ to the initial energy reserve of the flow going through the injector:

$$E_0 = \frac{G_\phi}{\rho} p_T.$$

(206)

Then, using equations (189), (190) and the continuity equation, we obtain after transformation[4]

$$\frac{\Delta E_\varkappa}{E_0} = \frac{p_T - p_{\varkappa\varkappa}}{p_T} \frac{\xi_\varkappa \varkappa}{(1+\xi_2)(\varkappa + \sqrt{1+\xi_1})}.$$

The mixing of the streams of fuel of both stages, entering the swirl chamber at various velocities, is connected with losses of energy. From the assumption that the mixing of flows occurs at constant pressure, it follows that energy losses are equal to the

139

difference of kinetic energies of the streams before and after mixing. Determining the flow velocity after mixing by formula (192), we find the loss of energy per second during mixing:

$$\Delta E_c = \frac{1}{2} \cdot \frac{G_1 G_2}{G_1 + G_2} (V_{1\infty} - V_{2\infty})^2.$$

Referring ΔE_c to the initial reserve of flow energy, we obtain with the help of the continuity equation and equations (189), (190) and (191):

$$\frac{\Delta E_c}{E_0} = \frac{p_T - p_{oc}}{p_T} \frac{\varkappa(\sqrt{1+\xi_2}-1)^2}{\sqrt{1+\xi_2}(\varkappa+\sqrt{1+\xi_2})^2}.$$

Let us determine $\dfrac{p_T - p_{oc}}{p_T}$.

Using equations (189) and (190) and the equation of flow rate in the form

$$G_\phi = G_1 + G_2 = \pi r_{cl}^2 \mu \sqrt{2\rho p_T}.$$

we obtain after transformations

$$\frac{p_T - p_{oc}}{p_T} = \mu^2 \frac{r_c^2(1+\xi_2)}{a_1 r_{1\infty}^2(\varkappa + \sqrt{1+\xi_2})^2}.$$

We will express the discharge coefficient by $\overline{A}$ according to the approximation formula (145):

$$\mu = \frac{A}{\overline{A}^m}.$$

where $\overline{A}$ is determined by formula (200), in which we assume that $\xi_1 = 0$. Then

$$\frac{p_T - p_{oc}}{p_T} = \frac{A^2 r_c^{2(2-m)}(1+\xi_2)(\varkappa + \sqrt{1+\xi_2})^{2(2m-1)}}{R^{2m} a_1^{2(1-m)} r_{1\infty}^{4(1-m)}(\varkappa + 1 + \xi_2)^{2m}}.$$

Total energy loss referred to the initial reserve of energy in the flow:

$$\frac{\Delta E}{E_0} = \frac{\Delta E_b + \Delta E_c}{E_0} = \frac{k^3 x r_c^{2(2-m)}(1+\xi_2)(x+\sqrt{1+\xi_2})^{4m-3}}{R^{2m} n_1^{2(1-m)} r_{3az}^{4(1-m)}(x+1+\xi_2)^2} \times$$

$$\times \left(\frac{\xi_2}{1+\xi_2} + \frac{(\sqrt{1+\xi_2}-1)^2}{\sqrt{1+\xi_2}(x+\sqrt{1+\xi_2})} \right). \tag{207}$$

From equation (207) it follows that at a certain value of ξ_2 the relative energy losses reach maximum. Designating

$$\sqrt{1+\xi_2} = x, \tag{208}$$

we transform equation (207):

$$\frac{\Delta E}{E_0} = \frac{k^2 x r_c^{2(2-m)}}{R^{2m} n_1^{2(1-m)} r_{3az}^{4(1-m)}} \frac{2x^3 + (x-2)x^2 - x}{(x^2+x)^{2m}(x+x)^{4(1-m)}}. \tag{209}$$

Differentiating equation (209) with respect to x and equating the derivative to zero, we obtain the equation determining the value of x*, for which losses of energy are maximum. This equation has the form

$$x^2 x + x^2[x^2(1-m) + x^3(3+m) - x(2-m) + m - 1] =$$
$$= x^3 - x x^2[x^2(3-4m) + 3x(2m-1) - 1 - 2m]. \tag{210}$$

Solving graphically equation (210) for different values of κ, we find x* and further from equation (209) the maximum losses of energy. When $\kappa = 4, 6, 8, 10$ we have accordingly x* = 5.1, 7.1, 9.0, 10.75 (k = 0.441, m = 0.67)

and

$$\left(\frac{\Delta E}{E_0} \right)_{max} = \tau_\kappa \frac{r_c^{2.66}}{R^{1.34} n_1^{0.66} r_{3az}^{1.32}}, \tag{211}$$

where

$$\tau_\kappa = \frac{x[2x^{*3} + (x-2)x^{*2} - x]}{(x^{*2}+x)^{1.34}(x^*+x)^{1.32}}.$$

Here $\tau_{\kappa=4} = 0.139$; $\tau_{\kappa=6} = 0.158$; $\tau_{\kappa=8} = 0.173$; $\tau_{\kappa=10} = 0.185$.

For two-stage injectors used in practice the coefficient of τ_κ does not exceed one. Consequently, maximum energy losses (for a wide range of values of κ) do not exceed 15-20% of the initial reserve of energy. For other relationships between fuel flow rate through the first and second stages energy losses will be less.

Thus, error from disregarding energy losses is comparatively small and is permissible in engineering calculation of flow rate and root angle of spray.

However, one should consider that energy losses lead to deceleration of the outflow, as a consequence of which when the second stage is cut in, the quality of atomization deteriorates.

In the swirl chamber of a two-stage injector imperfection of the mixing of the fuel streams from both stages also leads to impairment of the quality of atomization.

This circumstance should be related to the deficiencies of two-stage injectors.

Above the effect of fuel viscosity on the work of the first stage of a two-stage injector was noted (prior to opening of control valve). The increase of discharge coefficient induced by friction does not permit obtaining small absolute values of flow rate in a two-stage injector, and, consequently, narrows the control range of productivity of the injector (especially when using viscous fuels).

Using formulas (195), (198), (200), it is easy to show (see § 4 Chapter III) that in the adjustment interval the equivalent characteristic of a two-stage injector is expressed by the formula

$$\bar{\lambda}_s = \frac{\sigma A_u}{1 + \frac{\lambda}{2}\sigma\left(\frac{B_n^2}{R_1} - A_u\right)}, \tag{212}$$

where $B_u = \frac{R}{r_{ux}}$, $\sigma -$ is determined by formula (201), and the coefficient of friction λ is a certain function of the Re number

142

(Fig. 41).

Let us turn to determination of the Re number for two-stage injectors.

As the characteristic dimension (in the adjustment interval) we take the mean arithmetical value of the diameter of the entrance channels of the individual stages:

$$d_{\scriptscriptstyle{ex}} = \frac{n_1 d_{1ex} + n_2 d_{2ex}}{n_1 + n_2}.$$ (213)

The resultant flow velocity on the swirl chamber entrance is determined by formula (196). Substituting in it the value of $V_{1\,ex.}$ expressed through the mass flow rate of the first stage, and replacing G_1 from expression (203) by G_ϕ, we obtain

$$V_{ex} = \frac{4 G_\phi}{n_1 \pi d_{1ex}^2 \rho}.$$

Then the expression for Re number will take the form

$$\mathrm{Re} = \frac{d_{ex} V_{ex}}{\nu} = \frac{4 G_\phi (n_1 d_{1ex} + n_2 d_{2ex})}{\pi n_1 d_{1ex}^2 (n_1 + n_2) \nu}.$$ (214)

Determining the Re number, we find by the curve on Fig. 41, the value of coefficient of friction λ and then by formula (212) the equivalent characteristic, by which we will calculate the hydraulic parameters of a two-stage injector.

The flow rate of a two-stage injector in the adjustment interval depends on the law by which the relationship of pressures in front of the injector stages changes. This law is given by the characteristics of the control valve.

On Fig. 62 are given the flow rate curves of an experimental two-stage injector for three transition modes (first stage of injector has two tangential channels of rectangular cross section 0.355 × 1.015 mm, the second stage has six tangential channels 1.05 × 1.015 mm; radius of swirl arm R_1 = 2.62 and R_2 = 2.65 mm respectively for each stage;
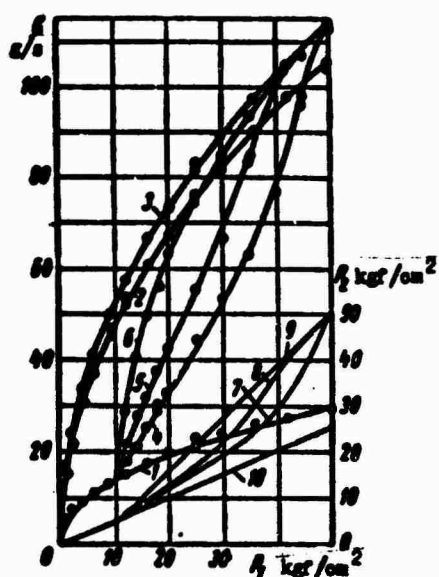
143

Fig. 62. Flow rate curves
of an experimental two-
stage injector: 1 — first
stage; 2 — second stage;
3 — both stages during
joint operation with
identical pressure; 4,
5 and 6 — transition
mode with change of
pressure in front of
second stage according
to curves 7, 8 and 9
respectively; 10 —
dependence of pressure
before second stage on
pressure before first
stage for a closed
control valve.

diameter of nozzle hole d_c = 2.12 mm). The same figure shows how
pressure before the second stage changes for a closed control valve
and for three transition modes. In all three cases the valve starts
to open at 10 kgf/cm^2, and is completely opened at 50 kgf/cm^2. In
the pressure interval from 3 to 50 kgf/cm^2 flow rate increases
15.2 times. Figure 62 also shows curves expressing the dependence
of flow rate on feed pressure for separate stages and for joint
operation of both stages with identical pressure before them.

The fact that the total flow rate through the injector (at
identical pressure before the stages) is less than the sum of flow
rates through the separate stages attracts our attention. This
result becomes understandable if we consider that the geometric
characteristic of the injector during joint operation of both stages
differs little from the characteristic of the second stage, for which
A = 1.38 (for joint operation of both stages A = 1.22) and
consequently, flow rates through the injector in these cases are close
to one another.

On transition modes depending upon the relationship of pressures
before the stages any kind of a flow rate can be obtained in accordance
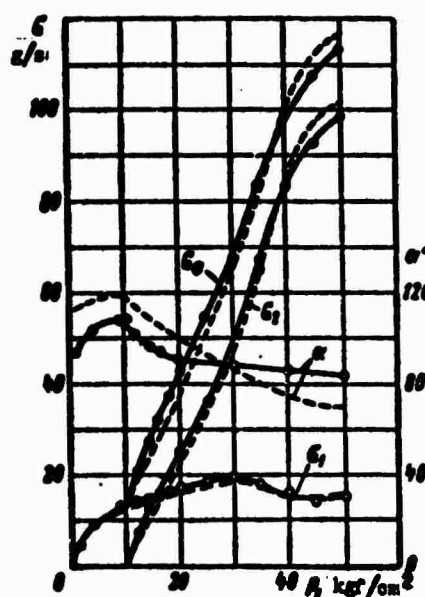with requirements on the adjustment of an engine and on the combustion
process.

Fig. 63. Dependence of flow rate and angle of spray on pressure for an experimental two-stage injector on transition modes: $\bullet$— flow rate through injector; G_1 — flow rate through first stage; G_2 — flow rate through second stage; α — angle of spray.

On Fig. 63 are given curves expressing the dependence of flow rate through injector and through each stage on feed pressure for a change of pressure before the second stage according to curve 5 on Fig. 62. Broken lines show calculated dependences, where it is accepted that the coefficient of contraction of the flow in the entrance channels of both stages is identical and equal to 0.90.

On the same figure are given comparative experimental and computed values of the root angle of spray.

As we see, for both flow rate and root angle of spray satisfactory agreement of calculated and experimental data is obtained. A similar result is obtained for other dependences $p_2 = f(p_1)$.

Flow rate through the first stage as the control valve opens at first increases, and then, passing through maximum, starts to decrease. This occurs because after the control valve is opened, pressure in the swirl chamber increases as compared to pressure during the operation of only the first stage (at the same feed pressure). The larger the cross section of the valve, the less the difference between pressure before the first stage and pressure in the swirl chamber, which also leads to a decrease of flow rate through this stage.

145

An essential deficiency of two-stage injectors observed during their joint operation on the header is the great irregularity in flow rates through separate injectors at pressures somewhat exceeding the pressure of opening the control valve. This irregularity is mainly due to the fact that for an insignificant difference in flow friction of the fuel duct of the first stage of separate injectors[5] pressure in the swirl chamber of these injectors will be different, and this causes an overflowing of fuel from one injector into the other when the control valve is closed and a great difference in flow rates through the second stage when the control valve is open.

Experiment shows that if in one of the injectors the fuel pipe drag of the first stage is increased (by putting a jet in it), when the control valve is opened the flow rate through this injector sharply increases (as compared to the flow rate through other injectors). The increase of flow rate is explained by the fact that in the swirl chamber this injector pressure turns out to be smaller than in the other, and the flow rate of fuel through channels of the second stage of the examined injector strongly increases.

This conclusion is confirmed by analysis of formula (200). Let us assume that the drag coefficient of the first stage of one of the injectors is equal to inifnity (channels of this stage are contaminated). Then from formula (200) it follows that $\bar{A}$ for this injector will be equal to the geometric characteristic of the second stage.

But since the geometric characteristic of the second stage is considerably less than the geometric characteristic of the first stage, the discharge coefficient essentially increases and there appears a considerable irregularity in flow rate through the separate injectors of the header.

An essential influence on irregularity in fuel flow rate through two-stage injectors is rendered also by the distinction in magnitude of the swirl arm for entrance channels of the first stage of separate injectors, since the pressure established in the swirl chamber depends on the magnitude of the swirl arm.

146

As follows from analysis of curves shown in Fig. 62, at pressures close to the pressure of switching in the second stage a small change of the difference of pressures before this stage and in the swirl chamber causes a considerable change in the flow rate of fuel through the injector.

Therefore two-stage injectors should be completed with an eye to the "counterpressure" in the swirl chamber, i.e., according to pressure in the fuel pipe of the second stage, when fuel is fed only into the first stage at a fixed pressure.

To decrease irregularity in flow rate so-called dual-chamber injectors are used, which are a variation of two-stage injectors. In the swirl chamber of these injectors is a diaphragm dividing the chamber into two cavities, one of which receives fuel from the first stage, and the other from the second. The flows are mixed in the injector nozzle and partially in the cavity of the first stage.

Since static pressure decreases as the axis of the swirl chamber is approached, then thanks to the diaphragm the change of pressure in the first stage more weakly affects pressure in the second stage than in a two-stage injector. Therefore the quantity of fuel overflowing from one injector into the other is considerably reduced, and thereby the fitting selection of injectors to a header is facilitated.

Uniformity of fuel distribution to the separate injectors is improved in dual-chamber injectors at the expense of a certain deterioration of the quality of atomization when the second stage is switched in, since in a dual-chamber injector the flows of both stages are mixed at high flow velocities and therefore it is accompanied by greater losses of energy than in the two-stage injectors. Furthermore, the mixing becomes less complete. These circumstances lead to a deterioration of the atomization when the second stage of a dual-chamber injector is switched in.

In quality of atomization dual-chamber injectors borrow a middle position between two-stage and two-nozzle injectors.

The study of hydraulic characteristics of dual-chamber injectors is the subject of a work by L. V. Kulagin [4].

§ 5. Adjustable Injector with Fuel Bypass

Of the examined adjustable injectors the greatest range of flow rates belongs to two-nozzle injector. Injectors with adjustable discharge coefficient ensure a somewhat smaller range of flow rates, since when flow rate is reduced the friction of the fuel on the swirl chamber wall does not permit obtaining the required small discharge coefficients. With decrease of the flow rate the coefficient of friction increases.

At the same time further expansion of the range of flow rates through two-nozzle injectors is limited not only by the effect of friction, but also by the fact that when the flow rate through the internal nozzle is reduced (by decreasing its diameter) the quality of atomization has impermissably deteriorated when the external nozzle is switched in.

However, in certain cases it is necessary to create adjustable injectors which can with satisfactory atomization in the whole flow rate range ensure smaller minimum flow rates than the injector examined above.

These requirements apparently can be satisfied by adjustable spill-type swirl fuel atomizers.

The schematic diagram of such an injector is shown in Fig. 64. The transfer valve is arranged in such a way that its cross section starts to decrease as valve pressure increases from p_{rn} to p_{rn_0} at which the cross section is zero (valve is closed). On conditions at which the transfer valve is open, only part of the fuel entering the injector is injected through the nozzle into the surrounding medium; the remaining fuel bypasses to the pump intake. The greater

148

the quantity of bypassed fuel (at a given pressure before the injector), the less the fuel flow rate through the nozzle and the bigger the root angle of the spray.
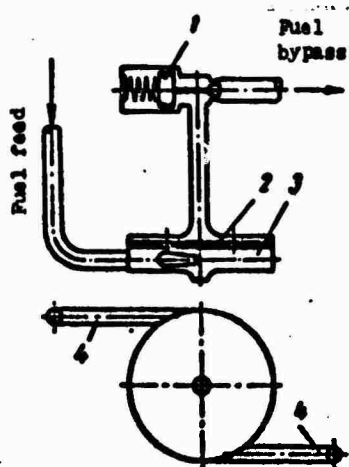

Fig. 64. Schematic diagram of injector with fuel bypass: 1 — bypass valve; 2 — bypass washer; 3 — nozzle hole; 4 — tangential channels.

At low feed pressures, while the cross section of the valve is constant, the discharge coefficient of the nozzle has a small constant value. With growth of pressure the valve cross section decreases, and the quantity of bypassed fuel drops. The discharge coefficient increases and attains maximum when the quantity of bypassed fuel is equal to zero (valve is closed).

Dependence of discharge coefficient of nozzle and root angle of spray on the quantity of bypassed fuel is determined by the change of initial angular momentum in the swirl chamber. The greater the flow rate of bypassing fuel, the greater the angular momentum on the swirl chamber entrance, and consequently, the less the discharge coefficient of the nozzle.

Since at low flow rates through the nozzle the overall flow rate through the swirl chamber is relatively great, fuel friction on the chamber wall has a considerably weaker effect on hydraulics of an injector with fuel bypass than on hydraulics of adjustable injectors of other types. Thanks to this, in an injector with bypass very small discharge coefficients can be obtained.

149

It is necessary to stress that adjustment of flow rate through a nozzle by means of fuel bypass can be carried out only in injectors of the centrifugal type, whose hydraulic parameters depend on the angular momentum on the swirl chamber entrance. In the case of jet injectors the quantity of bypassing fuel does not essentially influence the flow rate through the nozzle (at a given feed pressure).

Let us find the connection between flow rate of fuel through the nozzle and flow rate of bypassing fuel.

The flow rate of fuel through the nozzle hole of an injector can be represented in the form

$$G_e = \pi r_e^2 \mu \sqrt{2\rho p_T}. \tag{215}$$

For a closed transfer valve the discharge coefficient of the nozzle (for an ideal liquid) is determined by the geometric characteristic of the injector

$$A_0 = \frac{R r_e}{i \, r_{ca}^2}. \tag{216}$$

In the case of fuel bypass the discharge coefficient depends no longer only on the geometric characteristic, but also on the flow rate of the bypassing fuel.

Let us express flow rate through the nozzle in the following way (see § 1 Chapter III):

$$G_e = \pi r_e^2 \rho \varphi w, \tag{217}$$

where ϕ — space factor; w — axial component of velocity in nozzle.

We determine w from the equation of energy

$$w = \sqrt{\frac{2}{\rho} p_T - u_m^2}.$$

where u_m — value of peripheral component of velocity on the air vortex boundary (at $r = r_m$).

For an ideal liquid the law of conservation of momentum holds in the case of fuel bypass. Then the velocity of liquid on the swirl chamber entrance can be expressed through the resultant flow rate:

$$V_{ac} = \frac{a_\phi}{\mu a x_{ac}^2}.$$

(218)

The resultant flow rate through the injector is composed of the flow rate through nozzle G_c and the flow rate of bypassing fuel G_u:

$$G_\phi = G_c + G_u.$$

We introduce coefficient η from the condition that

$$G_\phi = \eta G_c = \eta \pi r_c^2 \mu \sqrt{2\rho p_r}.$$

(219)

Obviously

$$\eta = 1 + \frac{a_u}{a_c} = \frac{a_\phi}{a_c}.$$

(220)

Coefficient $\eta \geq 1$ shows how many times the resultant flow rate through the injector exceeds the flow rate through the nozzle. Let us call it the coefficient of multiplicity. If the flow rate of bypassing fuel is equal to zero, then $\eta = 1$.

Replacing G_ϕ by its expression from formula (219), we obtain

$$u_m = \frac{\eta \mu R r_c^2}{a_m r_{ac}^2} \sqrt{\frac{2}{\rho} p_r}$$

Substituting u_m in the formula determining w, we find

$$w = \sqrt{\left(1 - \frac{\eta^2 \mu^2 R^2 r_c^4}{a^2 r_m^2 r_{ac}^2}\right) \frac{2}{\rho} p_r}.$$

Then equation (217) will take the form

$$G_c = \pi r_c^2 \phi \sqrt{\left(1 - \frac{\mu^2 \eta^2 A_0^2}{1 - \phi}\right) 2 \phi p_r}.$$

151

Comparing the obtained expression for G_c with expression (215), we have

$$\mu = \varphi \sqrt{1 - \frac{\eta^2 \mu^2 A_0^2}{1 - \varphi}}.$$

Solving this equation with respect to the discharge coefficient, we obtain

$$\mu = \frac{1}{\sqrt{\frac{1}{\varphi^2} + \frac{\eta^2 A_0^2}{1 - \varphi}}}. \tag{221}$$

The formula of the discharge coefficient for an injector with bypass differs from the corresponding formula for a simple swirler (see § 1 Chapter III) in the replacement of geometric characteristic A_0 by the product ηA_0.

The connection between the space factor of the nozzle ϕ and the product ηA_0 is found by using the principle of maximum flow rate, according to which in the injector an air vortex of such dimensions is established that the flow rate at a given pressure is maximum (at a fixed flow rate of bypassing fuel), i.e., $d\mu/d\phi = 0$.

Analysis shows that the coefficient of multiplicity depends on ϕ, but at values of ϕ corresponding to maximum flow rate, the change of η is so small that it can be disregarded.

Then it is clear that the dependence of discharge coefficient on the product ηA_0 (we will call this product the effective characteristic of an injector with bypass) has the same form as the dependence of μ on A_0 for a simple swirler.

A similar result can also be obtained for the root angle of the spray.

Thus, the hydraulic parameters of a spill-type swirl fuel atomizer are determined (for an ideal liquid) by the effective characteristic $A = \eta A_0$.

152

As the coefficient of multiplicity increases, the discharge coefficient of the nozzle decreases, and the root angle of the spray increases.

As essential advantage of an injector with bypass over those examined above is that in connection with the high flow velocities in the swirl chamber, the effect of friction (for correct arrangement of the fuel bypass) can be minimized, which is especially important at low flow rates of fuel.

In order to clarify how the shape of the bypass disk influences hydraulics of the injector, we will examine the results of tests on an experimental injector with different bypass disks. Figure 65 shows an injector and three disks. Fuel is fed into the swirl chamber
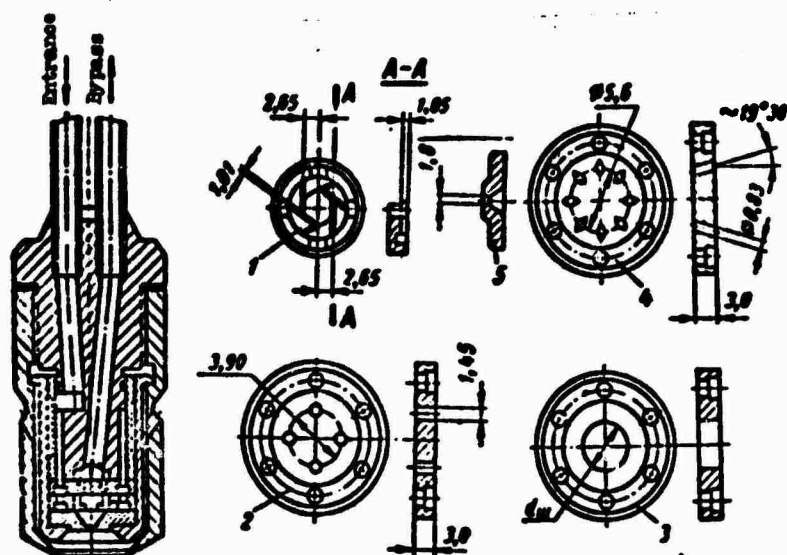
Fig. 65. Experimental injector with bypass (BI): 1 — swirl vane; 2, 3 and 4 — bypass disks; 5 — nozzle.

through six tangential channels of rectangular cross section (1.06 × 1.015 mm) with swirl arm R = 2.65 mm. From the swirl chamber part of the fuel enters the nozzle (d_c = 1.80 mm), and the remaining fuel bypasses through holes in the disk and regulating cock back into the tank. The injector has the following characteristics: A_0 = 1.17; B_0 = 4.55; C_0 = 2.94.

153

Disk 2 has four holes equispaced on a circumference 3.90 mm in diameter. In disk 4 the bypass is on the periphery of the swirl chambers through eight slanted holes. Disk 3 has one central hole.

The resultant areas of the bypass holes are given in Table 3.

Table 3.

Parameters	Disk (Fig. 65)					
	2	3				4
Diameter of hole d_m in mm	1.45	2.03	3.05	4.5	6.65	0.83
Overall area of holes F_m in mm^2	6.7	3.23	7.3	15.9	34.7	4.38

Flow rate curves for an injector with different disks when the cock is closed are shown in Fig. 66. The flow rate for an ideal liquid (μ_{us} = 0.40) is also shown.
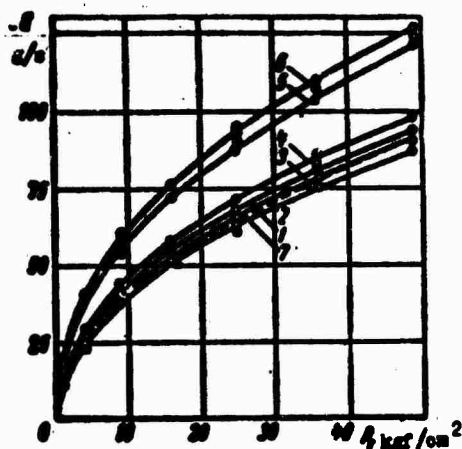
Fig. 66. Flow rate curves for a bypass injector with various bypass disks when the bypass cock is closed. 1 — with disk 2; 2 — with disk 4; 3, 4, 5 and 6 — with disk 3 at d_m = 2.03, 3.05, 4.50 and 6.65 mm respectively; 7 — rated curve for an ideal liquid.

Since the complex $(B_0^2/n) - A_0$ for a bypass injector is 2.28 in all, the flow rate through the injector should be close to the rated in the case of an ideal liquid, if the height of the swirl chamber insignificantly exceeds the height of the entrance channels.

Actually, the flow rates of an injector with disks 2 and 4 and disk 3 when the diameter of its hole d_m = 2.03 mm, are close to that

154

for an ideal liquid. At the same time the flow rate of fuel through
an injector with disk 3 increases as the diameter of the hole in
the disk increases. An especially intense growth of flow rate is
observed at $d_{w} = 4.50$ and 6.65 mm. The fact is that as the diameter
of the hole in the disk increases, the liquid filling the cavity
behind the disk has an even greater influence on the flow. An
increase of the diameter of the hole in the disk, as it were,
increases the height of the swirl chamber, which leads to an increase
of the flow rate.

The drag of the disks was determined by testing an injector
with a plugged nozzle. In these conditions the flow rate through the
injector is equal to the flow rate of the bypassing fuel. The change
of flow rate through the injector (plugged nozzle) depending upon
bypass pressure (i.e., pressure in front of bypass channel) at
constant pressure in front of the injector $p_{T} = 30$ kgf/cm^2 is
represented on Fig. 67.
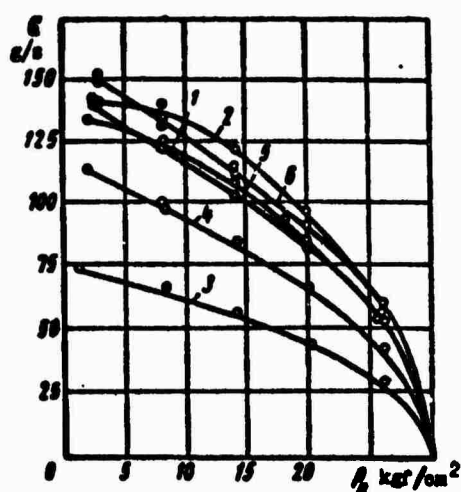
Fig. 67. Dependence of
flow rate through injector
on bypass pressure with a
plugged nozzle $p_{T} = 30$
kgf/cm^2): 1 — with disk 2;
2 — with disk 4; 3, 4, 5,
6 — with disk 3 at $d_{w} = 2.03$,
3.05, 4.50 and 6.65 mm
respectively.

The less the flow rate at a given bypass pressure, the greater
the drag of the disk. In order of growth the drags of the disk
are plotted in the following way; disk 4, disk 3 with $d_{w} = 6.65$, disk
2, disk 3 with $d_{w} = 4.5$, 3.05, 2.03 mm.

The drag of the bypass disk does not directly agree with the
area of the bypass holes. Thus, for example, disk 4 has the least

155

drag, although all remaining disks (with the exception of disk 3 with $d_w = 2.03$ mm) have a large passage area. This phenomenon is explained by the fact that the swirl energy of the flow through the bypass disk is lost either in the disk itself or further in the bypass pipeline.

Near the axis of the chamber the swirl velocity increases (for an ideal liquid in inverse proportion to the radius).

In disk 4 fuel bypasses to the periphery of the chamber and, consequently, losses on flow swirling are minimum. In disk 2 these losses are large, but also comparatively small. Since through disk 3 fuel bypasses with large peripheral components of velocity, the losses in it are the greatest.

Thus, to decrease the drag it is advisable to have the fuel bypass on the periphery of the swirl chamber.

Flow rate for a closed and completely open bypass valve with various bypass disks at constant pressure in front of the injector $p_T = 30$ kgf/cm^2 are given in Table 4.

Table 4.

Parameters	Disk (Fig. 65)					
	2	3				4
Diameters of hole d_w in mm . .	1,45	2,03	3,05	4,5	6,65	0,83
Flow rate of fuel in g/s $G_{c\,min}$	3,6	36,7	5,5	4,2	16,15	8,15
$G_{c\,max}$	74	71	76,5	95	100	69
$\dfrac{G_{c\,max}}{G_{c\,min}}$	20,55	1,94	13,93	22,6	6,2	8,47

The greatest range of change of the flow rate is ensured by using disk 2 and disk 3 with $d_w = 4.50$ mm. For disk 3 a greater range of flow rate than prior to disk 2 is obtained due to the greater value of $G_{c\,max}$, whereas $G_{c\,min}$ is less for disk 2.

156

The relatively small range of flow rate for disk 4 and disk 3 with $d_w = 6.65$ mm is caused by the increase of flow rate through the nozzle when the cock is completely open in connection with the effect of friction. Since in disk 4 fuel bypasses on the periphery, the mean free path of the liquid particles entering the nozzle is increased (due to the decrease of radial velocities), and the angular momentum of these particles decreases, which leads to an increase of flow rate when the cock is open. For disk 3 with $d_w = 6.65$ mm the increase of flow rate through the nozzle is connected with the great height of the swirl chamber.

For disk 3 with $d_w = 2.03$ and 3.05 mm the range of flow rate decreases due to the reduced flow rate of the bypassing fuel (large drag of disk).

As was noted, to decrease drag it is advisable to bypass fuel on the periphery of the swirl chamber. However, the effect of friction on the flow entering the nozzle is increased, causing an increase of flow rate through the nozzle.

Apparently, bypassing fuel through a series of holes or a circular slot on the radius is optimum, on the average between $r = 0$ and $r = R_w$ (R_w — radius of swirl chamber). These requirements are satisfied, for example by disk 2.

On Fig. 68 are shown the flow rate curves for a bypass injector with disk 2 for three laws of change of bypass pressure depending upon pressure before the injector. Corresponding dependences of bypass pressure on pressure before the injector are shown in the same figure. In all three cases the bypass cock at a pressure not exceeding $p_T = 10$ kgf/cm^2 is open completely, starts to close as pressure increases, and at $p_T = 50$ kgf/cm^2 is closed.

As can be seen, an injector with disk 2 possesses a sufficiently great range of flow rates. Thus, in the interval from $p_T = 3$ to $p_T = 50$ kgf/cm^2 the flow rate through the nozzle changes from $G_c = 1.1$ to $G_c = 95$ g/s, i.e., by 86.5 times. For nonadjustable
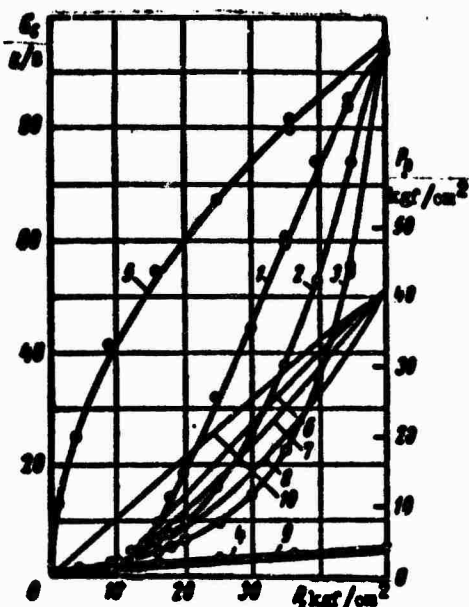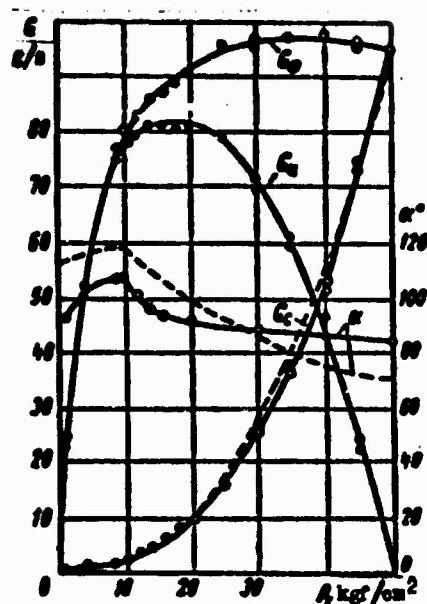
157

Fig. 68.   Fig. 69.

Fig. 68. Flow rate curves of a bypass injector with
disk 2 on transition mode: 1, 2, 3 — flow rate
through nozzle on transition mode when bypass pressure
changes according to curves 7, 8 respectively; 4, 5 —
flow rate through nozzle for a completely open and
closed cock respectively; 9, 10 — pressure before
bypass cock for completely open and closed cock
respectively.

Fig. 69. Dependence of flow rate and angle of spray
on pressure in the operation of a bypass injector on
the transition mode: G_c — flow rate through nozzle;
G_ϕ — flow rate through injector; G_q — flow rate of
bypassing fuel; α — angle of spray.

injectors in the shown interval of pressures flow rate is changed
in all by 4.1 times.

Dependences of flow rate through the nozzle G_c, flow rate of
bypassing fuel G_q and resultant flow rate through the injector G_ϕ,
and also the root angle of the spray on pressure before the injector
when bypass pressure changes according to curve 7 (see Fig. 68), are
represented on Fig. 69.

For low flow rates through the nozzle (bypass cock is open)
the coefficient of multiplicity reaches 50, but then as the drag
of the cock increases, it drops rapidly.

158

Broken lines on Fig. 69 correspond to computed values of flow rate through the nozzle G_c and the root angle of the spray. Calculation with respect to the effective characteristic satisfactorily agrees with experimental data. An analogous result is obtained for other dependences $p_a = f(p_T)$.

Satisfactory agreement of experimental and calculated values of the discharge coefficient of the nozzle and root angle of the spray is obtained when the flow rate of the bypass injector for a closed bypass cock (valve) is close to that for an ideal liquid.

Otherwise it is necessary to introduce corrections to the effect of liquid viscosity on hydraulic parameters of the injector. Certain experimental data referred to this question are contained in a work by S. L. Briskin [2].

A basic deficiency of injectors with bypass is the necessity of much circulation of fuel through the injector (on low flow rates circulation of fuel through the injector exceeds flow rate through the nozzle by tens of times).

However, in spite of this deficiency, a fuel system using bypass injectors has been designed which satisfies the requirements of aviation gas turbine engines [7].

§ 6.   Two-Component Centrifugal Injectors (Swirlers)

Two-component swirlers are injectors intended for mixing and atomization of two different liquids (for example, fuel and oxidizer in liquid-propellant rocket engines).

We distinguish two-component injectors with external and internal mixing. Injectors with internal mixing of components are sometimes called air-boost injectors.

Furthermore, there exist designs of two-component injectors in which liquids are mixed in the injector nozzle.

159

Schematic diagrams of two-component injectors with external and internal mixing differ accordingly from two-nozzle and two-stage injectors (see Fig. 52 and 60) only in the absence of a regulating valve.

A two-component nozzle with external mixing is designed in the same way as a two-nozzle injector with the only difference being that the difference in density of components must be considered.

Calculation of a two-component air-boost system, although in many respects analogous to calculation of a two-stage injector, still deserves independent consideration.

Let us conduct this consideration in reference to the air-boost systems of liquid-fuel rocket engines.

We will consider the oxidizer and fuel as ideal liquids. At values of the Reynolds criterion characteristic for injectors of a liquid-fuel rocket engine this assumption is fully permissible.

In the swirl chamber of an air-boost system the oxidizer proceeds along tangential channels $d_{вхо}$ and fuel along channels of diameter $d_{вхг}$ located on swirl radius R. The number of channels of oxidizer and fuel are designated accordingly n_o and $n_г$.

We assume for simplicity of calculation that oxidizer and fuel are fed into the injector under an identical pressure drop.

Then from the Bernoulli equation for flow in inlet channels we have

$$p_T = p_{вхо} + \frac{\rho_o V^2_{вхо}}{2} = p_{вхг} + \frac{\rho_г V^2_{вхг}}{2}. \tag{222}$$

Since entrance channels for both components lead into a general swirl chamber, then $p_{вхо} = p_{вхг}$.

160

Then from equation (222) we obtain

$$V_{a,u} = \sqrt{m}\, V_{a,uo}$$ (223)

where $m = \dfrac{\rho_o}{\rho_e}$ — density ratio of oxidizer and fuel.

The ratio of flow rates of oxidizer and fuel, as can be easily shown, will be determined from the expression

$$k = \frac{G_o}{G_e} = \sqrt{m}\, \frac{n_o f_{axo}^2}{n_e f_{axe}^2}.$$ (224)

Hence by the rated value of k, selecting beforehand the number of channels of oxidizer and fuel, we find the ratio of their diameters.

The resultant flow rate through the injector is equal to the sum of flow rates of components of the mixture

$$G_1 = G_o + G_e = \frac{k+1}{k}\, G_o = \frac{k+1}{k}\, n_o \pi r_{ax}^2 \rho_o V_{axo}$$

or, designating

$$\bar{r}_{a,u} = r_{axo}\sqrt{\frac{k+1}{k}},$$ (225)

we obtain

$$G_1 = n_o \pi \bar{r}_{ax}^2 \rho_o V_{axo}.$$ (226)

Streams of oxidizer and fuel are mixed in the swirl chamber of the injector and will form a general emulsion flow whose resultant angular momentum will be determined from the equation of conservation

$$G_1 R V_{a1} = G_o R V_{a,uo} + G_e R V_{a,ue}.$$

Consequently, the resultant velocity of swirling the emulsion flow on radius R will be

$$V_{a1} = \frac{V_{a,uo}\rho_o + V_{a,ue}\rho_e}{G_1} = V_{a,uo}\, \frac{k + \sqrt{m}}{k+1}.$$ (227)

Let us designate

$$\overline{R} = R \frac{k + \sqrt{m}}{k+1}. \tag{228}$$

Then the angular momentum for a volume unit of emulsion in the swirl chamber will be written in the form

$$M = \rho R V_{ur} = \rho \overline{R} V_{o,xo}. \tag{229}$$

where ρ — emulsion density:

$$\rho = \rho_o \frac{k+1}{k+m}. \tag{230}$$

As calculation shows, energy losses in mixing oxidizer and fuel are small and can be completely disregarded. Then, using formulas (226) and (229) and repeating the derivation of the fundamental equations for a simple swirler (see § 3 Chapter III), we conclude that hydraulic parameters of the air-boost system (discharge coefficient μ, space factor of nozzle ϕ, root angle of spray α) are determined by

$$\overline{A} = \frac{k(k + \sqrt{m})}{(k+1)(k+m)} \cdot \frac{R r_e}{n_e r_{exo}^2}. \tag{231}$$

The dependence of μ, ϕ and α on $\overline{A}$ remains the same as the dependence of these parameters on geometric characteristic A for a simple swirler.

The resultant flow rate through an air-boost system is determined by the usual formula

$$G_1 = \pi r_{e\mu}^2 \sqrt{2 \phi \rho_T}. \tag{232}$$

In the case of air-boost systems with large nozzle "opening," i.e., injectors for which $C = \frac{R}{r_e} < 3$, calculation must include a correction for energy losses in entrance channels (see § 5 Chapter III).

162

Literature

1. Alekseyev A. V. i Kondak N. M. Tsentrobezhnyye forsunki gazoturbinnykh dvigateley (Swirlers of gas turbine engines). Gostekhizdat, USSR, 1958.

2. Briskin S. L. K opredeleniyu koeffitsienta raskhoda tsentrobezhnykh forsunok s obratnym slivom (Determination of the discharge coefficient of swirlers with reverse overflow). "Teplo-energetika", 1963, No. 10.

3. Vitman L. A., Katsnel'son B. D. i Paleyev I. I. Raspylivaniye zhidkosti forsunkami (Atomization of liquid injectors). M.-L., Gosenergoizdat, 1962.

4. Kulagin L. V. Issledovaniye raboty dvukhkonturnykh forsunok (A study of two-loop injectors). "Teploenergetika", 1963, No. 11.

5. Kulagin L. V. Issledovaniye raboty dvukhsoplovykh dvukhstupenchatykh forsunok (A study of two-nozzle two-stage injectors). M., Transzheldorizdat, 1962 (Trudy Vsesoyuznogo nauchno-issledovatel'skogo instituta zheleznodorozhnogo transporta. Vyp. 241).

6. Prakhov A. M. Nekotoryye osobennosti tsentrobezhnykh forsunok GTD (Certain features of swirlers in a gas turbine). In the collection "Avtomaticheskoye regulirovaniye aviadvigateley", Vyp. 4. M., Oborongiz, 1962.

7. Carey F. The development of the spill flow burner and its control system for gas turbine engines. Journal of the Royal Aeronautical Society. V. 58 No. 527, 1954.

8. Gas-turbine sprayer design. Oil Engine and Gas Turbine. V. 17, No. 202, 1950.

9. The Dowty Spill-Burner Fuel System. Aircraft Engineering. V. 25, No. 291, 1955.

Footnotes

[1] Construction of adjustable injectors used in different areas of technology are described in literature [1, 3, 6, 8, 9].

[2] The continuity equation for flow in the swirl chamber is written in the form $Q = 2\pi r \delta V_m$, where $\delta = n 2 r_{ss}$ — height of swirl chamber, V_m — radial component of velocity.

[3] Characteristics of flow rate do not coincide with an increase and decrease of pressure.

[4] For simplicity, here and subsequently during determination of energy losses the drag coefficient of fuel pipe in the first stage is equated to zero in view of its insignificant value.

⁸Here is included the drag of the tangential channels themselves in the first stage.

CHAPTER V

THEORY OF THE DISINTEGRATION OF STREAMS, FILMS AND DROPS OF LIQUID

§ 1. Survey of Theoretical Investigations of the Disintegration of Streams, Films and Drops of Liquid

In Chapter I it was shown that when liquid flows from holes of injectors on the surface of the stream or film there appear waves, propagating along the stream. They are waves of capillary nature and will be formed as a result of an oscillatory process, in which the role of restoring forces is played by capillary forces. The same waves form on the surface of separate drops of liquid moving in a gaseous environment. Capillary waves play an essential role in the disintegration of a stream, film or drop on a multitude of small drops.

Disintegration causes waves, whose amplitude most rapidly grows in time; thus, disintegration of streams, films and drops of liquid is intimately connected with instability of their motion, with the appearance and development of capillary waves propagating along the surface.

The problem of disintegration of streams, films and drops is one of the important problems of capillary hydrodynamics which has attracted attention of many great scientists, such as Rayleigh, Niels Bohr and others.

Theoretical works have developed basically in two directions:

1. Study of stability and disintegration of streams, films and

165

drops, founded on use of the method of small disturbances with subsequent determination of diameters of the drops forming as a result of disintegration.

2. Determination of the dimensions of drops founded on the assumption that atomization of a stream near the nozzle hole occurs under the effect of turbulent pulsations appearing in the injector channel.

The largest part of these works belongs to the first area.

For the first time the problem about oscillations of a cylindrical thread of inviscid liquid, quiescent in a vacuum, was solved by Rayleigh [17]. He showed that the most rapidly growing amplitude is possessed by the disturbance which corresponds to value of wave number k for which the expression

$$Y = \frac{ka I_0'(ka)}{I_0(ka)} (1 - k^2 a^2)$$ (233)

has its maximum,

where $I_0'(x)$ — Bessel derivative with respect to the argument; $I_0(x)$ — Bessel function of zero order of an imaginary argument; $k = \frac{2\pi}{\lambda}$ — wave number (λ — wavelength); a — radius of cylindrical thread of liquid.
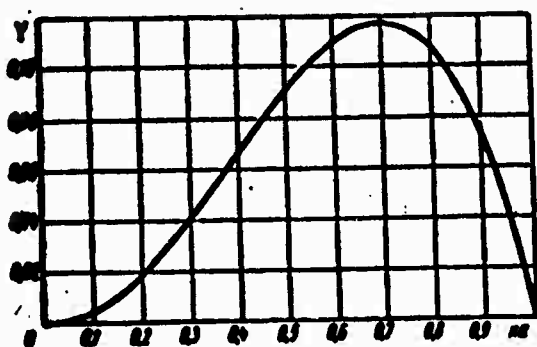
Fig. 70. Dependence of the square of the increment on dimensionless wave number ka for the case of oscillations of a cylindrical thread of inviscid liquid, quiescent in a vacuum (Rayleigh).

The corresponding critical value of the square of dimensionless wave number $k^2 a^2$ = 0.4858, whence for a wavelength corresponding to the greatest instability (Fig. 70), we find the value

166

$$\lambda = \frac{2\pi}{k} = 4.508 \cdot 2a. \qquad (234)$$

A disturbance having a wavelength 4.508 times greater than the diameter of the thread will increase faster than the others, and finally the thread will disintegrate into drops of identical diameter.

Allowing that the volume of the drop which forms is equal to the volume of the initial (undisturbed) cylinder with a length equal to the wavelength of the disturbance, Rayleigh calculated the diameter of drops into which a cylindrical thread, quiescent in a vacuum, disintegrates. His results agree well with experiments conducted with streams coming from round holes at minute velocities.

In subsequent works Rayleigh considered also the viscosity of liquid of stream. It turned out that viscosity decreases the rate of accretion of disturbances, but the ratio of optimum wavelength to diameter of stream remains constant.

G. I. Petrov and T. D. Kalinina, and also Yu. M. Shekhtman [20] examined the disintegration of a cylindrical stream of ideal liquid flowing into another ideal liquid. Shekhtman obtained for the increment of oscillations the following expression:

$$\gamma_k = \frac{-k(U_2 - U_1)A'}{A' + \rho_1 I_0(ka)} \pm$$

$$\pm \frac{i\sqrt{\rho_1 I_0(ka) A' k^2 (U_2 - U_1)^2 + [A' + \rho_1 I_0(ka)]\frac{\sigma}{a^2} k I_1(ka)(1 - k^2 a^2)}}{A' + \rho_1 I_0(ka)}, \qquad (235)$$

where

$$A' = \rho_2 \frac{I_1(ka)}{K_1(ka)} K_0(ka);$$

U_1, U_2 — velocity of liquid stream and of medium; ρ_1, ρ_2 — density of these liquids; σ — coefficient of surface tension of liquid of stream with respect to liquid of medium.

This formula makes it possible to find optimum wavelengths for

which the most rapidly increasing disturbances are realized.

Stability and disintegration of a fixed cylindrical liquid film in a vacuum were examined by Binni and Davidson [21]. The effect of velocity and ambient density, and also viscosity of the liquid on stability and disintegration of a cylindrical film was examined by A. S. Lyshevskiy [11, 12].

Stability and disintegration of a flat spray of inviscid liquid were studied by Jark, Stubbs and Tek [25], Hagerty and Shea [22] and others.

Along with the above-mentioned work of Rayleigh, the effect of viscosity of liquid on disintegration of a cylindrical stream was studied in the works of Tomatika [31], Weber [1], V. G. Levich [10] and A. S. Lyshevskiy [14]. Tomatika, besides viscosity of the liquid of a stream, considered also density and viscosity of the medium. For the case of a small exit velocity results of calculations agree well with experimental data.

The problem about stability and disintegration of a drop of liquid was examined in a number of theoretical works.

Oscillations of a drop of ideal liquid quiescent in a vacuum were studied by Rayleigh [17]. Using the method of small disturbances, he obtained a formula for the frequency of natural neutral oscillations. Lamb [9], using the same method, considered the density of a gaseous environment surrounding a drop, and obtained the following formula for the square of the frequency of natural oscillations:

$$\nu^2 = \frac{\sigma}{a^3} \cdot \frac{n(n+1)(n-1)(n+2)}{(n+1)\rho_1 + n\rho_2}, \qquad (236)$$

where σ — coefficient of surface tension; a — radius of drop; n — integers (n = 0, 1, 2, ...); ρ_1 and ρ_2 — densities of the liquid of the drop and of the environment.

A considerably more complex problem appears in examining the splitting of a drop by a gas flow streamlining it. Attempts were

made to determine the size of a stable drop of the critical value of Weber criterion $W_\kappa = \frac{\rho_2 V^2 a}{\sigma}$ from the condition of equilibrium of the force of surface tension and aerodynamic pressure of the medium on the drop [7, 10, 27]. Since the condition of equilibrium contains an unknown drag coefficient of a deformed drop, these attempts were unsuccessful.

Close to the above-indicated works is a work by L. A. Klyachko [8]. He examines conditions of static equilibrium of a drop. It is assumed that a drop under the action of gas flowing around it is deformed into an oblate ellipsoid of revolution with its axis parallel to the direction of the incident flow. As deformation develops, the ratio of the semiaxes increases, and when the Weber criterion exceeds 1.875, equlibrium is disturbed and the drop disintegrates.

Hinze [23] and Isshiki [24] used the method of small perturbations to calculate W_κ. It was assumed that deformations of the drop were symmetric with respect to the direction of gas flow, and that the distribution of normal and tangent components of aerodynamic force is not changed during deformation of the drop. The dependences of W_κ on Laplace criterion $Lp = \frac{\rho_1 \sigma a}{\mu_1^2}$ and distribution of pressure on the surface of the drop were obtained.

The method of small perturbations was used also by A. S. Lyshevskiy [13], A. M. Golovin [3, 4], V. A. Borodin, Yu. F. Dityakin, and V. I. Yagodkin [2].

On the basis of a very rough assumption about pressure distribution of the incident airflow A. S. Lyshevskiy obtained $W_\kappa = 6$. Borodin, Dityakin, and Yagodkin [2] examined different forms of perturbations of the surface of a drop. $W_\kappa = 1.63$ was obtained, corresponding to the lowest form — splitting of a drop in the direction of the flow and formation of a torus. Golovin took into account swirl flow inside the drop and determined W_κ under different assumptions about the character of motion and deformation. He showed that the boundary condition used in works [2, 13] connecting normal components of the velocity of liquid and gas is composed inaccurately and should be written for the perturbed surface of the drop [2, 13].

169

It is necessary to make general remarks about applicability of the method of small perturbations to calculation of W_{K} . Losses cf stability of the drop with respect to small perturbations occurs during nonstationary undisturbed motion of drop and medium. Therefore there appears a problem about the stability of nonstationary motion of a drop, which is incomparably more complex than the problem of the stability of stationary motion, and methods of its solution are not known, with the exception, for example, of the simple case of stabilized periodic oscillation of the density of a medium.

Golovin and Lyshevskiy [3, 4, 13] investigated the case of stability of a drop during the steady motion of both media, which naturally strongly differs from real conditions. Thus, the method of small perturbations, based on finding elementary waves, cannot be used for calculation of W_{K}. It is possible that this method will be useful for calculation of the characteristics of stability and forms of perturbations of a drop for large W criterion, when the growing perturbations are great as compared to deformations of the basic motion of the drop.

V. Ya. Natanzon [16] assumed that the only cause of disintegration of a stream is turbulence of the fluid flow in the channel of the injector. The size of the drop is determined from the relationship between the pulsational energy of isotropic turbulent motion and surface energy of the liquid at atomization. The distinction of computed values of the diameter of a drop from those measured is explained by the disregard of the effect of the density of the gaseous environment and other assumptions.

I. I. Bogdanovich considers that primary disintegration of a stream occurs basically under the effect of anisotropic large-scale turbulent pulsations of the flow, appearing in the injector channel. Due to the absence of data about the pulsational velocity in the injector channel use of the author's proposed formula for calculation of the diameter of the drop is very difficult.

The majority of theoretical works dedicated to the study of the disintegration of streams, films and drops use the method of small

perturbations.

This method, widely used in mechanics in solving problems about stability of motion, consists in imposing oscillations on the primary flow of liquid. Formally this is expressed in the fact that in equations of hydrodynamics instead of velocities and pressures of the primary flow, the values of velocities and pressures of perturbed motion are introduced, i.e., to parameters of the primary flow are added small perturbations.

During the study of oscillations and disintegration of streams, films and drops of liquid it is possible to see that their particles in their own motion obtain, besides basic velocities (undisturbed flow), still small perturbations with a wide spectrum of frequencies, appearing due to various kinds of flow disturbances (deflection from geometrically correct form of holes in injector nozzles, roughness of nozzle walls, periodic change of parameters of environment, etc.).

After linearization and integration of equations hydromechanics solutions are put into boundary conditions of the problem, as a result of which a system of linear equations is obtained, uniform relative to arbitrary constant equations. The condition of compatibility of these equations (characteristic equation) makes it possible to investigate the change of character of oscillations (accretion or damping) depending upon frequency. It turns out to be possible to establish for what frequencies the oscillations grow and at what frequencies this accretion is especially intensive. Further a conclusion is made about the most probable type of disintegration, about possible dimensions of the drops into which the stream, film or drop of liquid disintegrates, etc.

§ 2.   Stability and Disintegration of a Cylindrical
         Film of Liquid in a Gas Medium

A film of liquid flowing from the nozzle of a swirler, near it has an approximate cylindrical shape (see § 3 Chapter II). Its disintegration usually occurs also near the nozzle, and for a theoretical study of disintegration it is advisable to establish the

171

problem about stability of a cylindrical film of liquid during its motion in a fixed gaseous medium.

Moreover as special cases of the formulated problem we can obtain Rayleigh's result, and the conclusion of Petrov, Kalinin, Shekhtman and others.

Let us consider a cylindrical film of ideal liquid, surrounded by another ideal liquid (Fig. 71), with external radius a and internal radius b. We will consider that the liquid moves forward along the x-axis with velocity V, and the liquid of the medium (on the outside and inside the film) is stationary.

Let us introduce system of cylindrical coordinates (r, ϕ, x), heading the x-axis along the axis of the film, and the r-axis along its radius.

Let us designate by

$$\Phi_k = \Phi_k(r, \varphi, x, t), \ k = 1, 2, 3. \tag{237}$$

The velocity potentials of the liquid of film and medium.

Index k = 1 refers to the liquid of the film, indices k = 2, k = 3 — to the liquid of the medium on the outside and inside the film respectively. Densitites of liquid of film and medium are designated by ρ_1 and ρ_2.
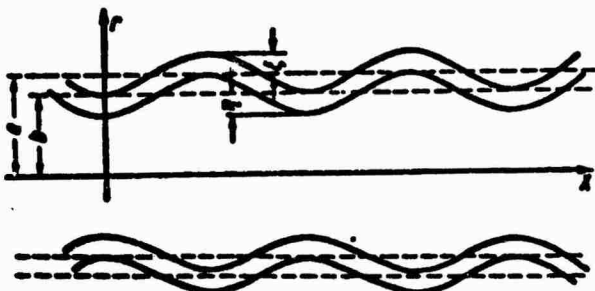
Fig. 71. Oscillations of a cylindrical film of liquid in a gaseous environment.

Velocity potential Φ_k should satisfy Laplace equation

$$\frac{\partial^2 \Phi_k}{\partial r^2} + \frac{1}{r} \cdot \frac{\partial \Phi_k}{\partial r} + \frac{\partial^2 \Phi_k}{\partial x^2} + \frac{1}{r^2} \cdot \frac{\partial^2 \Phi_k}{\partial \varphi^2} = 0. \tag{238}$$

172

Components of velocity of the flow will have the form:

$$
\left.
\begin{aligned}
V_{xx} &= V_x + v_{xx}, \quad k = 1, 2, 3; \\
V_{rx} &= v_{rx}, \quad V_1 = V, \quad V_2 = V_3 = 0; \\
V_{\varphi x} &= v_{\varphi x}, \quad v_{xx} = \frac{\partial \Phi_x}{\partial x}, \quad v_{rx} = \frac{\partial \Phi_x}{\partial r}; \\
v_{\varphi x} &= \frac{1}{r} \cdot \frac{\partial \Phi_x}{\partial \varphi}.
\end{aligned}
\right\}
\tag{239}
$$

The solution of equation (238) is represented in the following form:

$$
\Phi_x(r, \varphi, x, t) = f_x(r) e^{i(\alpha x + s\varphi - \beta t)}; \quad k = 1, 2, 3,
\tag{240}
$$

where $\alpha = \frac{2\pi}{\lambda}$ — space angular frequency of oscillations (wave number) (λ — wavelength of imposed perturbation); $\beta = \beta_r + i\beta_1$ — overall frequency of oscillations in time (β_r — real frequency of oscillations; β_1 — increment or decrement of oscillations).

Placing expression (240) in equation (238), we obtain

$$
f_x'' + \frac{1}{r} f_x' - \left(\alpha^2 + \frac{s^2}{r^2} \right) f_x = 0; \quad k = 1, 2, 3,
\tag{241}
$$

the solution of which has the form

$$
f_x = A_x I_s(\alpha r) + B_x K_s(\alpha r); \quad k = 1, 2, 3,
\tag{242}
$$

where A_K, B_K — arbitrary constants; $I_s(x)$, $K_s(x)$ — Bessel function of order s of an imaginary argument.

Proceeding from conditions of the finiteness of velocities when r = 0 and r = ∞, velocity potentials for the motion of liquid in a sheet and in the surrounding medium must be written in the following way:

$$
\left.
\begin{aligned}
\Phi_1 &= e^{i(\alpha x + s\varphi - \beta t)} [A_1 I_s(\alpha r) + B_1 K_s(\alpha r)]; \\
\Phi_2 &= e^{i(\alpha x + s\varphi - \beta t)} B_2 K_s(\alpha r); \\
\Phi_3 &= e^{i(\alpha x + s\varphi - \beta t)} A_3 I_s(\alpha r).
\end{aligned}
\right\}
\tag{243}
$$

173

On the border of the film of liquid and the medium, the following conditions must be fulfilled.

On external and internal surfaces of the film difference of pressures should be balanced by the pressure of surface tension:

$$p_2 - p_1 = \sigma\left[-\frac{1}{a} + \frac{\xi}{a^2} + \frac{\partial^2\xi}{\partial x^2} + \frac{1}{a^2}\cdot\frac{\partial^2\xi}{\partial \varphi^2}\right] \text{ when } r = a;$$

$$p_3 - p_1 = \sigma\left[\frac{1}{b} - \frac{\eta}{b^2} - \frac{\partial^2\eta}{\partial x^2} - \frac{1}{b^2}\cdot\frac{\partial^2\eta}{\partial \varphi^2}\right] \text{ when } r = b, \qquad (244)$$

where p_1, p_2, p_3 — pressure respectively in liquids of film, external and internal medium; σ — coefficient of surface tension of liquid of sheet with respect to liquid of medium; ξ and η — deflection of particles of liquid from external and internal surfaces of undisturbed sheet (Fig. 71) respectively, where

$$r_{ext} = a + \xi, \quad r_{int} = b + \eta. \qquad (245)$$

Expressions for pressures are obtained from the Lagrange-Cauchy integral in the following form:

$$\left.\begin{aligned}
\frac{p_1}{\rho_1} &= -\left(\frac{\partial \Phi_1}{\partial t} + V\frac{\partial \Phi_1}{\partial x}\right) + \frac{p_0}{\rho_1}, \\
\frac{p_2}{\rho_2} &= -\frac{\partial \Phi_2}{\partial t} + \frac{p_0}{\rho_2} - \frac{\sigma}{a\rho_2}; \\
\frac{p_3}{\rho_3} &= -\frac{\partial \Phi_3}{\partial t}\frac{\partial \Phi_3}{\partial x} + \frac{p_0}{\rho_3} + \frac{\sigma}{b\rho_3},
\end{aligned}\right\} \qquad (246)$$

where p_0 — pressure of liquid of undisturbed film.

Let us assume that deflections ξ and η are periodic functions of t and x in the following form:

$$\left.\begin{aligned}
\xi &= \bar{\xi}e^{i(\omega t + m - kx)}; \\
\eta &= \bar{\eta}e^{i(\omega t + m - kx)},
\end{aligned}\right\} \qquad (247)$$

where $\bar{\xi}$, $\bar{\eta}$ — amplitudes of deflections of liquid particles from external and internal surfaces of undisturbed film respectively.

Differentiating the expressions for velocity potential Φ_1, Φ_2, Φ_3

174

(243), we obtain after substitution of derivatives into equations (246):

$$
\left.
\begin{aligned}
p_1 &= i\rho_2 e^{i(\alpha x + \varkappa - \beta t)}(\beta - \alpha V) \times \\
&\times [A_1 I_s(\alpha r) + B_1 K_s(\alpha r)] + p_0; \\
p_2 &= i\rho_2 \beta e^{i(\alpha x + \varkappa - \beta t)} B_2 K_s(\alpha r) + \\
&+ p_0 - \frac{\sigma}{a}; \\
p_3 &= i\rho_2 \beta e^{i(\alpha x + \varkappa - \beta t)} A_3 I_s(\alpha r) + \\
&+ p_0 + \frac{\sigma}{b}.
\end{aligned}
\right\}
\tag{248}
$$

Using equations (247) and (248) from boundary conditions (244), we obtain

$$
\left.
\begin{aligned}
&i\rho_2\beta K_s(\alpha a) B_2 - i\rho_1 (\beta - \alpha V)[A_1 I_s(\alpha a) + \\
&+ B_1 K_s(\alpha a)] + \sigma\left(\alpha^2 - \frac{1}{a^2} + \frac{\sigma^2}{a^2}\right)\bar{\xi} = 0; \\
&i\rho_2\beta I_s(\alpha b) A_3 - i\rho_1 (\beta - \alpha V)[A_1 I_s(\alpha b) + \\
&+ B_1 K_s(\alpha b)] + \sigma\left(-\alpha^2 + \frac{1}{b^2} - \frac{\sigma^2}{b^2}\right)\bar{\eta} = 0.
\end{aligned}
\right\}
\tag{249}
$$

The total differentials of deflections of liquid particles from the surface of undisturbed film have the form

$$
\begin{aligned}
d\xi &= \frac{\partial \xi}{\partial x}\,dx + \frac{\partial \xi}{\partial t}\,dt; \\
d\eta &= \frac{\partial \eta}{\partial x}\,dx + \frac{\partial \eta}{\partial t}\,dt,
\end{aligned}
$$

whence normal components of the rates of displacement of liquid particles on external and internal surfaces of the film will be

$$
\begin{aligned}
v_{r1} &= \frac{\partial \xi}{\partial x}V + \frac{\partial \xi}{\partial t} \quad \text{when } r = a; \\
v_{r2} &= \frac{\partial \eta}{\partial x}V + \frac{\partial \eta}{\partial t} \quad \text{when } r = b; \\
v_{r3} &= \frac{\partial \xi}{\partial t} \quad \text{when } r = a; \\
v_{r4} &= \frac{\partial \eta}{\partial t} \quad \text{when } r = b.
\end{aligned}
$$

Considering expressions (247), we obtain:

175

$$v_{ri} = \bar{k}e^{i(\omega t + \omega - \beta t)}(\alpha V - \beta) \text{ when } r = a;$$
$$v_{ri} = \bar{\eta}e^{i(\omega t + \omega - \beta t)}(\alpha V - \beta) \text{ when } r = b;$$
$$v_{r0} = -\bar{k}e^{i(\omega t + \omega - \beta t)} \text{ when } r = a;$$
$$v_{r0} = -\bar{\eta}e^{i(\omega t + \omega - \beta t)} \text{ when } r = b.$$

(250)

On the other hand, using formulas (239) and (243), expressions
for normal velocities can be written in the following way:

$$v_{ri} = \alpha e^{i(\omega t + \omega - \beta t)}[I_s'(\alpha r) A_1 + K_s'(\alpha r) B_1];$$
$$v_{ri} = \alpha e^{i(\omega t + \omega - \beta t)} K_s'(\alpha r) B_2;$$
$$v_{r0} = \alpha e^{i(\omega t + \omega - \beta t)} I_s'(\alpha r) A_3.$$

(251)

where the primes designate differentiation of Bessel function with
respect to the argument.

Equating the right sides of equalities (250) and (251), we
obtain: for external surface of film

$$\alpha [I_s'(\alpha a) A_1 + K_s'(\alpha a) B_1] = \bar{k}(\alpha V - \beta);$$
$$\alpha K_s'(\alpha a) B_2 = -\beta \bar{k}.$$

(252)

and for internal surface of film

$$\alpha [I_s'(\alpha b) A_1 + K_s'(\alpha b) B_1 = \bar{\eta}(\alpha V - \beta);$$
$$\alpha I_s'(\alpha b) A_3 = -\beta \bar{\eta}.$$

(253)

From equations (252) and (253) we have

$$\bar{k} = \frac{\alpha [I_s'(\alpha a) A_1 + K_s'(\alpha a) B_1]}{i(\alpha V - \beta)} = -\frac{\alpha K_s'(\alpha a) B_2}{\beta};$$
$$\bar{\eta} = \frac{\alpha [I_s'(\alpha b) A_1 + K_s'(\alpha b) B_1]}{i(\alpha V - \beta)} = -\frac{\alpha I_s'(\alpha b) A_3}{\beta}.$$

(254)

Placing the values for $\bar{k}$, $\bar{\eta}$ from equations (254) in expressions
(249), we obtain together with equations (254) a system of four linear
equations relative to arbitrary constants:

176

$$\beta I_0'(ab) A_1 + \beta K_0'(ab) B_1 + (\alpha V - \beta) I_0'(ab) A_3 = 0;$$
$$\beta I_0'(aa) A_1 + \beta K_0'(aa) B_1 + (\alpha V - \beta) K_0'(aa) B_2 = 0;$$

$$\rho_2 \beta (\alpha V - \beta) I_0(aa) A_1 + \rho_1 \beta (\alpha V - \beta) K_0(aa) B_1 +$$
$$+ \left[\rho_2 \beta^2 K_0(aa) + \alpha a \left(\alpha^2 - \frac{1}{a^2} + \frac{a}{a^2} \right) K_0'(aa) \right] B_2 = 0;$$
$$\rho_2 \beta (\alpha V - \beta) I_0(ab) A_3 + \rho_1 \beta (\alpha V - \beta) K_0(ab) B_1 +$$
$$+ \left[\rho_2 \beta^2 I_0(ab) + \alpha a \left(-\alpha^2 + \frac{1}{b^2} - \frac{a}{b^2} \right) I_0'(ab) \right] A_3 = 0.$$

(255)

Introducing dimensionless parameters

$$Z = \beta \sqrt{\frac{\rho_1 a^2}{a}}, \quad W = \frac{\rho_1 a V^2}{a},$$
$$M = \frac{\rho_2}{\rho_1}, \quad m = aa, \quad n = ba,$$
$$S = \sqrt{\frac{W}{M}}, \quad a = \frac{a}{b} = \frac{l m}{n}$$

(256)

and the following designations:

$$A_0(x) = \frac{I_0(x)}{K_0(x)},$$
$$A_{0+1}(x) = \frac{I_0'(x)}{-K_0'(x)};$$
$$t = Z - mS, \quad B(x) = -\frac{K_0'(x)}{K_0(x)},$$

(257)

after substituting parameters (256) into equations (255) we obtain:

$$Z I_0'(n) A_1 + Z K_0'(n) B_1 + (mS - Z) I_0'(n) A_3 = 0;$$
$$Z I_0'(m) A_1 + Z K_0'(m) B_1 + (mS - Z) K_0'(m) B_2 = 0;$$
$$Z(mS - Z) I_0(m) A_1 + Z(mS - Z) K_0(m) B_1 +$$
$$+ [MZ^2 K_0(m) + m(m^2 - 1 + s^2) K_0'(m)] B_2 = 0;$$
$$Z(mS - Z) I_0(n) A_1 + Z(mS - Z) K_0(n) B_1 +$$
$$+ [MZ^2 I_0(n) - m(m^2 - t^2 + s^2 t^2) I_0'(n)] A_3 = 0.$$

(258)

Excluding from the equations of a homogeneous system (258) arbitrary constants, after transformations we obtain

$$
\begin{vmatrix}
I'_0(n) & K'_0(n) & 0 & I'_0(n) \\
I'_0(m) & K'_3(m) & K'_0(m) & 0 \\
(mS-Z)^2 I_0(m) & (mS-Z)^2 K_0(m) & MZ^2 K_0(m)+ & 0 \\
& & +m(m^2-1+ & \\
& & +s^2)K'_0(m) & \\
(mS-Z)^2 I_0(n) & (mS-Z)^2 K_0(n) & 0 & MZ^2 I_0(n)- \\
& & & -m(m^2-s^2+ \\
& & & +s^2 s^2)I'_0(n)
\end{vmatrix}
= 0. \tag{259}
$$

Using designations of expressions (257), after elementary transformations we bring equation (259) to the form

$$
\begin{vmatrix}
A_{n+1}(n) & -1 & 0 & 1 \\
A_{n+1}(m) & -1 & -1 & 0 \\
\tau^2 A_0(m) & \tau^2 & M(mS+\tau)^2-mX & 0 \\
& & \times(m^2-1+s^2)B(m) & \\
\tau^2 A_0(n) & \tau^2 & 0 & M(mS+ \\
& & & +\tau)^2 \dfrac{A_0(n)}{A_{n+1}(n)}- \\
& & & -m(m^2-s^2+ \\
& & & +s^2 s^2)B(n)
\end{vmatrix}
= 0. \tag{260}
$$

Roots of equation (260) can be represented in the form of a series in powers of $M^{1/2}$ (after the replacement $S = \sqrt{\dfrac{W}{M}}$):

$$
\tau^2 = Z_0 + Z_1 M^{1/2} + Z_2 M + \ldots \tag{261}
$$

For the majority of cases M is minute (for example, a water film in air $M = 1.2 \cdot 10^{-3}$), therefore in the expansion of series (261) we limit ourselves to one member, setting $\tau = Z_0$. Then from equation (260) we obtain

$$
\begin{vmatrix}
A_{n+1}(n) & -1 & 0 & 1 \\
A_{n+1}(m) & -1 & -1 & 0 \\
Z_0^2 A_0(m) & Z_0^2 & m^2 W+m(1- & 0 \\
& & -m^2-s^2)B(m) & \\
Z_0^2 A_0(n) & Z_0^2 & 0 & m^2 W \dfrac{A_0(n)}{A_{n+1}(n)}+ \\
& & & +m(-m^2+s^2- \\
& & & -s^2 s^2)B(n)
\end{vmatrix}
= 0. \tag{262}
$$

178

Expanding determinant (262), we obtain

$$[A_0(m) - A_s(n)] Z_0^4 + \{[A_s(n) + A_{s+1}(m)][m^3 W +$$
$$+ m(1 - m^2 - s^2) B(m)] + [A_s(m) + A_{s+1}(n)]\left[m^3 W \frac{A_0(n)}{A_{s+1}(n)} +\right.$$
$$\left.+ m(e^2 - m^2 - s^2 e^2) B(n)]\right\} Z_0^2 + [A_{s+1}(m) - A_{s+1}(n)] \times$$
$$[m^3 W + m(1 - m^2 - s^2) B(m)]\left[m^3 W \frac{A_0(n)}{A_{s+1}(n)} +\right.$$
$$\left.+ m(e^2 - m^2 - s^2 e^2) B(n)] = 0.\right. \tag{263}$$

Let us examine several special cases of our problem neglecting the effect of tangential waves, i.e., development of axisymmetrical waves, for which we assume that in equation (263) s = 0:

$$[A_0(m) - A_0(n)] Z_0^4 + \{[A_0(n) + A_1(m)][m^2 W + m(1 - m^2)B(m)] +$$
$$+ [A_0(m) + A_1(n)]\left[m^3 W \frac{A_0(n)}{A_1(n)} + m(e^2 - m^2) B(n)]\right\} Z_0^2 +$$
$$[A_1(m) - A_1(n)][m^3 W + m(1 - m^2) B(m)] \times$$
$$\times \left[m^3 W \frac{A_0(n)}{A_1(n)} + m(e^2 - m^2) B(n)] = 0.\right. \tag{264}$$

We investigate a film with internal cavity of small diameter, assuming that in equation (264) $e = \frac{a}{b} \gg 1$, i.e., a >> b or m >> n, and disregarding in the coefficients $A_0(n)$ and $A_1(n)$ as compared to functions of m. Then we obtain

$$A_0(m) Z_0^4 +$$
$$+ \{[A_1(m)[m^2 W + m(1 - m^2) B(m)] + A_0(m)[m^3 W \times$$
$$\times \frac{A_0(n)}{A_1(n)} + m(e^2 - m^2) B(n)]\} Z_0^2 + A_1(m)[m^3 W + m(1 - m^2) \times$$
$$\times B(m)]\left[m^3 W \frac{A_0(n)}{A_1(n)} + m(e^2 - m^4) B(n)] = 0.\right. \tag{265}$$

Solving equation (265) relative to Z_0^2, we will have

$$(Z_0^2)_1 = -\frac{A_1(m)}{A_0(m)}[m^3 W + m(1 - m^2) B(m)]; \tag{266}$$

$$(Z_0^2)_2 = -\left[m^3 W \frac{A_0(n)}{A_1(n)} + m(e^2 - m^2) B(n)].\right. \tag{267}$$

179

The root $(z_0^2)_1$ (265) is the solution for the case of a solid cylindrical stream (b = 0, n = 0). This solution can be obtained also with the help of corresponding passage to the limit from equation (264). Dividing the left and right side of this equation by $m^2 W \frac{A_0(n)}{A_1(n)} + m(e^2 - m^2)B(n)$ and directing n to zero, we obtain equation (266). Using the designations of (257), from equation (266) we obtain

$$z_{01}^2 = \frac{m^2 W I_1(m) K_0(m) + m(1-m^2) I_1(m) K_1(m)}{I_0(m) K_1(m)}, \tag{268}$$

which corresponds to equation (235), obtained by Shekhtman [20]. Furthermore, we have $Z_r = mS$, if $z_0^2 < 0$ and $Z_1 = 0$, $Z_r = mS + Z_0$, if $z_0^2 > 0$.

On Fig. 72 is shown the graph of the dependence of the square of the increment of oscillations z_{01}^2 on dimensionless wave number m for various values of Weber criterion W, calculated by formula (268) or (266). The broken line on the same graph is the dependence for $(z_{01}^2)_2$ on m, calculated by formula (267).

Let us determine approximately the locus of the maximum of the square of the increment of oscillations depending upon Weber number W for large wave numbers m >> 1.

Using asymptotic formulas for the Bessel function

$$\left. \begin{array}{l} I_0(x) \approx I_1(x) \approx \frac{e^x}{\sqrt{2\pi x}}; \\ K_0(x) \approx K_1(x) \approx e^{-x}\sqrt{\frac{\pi}{2x}}. \end{array} \right\} \tag{269}$$

from expressions (257) we obtain s = 0

$$\frac{A_1(x)}{A_0(x)} = 1, \ B(x) = 1,$$

and instead of equation (266) we will have for m >> 1

$$(z_{01}^2)_1 \approx m^2 W + m(1 - m^2). \tag{270}$$

180

Differentiating expression (270) and equating the derivative to zero, we obtain

$$2m_0 W + 1 - 3m_0^2 = 0.$$

In the obtained equation we can disregard one as compared to the other large components, which gives

$$m_0 = \frac{2}{3} W, \tag{271}$$

where m_0 — critical value of wave number, corresponding to maximum of square of increment.
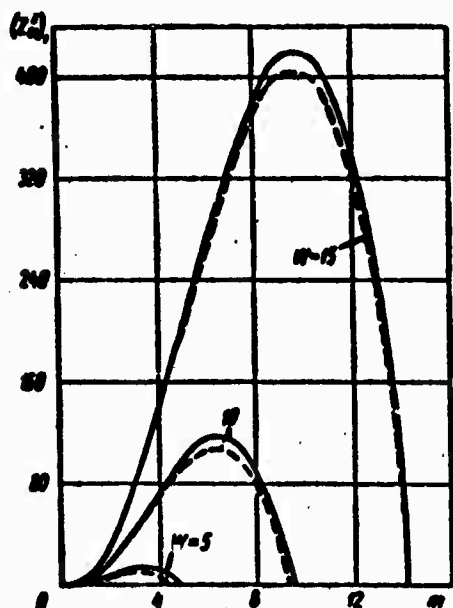
Fig. 72. Dependence of square of increment $(Z_{01}^2)_1$ (first root) on dimensionless wave number m at various values of Weber criterion W for the case of oscillations of a solid cylindrical stream of liquid, calculated by formula (266) or (268) (solid line). The dotted line shows the dependence of $(Z_{01}^2)_2$ on m, calculated by formula (267).
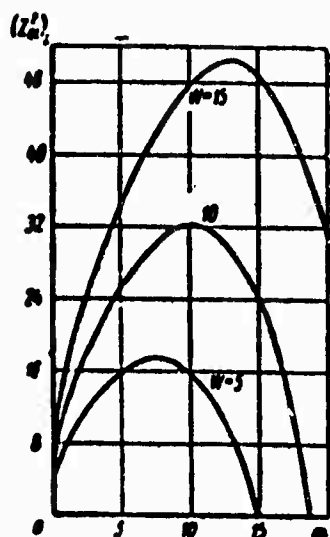
Fig. 73. Dependence of square of increment $(Z_{01}^2)_2$ (second root) on wave number m for various W for the case of oscillations of a cylindrical film of liquid (n = 0.1 m).

181

Figure 73 is the graph of the dependence of the square of the increment of oscillations $(Z_{01}^2)_2$ on wave number m for various values of W, calculated by formula (267).

Also it is possible to determine approximately the locus of the maximum of the square of the increment $(Z_{01}^2)_2$ for large wave numbers.

In this case we obtain

$$(Z_{01}^2)_2 = m^3 W + m(\varepsilon^2 - m^5)$$

and after equating the derivative to zero we will have

$$2W m_0 - 3m_0^2 + \varepsilon^2 = 0,$$

whence

$$m_0 = \frac{W + \sqrt{W + 3\varepsilon^2}}{3}. \qquad (272)$$

As the next special case we will examine the case of total absence of velocity. Assuming that in equation (264) W = 0, we obtain

$$[A_0(m) - A_0(n)] Z_0^2 + \{[A_0(n) + A_1(m)] m(1 - m^2) B(m) + \\ + [A_0(m) + A_1(n)] m(\varepsilon^2 - m^2) B(n)\} Z_0^2 + [A_1(m) - \\ - A_1(n)] m^2 (1 - m^2)(\varepsilon^2 - m^2) B(m) B(n) = 0. \qquad (273)$$

In Fig. 74 are given the graphs for the dependence of the square of the increment of oscillations $(Z_{01}^2)_1$ on the wave number for various thicknesses of film, i.e., various values of parameter ε at W = 0, calculated by equation (273). In the same place is given the graph for the maximum case of a solid stream (Rayleigh's case n = 0), coinciding with that shown earlier in Fig. 70.

In Fig. 75 is given the graph of the analogous dependence for the second root of equation (273).

From equation (273) can be obtained the case of oscillations of a plane film assuming that m >> 1, n >> 1, m - n ≈ 1 (radii of film a and b

182
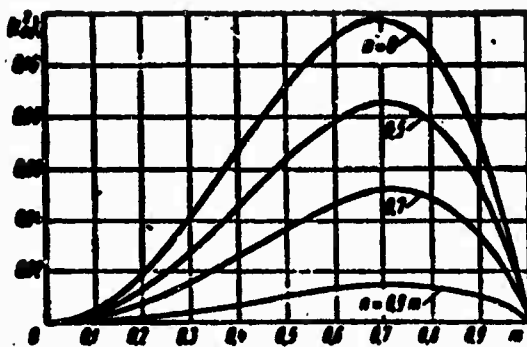
Fig. 74. Dependence of square of increment $(z_{01}^2)_1$ (first root) on wave number m at W = 0 for various values of ε = m/n.

are great as compared to wavelength λ).

Then equation (273) will take the form

$$z_0^4 - 2m^3 z_0^2 + m^6 = 0, \qquad (274)$$

whence $z_0^2 = m^3$, i.e., $Z_1 = 0$, $Z_r = \pm m^{3/2}$. From this it follows that a plane film in the absence of velocity is stable [22].
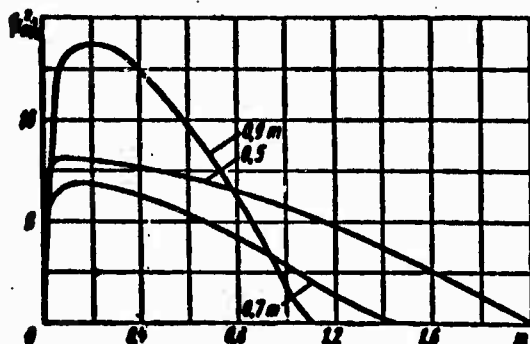
Fig. 75. Dependence of square of increment $(z_{01}^2)_2$ (second root) on wave number m at W = 0 for various values of ε = m/n.

Let us examine the case of high flow velocities of the liquid of a sheet W >> 1, m >> 1, m - n $\approx$ 1.
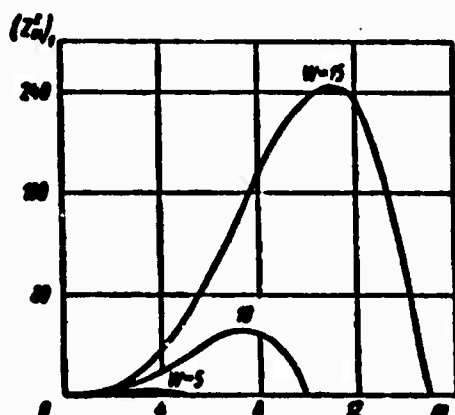
Fig. 76. Dependence of square of increment $(z_{01}^2)_1$ on wave number m(W >> 1) for various values of W at n = 0.9 m.

183
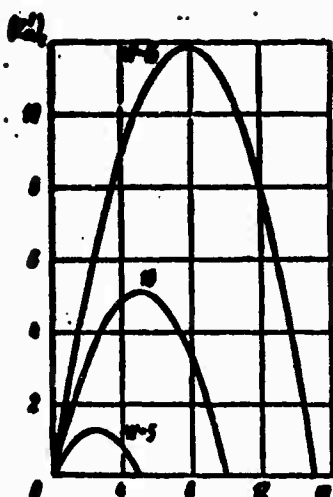
Fig. 77. Dependence of square of increment $(Z_{01}^2)_2$ on wave number $m(W \gg 1)$ for various values of W at $n = 0.9$ m.

Using asymptotic expressions (269) for Bessel functions at large arguments, we obtain

$$A_0(x) \approx A_1(x) \approx \frac{e^x}{x}, \quad B(x) = 1.$$

Placing the obtained expressions in equation (264), we will have

$$Z_0^4 + 2m^2(W-m)\,\text{cth}\,(m-n)\,Z_0^2 + m^4(W-m)^2 = 0, \tag{275}$$

whence

$$\left.\begin{array}{l} (Z_{01}^2)_1 = m^2(W-m)\,\text{th}\,\dfrac{m-n}{2}; \\[2mm] (Z_{01}^2)_2 = m^2(W-m)\,\text{cth}\,\dfrac{m-n}{2}. \end{array}\right\} \tag{276}$$

This gives instability at $W > m$ and stability at $W < m$. In Figs. 76 and 77 are given the graphs of dependences of the square of the increment on the wave number for various values of W and thickness of film corresponding to $n = 0.9$ m, ($\varepsilon = 1/0.9$), calculated by the formulas (276). In Figs. 78 and 79 are given the same dependences for $W = 5$ and various film thicknesses.

In order to find loci of maxima on curves expressing the above dependence, we differentiate expression (276) for the squares of increments with respect to m and equate the derivatives to zero.

184

Fig. 78. Dependence of square of increment $(z_{01}^2)_1$ on wave number m at W = 5 for various values of $\varepsilon = m/n$.

Solving the obtained equations with respect to W, we obtain for $(z_{01}^2)_1$

$$W = m_0 \frac{km_0 + \frac{3}{2} \, sh \, 2km_0}{km_0 + sh \, 2km_0} \tag{277}$$

and for $(z_{01}^2)_2$

$$W = m_0 \frac{3 \, sh \, 2km_0 - 2km_0}{3 \, (sh \, 2km_0 - km_0)} . \tag{278}$$

where $k = \frac{e-1}{2\pi}$.

As the wave number increase, expressions (277) and (278) tend to the same limit

$$W = \frac{3}{2} \, m_0.$$

which will agree with expression (271).

Dependences (277) and (278) are given on graphs of Fig. 80 for various ε.

We will examine, finally, the case of oscillations of a film of liquid, considering the effect of transverse waves, in the presence of large flow velocities of liquid, W >> 1.

185
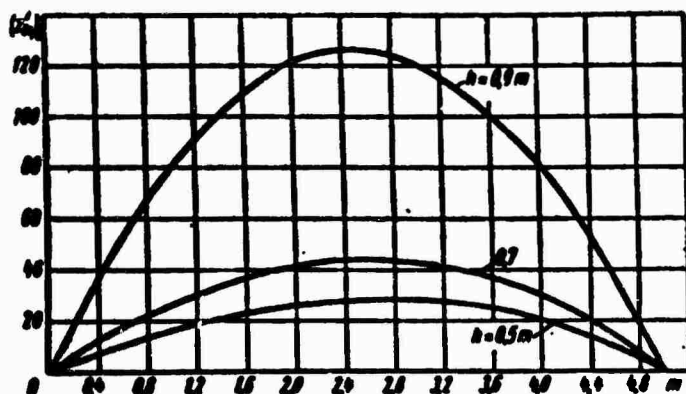
Fig. 79. Dependence of square of increment $(z_{01}^2)_2$ on wave number m at W = 5 for various values of ϵ = m/n.

Under this condition one should examine only the region of large wave numbers m >> 1, n >> 1, in which W >> 1 lies the curve of dependence of increments on wave number. Using equation (263) and asymptotic expressions for Bessel functions with a large argument

$$A_s(x) \approx A_{s+1}(x) \approx \frac{e^{sx}}{x}, \; B(x) \approx 1,$$

we obtain

$$Z_0^4 + \text{cth}\,(m-n)\,[2m^2W + m(1-m^2-s^2) + m(\epsilon^2 - m^2 - \\ - s^2\epsilon^2)]\,Z_0^2 + [m^2W + m(1-m^2-s^2)]\,[m^2W + \\ + m(\epsilon^2 - m^2 - s^2\epsilon^2)] = 0.$$

Considering that m − n >> 1 and cth (m − n) $\approx$ 1 and that it is possible to disregard unity as compared to s^2, we obtain from the preceding equation:

$$Z_0^4 + [2m^2(W-m) - ms^2(1+\epsilon^2)]\,Z_0^2 + [-m^2(W-m) + \\ + ms^2\epsilon^2]\,[-m^2(W-m) + ms^2] = 0.$$ (279)

Solving equation (279), we obtain

$$\begin{aligned}
(Z_0^2)_1 &= -m^2(W-m) + ms^2\epsilon^2; \\
(Z_0^2)_2 &= -m^2(W-m) + ms^2.
\end{aligned} \tag{280}$$

Graphs of dependences (280) are given by broken line on Fig. 73.

186
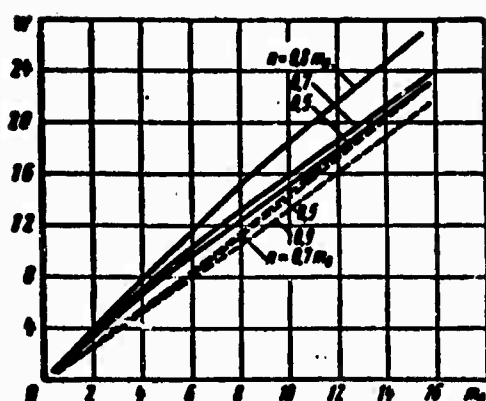
Fig. 80. Dependence of the critical value of wave number m_0 (corresponding to maximum of increment of oscillations) on Weber criterion W for various film thicknesses calculated by formula (277) — solid line and (280) — shading.

Further, it is advisable to study the forms of perturbations predominating in different cases, for which increments of oscillations were determined above.

To the determinant of expression (262) at $s = 0$ corresponds the following system of equations:

$$
\left.
\begin{aligned}
& C_2 A_1(n) - C_3 + C_4 = 0; \\
& C_2 A_1(m) - C_3 - C_3 = 0; \\
& C_2 Z_0^2 A_0(m) + C_3 Z_0^2 + C_3 [m^2 W + m(1 - m^2) B(m)] = 0; \\
& C_2 Z_0^2 A_0(n) + C_3 Z_0^2 + \\
& + C_4 \left[m^2 W \frac{A_0(n)}{A_1(n)} - m(m^2 - e^2) B(n) \right] = 0.
\end{aligned}
\right\}
\tag{281}
$$

Taking the first three equations of system (281), dividing their left and right side by C_1, subtracting the first from the second and adding the second to the third, we obtain

$$
A_1(m) - A_1(n) - \frac{C_2}{C_1} - \frac{C_4}{C_1} = 0;
$$

$$
A_0(m) + A_1(m) - \frac{C_2}{C_1} + \frac{C_3}{C_1} [m^2 W + m(1 - m^2) B(m)] \frac{1}{Z_0^2} = 0.
$$

whence

$$
\left.
\begin{aligned}
& \frac{C_2}{C_1} = \frac{Z_0^2 [A_0(m) + A_1(m)]}{Z_0^2 - m^2 W - m(1 - m^2) B(m)}; \\
& \frac{C_4}{C_1} = A_1(m) - A_1(n) - \frac{Z_0^2 [A_0(m) + A_1(m)]}{Z_0^2 - m^2 W - m(1 - m^2) B(m)}
\end{aligned}
\right\}
\tag{282}
$$

187

Using expressions (254) for amplitudes of the deflections of liquid particles on external and internal surfaces of a film at s = 0, we write out their ratio:

$$\frac{\zeta}{\eta} = -\frac{C_3}{C_4} \cdot \frac{K_1(m)}{I_1(m)}. \tag{283}$$

Determining $\frac{C_3}{C_4}$ from expression (282) and placing it in expression (283), we obtain for ξ, characterizing the sign of the ratio of deflections of liquid particles, the following expression:

$$\zeta = \frac{\zeta}{\eta} \frac{I_1(n)}{K_1(m)[A_0(m) + A_1(m)]} =$$

$$= \frac{z_0^2}{z_0^2[A_0(m) + A_1(n)] + [A_1(m) - A_1(n)][m^2 W + m(1 - m^2) B(m)]}. \tag{284}$$

since

$$\frac{I_1(n)}{K_1(m)[A_0(m) + A_1(m)]} > 0.$$

Putting into expression (284) the square of the increment of oscillations z_0^2, obtained for any case, we will be able to determine the sign of the amplitude ratio for deflections of liquid particles from external and internal surfaces of a film and to determine the phase shift of oscillations on these surfaces.

For the case of motion of a film of liquid with internal cavity of small diameter we place the first root of equation (266) into equality (284). The quantity $A_1(n)$ in the denominator may be disregarded, since it is small as compared to $A_0(m)$ and $A_1(m)$. Then we obtain $\zeta = \infty$, which shows the smallness of the amplitudes of waves (corresponding to first root) along the internal surface of the film as compared to amplitudes of waves on the external surface. In the limit amplitudes of these waves tend to zero as the diameter of the internal cavity of the film decreases.

Placing the second root of equation (267) into equality (284) and also disregarding $A_1(n)$ in the denominator, we obtain

188

$$\zeta = \frac{-\left[m^2 W \frac{A_2(n)}{A_1(n)} + m(n^2 - m^2) B(n)\right]}{-A_0(m)\left[m^2 W \frac{A_2(n)}{A_1(n)} + m(n^2 - m^2) B(n)\right] + A_1(m)\left[m^2 W + m(1 - m^2)\Delta(n)\right]}. \quad (285)$$

The augend of the denominator in expression (285) is considerably less than the first, therefore $\zeta > 0$ and amplitudes $\bar{\xi}$, $\bar{\eta}$ are of one sign.
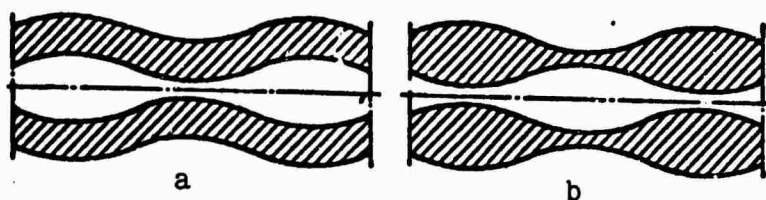

Fig. 81. Forms of perturbations on external and internal surfaces of a film (internal cavity of film is of small diameter): a) second root — identical phases; b) first root — opposite phases.

Consequently, along external and internal surfaces of a film with internal cavity of small diameter propagate waves (corresponding to second root) in identical phase (Fig. 81a).

For the case of an almost motionless film (analogous to the Rayleigh problem), taking the value of roots $(z_0^2)_{1,2}$ of equation (273) from the graphs of Figs. 74 and 75 and placing them for corresponding values of wave numbers m and n into equation (284), it is easy to check that to the first root corresponds inequality $\zeta < 0$ (surfaces of film oscillate in opposite phases (Fig. 81b), and to the second root — inequality $\zeta > 0$ (surfaces oscillate in the same phase — Fig. 81a).

For the case of motion of a film with high velocities substitution of roots $(z_0^2)_{1,2}$ from expression (276) into equation (284) also shows that to the first root corresponds inequality $\zeta < 0$, and to the second $\zeta > 0$.

Consequently, it is possible to say that for all three examined special cases to the first root with the plus sign before the radical in the solution of equation (264) quadratic relative to z_0^2

corresponds inequality $\zeta < 0$, which gives various signs of amplitudes of the rise of liquid particles $\bar{\xi}$ and $\bar{\eta}$ on external and internal surfaces of a film, i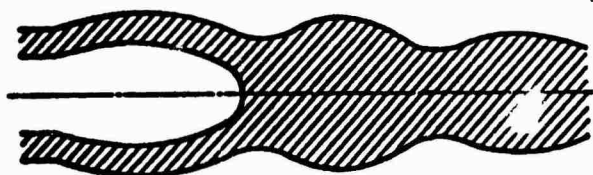.e., these surfaces oscillate in opposite phases (Fig. 81b). To the second root with the minus sign before the radical in the solution of quadratic equation (264) corresponds inequality $\zeta > 0$, which gives identical signs of amplitudes of rise of liquid particles $\bar{\xi}$ and $\bar{\eta}$ on external and internal surfaces of the sheet, i.e., these surfaces oscillate in the same phase (Fig. 81a).

Fig. 82. Closing of internal cavity of film of liquid at small values of Weber W criterion.

Further we will attempt to make certain (basically qualitative) conclusions concerning the mechanism of disintegration of a liquid film proceding from obtained theoretical results. It is necessary to say that in real conditions the flow of a liquid film into a gaseous medium from any nozzle in the initial section has an unsteady character, whereas our theoretical problem assumes the presence of a steady flow, examined as initial undisturbed motion.

From consideration of data about change of the increment of oscillations depending upon wave number for the considered special cases of the motion of a liquid film in a gaseous medium, we can make the following conclusions.

For small values of Weber number W, if one were to not consider the influence of transverse waves when $s = 0$, from the fact that the second root $(z_{01}^2)_2$ considerably exceeds the first $(z_{01}^2)_1$ (see Figs. 74 and 75) and from the principle of Rayleigh, we can conclude that after leaving the opening on the liquid film there appear waves in identical phase on the external and internal surfaces. Since the amplitudes of the oscillations grow rapidly (increment is great), this leads to a closing of the internal cavity in the film (Fig. 82), after which the film turns into a solid stream, disintegrating according to Rayleigh (at minute Weber numbers W) or according to

190

Petrov and Shekhtman. In this case disintegration is described by a form of oscillations corresponding to the first root of equation (265).

For large Weber numbers W and at s = 0 one should examine two cases: for Weber numbers $3 < W_h < 10$ there appear surface oscillations on the film in one phase with wavelength of the order of its thickness $\lambda \approx h = a - b$, and upon disintegration the integrity of the film can be immediately disturbed as a result of being strongly stretched (Fig. 83). For Weber numbers $W_h > 10$ on both surfaces of the film appear waves on one of the two examined types, which are short as compared to thickness (in identical phase, which corresponds to the second root, or in various phases, which corresponds to first root); the appearance of waves of both types is apparently equiprobable in view of the proximity of increments of oscillations (here $W_h = -\frac{\rho_2(a-b)V^2}{\sigma}$). In this case apparently disintegration occurs according to the pattern proposed by Taylor and consisting in tearing drops of liquid with diameter of the order of a wavelength from both surfaces of the film without preliminary disturbance of its integrity. Wavelength corresponds to wave number $m_0 = (2/3)W$, i.e., it is the same as for the case of disintegration of a plane film. Here cylindricity of the film ceases to affect disintegration, and from both surfaces occurs a breakaway of drops of liquid of diameter

$$d \approx \lambda = \frac{3\pi\sigma}{\rho_2 V^2}. \tag{286}$$

A breakaway of rings of liquid from the film apparently is improbable, and can occur possibly only in a narrow range of Weber numbers, somewhere near $W_h = 10$. As can be seen from Fig. 72, transverse waves have little effect on the increment of oscillations, changing it in the direction of a decrease.
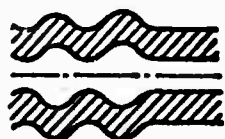

Fig. 83. Waves (in identical phase) on the surfaces of a film of liquid (wavelength — of the order of film thickness) for large Weber criterion W.

It is necessary to say that the conclusion concerning dimensions of drops detached from the film surfaces is not completely exact, because the forces of friction in the liquid are disregarded. Experiments show that the size of the drops is affected by Laplace number

$$Lp = \frac{a\sigma\rho_1}{\mu_1^2},$$

where a — diameter of stream; σ — coefficient of surface tension; ρ_1 — density of liquid; μ_1 — coefficient of absolute viscosity of liquid.

The action of a viscosity of a liquid on its disintegration can be examined from two points of view. First, viscous forces lead to a change of the primary flow — a boundary layer will form, whose presence should lead to a change of the wave formation. Secondly, viscous forces can directly influence the development of perturbations at a given primary flow profile. An analysis of stability should settle no longer on equations of an ideal liquid, but on Navier-Stokes equations, which strongly complicates the investigation. Tomatika's study [31] indicates that the influence of viscosity on liquids which are not too viscous is very small. In view of this it seems to us that the basic role is played only by a change of the velocity profile and the behavior of the perturbations is described by the same equations of an ideal liquid which were used above.

§ 3. Stability of Motion of the Plane Interface of Two Liquids

Let us consider the flow of three liquids, for which densities ρ_1, ρ_2, ρ_3 have two parallel plane interfaces (for example, water, steam, and air).

We will consider that a space is divided into four zones: in first and second flows a liquid with density ρ_1, forming a boundary layer of thickness h_1. In the third zone flows a liquid with density ρ_2, forming a boundary layer of thickness h_2, and in fourth zone rests a liquid with density ρ_3 (Fig. 84). On the interface between
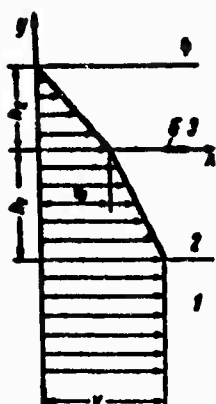
192

Fig. 84. Flow of liquids with plane interface.

the second and third zones act forces of surface tension (coefficient of surface tension σ); velocity in the boundary layer changes linearly with respect to the coordinate. Values of parameters are given in Table 5.

Table 5.

Zone (Fig. 84)	Values of ordinate	Density of liquid	Velocity
1	$-\infty < y < -h_1$	ρ_1	$V_1 = V$
2	$-h_1 < y < 0$	ρ_1	$V_2 = V - \dfrac{V - V_0}{h_1}(h_1 + y)$
3	$0 < y < h_2$	ρ_2	$V_3 = V_0 - \dfrac{V_0}{h_2} y$
4	$h_2 < y < \infty$	ρ_2	$V_4 = 0$

The stream function of the flow we express in the following way:

$$\psi = \varphi(y)e^{i(\alpha x - \beta t)}. \tag{287}$$

Velocity components are written so:

$$u' = \frac{\partial \psi}{\partial y}, \quad v' = -\frac{\partial \psi}{\partial x}. \tag{288}$$

and for function $\phi(y)$ the solution in zones 1, 2, 3, and 4 will be of the following form:

193

$$\varphi_1 = C_1 e^{\alpha y}; \quad \varphi_2 = C_2 e^{-\alpha y} + C_3 e^{\alpha y};$$
$$\varphi_3 = C_4 e^{-\alpha y} + C_5 e^{\alpha y};$$
$$\varphi_4 = C_6 e^{-\alpha y}. \tag{289}$$

Boundary conditions of the problem are formulated thusly: on borders 1-2 ($y = -h$), 2-3 ($y = 0$), 3-4 ($y = h_2$), normal components of velocity and pressure gradients along the x-axis are continuous.

Equation of motion gives the expression for pressure gradient:

$$\frac{\partial p}{\partial x} = -\rho \left(\frac{\partial u'}{\partial t} + V \frac{\partial u'}{\partial x} + v' \frac{dV}{dy} \right). \tag{290}$$

and if we have in mind that by formulas (288) and (289)

$$u' = \varphi'(y) e^{i(\alpha x - \beta t)};$$
$$v' = -i\alpha \varphi(y) e^{i(\alpha x - \beta t)}, \tag{291}$$

it is possible to write:

$$\frac{\partial p}{\partial x} = i\rho \left[(\beta - \alpha V) \varphi' + \alpha \varphi \frac{dV}{dy} \right] e^{i(\alpha x - \beta t)}. \tag{292}$$

Lifting a particle of liquid above the undisturbed surface of an interface is represented in the form

$$\eta = \bar{\eta} e^{i(\alpha x - \beta t)} \tag{293}$$

$$\frac{\partial \eta}{\partial t} = v' - \frac{\partial \eta}{\partial x} V = -i\beta \bar{\eta} e^{i(\alpha x - \beta t)} =$$
$$= -i\alpha \varphi e^{i(\alpha x - \beta t)} - i\alpha \bar{\eta} V e^{i(\alpha x - \beta t)},$$

whence

$$\bar{\eta} = \frac{\alpha \varphi}{\beta - \alpha V}. \tag{294}$$

Formulated boundary conditions give

194

$$\text{when} \quad y = -h_1 \; \varphi_1 = \varphi_2, \; \frac{\partial p_1}{\partial x} = \frac{\partial p_2}{\partial x} \; ;$$

$$\text{when} \quad y = 0 \; \varphi_2 = \varphi_3, \; \frac{\partial p_3}{\partial x} - \frac{\partial p_2}{\partial x} = -\sigma \frac{\partial^2 \eta}{\partial x^2} = \sigma i \eta \alpha^2 \; ; \tag{295}$$

$$\text{when} \quad y = h_2 \; \varphi_3 = \varphi_4, \; \frac{\partial p_3}{\partial x} = \frac{\partial p_4}{\partial x} \; .$$

Using expressions (289), (292), (293), and (294) upon substitution into expressions (295), after certain transformations we obtain

$$C_2 e^{-\alpha h_1} = C_2 e^{\alpha h_1} + C_3 e^{-\alpha h_1}; \quad C_2 + C_3 = C_4 + C_5;$$

$$C_4 e^{-\alpha h_2} + C_5 e^{\alpha h_2} = C_6 e^{-\alpha h_3};$$

$$(\beta - \alpha V) C_1 e^{-\alpha h_1} = (\beta - \alpha V)[-C_2 e^{\alpha h_1} + C_3 e^{-\alpha h_1}] +$$

$$+ [C_2 e^{\alpha h_1} + C_3 e^{-\alpha h_1}] \left(-\frac{V - V_0}{h_1}\right);$$

$$\rho_2 \{\beta[-C_4 e^{-\alpha h_2} + C_5 e^{\alpha h_2}] - \frac{V_0}{h_2}[C_4 e^{-\alpha h_2} + C_5 e^{\alpha h_2}]\} =$$

$$= \rho_3(-\beta C_6 e^{-\alpha h_3}); \tag{296}$$

$$\rho_1 \left\{(\beta - \alpha V_0)[-C_2 + C_3] + (C_2 + C_3)\left[-\frac{V - V_0}{h_1}\right]\right\} -$$

$$- \rho_2 \left\{(\beta - \alpha V_0)[-C_4 + C_5] + (C_4 + C_5)\left[-\frac{V_0}{h_2}\right]\right\} =$$

$$= \frac{\sigma \alpha^2}{\beta - \alpha V_0}(C_2 + C_3).$$

Let us introduce the following dimensionless quantities:

$$m_1 = \alpha h_1, \; m_2 = \alpha h_2, \; M = \frac{\rho_2}{\rho_1}, \; N = \frac{\rho_3}{\rho_2}. \tag{297}$$

After substitution of these quantities into expressions (296) we obtain

$$C_2 e^{-m_1} - C_2 e^{m_1} - C_3 e^{-m_1} = 0; \quad C_2 + C_3 - C_4 - C_5 = 0;$$

$$C_4 e^{-m_2} + C_5 e^{m_2} - C_6 e^{-m_3} = 0;$$

$$C_1(h_1 \beta - m_1 V) e^{-m_1} + C_2[(h_1 \beta - m_1 V) + (V - V_0)] e^{m_1} -$$

$$- C_3[(h_1 \beta - m_1 V) - (V - V_0)] e^{-m_1} = 0; \tag{298}$$

$$C_4[-(h_2 \beta + V_0) e^{-m_2}] + C_5[(h_2 \beta - V_0) e^{m_2}] +$$

$$+ C_6 N h_2 \beta e^{-m_3} = 0;$$

195

$$C_2\left\{-(\beta-\alpha V_0)-\frac{V-V_0}{h_1}-\frac{\sigma\alpha^2}{\rho_1(\beta-\alpha V_0)}\right\}+C_3\left\{(\beta-\alpha V_0)-\right.$$
$$\left.-\frac{V-V_0}{h_1}-\frac{\sigma\alpha^2}{\rho_1(\beta-\alpha V_0)}\right\}+C_4 M\left\{(\beta-\alpha V_0)+\frac{V_0}{h_2}\right\}+$$
$$+C_5 M\left\{-(\beta-\alpha V_0)+\frac{V_0}{h_2}\right\}=0. \tag{298}$$

Composing a determinant from coefficients for arbitrary constants of system (298) and equating it to zero, we obtain

$$\begin{vmatrix} e^{-m_1} & -e^{-m_1} & -e^{-m_1} & 0 & -1 & 0 \\ e & 1 & 1 & -1 & e^{-m_2} & 0 \\ \eta e^{-m_1} & (\eta+g_1)e^{-m_1} & -(\eta-g_1)e^{-m_1} & 0 & 0 & -e^{-m_3} \\ 0 & 0 & 0 & -(\beta+g_2)e^{-m_2} & (\beta-g_2)e^{m_2} & N\beta e^{-m_3} \\ 0 & -[\eta_0^2+g_1\eta_0+\tau] & \eta_0^2-g_1\eta_0-\tau & M[\eta_0^2+g_2\eta_0] & M[-\eta_0^2+g_2\eta_0] & 0 \end{vmatrix}=0, \tag{299}$$

where

$$\eta=\beta-\alpha V;\quad \eta_0=\beta-\alpha V_0;$$
$$g_1=\frac{V-V_0}{h_1};\quad g_2=\frac{V_0}{h_2};\quad \tau=\frac{\sigma\alpha^2}{\rho_1}. \tag{300}$$

Expanding determinant (299), we obtain a characteristic equation in the following form:

$$-[2\eta+g_1(1-e^{-2m_1})]\{2M\eta_0^2[(1-N)\beta+g_2]e^{-2m_1}-$$
$$-M(\eta_0^2+g_2\eta_0)[\beta((1+N)+(1-N)e^{-2m_0})-$$
$$-g_2(1-e^{-2m_0})]\}+\{\beta[(1+N)+(1-N)e^{-2m_0}]-$$
$$-g_2(1-e^{-2m_0})\}\{[2\eta+$$
$$+g_1(1-e^{-2m_0})][\eta_0^2-g_1\eta_0-\tau]+2\eta_0^2 g_1 e^{-2m_1}\}=0. \tag{301}$$

We will examine a special case of the problem in which densities of liquids in zones 3 and 4 are equal (i.e., for example, for the case water-steam-air instead of vapor air of the same density as in zone 4 is also in motion; then $\rho_2 = \rho_3$, $N = 1$. Instead of equation (301) we obtain

$$-[2\eta+g_1(1-e^{-2m_0})]\{2M\eta_0^2 g_2 e^{-2m_1}-M(\eta_0^2+g_2\eta_0)[2\beta-$$
$$-g_2(1-e^{-2m_0})]\}+\{2\beta-g_2(1-e^{-2m_0})\}\{[2\eta+g_1(1-$$
$$-e^{-2m_0})][\eta_0^2-g_1\eta_0-\tau]+2\eta_0^2 g_1 e^{-2m_1}\}=0. \tag{302}$$

196

Thus, equation (302) corresponds to the problem of stability of the interface of two liquids with densities ρ_1 and ρ_2 (for example, water and air) when in the first is a layer of thickness h_1, and in the second, a boundary layer of thickness h_2.

Let us set

$$h_1 = h; \ (m_1 = m); \ h_2 = kh; \ (m_2 = km); \ V_0 = \frac{k}{k+1}V. \tag{303}$$

then

$$\left.\begin{array}{l}
\eta \dfrac{k}{V} = H - m; \ \eta_0 \dfrac{k}{V} = H - \dfrac{k}{k+1}m = R; \\[2mm]
H = \beta \dfrac{k}{V}; \ g_1 \dfrac{k}{V} = g_2 \dfrac{k}{V} = \dfrac{1}{k+1}; \\[2mm]
\tau \dfrac{k^2}{V^2} = M \dfrac{\pi^2}{W} = D; \ W = \dfrac{\rho_1 h V^2}{e}.
\end{array}\right\} \tag{304}$$

After substitution of equations (303) and (304) into equation (302), we obtain

$$-(R+p)\{M\,bR^2 - M\left(R^2 + \frac{1}{k+1}R\right)(R+q)\} +$$
$$+(R+q)\left\{(R+p)\left(R^2 - \frac{1}{k+1}R - D\right) + aR^2\right\} = 0. \tag{305}$$

where

$$\left.\begin{array}{l}
p = -\dfrac{m}{k+1} + \dfrac{1-e^{-2m}}{2(k+1)}; \ q = \dfrac{k}{k+1}m - \dfrac{1-e^{-2km}}{2(k+1)}; \\[2mm]
a = \dfrac{e^{-2m}}{k+1}; \ b = \dfrac{e^{-2km}}{k+1}.
\end{array}\right\} \tag{306}$$

Transforming equation (305), we obtain

$$(1+M)R^4 + [(p+q)(1+M) - \frac{1}{k+1}(1-M) + a - bM]R^3 +$$
$$+ [pq(1+M) - (p+q)\frac{1}{k+1}(1-M) + aq - bpM - D]R^2 -$$
$$- \left[pq\frac{1}{k+1}(1-M) + (p+q)D\right]R - pqD = 0. \tag{307}$$

Let us investigate the special case when the boundary layer in zone 3 is absent, i.e., oscillations of the interface of two liquids

197

(for example, water-air), considering only the boundary layer in one
of them (in water).

Assuming that in equation (306) k = 0, we obtain

$$p = -m + \frac{1-e^{-2m}}{2}; \quad q = 0; \quad a = e^{-2m}; \quad b = 1 \tag{308}$$

and, placing these values in equation (307), we will have

$$H^3 + p_2 H^2 + p_1 H + p_0 = 0, \tag{309}$$

where

$$p_2 = -\frac{n_1 + M n_2}{1+M}; \quad p_1 = \frac{n_2 - D}{1+M};$$

$$p_0 = \frac{n_2 D}{1+M}; \quad n_1 = n + A; \quad n_2 = m - A; \quad A = \frac{1-e^{-2m}}{2}. \tag{310}$$

Equation (309) for the relevant range of values of the coefficient
of parameters has one real root H_1 = a and two complex conjugate roots
$H_{2,3}$ = b ± ic. Between the roots and coefficients of this equation,
using certain Vieta formulas, we can establish the following connection:

$$\begin{cases} a + 2b = -p_2; \\ 2ab + b^2 + c^2 = p_1; \\ a(b^2 + c^2) = -p_0. \end{cases} \tag{311}$$

Excluding from expressions (311) a and b, we obtain the equation
for the square of the imaginary part of root $c^2 = H_1^2 = \chi$:

$$64\chi^3 + 32(p_2^2 - 3p_1)\chi^2 + 4(p_2^2 - 3p_1)^2 \chi - (p_2^2 - 3p_1)^3 F = 0, \tag{312}$$

where

$$F = \frac{27p_0^2 + 4p_1^3 + 4p_0 p_2^3 - 18p_0 p_1 p_2 - p_1^2 p_2^2}{(p_2^2 - 3p_1)^3}. \tag{313}$$

Setting

$$\chi = \frac{1}{4}(\rho_1^2 - \psi_1)\psi,$$

we obtain the equation

$$\psi(\psi + 1)^2 = F,$$ (314)

from which one should determine only real roots.

This equation is easily solved graphically with the help of two graphs for $F = \psi(\psi + 1)^2$ and $F = F(m, W)$ (Fig. 85).

The result of the solution of equation (312) is given on Figs. 86, 87, and 88, which show the dependences of the square of dimensionless increment H_1^2 on the dimensionless wave number for various values of W and the dependence of the value of optimum wave number m_0 on Weber number W (at $M = 1.2 \cdot 10^{-3}$, water-air).

Let us now consider certain special cases.

Let us assume that thickness of boundary layer h tends to zero. Then from equation (309)

$$\rho_i = \sqrt{MV^2\alpha^2 - \frac{\alpha^3\sigma}{\rho_1}}.$$ (315)

This result was obtained by Jork and Stubbs. In the absence of velocity or a second liquid ($V = 0$ or $M = 0$) for increment of
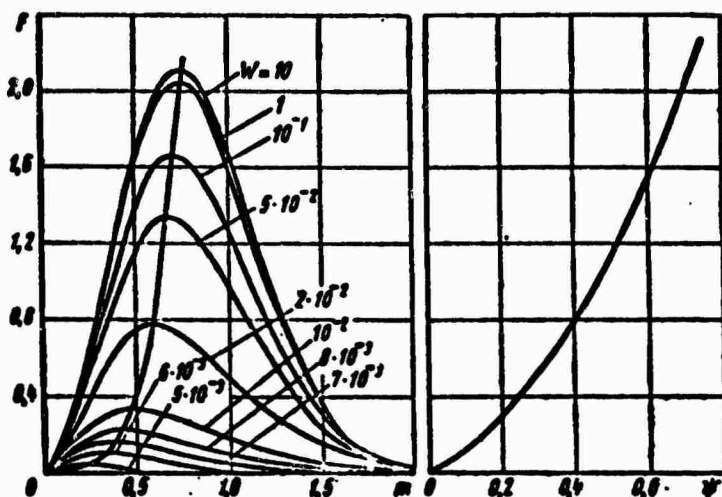
Fig. 85. Function $F = \psi(\psi + 1)^2$ and $F = f(m, W)$ for the solution of equation (312) (calculation of square of increment of oscillations $\chi = H_1^2$).
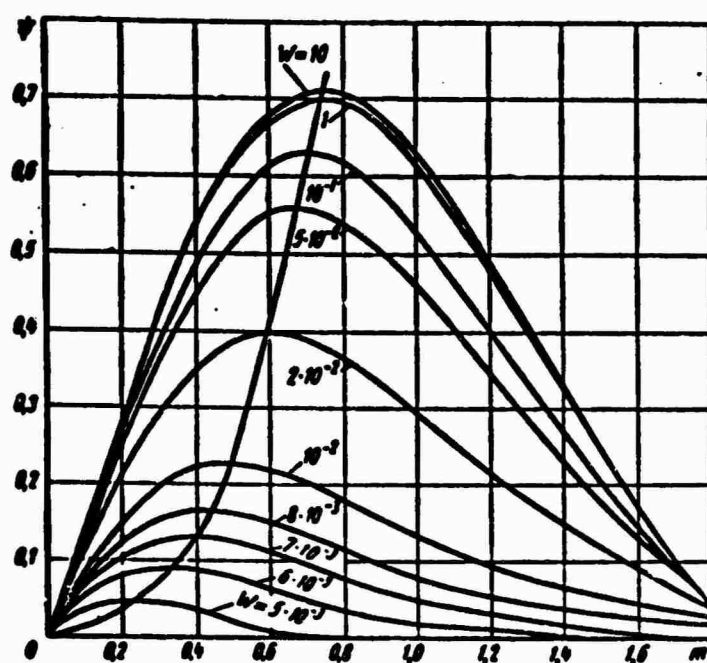
Fig. 86. Auxiliary graph of the dependence of ψ on wave number m for calculation of the unknown connections between H_1^2 and m for various W.

oscillations β_1 an imaginary number is obtained which shows that motion in this case is stable.

Squaring equation (315) differentiating the expression for square of the increment with respect to α and equating the derivative to zero, we obtain the expression for wavelength of the optimum perturbation (corresponding to maximum of increment of oscillations):

$$\lambda_m = \frac{3\pi\sigma}{\rho_1 V^2}.$$

(316)

For oscillations of the interface of two liquids the same result is obtained as for a cylindrical film of liquid in a gaseous environment, expressed by formula (286) for the case of large Weber numbers W >> 1. This shows the accuracy of the earlier affirmation that curvature of the film does not affect disintegration when Weber numbers are large.

In another maximum case when W = ∞ from the solution of equation (309), setting D = 0, we can obtain the value of optimum wave number
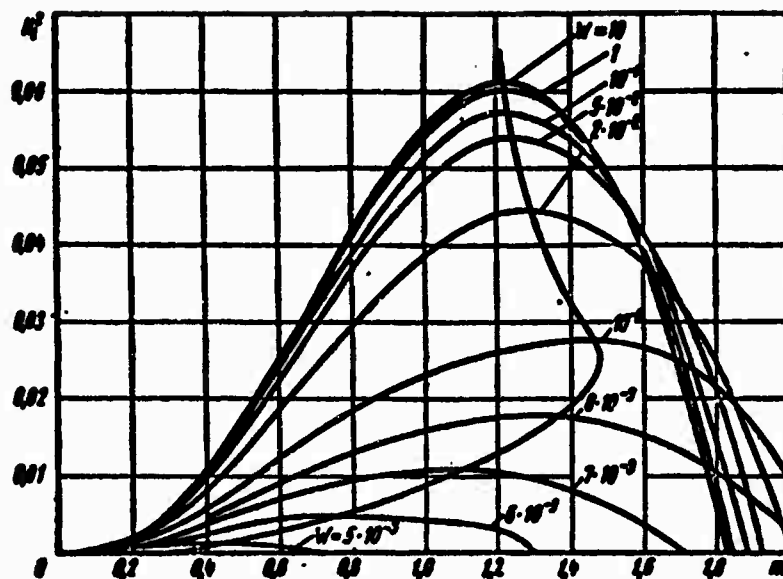
Fig. 87. Dependence of the square of dimensionless increment of oscillations H_1^2 on wave number m for various Weber numbers W for the case of oscillations of the interface of two liquids taking into account the boundary layer in one of them (water-air, boundary layer in water, M $=$ $1.2 \cdot 10^{-3}$).

m, corresponding to the asymptote on Fig. 88:

$$m_\infty = 1.225,$$ (317)

whence we obtain the limit wavelength in the presence of a boundary layer in liquid as W $\to \infty$ (practically, at W > 0.1):

$$\lambda_m > \frac{2\pi h}{1.225} = 5.12\, h.$$ (318)

Consequently, in this maximum case in the presence of a boundary layer in the liquid wavelength cannot be less than approximately five times the thickness of the boundary layer any velocity of the liquid.

In general, as follows from Fig. 88, the dimensionless wave number does not exceed $m_0 = 1.5$, which corresponds to wavelength $\lambda_m \geq 4.2$ h. On the same graph it is clear that when Weber number W ≤ 0.004 the interface becomes stable.

201
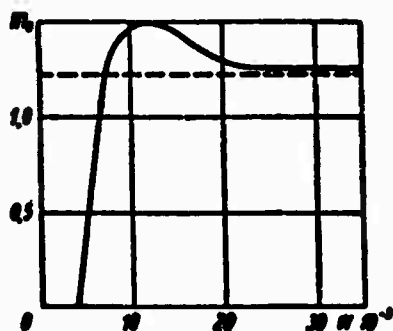
Fig. 88. Dependence of optimum wave number m_0 on W.

The examined problem about oscillations of the interface of two liquids taking into account the boundary layer in one of them (more dense) is the most important, inasmuch as the boundary layer in a less dense liquid weakly affects oscillations.

This may be seen from the following considerations. From equation (307) at $D = 0$ (no influence of capilarity) simple equations can be obtained corresponding to:

1. The case of oscillations of the interface of two liquids taking into account the boundary layer only in the more dense liquid

$$(M+1)H^2 - (Mn_2 + n_1)H + n_2 = 0;$$

2. The case of oscillations of the interface of two liquids taking into account the boundary layer only in the less dense liquid

$$(M+1)H^2 - (n_2 + Mn_1)H + Mn_2 = 0.$$

The solution of these equations and transformation of equation (315), corresponding to the case of oscillations of the interface of two liquids during discontinuous velocity distribution, permit making the following conclusions:

1. The presence of a boundary layer in a liquid with greater density strongly increases the increment of oscillations as compared to the case of discontinuous velocity distribution on the interface (liquid with small density influences weakly).

202

2. Presence of a boundary layer in a liquid with less density (due to its small density) gives increments of oscillations comparable with those obtained in the case of discontinuous velocity distribution.

§ 4. Influence of External Perturbations of Primary Motion on Stability and Disintegration of a Cylindrical Stream of Liquid

It is worthwhile to establish the effect of changes of certain parameters of primary motion on stability and disintegration of a stream of liquid, since in most cases in practice they can be changed for various reasons.

Let us consider the effect on stability and disintegration of a round cylindrical stream of liquid of periodic oscillations of velocity and density of the medium.

The system of coordinates is selected so that the stream is considered motionless, and the surrounding medium moves at velocity U. Densities of stream and medium are designated by ρ_1 and ρ_2 respectively. We will consider that U and ρ_2 are periodic functions of time. Liquid of the stream and medium are considered ideal, and the flow is potential.

Equation (238) will be the equation of the velocity potential in a cylindrical system of coordinates (r, ϕ, x) at k = 1.2.

It is known that on the surface of the stream the following boundary conditions must be fulfilled [20]:

a) equality of normal velocities (at r = a)

$$\frac{\partial \xi}{\partial t} + \frac{\partial \xi}{\partial x} U = \frac{\partial \Phi_2}{\partial r} ; \quad \frac{\partial \xi}{\partial t} = \frac{\partial \Phi_1}{\partial r} . \tag{319}$$

where ξ — radial deflection of particle of liquid from undisturbed surface of stream; indices 1 and 2 refer to stream and medium respectively;

b) equality of the difference of pressures in stream and medium and the pressure of surface tension

$$p_1 - p_2 = -\sigma\left(\frac{\xi}{a^2} + \frac{1}{a^2}\cdot\frac{\partial^2\xi}{\partial\varphi^2} + \frac{\partial^2\xi}{\partial x^2}\right). \tag{320}$$

where σ — coefficient of surface tension of liquid of stream with respect to liquid of medium; p_1 and p_2 — pressure during perturbed motion, determined by Lagrange-Cauchy integral:

$$\left.\begin{array}{c}
p_1 = -\rho_1\dfrac{\partial\Phi_1}{\partial t}; \\[2mm]
p_2 = -\rho_2\left(\dfrac{\partial\Phi_2}{\partial t} + \dfrac{\partial\Phi_2}{\partial x}U\right).
\end{array}\right\} \tag{321}$$

Integrating equation (238) by the method of separation of variables, we obtain:

$$\left.\begin{array}{ll}
\text{for stream} & \Phi_1 = A(t)I_m(kr)e^{im\varphi + ikx}; \\[1mm]
\text{for medium} & \Phi_2 = B(t)K_m(kr)e^{im\varphi + ikx}.
\end{array}\right\} \tag{322}$$

where $A(t)$, $B(t)$ — function of time; $k = \dfrac{2\pi}{\lambda}$ — wave number; λ — wavelength of perturbation along the x-axis; m — number of waves along the circumference of the stream cross section; $I_m(a)$, $K_m(a)$ — Bessel function of imaginary argument of order m.

Radial deflection of surface from the initial position of the undisturbed stream can be represented in the form

$$\xi = \bar{\xi}e^{im\varphi + ikx}. \tag{323}$$

Placing in boundary conditions (319) and (320) expressions (321), (322) and (323) we obtain

$$\left.\begin{array}{c}
\bar{\xi}' = kA(t)I_m'(ka); \\[1mm]
\bar{\xi}' + ikU\bar{\xi} = kB(t)K_m'(ka); \\[1mm]
-\rho_1 A'(t)I_m(ka) + \rho_2 B'(t)K_m(ka) + \rho_2 ikUB(t)K_m(ka) = \\[1mm]
= -\dfrac{1}{a^2}\sigma\bar{\xi}(k^2a^2 + m^2 - 1).
\end{array}\right\} \tag{324}$$

where the prime for ξ — signifies differentiation with respect to t, and for Bessel functions — differentiation with respect to the argument. Excluding from this ystem functions A and B and introducing dimensionless quantites

$$M = \frac{n}{n}, \quad a = ka, \quad S = U\sqrt{\frac{\rho\epsilon}{\epsilon}},$$
$$\tau = t\sqrt{\frac{\epsilon}{n^2}}.$$

(325)

we obtain an equation relative to $\bar{\xi}(\tau)$:

$$\bar{\xi}''(MK - I) + 2ia MSK\bar{\xi}' - [a^2 MS^2 K + \\ + a(a^2 + m^2 - 1) - ia MS'K]\xi = 0,$$

(326)

where

$$I = \frac{I_m(a)}{I'_m(a)}, \quad K = \frac{K_m(a)}{K'_m(a)}.$$

(327)

We reduce equation (326) to normal form:

$$u'' + Ju = 0,$$

(328)

where

$$u(\tau) = \xi \exp\left\{\frac{1}{2}\int \frac{g}{f} d\tau\right\}; \quad J = \frac{h}{f} - \frac{1}{4}\left(\frac{g}{f}\right)^2 - \frac{1}{2}\left(\frac{g}{f}\right)'$$

is the invariant of the differential equation, and

$$f = MK - I; \quad g = 2ia MSK;$$
$$h = - [a^2 MS^2K + a(a^2 + m^2 - 1)] + ia MS'K.$$

Thus,

$$u(\tau) = \bar{\xi}(\tau) \exp\left\{ia K \int \frac{MS}{MK - I} d\tau\right\}$$

(329)

$$J = \frac{1}{(MK - I)^2} [a^2 MS^2KI - a(a^2 + m^2 - 1)(MK - I) + \\ + ia KSM'I].$$

Let us examine first the effect of oscillation of the flow rate, i.e., parameter S, on disintegration of a stream during constant density of medium (M = const).

Dimensionless velocity S is represented in the following form:

$$S = S_0 [1 + \epsilon \psi(\nu\tau)] \left(\nu = \omega \sqrt{\frac{\rho_0 d^2}{\sigma}} \right).$$

where ϵ — relative amplitude of oscillations of velocity of the medium, which we consider small as compared to unity; ψ — periodic function with period 2π; ν — dimensionless frequency of imposed oscillations; ω — angular frequency.

Then from expression (329) we obtain

$$u(\tau) = \bar{\xi}(\tau) \exp \left\{ \frac{MK}{MK - 1} \int S \, d\tau \right\}; \tag{330}$$

$$J = \frac{1}{(MK - 1)^2} [\alpha^2 M K I S_0^2 - \alpha(\alpha^2 + m^2 - 1)(MK - 1) + 2\alpha^2 M K I S_0^2 \epsilon \psi(\nu\tau)].$$

Designating $\nu\tau$ = x, we reduce equation (326) to the form

$$u'' + [\lambda + \gamma \psi(x)] u = 0, \tag{331}$$

where

$$\left. \begin{array}{l} \lambda = \frac{1}{\nu^2 (MK - 1)^2} [\alpha^2 M K S_0^2 - \alpha)(\alpha^2 + m^2 - 1)(MK - 1)]; \\[2mm] \gamma = \frac{2\alpha^2 M K I S_0^2}{\nu^2 (MK - 1)^2} . \end{array} \right\} \tag{332}$$

Equation (331) is Hill's equation. Its general solution has the form [19]

$$u = C_1 e^{\mu x} \varphi(x) + C_2 e^{-\mu x} \varphi(-x). \tag{333}$$

where $\varphi(x)$ — periodic function; μ — characteristic index, depending on parameters λ and γ and determining the character of the solution.

Solutions increasing in time correspond to Re $\mu > 0$.

At first we will examine the simplest case of pulse oscillations of the form

$$\psi(x) = \begin{cases} 1 \, (-\pi < x < 0); \\ -1 \, (0 < x < \pi). \end{cases} \qquad (334)$$

In this case the solution of equation (331) is expressed in trigonometric functions, and the index μ is calculated by the formula [18].

$$ch\, 2\pi\mu = \cos x_1 \cos x_2 - \frac{1}{2}\left(\frac{x_1}{x_2} + \frac{x_2}{x_1}\right)\sin x_1 \sin x_2, \qquad (335)$$

where

$$x_1 = \pi\sqrt{\lambda + \gamma}; \; x_2 = \pi\sqrt{\lambda - \gamma}.$$

With the help of this equation it is possible to construct boundary curves between regions of stable and unstable solutions, corresponding to ch $2\pi\mu = \pm 1$. On Fig. 89 such curves are constructed in coordinates λ, γ and regions corresponding to stable solutions are shown (shaded).
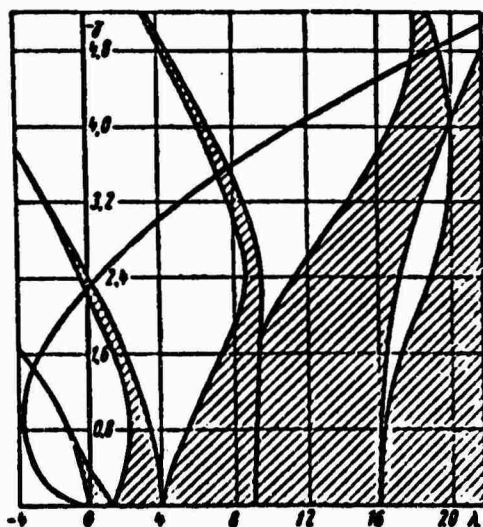
Fig. 89. Regions of stable and unstable solutions of Hill's equation.

Parameters of Hill's equation λ and γ in the examined case depend on M, S_0, m, ν, ϵ, and also on wave number α. After excluding α

from formulas (332) it is possible to construct the curve of $\lambda(\gamma)$ for selected values of the parameters.

The curve of $\lambda(\gamma)$ goes beyond the origin of coordinates and consecutively intersects all regions of instability. With distance from the origin of coordinates to points of the curve correspond ever increasing values of wave numbers α.

To investigate the effect of oscillations of velocity of the medium (or exit velocity of liquid) it is necessary to construct curves of the dependence of the increment of oscillations of perturbed motion on wave number for different regions of unstable (growing) oscillations.

Since accurate to the periodic factor

$$\bar{\xi} \sim u \sim e^{i\lambda \tau} = e^{i\mu\nu\tau}, \tag{336}$$

the dimensionless increment of oscillations is equal to

$$Z = \mu\nu. \tag{337}$$

In Fig. 90 are constructed curves of $Z(\alpha)$ for two frequencies of oscillations $\nu = 0.6$, 2 for parameters $M = 10^{-3}$, $m = 0$, $S_0 = 40$, $\varepsilon = 0.4$. In the same place is constructed the curve of $Z(\alpha)$ for the case of no velocity oscillations ($\varepsilon = 0$); this curve has a maximum at $\alpha \approx 1.3$ [20].
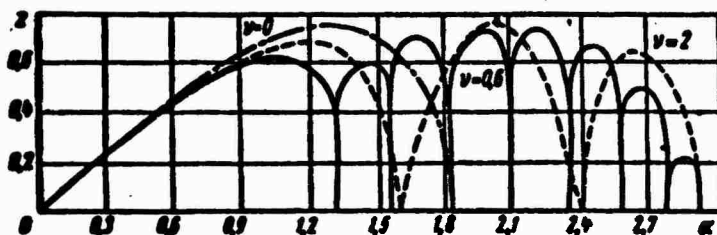
Fig. 90. Dependence of increment of oscillations on wave number when oscillations are imposed on the stream exit velocity.

When velocity oscillations are imposed the character of disintegration of the stream is changed: there appears a multitude (in principle infinitely large) of regions of instability in coordinates λ, γ. Each of these regions has a defined width with respect to wave numbers (wavelengths) and maximum increment of oscillations.

If it is considered that the size of the drops forming as a result of disintegration of a stream is determined by the wavelength corresponding to maximum increment over all regions of instability, then from Fig. 89 a decrease of the size of drops in the case of oscillations of flow rate can be concluded.

There are experimental data about the effect on a stream of liquid of oscillations of flow rate. It developed that these oscillations lead to a decrease of the size of drops -- average diameter of the drops under experimental conditions decreased approximately by half.

Thus, these experiments confirm the above theoretical conclusion.

Within limits of selected parameters the frequency shift of oscillations ν causes redistribution of regions of instability with respect to wave numbers (wavelengths); the maximum increment of oscillations hardly changes.

Further, let us turn to an investigation of the effect of oscillations of the density of a medium (M) on disintegration of a stream, considering the flow rate as constant (S = const).

We will consider that M is a periodic function of time

$$M = M_0(1 + \delta \cos \nu\tau). \tag{338}$$

where δ is the amplitude.

From formulas (328) and (329) we obtain the expressions for the invariant of the differential equation ($\nu\tau = 2x$):

209

$$J(x) = \theta_0 - 2\theta_1 \cos 2x - 2i\theta_2 \sin 2x, \qquad (339)$$

where

$$\theta_0 = \frac{4}{\nu_1(M_0 K - I)^2}[\alpha^2 M_0 S^2 KI - \alpha(\alpha^2 + m - 1)(M_0 K - I)];$$

$$\theta_1 = -\frac{2M_0 K \alpha \delta}{\nu^2 (M_0 K - I)^2}[\alpha S^2 I(1 - 2KM_0) + (\alpha^2 + m^2 - 1)(KM_0 - I)];$$

$$\theta_2 = -\frac{2\alpha M_0 KIS\delta}{\nu(M_0 K - I)^2}. \qquad (340)$$

Then equation (326) takes the form of Hill's equation:

$$u'' + (\theta_0 - 2\theta_1 \cos 2x - 2i\theta_2 \sin 2x)u = 0. \qquad (341)$$

Its solution also can be represented by expression (333)

For an analysis of stability of the solutions of equation (341) we will present it in the following way:

$$u'' + [\theta_0 - (\theta_1 + \theta_2)e^{2ix} - (\theta_1 - \theta_2)e^{-2ix}]u = 0, \qquad (342)$$

and its solution in the form

$$u = e^{\mu x} \sum_{-\infty}^{+\infty} a_{2r+p} e^{(2r+p)ix}. \qquad (343)$$

Putting the solution of (343) into equation (342), we obtain the relationship for coefficients

$$[\theta_0 - (2r + p - i\mu)^2]a_{2r+p} - (\theta_1 + \theta_2)a_{2r+p-2} - (\theta_1 - \theta_2)a_{2r+p+2} = 0. \qquad (344)$$

To calculate μ we will use the method of Einz [Editor's Note: exact translation of name not found] [15]. We have

$$\frac{a_{2r+p}}{a_{2r+p-2}} = \frac{\theta_1 + \theta_2}{\theta_0 - (2r + p - i\mu)^2 - (\theta_1 - \theta_2)\dfrac{a_{2r+p+2}}{a_{2r+p}}} \qquad (345)$$

210

where $(r = 1, 2, 3, \ldots)$;

$$\frac{a_{2r+\rho}}{a_{2r+\rho+2}} = \frac{\theta_1 - \theta_2}{\theta_0 - (2r+\rho - i\mu)^2 - (\theta_1 + \theta_2)\frac{a_{2r+\rho-2}}{a_{2r+\rho}}} \tag{346}$$

where $(r = 0, -1, -2 \ldots)$.

From expressions (345) and (346) it follows that

$$\frac{a_{2+\rho}}{a_\rho} = \frac{\theta_1 + \theta_2}{\theta_0 - (2+\rho - i\mu)^2 - \dfrac{\theta_1^2 - \theta_2^2}{\theta_0 - (4+\rho - i\mu)^2 - \ldots}}, \tag{347}$$

$$\frac{a_\rho}{a_{2+\rho}} = \frac{\theta_1 - \theta_2}{\theta_0 - (\rho - i\mu)^2 - \dfrac{\theta_1^2 - \theta_2^2}{\theta_0 - (-2+\rho - i\mu)^2 - \ldots}}$$

We set

$$W_\rho(\mu) = \frac{a_{2+\rho}}{a_\rho}(\theta_1 - \theta_2). \tag{348}$$

Then at $\rho = 0$

$$W_0(\mu) = \theta_0 + \mu^2 - \overline{W_0(\mu)}; \tag{349}$$

for $\rho = 1$

$$W_1(\mu) = \theta_0 - (1 - i\mu)^2 - \frac{\theta_1^2 - \theta_2^2}{\theta_0 - (1 - i\mu)^2 - \overline{W_1(\mu)}}. \tag{350}$$

where the line signifies a complex conjugate number.

Then

$$\left.\begin{array}{c} W_0(\mu) + \overline{W_0(\mu)} = \theta_0 + \mu^2; \\ \theta_1^2 - \theta_2^2 = [\theta_0 - (1 + i\mu)^2 - \overline{W_1(\mu)}][\theta_0 - \\ - (1 - i\mu)^2 - W_1(\mu)]. \end{array}\right\} \tag{351}$$

To analyze the stability of solutions of equation (342) it is possible to construct a diagram of eigenvalues $\theta_0 = f(\theta_1^2 - \theta_2^2)$ similar to the diagram for the Mathieu equation [15], considering in formulas (349), (350), and (351) that Re $\mu = 0$. This diagram we give

211

in coordinates θ_0, Q, where

$$Q = \sqrt{|\theta_1^2 - \theta_2^2|}\, \text{sign}(\theta_1^2 - \theta_2^2). \tag{352}$$

When Q > 0 the diagram becomes the ordinary diagram of a - q for the Mathieu equation (a = θ_0 and q = Q). When Q < 0 curves θ_0 = f(Q) (θ_0 is real) correspond to even periodic solutions of the Mathieu equation with purely imaginary parameter q and can be constructed by the shown method (ρ = 0).

However, for th. investigated case of the effect of oscillations of density of a medium on the disintegration of a stream of liquid, it turns out that for selected parameters M, S (we examine disintegration of a stream of water in air) Q > 0. Consequently, to analyze the stability of a stream, the usual diagram for Mathieu functions can be used (Fig. 91), where a = θ_0 and q = Q.
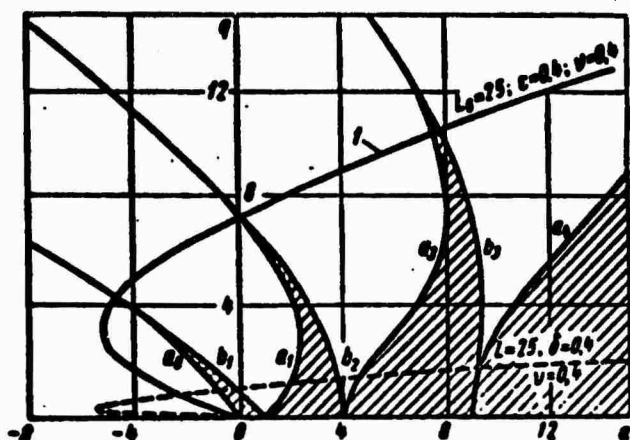
Fig. 91. Regions of stable and unstable solutions of the Mathieu equation.

On Fig. 91 the broken line is the a(q) curve, calculated by the formulas of (340) for S = 25, ν = 0.4 and δ = 0.4. The solid curve is the dependence of a(q) for the case of harmonic oscillations of velocity.

Comparing these curves, we see that at identical values of parameters M, S, frequencies and amplitudes of the curve characterizing oscillation of density of the medium becomes more hollow. As

calculations show, curves for μ = const lie in every region of instability of the diagram (Fig. 91) such that with distance from the origin of the region along the q-axis the index μ increase. This means that under identical conditions the increments Z in the case of oscillations of the density of a medium will be less in absolute value than their values for the case of oscillations of flow rate.

Consequently, oscillations of the density of the medium surroundin a stream of liquid render a smaller influence on disintegration of the stream than oscillation of the flow rate. If one were to construct for this case the curve of Z(α), similar to curve on Fig. 90, then it is possible to establish the same effect of oscillations of the density of the medium, as during oscillations of velocity.

The above conclusions concerning the effect of oscillations of the density of a medium are qualitatively confirmed by the results of experiments, published in the work by Miesse [29].

§ 5. The Effect of Periodic Oscillations of the Density of a Medium on the Stability of the Liquid Drops

It is known that oscillations of the density of a medium influence the dimensions of drops forming during disintegration of a stream of liquid [6, 29].

There are cases when the density of the medium in which drops of liquid move experiences periodic oscillations. It is worthwhile to investigate the stability of a drop of liquid with respect to small perturbations of the parameters of motion and the physical state.

Let us consider a spherical drop of radius R, suspended in a motionless gaseous environment. We will consider that the density of the medium in all its points oscillates periodically and synchronously.

Velocity potential of the perturbed motion of a drop and the surrounding medium satisfies the Laplace equation, having in spherical system of coordinates (r, θ, φ) the following form:

$$\frac{\partial}{\partial r}\left(r^2\frac{\partial\Phi}{\partial r}\right)+\frac{1}{\sin\theta}\cdot\frac{\partial}{\partial\theta}\left(\sin\theta\frac{\partial\Phi}{\partial\theta}\right)+\frac{1}{\sin^2\theta}\cdot\frac{\partial^2\Phi}{\partial\varphi^2}=0, \tag{353}$$

where the rates of the perturbations will be equal to

$$v_r=\frac{\partial\Phi}{\partial r}; \quad v_\varphi=\frac{1}{r\sin\theta}\cdot\frac{\partial\Phi}{\partial\varphi}; \quad v_\theta=\frac{1}{r}\cdot\frac{\partial\Phi}{\partial\theta}. \tag{354}$$

Pressure is determined by the Lagrange-Cauchy integral, having the form

$$\frac{p}{\rho}=-\frac{\partial\Phi}{\partial t}. \tag{355}$$

Density of the liquid of the drop is considered constant and equal to ρ_1, and the velocity potential is equal to $\Phi_1(r,\varphi,\theta,t)$. Density of the liquid of the medium is considered as changing in time and equal to ρ_2, and the velocity potential equal to $\Phi_2(r,\varphi,\theta,t)$. Velocity potentials are represented in the form

$$\Phi_1=u_1A(t); \quad \Phi_2=u_2B(t), \tag{356}$$

where $u_1(r,\varphi,\theta); u_2(r,\varphi,\theta)$ are solutions of equation (353) accordingly for the space inside and outside the sphere, and $A(t)$, $B(t)$ are functions of time, determined by boundary conditions. From expressions (355) and (356) we have

$$\frac{p_1}{\rho_1}=-u_1A'(t); \quad \frac{p_2}{\rho_2}=-u_2B'(t). \tag{357}$$

Boundary conditions of the problem can be formulated in the following way:

1. Normal velocity components on the interface are continuous:

$$\frac{\partial\Phi_1}{\partial r}=\frac{\partial\Phi_2}{\partial r} \text{ when } r=R. \tag{358}$$

2. The difference of pressures inside and outside the sphere is equal to the pressure of surface tension:

$$p_1-p_2=\sigma H, \tag{359}$$

214

where σ coefficient of surface tension of the liquid of the drop with respect to the liquid of the medium; H — mean curvature of perturbed surface of drop;

$$H = -\frac{2}{R^0}\xi - \frac{1}{R^2}\left\{\frac{1}{\sin\theta}\cdot\frac{\partial}{\partial\theta}\left(\sin\theta\frac{\partial\xi}{\partial\theta} + \frac{1}{\sin^2\theta}\cdot\frac{\partial^2\xi}{\partial\varphi^2}\right)\right\},$$

(360)

where ξ — radial displacement of surface of drop, determined by the relationship

$$\frac{\partial\xi}{\partial t} = \frac{\partial u_1}{\partial r}A(t) \qquad \text{when } r = R.$$

(361)

From expressions (358) and (359) it follows that

$$\frac{\partial u_1}{\partial r}A(t) = \frac{\partial u_2}{\partial r}B(t) \qquad \text{when } r = R$$

(362)

and

$$-\rho_1 u_1 A'(t) + \rho_2 u_2 B'(t) = \sigma H \qquad \text{when } r = R.$$

(363)

To exclude one function of time we differentiate relationships (362) and (363) and, considering that

$$H' = \frac{\partial H}{\partial t} = \frac{\partial}{\partial r}\left\{-\frac{2}{R^2}\Phi_2 + \frac{1}{R^2}\cdot\frac{\partial}{\partial r}\left(r^2\frac{\partial u_2}{\partial r}\right)\right\} =$$
$$= \left(\frac{\partial^2 u_2}{\partial r^2} + \frac{4}{R}\cdot\frac{\partial u_2}{\partial r^2}\right)B(t) \qquad \text{when } r = R,$$

(364)

we obtain

$$-\rho_1 u_1 \frac{\partial u_2/\partial r}{\partial u_1/\partial r}B'(t) + \rho_2 u_2 B'(t) + \rho_2 u_2 B'(t) =$$
$$= \sigma\left(\frac{\partial^2 u_2}{\partial r^2} + \frac{4}{R}\cdot\frac{\partial u_2}{\partial r^2}\right)B(t) \qquad \text{when } r = R.$$

(365)

Solutions of equation (253) for regions inside and outside the sphere have the form

$$u_1 = \left(\frac{r}{R}\right)^n S_{mn}; \quad u_2 = \left(\frac{r}{R}\right)^{-n-1}S_{mn}.$$

(366)

215

where $S_{mn}(\theta, \varphi)$ — surface spherical function; m and n — eigenvalues.

Putting equation (366) into equation (365), we obtain the equation for B(t):

$$[\rho_1(n+1) + \rho_2 n]B''(t) + \rho_2' n B'(t) +$$
$$+ \frac{\sigma}{R^2} n(n-1)(n+1)(n+2)B(t) = 0. \tag{367}$$

We designate the density ratio in the following way:

$$\frac{\rho_2}{\rho_1} = M \tag{368}$$

and consider that ρ_2 is a periodic function of time, i.e.,

$$M = M_0(1 + \varepsilon \cos \omega t), \tag{369}$$

where M_0 — ratio of density of medium to density of liquid of drop averaged in time; ε — dimensionless amplitude of oscillations of the density of the medium; ω — angular frequency of imposed oscillations of density.

Let us introduce dimensionless quantities:

$$x = \omega t = \nu\tau; \quad \tau = t\sqrt{\frac{\sigma}{\rho_1 R^3}}; \quad \nu = \omega\sqrt{\frac{\rho_1 R^3}{\sigma}}. \tag{370}$$

Then equation (367) is written as:

$$(n+1+Mn)y'' + M'ny' + \frac{n(n-1)(n+1)(n+2)}{\nu^2} y = 0, \tag{371}$$

where $y(x) = B(t)$, and the primes designate differentiation with respect to x.

Normalizing equation (371), we obtain

$$z'' + Jz = 0, \tag{372}$$

where

216

$$z = y \sqrt{Mn + n + 1};$$

$$J = \frac{n(n-1)(n+1)(n+2)}{v^2(Mn+n+1)} - \frac{1}{4} \cdot \frac{M'^2 n^2}{(Mn+n+1)^2} -$$

$$- \frac{1}{2} \left(\frac{M'n}{Mn+n+1} \right)'. \qquad (373)$$

For the case of drops suspended in a gaseous medium, one may assume that $M_0 \ll 1$. Then the expression for J, if we consider expression (369), will take the form

$$J = \frac{n(n-1)(n+2)}{v^2} - \frac{M_0^2 n^2 \varepsilon^2}{4(n+1)^2} \sin^2 x + \frac{M_0 n \varepsilon}{2(n+1)} \cos x. \qquad (374)$$

The augend in expression (374) can be rejected in view of its smallness as compared to the third term. Then equation (372) passes into a Mathieu equation [15]:

$$z'' + (a - 2q \cos 2x) z = 0, \qquad (375)$$

where

$$a = \frac{4n(n-1)(n+2)}{v^2}; \quad q = - \frac{M_0 n \varepsilon}{n+1}. \qquad (376)$$

The general solution of equation (375) can be written in the form [15]:

$$z = C_1 e^{\mu x} \varphi(x) + C_2 e^{-\mu x} \varphi(-x). \qquad (377)$$

where μ — characteristic exponent, depending on parameters a and q and determining the character of the solution; $\varphi(x)$ — periodic function.

We will examine solutions growing in time, i.e., corresponding to Re $\mu > 0$. Deflection of the surface of a drop accurate to the periodic factor will be proportional to $e^{\mu x} = e^{Zt}$, where Z is the increment of oscillations of the drop:

$$Z = \mu \omega. \qquad (378)$$

Characteristic index μ is calculated according to the method of Whittaker, according to whom μ is determined from system of equations:

$$\left. \begin{aligned} a &= 1 - q\cos 2\sigma_1 + \frac{1}{4}q^2\left(-1 + \frac{1}{2}\cos 4\sigma_1\right) + \ldots; \\ \mu &= -\frac{1}{2}q\sin 2\sigma_1 + \frac{3}{128}q^3\sin 2\sigma_1 - \frac{3}{1024}q^4\sin 4\sigma_1 - \ldots \end{aligned} \right\} \tag{379}$$

Let us find the value of a corresponding to the maximum value of μ between curves a_1, b_1 on the diagram of stability of solutions of the Mathieu equation.

From equation (379) we have

$$\frac{d\mu}{da} = \frac{d\mu}{d\sigma_1} \cdot \frac{d\sigma_1}{da} = 0,$$

i.e.,

$$\frac{d\mu}{d\sigma_1} = -q\cos 2\sigma_1 + \frac{3}{64}q^3\cos 2\sigma_1 - \cdots = 0.$$

In view of the smallness of q being limited to two terms of the series, we obtain

$$\cos 2\sigma_1 = 0, \quad \text{т. е.} \quad \sigma_1 = \frac{\pi}{4} + \pi n \quad (n=0, 1, 2, \ldots). \tag{380}$$

Putting the obtained value of σ_1 into equation (379), we obtain

$$\mu_{\text{max}} = -\frac{1}{2}q + \frac{3}{128}q^3 \tag{381}$$

and

$$a = 1 - \frac{3}{8}q^2. \tag{382}$$

For small values of q the maximum value of characteristic index μ_{max}, considering relationship (376), can be represented in the following form:

218

$$\mu_{max} \approx \frac{1}{2} \cdot \frac{M_0 n s}{n+1} \cdot \tag{383}$$

Frequency of oscillations of density of the medium, corresponding to μ_{max} (resonance frequency), is approximately equal to

$$\omega_p \approx \sqrt{\frac{\sigma}{\rho_1 R^3}} \sqrt{n(n-1)(n+2)}, \tag{384}$$

i.e., naturally coincides with the frequency of neutral oscillations of a spherical drop [9].

The maximum increment of oscillations of a drop

$$Z_{max} = \mu_{max}\omega_p = \frac{M_0 n s}{n+1} \sqrt{\frac{\sigma}{\rho_1 R^3}} \sqrt{n(n-1)(n+2)}. \tag{385}$$

Thus, under conditions of resonance the higher the form of oscillations of a drop, characterized by eigenvalue n, the faster and into a greater number of parts the drop disintegrates.

Decay time of a drop under the influence of imposed oscillations of the density of the medium will be expressed in the following way:

$$t_{pacn} = -\frac{1}{\mu_{max}\omega_p} \ln \frac{\xi_{0\,max}}{R} ; \tag{386}$$

where $\xi_{0\,max}$ - initial maximum deviation of the surface of drop from spherical.

In dimensionless form, using expression (385), we obtain

$$\tau_{pacn} = -\frac{n+1}{n\sqrt{n(n-1)(n+2)}} \cdot \frac{1}{M_0 s} \ln \bar{\xi}_{0\,max}. \tag{387}$$

where $\tau_{pacn} = t_{pacn} \sqrt{\frac{\sigma}{\rho_1 R^3}}$ - dimensionless decay time of drop; $\bar{\xi}_{0\,max} = \frac{\xi_{0\,max}}{R}$ - relative initial maximum deflection of the surface of a drop from spherical.

219

Let us consider disintegration of a drop under the influence of oscillations of the density of the medium. We will consider that the drop has only just now formed during the disintegration of a stream of liquid, and therefore is elongated (for example, as a spheroid).

From formula (384) and (387) we obtain the expression for the ratio of decay time of drop $t_{\text{расп}}$ to period of oscillations θ, accomplished with resonance frequency ω_p:

$$\frac{t_{\text{расп}}}{\theta} = -\frac{n+1}{2\pi n} \cdot \frac{1}{M_0 \beta} \ln \bar{\xi}_{0\max}. \tag{388}$$

If we designate by $\alpha = \dfrac{b}{a}$ the ratio of semiaxes of a spheroid, then

$$\bar{\xi}_{0\max} = \alpha^{2/3} - 1.$$

Putting the value of $\bar{\xi}_{0\max}$ into expression (388), we obtain

$$\alpha = \left(1 + e^{-\frac{2\pi n}{n+1} M_0 \beta \frac{t_{\text{расп}}}{\theta}}\right)^{3/2}. \tag{389}$$

Figure 92 shows the dependence of $\dfrac{t_{\text{расп}}}{\theta}$ on α for $n = 2$ (splitting of drop) and the values $M_0 = 1/7$ and $\varepsilon = 0.2$. As the ratio α increases, decay time of the drop decreases.
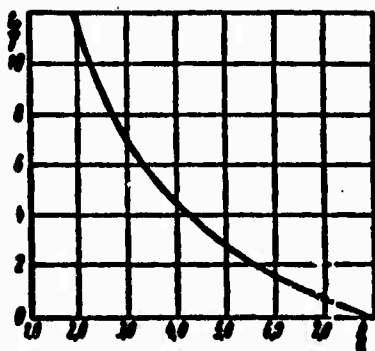
Fig. 92. Dependence of the ratio of decay time to period of oscillation with resonance frequency $\dfrac{t_{\text{расп}}}{\theta}$ on the ratio of semiaxes of a spheroid (initial form of drop).

Let us assume that a drop of liquid is in a volume in which the gas density oscillates with period θ; the time for which drops stay in this volume is $t_{\text{преб}}$.

Plotting $\frac{l_{npe\delta}}{\theta}$ along the axis of ordinates, from the curve we find that those drops which are stretched to the determined ratio of the semiaxes α will disintegrate during $t_{npe\delta}$. Thus, for example, at $\frac{l_{npe\delta}}{\theta} = 5$ for the above values of M_0 and ε those drops for which the ratio of longitudinal and transverse dimensions is α = 3.75 will split.

This example shows that under certain conditions of vibration burning in a jet engine chamber, fine subdivision of fuel drops is possible under the effect of pulsations of the density of the medium.

§ 6.   The Disintegration of a Liquid Torus into Drops

In § 1 of this chapter the difficulties encountered during an investigation of stability and disintegration of drops of liquid in a gas flow were indicated. It is necessary to note one phenomenon, which apparently sometimes occurs during disintegration of drops subjected to the action of a gas flow.

Under certain conditions a drop of liquid streamlined by an external flow of another liquid, can as a result of deformation turn into a liquid ring (torus).

To confirm this phenomenon the following experiment was carried out.

From a small distance above the free surface of water fell a drop of ink. In Fig. 93a-d are the consecutive pictures of the drop descending into the water (pictures were taken from above). It is clear that from the ink drop appears a ring (torus) on which crests subsequently form, and the ring then bursts into drops, each again turning into a torus on which crests again appear, etc.

We must note that the number of crests appearing on the torus may be two, three or more; it decreases with a decrease of the diameter of the torus.

The theoretical problem of oscillations and breaking up of a liquid torus has been apparently examined only in a work by S. Oka [30].

Fig. 93. Consecutive photographs of a drop of ink moving in water.

The complex calculation of the number of drops into which a motionless torus disintegrates, depending upon the ratio of the radius of the torus to the radius of its cross section R/r was carried out only for values of R/r ≥ 5. Oka's work [30] gives the following data:

$\frac{R}{r}$ 5 6 7 8 9 10 11 12

m 3 4 5 6 6 7 8 8

From the formula given in Oka's work it follows that when R/r = 3-4, m = 2.

These results, obtained by Oka by integrating the differential equation describing the phenomenon, in toroidal coordinates, can be established from the following absolutely elementary considerations.

If R/r is large (for Oka R/r ≥ 5), then the breaking up of the torus can be examined as the breaking up of a linear cylindrical stream of circular section under the condition that on length 2πR

is a whole number of waves m.

Since the maximum of instability corresponds to $\frac{2\pi r}{\lambda} = 0.697$, under the condition $m\lambda = 2\pi R$ we obtain [17]:

$$m = \left\{ 0.697 \frac{R}{r} \right\}, \tag{390}$$

where $\{x\}$ is the nearest integer (from below or above) to the x number. Formula (390) gives all values given by Oka's work, and also the values m = 2 and 3 for R/r = 3 and 4.

The above shows that the consideration of being toroid does not influence the number of drops forming from a torus. Division of a torus into two drops is possible only when the inequalities

$$\frac{R}{r} > \frac{2}{0.697} = 2.87 \quad \text{or} \quad \frac{R}{a} > 1.2 \tag{391}$$

hold, and into three drops — when $\frac{R}{r} > \frac{3}{0.697} = 4.3$ or $\frac{R}{a} = 1.58$, where a is the radius of the initial drop.

A comparison of these results with the above experiments may be made only for a very slowly moving torus. Thus, on Fig. 93 it is clear that the ratio R/a for the case of a torus divided into three drops is approximately equal to two. The circumstance that in experiments R/a considerably is larger than in formulas (391), is apparently explained by the effect of transverse streamlining of a thread on a wavelength of maximally growing perturbation.

§ 7. The Effect of Viscosity on Oscillations of the Surface of a Liquid Streamlined by a Gas Flow

When the thickness of the boundary layer in a liquid or gas is small, viscosity of the liquid or gas can directly influence the formation of waves. The problem about direct influence of viscosity on wave formation, neglecting the velocity of the liquid, was solved by Lamb [9], who established that viscosity causes a damping of oscillations according to the following law:

223

$$A = A_0 e^{-2\nu\alpha^2 t},$$ (392)

where A — amplitude of wave; A_0 — initial amplitude; ν — kinematic viscosity of liquid; α — wave number.

Hence time τ of an amplitude decrease by a factor of e is expressed in the following way:

$$\tau = \frac{\lambda^2}{8\pi^2\nu}.$$ (393)

This means that viscosity affects waves of only small length.

It is worthwhile to compare the direct influence of viscosity on oscillations with the boundary layer effect considering the liquid to have velocity.

To determine wavelength we use, just as Mayer [28], the formula for the derivative of wave amplitude A with respect to time [9]:

$$\frac{dA}{dt} = \frac{C}{2\rho_1 c} - 2\nu_1\alpha^2 A,$$ (394)

where $c = \sqrt{\dfrac{\sigma\alpha}{\rho_1}}$ — propagation velocity of capillary waves;

$\nu_1 = \dfrac{\mu_1}{\rho_1}$ — coefficient of kinematic viscosity of liquid;

$\alpha = \dfrac{2\pi}{\lambda}$ — wave number (λ — wavelength).

According to Jeffry, gas pressure on a traveling wave crest may be represented as

$$\bar{s}\rho_2\,(U_2 - c)^2\,\frac{\partial\eta}{\partial x},$$

where $\bar{s} < 1$ — factor characterizing distribution of gas pressure on wave crest;
U_2 — gas velocity;
$\dfrac{\partial\eta}{\partial x}$ — derivative of the rise of the liquid surface with respect to the coordinate in direction of velocity U_2. Then

$$C = \bar{s}\rho_2(U_2 - c)^2\alpha A.$$ (395)

224

Putting values of C and c into expressions (395) and disregarding propagation velocity of waves c in comparison with U_2, we obtain

$$\frac{dA}{dt} = \frac{A}{\tau},$$ (396)

where

$$\frac{1}{\tau} = \frac{\xi}{2} \cdot \frac{\rho_1}{\rho_1} \cdot \frac{U_{\phi a}^2}{\gamma_{\alpha a}} \sqrt{\rho_1} - 2\frac{\mu_1}{\rho_1}\alpha^2.$$ (397)

Amplitude A has its maximum value when $1/\tau = 0$.

Hence we obtain the following connection between $W_\lambda = \frac{\rho U_{\phi}^2 \lambda}{\sigma}$ and $L_{p\lambda} = \frac{\lambda \sigma \rho_1}{\mu_1^2}$:

$$W_\lambda = \frac{4\pi \sqrt{\rho_1}}{\beta \sqrt{L_{p\lambda}}}.$$ (398)

Optimum wavelength

$$\lambda = \frac{2\pi A}{m_0(W)},$$ (399)

The value of $m_0(W)$ should be taken from the graph on Fig. 88.

Placing expression (399) into expression (398), we obtain for a consideration of a boundary layer only in the liquid:

$$L_p = \frac{16[m_0(W)]^2}{W^2},$$ (400)

where $\bar{\beta} = 1/2$, and W and Lp are determined by the thickness of the boundary layer h.

Equation (400) is obtained from the condition of equality of optimum wavelength of perturbation, determined by taking into account the boundary layer, but neglecting viscosity, on one hand and wavelength obtained taking into account viscosity with discontinuous velocity distribution on the interface.
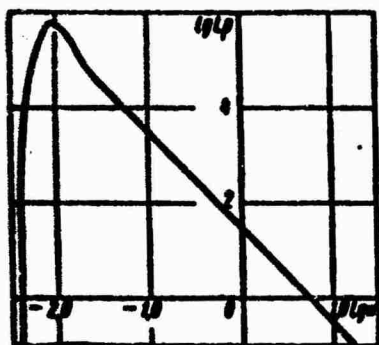
Fig. 94. Curve separating the region of boundary layer influence on disintegration in a liquid from the region where viscosity directly influences.

With the help of this equation it is possible to establish approximately the region of applicability of the expounded theory.

The graph on Fig. 94 is constructed according to equation (400) and shows that for low-viscosity liquids (water and others) the direct influence of viscosity is immaterial; for example, at U_2 = 100 m/s and h = 0.02 cm for water we have W = 37, Lp = 13,460 and the point corresponding to these values of W, Lp lies considerably above the curve on Fig. 94.

Literature

1. Veber K. Raspad strui zhidkosti (Desintegration of a liquid jet). In the collection "Dvigateli vnutrennego sgoraniya." T. I. M.-L., ONTI, 1936.

2. Borodin V. A., Dityakin Yu. F. i Yagodkin V. I. O droblenii sfericheskoy kapli v gazovom potoke (The breaking up of a spherical drop in a gas flow). "Prikladnaya mekhanika i tekhnicheskaya fizika," 1962, No. 1.

3. Golovin A. M. K teorii kolebaniy i drobleniya kapli v gazovom potoke pri nalichii vikhrevogo dvizheniya vnutri kapli (The theory of oscillations and breaking up of a drop in a gas flow, considering a swirl flow inside the drop). "Izvestiya AN SSSR. Seriya geofizicheskaya." 1964, No. 7.

4. Golovin A. M. K teorii kolebaniy i drobleniya kapli v gazovom potoke pri nalichii potentsial'nogo dvizheniya znutri kapli (The theory of oscillations and breaking up of a drop in a gas flow, considering irratational motion inside the drop). "Izvestiya AN SSSR. Seriya geofizicheskaya.," 1964, No. 8.

5. Gradshteyn I. S. i Ryzhik I. M. Tablitsy integralov, summ, ryadov i proizvedeniy (Tables of integrals, sums, series and products). M., Fizmatgiz, 1962.

6. Dityakin Yu. F. i Yagodkin V. I. Vliyaniye periodicheskikh kolebaniy skorosti i plotnosti sredy na raspad zhidkikh struy (Influence of periodic oscillations of velocity and density of a medium on the disintegration of liquid jets). "Izvestiya AN SSSR. Otd. tekhn. nauk," 1957, No. 4.

7. Klyuzener O. Protsess vpryskivaniya v beskompressornykh dizelyakh (Injection in compressorless diesel engines). In the collection "Dvigateli vnutrennego sgoraniya." T. 1. M.-L., ONTI, 1936.

8. Klyachko L. A. K teorii drobleniya kapli potokom gaza (The theory of the breaking up of a drop by a gas flow). "Inzhenernyy zhurnal AN SSSR." T. III. 1963, No. 3.

9. Lamb G. Gidrodinamika (Hydrodynamics). M., OGIZ. 1947.

10. Levich V. G. Fiziko-zhimicheskaya gidrodinamika (Phisico-chemical hydrodynamics). M., Fizmatgiz. 1959.

11. Lyshevskiy A. S. Ob ustoychivosti i raspade poloy strui vyazkoy zhidkosti, dvizhushcheysya s malymi skorostyami (The stability and disintegration of a hollow jet of viscous liquid, moving at low velocities). "Izvestiya vuzov. Energetika." 1958. No.3.

12. Lyshevskiy A. S. O vliyanii okruzhayushchey sredy na raspad poloy strui zhidkosti (About the ambient effect on disintegration of hollow stream of liquid). "Izvestiya vuzov. Energetika," 1958, No. 6.

13. Lyshevskiy A. S. O kriterii drobleniya zhidkikh kapel' (The criterion of breaking up of liquid drops). Novocherkassk, 1959. (Trudy Novocherkasskogo politekhnicheskogo instituta No. 86).

14. Lyshevskiy A. S. Neustoychivost' i raspad krugloy strui vyazkoy zhidkosti, okruzhennoy nevyazkoy zhidkost'yu (Instability and disintegration of a round jet of viscous liquid surrounded by an inviscid liquid). Novocherkassk, 1958 (Trudy Novocherkasskogo politekhnicheskogo instituta. T. 46/60).

15. Mak-Lakhlan. Teoriya i prilozheniya funktsiy Mat'ye (Theory and application of Mathieu functions). M., Izd-vo IL, 1953.

16. Natanzon V. Ya. O raspylivanii topliva v dvigatelyakh dizelya (Atomization of fuel in diesel engines). "Dizelestroyeniye," 1938, No. 3-5.

17. Reley. Teoriya zvuka (Theory of sound). T. 2 M., OGIZ, 1944.

18. Strett. Funktsii Lyame, Mat'ye i rodstvennyye im v fizike i tekhnike (Lame, Mathieu and related functions in physics and technology). Khar'kov-Kiyev, ONTI, 1935.

19. Uitteker Ye. T. i Vatson G. N. Kurs sovremennogo analiza. Ch. 2 (Contemporary analysis. Pt. 2). M.-L., Fizmatgiz, 1963.

20. Shekhtman Yu. M. K voprosu o vliyanii okruzhayushchey sredy na ustoychivost' zhidkikh struy (The ambient effect on the stability of liquid jets). "Izvestiya AN SSSR. Otd. tekhn. nauk," 1946, No. 11.

21. Blaal A., Davidson J. The flow under gravity of a swirling liquid through an orifice—plate. Proceedings of the Royal Society, V. 199, No. 1059, 1949.

22. Hagerty W., Shea J. Study of the stability of plane liquid sheets Journal of Applied Mechanics, V. 22, No. 4, 1955.

23. Hinze J. Fundamentals of the hydrodynamic mechanism of splitting in dispersion process. American Institute Chemical Engineering Journal, No. 1, 1955.

24. Isahiki N. Theoretical and experimental study of atomisation of liquid drop in high speed gas stream. Reports of Transport Technical Research Institute, No. 35, 1959.

25. Jork J., Stubbs H., Tak M. Mechanism of disintegration of liquid sheets. Transactions of the ASME, V. 75, No. 7, 1953.

26. Lane W. Shatter of drops in streams. Industrial and Engineering Chemistry, V. 43, No. 6, 1951.

27. Littaya G. Sur l'atomisation d'un jet liquide. Comptes Rendus hebdomadaires des séances de l'Académie des sciences, V. 219, No. 15, 1944.

28. Mayer E. Theory of liquid atomization in high velocity gas streams. American Rocket Society Journal, V. 31, No. 12, 1961.

29. Miease C. The effect of ambient pressure oscillation on the disintegration and dispersion of a liquid jet. Jet Propulsion, V. 25, No. 10, 1955.

30. Oka S. On the instability and breaking up of a ring of liquid into small drops. Proceedings of the Physical—Mathematical Society of Japan, 3—rd Series, V. 18, No. 9, 1936.

31. Tomatika S. The instability of a cylindrical thread of a liquid surrounded by another viscous fluid. Proceedings of the Royal Society. V. 130, No. 870, 1935.

C H A P T E R VI

THE EFFECT OF PARAMETERS OF INJECTORS AND LIQUID PROPERTIES ON THE SHAPE OF THE STREAM (JET) AND THE FINENESS OF ATOMIZATION

At present theory of the disintegration of a liquid jet still cannot serve as the basis for establishing quantitative regularities, in particular, the connections between the size of drops or the length of an undisintegrated section of the stream, parameters of injectors and quantities expressing the properties of the liquids; therefore, during calculations it is necessary to use appropriately treated experimental data. But before we go to such treatment, we should examine the fineness of atomization, and also the effect of basic parameters of injectors and liquid properties on the shape of the streams (films) and size of the drops obtained upon atomization of a liquid by different injectors.

§ 1.   The Fineness of Atomization

Experimental studies of atomization show that as a result of this process a large quantity of different sized drops will be formed, composing a spray of atomized liquid.

In order to determine the degree of atomization (dispersiveness), it is necessary to introduce corresponding characteristics.

Since the number drops per volume unit of a spray of atomized liquid is very great ($\sim 10^6/cm^3$), during an investigation it is advisable to use statistical methods.

The objects of the studied statistical totality are drops having a practically spherical shape. Therefore it is sufficient to investigate only the distribution drops with respect to their diameters. Thus, the diameter of a drop x is the argument and its values will form a sequence of the totality. The least and greatest values of argument x limit the interval of variation.

Let us designate by i the quantity drops of diameter x, and by i_{max} the total amount of all measured drops.

In statistics the totality of any items is measured by means of separation into classes (group) with interval Δx. The magnitude Δx is established basically depending upon the method of measurement and the measuring instrument (scale division of microscope eyepiece, difference of the size of sections of the screens used consecutively during screening, etc.).

Drops with diameters within limits from $x_n - \frac{\Delta x}{2}$ to $x_n + \frac{\Delta x}{2}$ will form a class corresponding to x_n. If we plot the values of the number of drops for all classes on a graph in the form of the ordinate for mean diameter x_n, we will obtain the mean distribution curve of the number of drops with respect to diameters (frequency curve):

$$f(x) = \frac{di}{dx}.$$ (401)

If we combine sequentially the number of drops in all classes and along the axis of ordinates plot the sum of the number of drops with diameters smaller than that given, then we obtain the resultant curve characterizing the distribution of the number of drops with respect to diameters:

$$f(x) = i = \int_0^{x_{max}} \frac{di}{dx}\, dx.$$ (402)

However, usually in practice the curves described by formulas (401) and (402) are used rarely, since they are not convenient for comparison with each other. We use instead the relative distribution frequencies of the number, surface or volume (mass) of drops with

respect to size

$$y_p = \frac{\frac{du}{dx} x^p}{\int_0^{x_{max}} \frac{du}{dx} x^p dx}.$$ (403)

For p = 0 we have the curve of relative distribution frequencies of the number of drops (y_0), for p = 2 — the curve of relative distribution frequencies of the surfaces of drops (y_2) and for p = 3 — the curve of the relative distribution frequencies of the volumes of drops (y_3).

Likewise, we use distribution curves of relative values of number, surface or volume of drops whose diameters are less than that assigned. These distribution curves are called total distirbution curves of the number, surface or volume of drops with respect to their diameters. The equation of these curves has the form

$$G_p = \frac{\int_0^x \frac{du}{dx} x^p dx}{\int_0^{x_{max}} \frac{du}{dx} x^p dx}.$$ (404)

For p = 0, 2, 3 we obtain respectively the relative total distribution curves of the number of drops G_0, surface of drops G_2, and volume of drops G_3.

The frequency curves described by formula (401) or (403) are called sometimes differential curves, but the resultant curves described by formula (402) or (404) are integral distribution curves of drops with respect to diameters.

For functions y_p and G_p different researchers studying the distribution of particles of solid materials and drops with respect to diameters proposed numerous equations [10]. To describe the distribution of drops of atomized liquid the most convenient equation of the resultant distribution curve of the volumes of drops with respect to diameters was proposed by Rozin-Rammler:

231

$$G_3 = 1 - e^{-\left(\frac{x}{\overline{x}}\right)^n}. \tag{405}$$

where $\overline{x}$ – constant of dimension: n – constant of distribution.

The frequency curve corresponding to the resultant curve described by formula (405) has the form

$$y_3 = \frac{dG_3}{dx} = x^0 \frac{d}{dx} = \frac{n}{x^n} x^{n-1} e^{-\left(\frac{x}{\overline{x}}\right)^n}. \tag{406}$$

Sometimes instead of G_3 we use another form of the resultant curve:

$$R = 1 - G_3 = e^{-\left(\frac{x}{\overline{x}}\right)^n}. \tag{407}$$

That part of the drops composed of drops whose diameter exceeds x is R_3.

On Fig. 95 are represented frequency y_3 and resultant G_3 and R_3 distribution curves of volumes of drops with respect to diameters.

We will examine the basic properties of these distribution curves.

The area lying between distribution curve y_3 and the axis of abscissas within limits of x from 0 to ∞ will be

$$\int_0^\infty y_3 \, dx = 1.$$

The maximum of the curve of frequencies y_3 corresponds to inflection points of resultant curves G_3 and R_3. The abscissa of the maximum of curve y_3 is called the mode and constitutes the diameter of the most frequently encountered drops.

The abscissa which divides the totality of drops into two equal parts ($G_3 = R_3 = 0.5$) is on the intersection of total distribution curves and is called the median or median diameter of drops.

232

With the help of equations (405) and (406) it is possible to express the most frequently encountered diameter of a drop $x_{\text{мод}}$, median diameter $x_{\text{мед}}$ through constants $\bar{x}$ and n:

$$\left. \begin{array}{c} x_{\text{мод}} = \bar{x}\left(\dfrac{n-1}{n}\right)^{\frac{1}{n}}; \\[12pt] x_{\text{мед}} = \bar{x}(\ln 2)^{\frac{1}{n}}. \end{array} \right\}$$

(408)

The curve of frequencies y_3 has maximum only when n > 1.
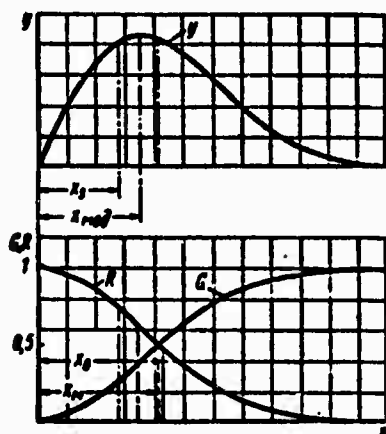
Fig. 95. Frequency and resultant distribution curves of volumes of drops with respect to diameters.

Together with the shown characteristics of the distribution curve of drops with respect to diameters we use different ideas of the mean diameter of drops. We use the following idea of the mean diameter of drops, each of which expresses those or other properties of the totality:

1) arithmetic mean diameter of drops (weighted with respect to the number of drops — surface and volume of all drops remain constant)

$$x_{10} = \frac{\Sigma i x}{\Sigma i}$$

(409)

(The 10 means that in the numerator the diameter of a drop is taken in the first degree and in the denominator — the zero);

2) mean surface diameter of drops (weighted with respect to the number of drops — surface of all drops remains constant)

233

$$x_{30} = \left(\frac{\sum i x^3}{\sum i}\right)^{\frac{1}{3}};$$

(410)

3) mean volume diameter of drops (weighted with respect to the number of drops — volume of all drops remains constant)

$$x_{30} = \left(\frac{\sum i x^3}{\sum i}\right)^{\frac{1}{3}};$$

(411)

4) mean diameter of drops weighted with respect to specific surface, or mean diameter according to Zauter.

$$x_{32} = \frac{\sum i x^3}{\sum i x^2}.$$

(412)

During treatment of the results of measurements of the size of drops using the formula of Rozin-Rammler (405) we can calculate the mean diameter of drops by the following general formula [10]:

$$x_{dq} = \left\{\frac{\Gamma\left(\frac{d-3}{a}+1\right)}{\Gamma\left(\frac{q-3}{a}+1\right)}\right\}^{\frac{1}{d-q}} \bar{x}.$$

(413)

Thus, for the mean diameter according to Zauter we obtain (d = 3, q = 2)

$$x_{32} = x_3 = \frac{1}{\Gamma\left(1-\frac{1}{a}\right)} \bar{x}.$$

(414)

and for the mean diameter of drops, weighted with respect to the volume of all drops (d = 4, q = 3), we obtain

$$x_{43} = \Gamma\left(\frac{1}{a}+1\right)\bar{x}.$$

(415)

We must note that x_{43} coincides with the abscissa of the center of gravity for the area lying under the frequency curve and that described by formula (406).

234

§ 2. Dimensions of Stream (Jet) and Diameters of Drops Forming upon the Atomization of Liquids by Jet Injectors

A description of the forms appearing upon the disintegration of a stream from a cylindrical hole was given in Chapter I. Let us consider further the dependence of the length of the undisintegrated section of the stream on exit velocity. The length of the undisintegrated section of the stream L has been measured by many researchers [10, 19]. On Fig. 96 is represented the dependence of the length of the undisintegrated part of the stream on the exit velocity of liquid into air at atmospheric pressure. Length L at first grows linearly, then upon achieving the first maximum drops and again grows up to the second maximum, after which it gradually drops. Line 1-1 designates the end of the linear section, line 2-2 — the transition from axisymmetrical disintegration to wave-like and, finally 3-3 is the transition from wave-like disintegration to atomization.

We will examine the influence on smallness of atomization of basic factors, determined by the jet injector and operating regime.

Exit velocity of liquid. Numerous experiments with jet injectors have shown that as exit velocity of the liquid (or pressure drop on injector) increases, the size of drops decreases. Moreover drops become more uniform.

If a liquid jet is streamlined by a coaxial gas flow, then as relative velocity increases the size of the drops also decreases. On Fig. 97 in logarithmic coordinates are represented the dependences of median diameter of drops on relative velocity when the jet is streamlined by a flow of air, the direction of which coincides with the direction of the liquid flow or is opposite to it [32]. As we see, the slope of the line in both cases does not change.

Diameter of nozzle hole and ratio of length of hole to diameters. An increase of the nozzle hole diameter causes a growth of the size of drops. Figure 98 shows the dependence of median diameter of drops on the nozzle hole diameter for constant pressure drop on the injector.

The influence of the ratio of hole length to diameter can be seen on Fig. 99, which gives the results of the experiments of different researchers.
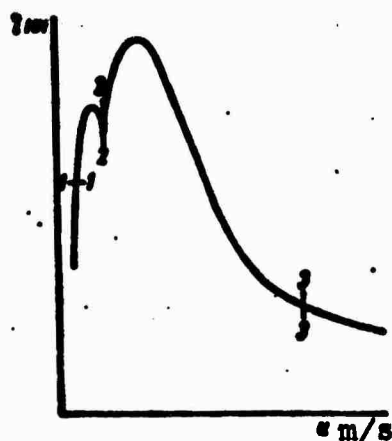
Fig. 96.
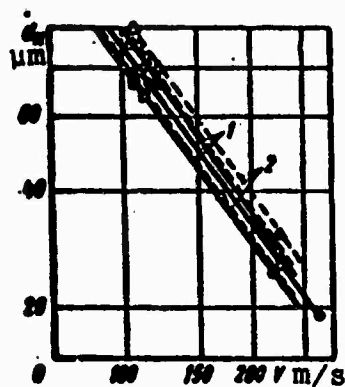
Fig. 97.

Fig. 96. Dependence of length of solid part of liquid jet on exit velocity.

Fig. 97. Dependence of median diameter of drops on relative velocity [32]. Diameter of nozzle hole 4.76 mm. Exit velocity of liquid: □ — 1.22 m/s; O — 3.65 m/s; Δ — 9.1-10.65 m/s; 1 — liquid flow against airflow; 2 — liquid flow with respect to airflow.

Fig. 98.
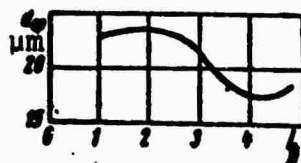
Fig. 99.

Fig. 98. Dependence of mean diameter of drops on nozzle diameter for a constant pressure drop. (Gas oil, pressure drop 278 kgf/cm^2).

Fig. 99. Influence of ratio of nozzle hole length to its diameter on mean diameter of drops. Diameter of hole 0.407 mm, pressure drop 242 kgf/cm^2.

Density of gaseous environment surrounding liquid jet.
Density of the gas surrounding the liquid jet has a certain influence
on the size of the drops. However, this influence depends on the
range of gas density change (pressure) in which atomization occurs.

Experimental data, mainly on injectors of internal-combustion
engines with compression ignition, show that as air density increases
6-20 times with respect to atmospheric density, the size of the drops
does not depend on air density.

If density (pressure) of air exceeds atmospheric density only by
2-3 times, then, as experiments show, an increase of the density
(pressure) of air leads to a certain decrease of the size of the
drops [32].

Figure 100 shows in logarithmic coordinates the dependence of
median diameter of drops on air pressure for different relative
velocities.

When air pressure goes below atmospheric, the effect of
density is more essential. Figure 101 shows the results of measure-
ments of drop size for heavy petroleum fuel which is atomized by a
jet injector into air of lowered density with respect to atmosphere
[30]. Along the axis of abscissas is plotted the ratio of average
diameter of drops to nozzle hole diameter, and along the axis of
ordinates — the ratio of the density of air surrounding the injector
in the pressure chamber, to the density of atmospheric air. In these
experiments pressure drop on the injector remained constant.

Change of mean diameter of drop with density of gaseous environ-
ment may be, as was earlier explained, the change of conditions of
stream disintegration with increase of density of the medium.

Viscosity of gaseous medium surr nding stream. It has been
experimentally established that an increase of viscosity of the gaseous
medium somewhat decreases the size of the drops [28, 30].
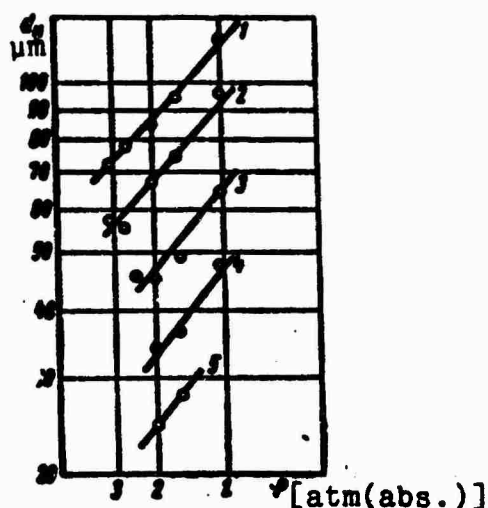
Fig. 100. Dependence of median diameter of drops on pressure of air at different relative velocities V [6, 4]:
1 — V = 76 m/s; 2 — V = 91.5 m/s; 3 — V = 121.8 m/s; 4 — V = 152.3 m/s; 5 — V = 182.6 m/s.
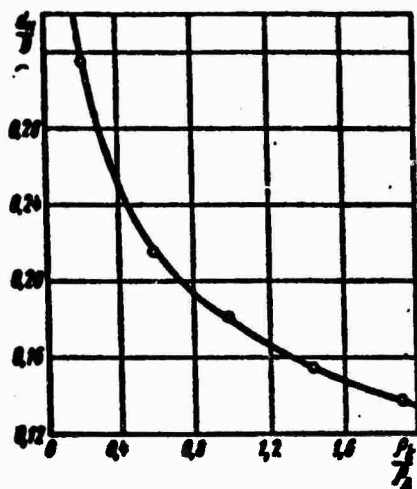
Fig. 101. Dependence of mean relative diameter of drops on the ratio of air density in pressure chamber to atmospheric density for constant pressure drop on injector [30].

In these experiments liquid was atomized into a medium whose gases (ethane and others) were selected so that their viscosities were various and their densities identical.

In Fig. 102 are given results of experiments in which viscosity of gas changed approximately by an order of 3 [30]. The size of the drops at such an increase of viscosity of the gaseous medium decreases insignificantly. In these experiments the boundary layer from the gas side on the surface of the liquid stream for practical purposes was absent. Frictional force on the surface of the stream, increasing in magnitude with increase of gas viscosity, was added to the normal

238

force of pressure and led to a breakaway of ridges of small waves from the surface of the stream. Consequently, here drops were smaller than in the case of smaller viscosity of the gaseous medium.

However, according to experiments of Weis and Worshem [32] the size of a drop is in a certain degree proportional to the coefficient of viscosity of the gaseous medium. This deviation apparently is connected with the presence of a thick gas boundary layer, growing on the stream (stream came from long tube, longitudinally stream-lined by a gas flow). The thick gas boundary layer weakens merging the effect of velocity on disintegration of the stream, and drops become bigger.
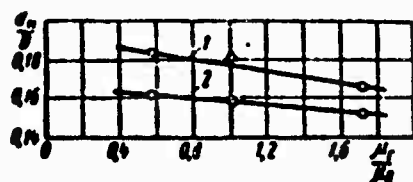
Fig. 102. Influence of ratio of gas viscosity to air viscosity (at 15°C) on dimensionless median diameter of drops [30]: 1 — flow velocity 52 m/s; 2 — flow velocity 63 m/s.

Physical properties of liquid. The basic physical constants of a liquid — coefficient of surface tension and viscosity — influence the size of drops.

On Fig. 103 are represented results of experiments in which the influence of the liquid viscosity on size of the drops was determined [32]. An increase of viscosity of the liquid results in an increase of the median drop diameter. This influence can be explained by the fact that as viscosity increases so does the thickness of boundary layer in the nozzle hole. But in accordance with Fig. 88 the wave length of the most unstable perturbation or the drop diameter for sufficiently large Weber criterion are proportional to the boundary layer thickness. Consequently, an increase of liquid viscosity is conjugate with enlargement of drops.

A similar influence of liquid viscosity was revealed even earlier in experiments of I. V. Astakhov [1].

The drop diameter is increased if the coefficient of surface

239

tension increases.
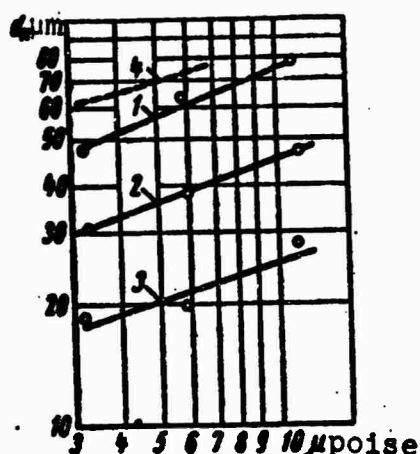
Fig. 103. Influence of liquid viscosity on median diameter of drops at different relative velocities V [32]: 1 — V = 106.6 m/s; 2 — V = 152.3 m/s; 3 — V = = 228.5 m/s; 4 — dependence for swirler (experiments of Marshall).

Let us examine the influence on the smallness of atomization of parameters and operating regimes of an injector with impinging jets. Such investigations have been made by Fry, Thomas [21], I. G. Panevin, Dombrovskiy and Hooper. Results of experiments of the last investigators are represented on Fig. 104. Average diameter of
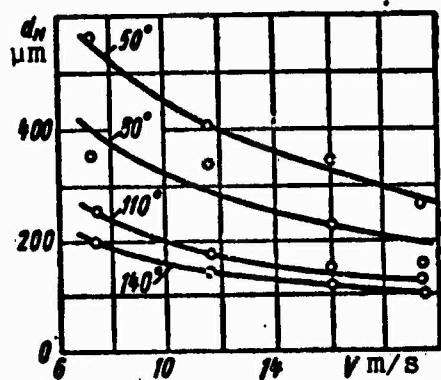
Fig. 104. Dependence of median diameter of drops on exit velocity at different angles between impinging jets (Dombrovskiy experiments).

drops decreases with increase of exit velocity, while the smaller the angle between the impinging jets, the bigger the drops into which the film forming upon inpingment of jets disintegrates. Influence of stream diameter on size of drops was studied by I. G. Panevin, who showed that an increase of stream diameter leads to growth of mean diameter of drops (Fig. 105).

240

The size of drops forming upon atomization of a liquid jet streamlined by a transverse gas flow was measured by Bitron [18], M. S. Volynskiy [5] and the authors. In the experiments of Bitron and M. S. Volyn streams of different liquids were atomized by supersonic airflows, and in the authors' experiments streams of liquified paraffin were atomized by a subsonic airflow.

On Fig. 106 are represented dependences of median and maximum diameters of a drop of liquified paraffin on airflow velocity in the diffuser throat.
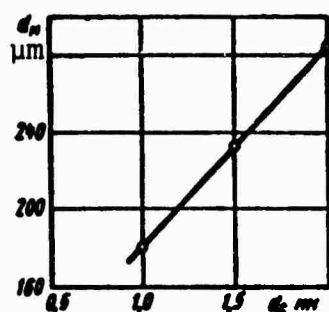
Fig. 105. Influence of diameter of stream on median diameter of drops at constant exit velocity (experiments of I. G. Panevin).
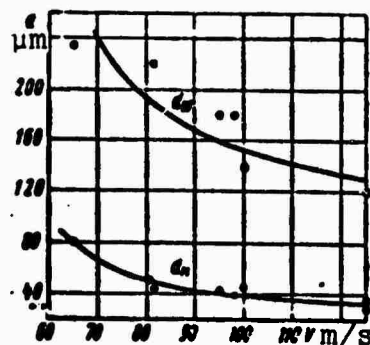
Fig. 106. Dependence of median and maximun diameter of drops of liquified paraffin on airflow velocity in the throat of a diffuser. Diameter of throat 11.5 mm, diameter of nozzle hole 1 mm. Ratio of volumetric flow rates of paraffin and air (0.96 - 0.59) × × 10^{-3}.

§ 3. Dimensions of Film and Diameters of Drops Forming upon Atomization of Liquids by Centrifugal Injectors (Swirlers)

Calculations of the shape of the film coming from a swirler (see Chapter II), and also analysis of photos of the sprays of atomized liquid show that with distance from the nozzle hole film thickness decreases. Film thickness at the site of disintegration can be determined if the length of its undisintegrated part

241

ℓ_p is known, i.e., the distance from the cut of the nozzle to the site where the film is broken up.

For small W the graph on Figure 23 can be used to measure film thickness, and for large W ($W \rightarrow \infty$) we can use the formula

$$\frac{\delta}{\delta_0} = \frac{1}{1+X \sin \alpha},$$

where $X = x/r_c$ is the dimensionless length of the film; α — half the root spray angle.

It is known that length X decreases with growth of exit velocity from nozzle.

Experiments conducted by Weinberg [31] in reference to a low pressure injector (range of pressure drop from 0.15 to 1.75 kgf/cm^2), during atomization of water established the connection of X with dimensionless criteria determining disintegration of the film.

The following empirical formula for determination of thickness of film δ in mm at the site of its disintegration was obtained:

$$\frac{\delta}{D} = 0.0075 \ln (28 \Delta p D),$$

where D — diameter of injector nozzle in mm; Δp — pressure drop on injector in kgf/cm^2.

We will examine the influence on smallness of atomization of basic factors determined by the swirler and its operating regime. It is obvious that the character of the effect of these factors will differ from that for a jet injector. This distinction is connected, for example, with the fact that the thickness of the film created by a swirler decreases with distance from the nozzle hole, that the film constitutes a hollow cone, etc.

Exit velocity of liquid. As also in the case of a jet injector, with increase of liquid exit velocity dimensions of drops decrease.

On Figure 107 is represented the dependence of median diameter on exit velocity.[1]

The curve consists of two parts. In the part corresponding to low flow velocity, the median diameter rapidly decreases as velocity increases. Further, with a growth of velocity the character of the curve changes; in the second part of the curve median diameters very weakly decrease with respect to exit velocity. Such a sharp change of the size of drops can be explained by the fact that at a low exit velocity the twisting of the flow in the nozzle hole becomes insufficient to maintain a hollow film up to its disintegration. Under the
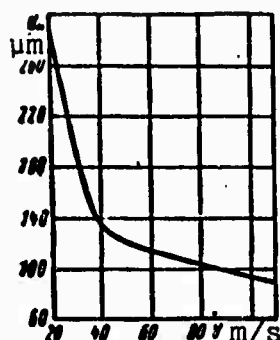
Fig. 107. Dependence of median diameter of drops on exit velocity of liquified paraffin. Swirler, geometric characteristic A = 0.758.

action of surface tension of the liquid the hollow film merges into a solid stream which breaks up into big drops. As velocity increases the film no longer merges into a stream; the film breaks into considerably smaller drops.

Thickness of film. On Figure 108 are represented the results of experimental investigation of a number of swirlers which did not differ structurally. Only the dimensions of the atomizer were changed; the film thickness was changed upon exit from nozzle hole. At a given pressure drop on the injector an increase of film thickness leads to a growth of median diameter of the drops. However, with an increase of pressure drop(Weber criterion) the slope of the lines decreases, i.e., at sufficiently high exit velocities the slanted lines will become horizontal. In this case wavelengths of maximally unstable perturbations (and, consequently, and the size of the drops) become significantly less than the thickness of the film δ and will not depend on δ_0 (see § 2, Chapter 5). In the maximum case of large Weber criterion the size of drops will depend only on the thickness

243

of the boundary layer of liquid.

Thus, the character of the dependence of median diameter of drop on film thickness is determined by the exit velocity (W).

Density of gaseous medium surrounding liquid film. The influence of the density of the gaseous medium ρ_2 in which liquid is atomized by the swirler has been less studied than for a jet injector. Available experimental data often are contradictory. In works by Manson and others [12] it has been established that when density is decreased the size of the drops decreases. The work of De Corso [20] shows that as ρ_2 increases the diameters of the drops at first decrease, and with a further increase of ρ_2 they increase. There are also works in which it is proved that with growth of density ρ_2 the size of the drops decreases. These contradictions can be organized if we consider that the length of the undisintegrated part of the film X strongly depends on density of the gaseous medium ρ_2; as density ρ_2 increases, length X decreases. At present there are no direct experimental proofs of this conclusion. However, it has been confirmed by many experiments with jets from cylindrical nozzle holes. This means that as density of the gaseous medium increases, the site where the film breaks up shifts nearer to the injector nozzle and the film thickness here increases. An increase of the thickness results in growth of the size of drops (Fig. 108).

Upon further increase of density ρ_2 there will be a moment when the site of breaking up of film comes close to the nozzle hole and the film thickness at the site of disintegration remains constant. For the case of large W formula (316) is valid, according to which the wavelength of the maximally unstable perturbation is inversely proportional to ρ_2. Consequently, the size of drops will decrease with growth of density ρ_2.

When density ρ_2 is reduced, the site where the film breaks up moves further from the nozzle hole. Consequently, lowering of density ρ_2 leads to a decrease of drop size.
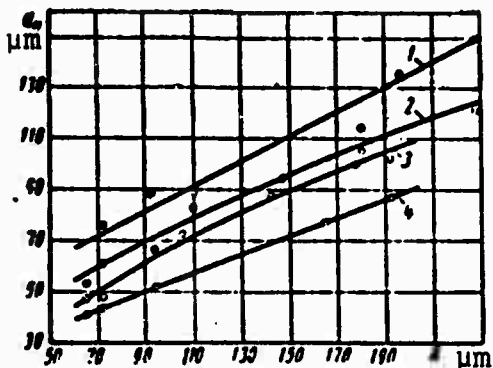
Fig. 108. Influence of film thickness on exit from nozzle hole of swirler on median diameter of drops of liquified paraffin at different pressure drops on injector: 1 — $\Delta p =$ = 8 kgf/cm^2; 2 — Δp = 10 kgf/cm^2; 3 — Δp = 20 kgf/cm^2; 4 — $\Delta p =$ = 40 kgf/cm^2.

Thus, when liquid is atomized by a swirler in a medium of variable density there can appear both a disintegration regime in which drop size decreases as ρ_2 increases, and also a regime in which drop size increases as ρ_2 decreases.

Viscosity of gaseous medium surrounding film. There have been no known experimental investigations of the influence of gas viscosity μ_2 on dimensions drop size. However, we can assume that this influence will be even less considerable than for a jet injector, since due to the small length of the undisintegrated part of the film the gas boundary layer on its surface does not grow.

Physical properties of liquid. The influence of liquid viscosity on drop size during atomization by a swirler is shown on Figure 103. As also for a stream coming from an injector, an increase of viscosity causes a growth of the median diameter of drops. But viscosity in this case has a somewhat weaker influence than during atomization by jet injector.

Growth of the coefficient of surface tension res .lts in an increase of drop size.

§ 4. Diameters of Drops Forming During Atomization of Liquids by Revolving Disks, Drums and Ultrasonic Injectors

Let us consider the influence on smallness of atomization of two basic parameters of a revolving disk: peripheral velocity of rotation on periphery of disk and thickness of liquid layer

245

,liquid flow rate).

On Figure 109 is represented the dependence of median diameter
of drops on peripheral velocity of rotation of disk at constant
flow rate of liquid, obtained experimentally by Marshall. With an
increase of peripheral velocity drop size decreases. On Fig. 110
? shown the influence of liquid flow rate (thickness of film
dropped from disk) on drop size; the peripheral velocity remained
unchanged. Increase of liquid flow rate leads to growth of median
diameter of drops. This increase of d_M is explained by growth of
the thickness of liquid film, as also in all injectors examined above.

In ultrasonic injectors, working on the principle of gas jet
radiators (Fig. 111), the liquid film is subjected to sound generated
by an oscillatory shock wave [8, 33]. Air flows through annular
let 2, formed by rod 4 and housing 1. In cavity of resonator 3
appear ultrasonic oscillations, creating pulsation of air density
on internal surface of the liquid circular film from the nozzle.
As was theoretically shown in § 5 Chapter 5, pulsation of
density results in decrease of drop size during disintegration of a
stream. In experiments of N. S. Lamekin [8] and Wilcox and Tate
[33] the size of drops forming upon disintegration of an annular
liquid film under the influence of pulsations of air density,
created by an oscillatory shock wave, were measured. In Table 6
are represented results of these measurements [33].

It is interesting to compare measured values of the average
diameter of drops with those calculated by the formulas proposed by
different researchers studying atomization of a liquid by gas
(pneumatic) injectors. Knowing only the ratio of the flow rates of
air and water, given in Table 6, by the formula of Nukiyama and
Tanazawa we find that $d_{cp} \approx 1400$ µm. Consequently, the influence
of pulsations of air density results in a considerable decrease of
drop size.

During electrical atomization of liquids a certain quantity of
liquid is reduced to the size of small drops with the help of an
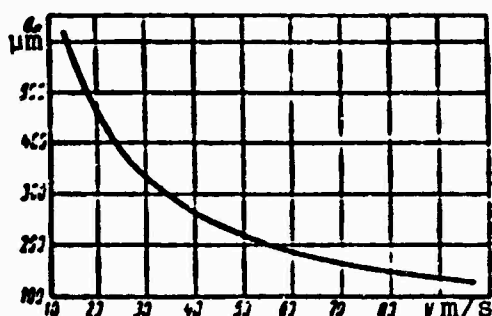electrical field applied from the outside. Electrical atomization

246

Fig. 109. Dependence of median diameter of drops on peripheral velocity of rotation of disk at constant flow rate of liquid (9 kg/min) (Marshall experiments).
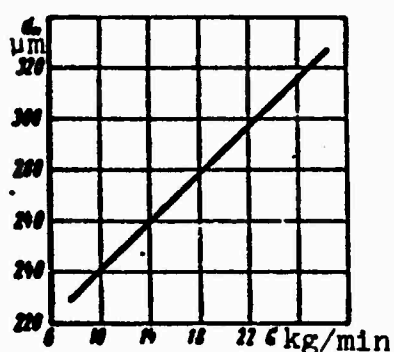

Fig. 110. Influence of flow rate of liquid passing along disk on drop size with constant circumference of velocity of disk (46 m/s) (Marshall experiments).
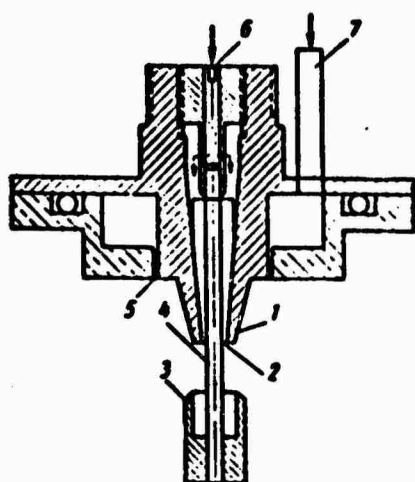

Fig. 111. Ultrasonic injector: 1 — housing; 2 — annular slot for air; 3 — resonator; 4 — rod; 5 — annular slot for liquid; 6 — feed of air; 7 — feed of liquid.

essentially differs from mechanical, which occurs in the absence of an electrical field. The atomized liquid is fed into a capillary tube from a tank in which pressure is insufficient to cause mechanical atomization. The stream of liquid from the tube is subjected to a longitudinal electrical field and disintegrates into smaller drops than when there is no field. It is obvious that drop size depends both on the magnitude of the electrical field and on the dielectric constants of the liquid

247

Table 6

Parameters	Experiment 1	Experiment 2
Flow rate of water in kg/h..............	465	700
Pressure of water in kgf/cm^2.............	1.4	2.8
Flow rate of air in kg/h................	30	16
Pressure of air in kgf/cm^2..............	6.3	2.8
Average surface (Zauterovskiy) diameter of drops in microns............	282	256

and surrounding gaseous medium [7]. Data on drop size during electrical atomization are very scarce. We can show only one work of R. Peskin and others [13], which gives materials about the influence of electrical parameters on drop size.

§ 5. Criteria of Similarity, Used During the Study of Atomization of a Liquid

We can assume that the average diameter of drops d_{cp} and the constant of distribution n are affected by the following:

D — characteristic linear dimension; V — relative velocity of liquid; σ — coefficient of surface tension of liquid; μ_1 — coefficient of absolute viscosity of liquid; ρ_1 — density of liquid; μ_2 — coefficient of absolute viscosity of gaseous medium; ρ_2 — density of gaseous medium.

In deriving criteria usually we use the theory of similitude, namely dimensional analysis. Using the Π-theorem, we obtain the following criterial equations relative to dimensionless diameter of the drops and the constant of distribution:

$$\frac{d_{cp}}{D} = F_1\left(\frac{V^2 \rho_1 D}{\sigma}, \frac{D\rho_1 \sigma}{\mu_1^2}, \frac{\rho_2}{\rho_1}, \frac{\mu_2}{\mu_1}\right);$$
$$n = F_2\left(\frac{V^2 \rho_1 D}{\sigma}, \frac{D\rho_1 \sigma}{\mu_1^2}, \frac{\rho_2}{\rho_1}, \frac{\mu_2}{\mu_1}\right).$$

(416)

A similar analogous criterial equation can obviously be obtained for other quantities characterizing the disintegration of a stream

or film, for example, for the dimensionless length of a solid (undisintegrated) section of a stream L/D.

These criteria can be obtained by another means — by considering conditions of disintegration of a stream of viscous liquid travelling in a viscous medium, i.e., just as in Chapter 5 for low viscosity liquids.

As characteristic linear dimension D we must take nozzle diameter, film thickness, thickness of boundary layer, depending upon conditions of flow of stream or film of liquid before breaking up.

First Weber criterion $W = \dfrac{V^2 \rho_2 D}{\sigma}$ constitutes the relationship of impact pressure to pressure of surface tension. Second Laplace criterion $Lp = \dfrac{D \rho_1 \sigma}{\mu_1^2}$ characterizes the relationship of the force of viscosity and the force of surface tension of the liquid. Criterion Lp is equal to the ratio of dimension D to certain fictitious length $\Delta = \dfrac{\mu_1^2}{\rho_1 \sigma}$, depending only on the physical constants of the liquid. For example, for hydrocarbon liquid fuels Δ will depend mainly on viscosity μ_1, since density ρ_1 and the coefficient of surface tension change insignificantly. Thus, Lp criterion characterizes the influence of the liquid viscosity.

Third criterion $M = \dfrac{\rho_2}{\rho_1}$ characterizes inertial properties of gaseous medium and liquid.

Finally, fourth criterion $N = \dfrac{\mu_2}{\mu_1}$ is the relationship of the forces of viscosity of the gaseous medium and atomized liquid.

The selected system of criteria is the most advisable of all which can be obtained instead of a given system of criteria for the following reasons. Velocity V enters only in criterion W, and not in any other (for example, in the Reynolds criterion, which is sometimes introduced in the number being determined along with criterion W). Application of Lp criterion is also advisable since it characterizes only physical properties of the atomized liquid, and physical properties of the gaseous medium are reflected in two other criteria.

249

Thus, the problem of experimental investigation of atomization consists in establishing the dependences:

$$\frac{d_{cp}}{D} = F_1(W, Lp, M, N); \qquad n = F_2(W, Lp, M, N).$$

The above characteristic criterion can be used also in the generalization of results of experimental determination of boundary curves for regions of disintegration of streams or films.

Ohnesorge [27] with the help of high-speed filming studied the transition from one form of stream disintegration to another. Streams of different liquids were used, flowing into the atmosphere from cylindrical nozzle holes of different diameters. On Fig. 112 in coordinates lg $Lp^{-1/2}$ and lg Re $\left(\text{where } Re = \sqrt{Lp}\frac{W}{M}\right)$ results of these experiments are represented in the form of straight lines, differentiating the region of axisymmetrical disintegration from the region of wave-like disintegration and the region of atomization. Equations of these curves have the form

$$\frac{\lg Re}{\lg Re_0} + \frac{\lg Lp^{-\frac{1}{2}}}{\lg Lp_0^{-\frac{1}{2}}} = 1 \qquad (417)$$

or

$$Lp = Lp_0 Re^{-\frac{\lg Lp_0}{\lg Re_0}}. \qquad (418)$$

where Re_0 is the Reynolds number corresponding to transition from one region of disintegration into another when Lp = 1 is the segment cut off by the boundary direct on the axis lg $Lp^{-1/2}$ at Re = 1. According to experiments of Ohnesorge Re = 240 and lg Lp_0 = -5.860.

Littaye [26] experimentally showed that an essential value during transition from the region of disintegration into the region of atomization belongs to properties of the nozzle hole, i.e., initial perturbations imposed on the stream. These experiments showed that on the diagram $Lp^{-1/2}$, Re (Fig. 112) regions of disintegration can shift
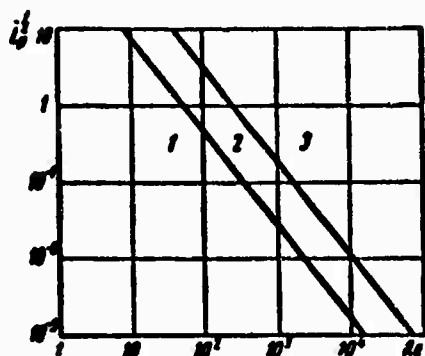
Fig. 112. Regions of disinte-
gration of cylindrical stream
[27]: 1 – axisymmetrical dis-
integration; 2 – wave-like
disintegration; 3 – atomization.

both toward large Re numbers (weak initial perturbations), and small
Re numbers (strong initial perturbations), while the boundary line
shifts parallel to itself. If we use in the form of equation (418)
the equation of the boundary curve, constituting a curve of parabolic
form (Fig. 113), then a change of the beginning perturbations (Re_0)
will elicit a change of the index in equation (418). Small initial
disturbances (large Re_0) result in the boundary curve approaching the
x-axis. Conversely, large initial disturbances (small Re_0) result
in a removal of the curve from the x-axis.

According to experiments of Ohnesarge and Littaye the Re_0 is a
characteristic of the initial disturbances, and the other quantity –
Lp_0 does not depend on initial disturbances, but is constant for a
given injector.
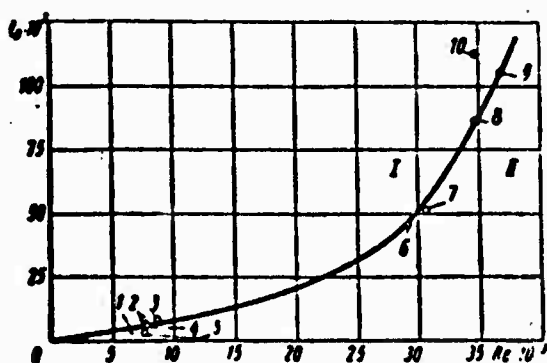
Fig. 113. Regions of
disintegration of film in
swirler in coordinates Re,
Lp: I – disintegration;
II – atomization.

Diameter of nozzle in mm	Point's of curve	
	Water	Kerosene
0.677	6	5
0.765	7	1
1.30	8	4
4.57	9	3
1.69	10	2

On Fig. 113 is represented the boundary curve characterizing transition from the "tulip" form of disintegration to atomization for five swirlers of identical construction with different nozzle diameters (from 0.677 to 1.69 mm) during the flow of water and kerosene into the atmosphere.[2] Transition to atomization was fixed by visual observation. In spite of the proximity of determination of the transition, the spread of points on Fig. 113 is not large. Consequently, the characteristic curves of initial disturbances for tested injectors are approximately identical.

Constants Re_0 and Lp_0, obviously depend also on $M = \frac{\rho_1}{\rho_1}$: with increase of M transition to atomization of streams or films occurs at smaller values of the exit velocity. Thus, boundary curves on Fig. 113 corresponding to higher M will be higher than the experimental curve corresponding to liquid flow into the atmosphere. Actually, if we turn to the empirical formula proposed by A. S. Lyshevskiy [10] for the connection between criteria Re, Lp and M upon transition from a mode of wave-like disintegration to a mode of atomization of a cylindrical stream of liquid

or
$$\left. \begin{array}{l} Re = 51,4 Lp^{0.434} M^{-0.4} \\ Lp = 0,1175 \cdot 10^{-3} M^{0.919} Re^{2.3} \end{array} \right\} \tag{419}$$

then we can find the connection of Re_0 and Lp_0 with M:

$$Lp_0 = 0,1175 \cdot 10^{-3} M^{0.919};$$
$$Re_0 = 31,6 M^{-0.368}.$$

§ 6. Breaking Up of a Drop of Liquid in a Gas Flow

Drops of liquid forming as a result of disintegration of a stream or film can be broken up into still smaller drops if there are corresponding conditions.

On the surface of a liquid drop streamlined by a flow of gas is created a certain distribution of pressures, which deforms the drop. The drop breaks up when the external forces on it overcome the forces

252

of surface tension.

The process of splitting of a drop has been studied by many researchers both theoretically and experimentally. In § 1 of Chapter V is given a survey of theoretical works on the breaking up of drops.

Experimental investigations of the breaking up of single drops have been carried out by many authors (Khokhshvender [14], Littaye [25], M. S. Volynskiy [6], Lane [24], Bukhman [3], Hanson and others [23], Haas [22] and others).

In these experiments the critical Weber number $W_{\kappa} = \frac{\rho_1 a V^2}{\sigma}$, at which a drop is broken up by a gas flow (where a — radius of drop, V — relative velocity), and also the influence of different factors on this quantity were determined.

In experiments of M. S. Volynskiy single drops of different liquids (radius was known beforehand), were scattered in a free jet of air. The breaking up was fixed by photographing the trajectory of the drop and catching it (or small drops when the drops were broken up) on screens. Experiments were conducted for comparatively big drops (1.5-2 mm) of different liquids (mercury, water, alcohol).

Experments showed that when the velocity of the air was sufficiently low, drops were not broken up but were attracted. As the velocity of the air is increased the drops lose stability and begin to break up into smaller drops. It was determined that when quantities in the expression $W_{\kappa} = \frac{\rho_1 a V^2}{\sigma}$, reach specific values, conditions for breaking up are created. The quantity W_{κ}, corresponding to the lower border of the interval of stability, turned out to equal 5.35, whereas for the upper stability limit $W_{\kappa} = 7$.

To the lower value $W_{\kappa} = 5.35$ correspond conditions at which a drop breaks into two parts (splitting). The higher $W_{\kappa} = 7$ corresponds to splitting of a drop into a certain number of fine drops.

253

Experiments with drops of a liquid having high viscosity showed that W_K depends on the viscosity of the liquid. Experiments with fine drops (up to 300 microns) established that when the drop diameter decreases, W_K increases, differing from the constant values 5.35 and 7.

The critical values $W_K = 5$-7 were confirmed in experiments of Isshiki. However, they are disputed by S. V. Bukhman [3], who experimentally obtained $W_K = 1.3$-1.8 for Reynolds numbers of the streamlining flow $(1.7$-$5.4) \times 10^3$. In these experiments both velocity of airflow and velocity of drops were measured, and therefore the relative velocity of drops was determined more exactly than in other works.

The above results pertain to the case of so-called "stationary" breaking up of a drop, when it is subjected to a gas flow with gradually increasing velocity incident drops; drops forming upon disintegration of stream [3, 6]). The case of "nonstationary" splitting of a drop is also interesting. This case occurs at the instantaneous influence of the gas flow, for example, influence of the flow behind the forward shock. Lane [24] and in special detail Hanson and others [23] studied this case of the breaking up of a drop. On Fig. 114 are shown the consecutive phases of deformation of a drop under the influence of a shock wave [23]. A spherical drop under the influence of pressure on its surface is turned into a body similar to an ellipsoid, which rapidly flattens in the center and turns into a liquid ring with a thin shell ("bag"). The liquid ring ever increases in diameter, the "bag" is destroyed and a multitude of fine drops forms. Finally, and the ring itself is crushed into fine drops.

On Figure 114 are shown photos of water drops of different diameters before the diaphragm of the shock tube ruptures and 1500 μs after the repture [23]. The fine drops still are only flattened, whereas big drops passing this stage are already destroyed (the "bag" bursts). Furthermore, certain specific peculiarities of "nonstationary" splitting were revealed: formation in the center of the "bag" of small holes. However, the conditions for these peculiarities have not been established.

The "nonstationary" splitting of drops of very viscous liquids is very interesting. On Fig. 115 are shown photos of drops of silicone (viscosity 100 cSt) of different diameters. In this case the "bag" has a neck and as a result of its disintegration not drops, but filaments will be formed.
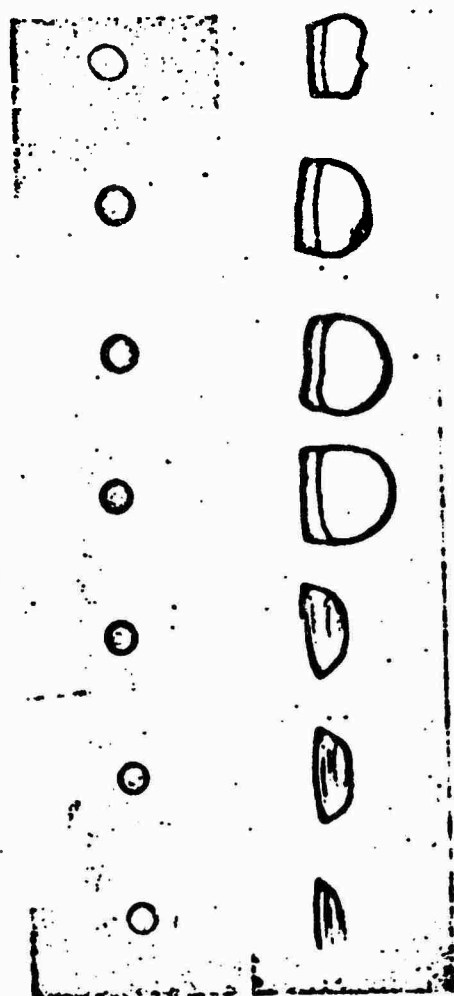
Fig. 114. Disintegration of water drops of different initial diameter [23]. Diameters of drops from top to bottom: 960, 900, 900, 810, 795, 788, 645 microns. Velocity of air 33.5 m/s.
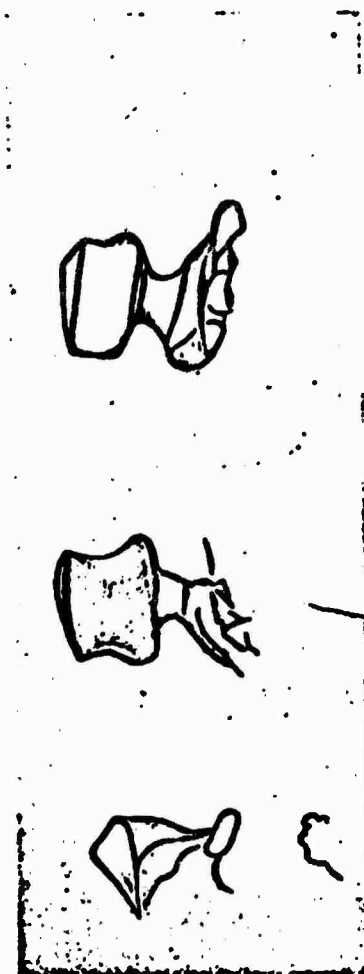
Fig. 115. Disintegration of drops of silicone of different initial diameter [23]. Diameters of drops from top to bottom: 165, 273, 270 microns. Velocity of air 36 m/s.

The influence of viscosity on W_K can be determined in accordance with $Lp = \frac{\rho\sigma}{\mu_1^2}$.

Figure 116 represents the dependence of W_R on Lp according to experiments of Hanson and others [23].
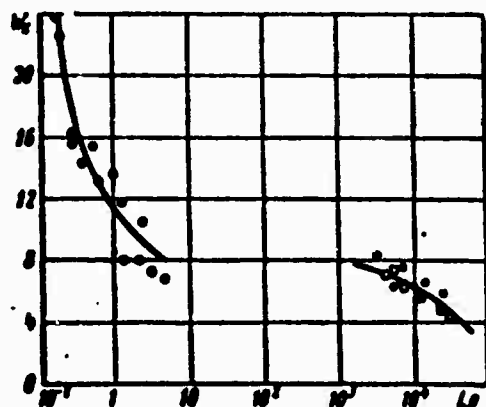
Fig. 116. Dependence of critical value of W_R on Lp according to experiments [23]: ● — methyl alcohol; ☐ — water; ○ — silicone.

§ 7. Treatment of Results for Investigations of the Atomization of Liquids in Dimensionless Criteria

Application of dimensionless criteria and theoretical relationships permits a correct approach to establishing empirical dependences describing the connection of basic characteristics of the atomization of liquids (length of solid section of stream, average diameter of drops, constant of distribution, etc.) with dimensionless criteria.

Let us examine these dependences for jet injectors.

A. S. Lyshevskiy [10] treated in dimensionless criteria both his own results and those of other researchers determining the dependence of the dimensionless length of the solid part of the stream. Below are formulas obtained from the corresponding formulas of A. S. Lyshevskiy during transition to criteria W, Lp, M.

For axisymmetrical disintegration of a stream on the linear section up to line 1-1 (see Fig. 96) the following formula is valid:

$$\frac{L}{e} = 29.6 \sqrt{\frac{W}{M}\left(1 + \frac{1}{\sqrt{3Lp}}\right)}. \qquad (420)$$

256

For axisymmetrical disintegration of a stream on the section between lines 1-1 and 2-2 (Fig. 96) we have the relationship

$$\frac{L}{a} = 53.2 \left(\frac{W}{M}\right)^{\frac{1}{3}} Lp^{-0.005} \exp\left(-0.474 \sqrt{\frac{W}{M}}\right). \qquad (421)$$

For wave-like disintegration and atomization of streams the following formulas are accurate:

$$\frac{L}{a} = 50.4 W^{-0.83} M^{-0.5} Lp^{-0.006}; \qquad (422)$$

$$\frac{L}{a} = 435 W^{-0.71} M^{-0.5} Lp^{-0.308}. \qquad (423)$$

Results of the measurements of drop size in the atomization of liquids by jet injectors have been treated by other researchers, however, they examined only the average diameter of drops and did not investigate the constant of distribution [10, 32].

We will look for the dependence of average diameter of drops on dimensionless criteria in the form of the exponential formula:

$$\frac{d_{cp}}{D} = C W^a Lp^b M^d N^f. \qquad (424)$$

For determination of C, a, b, d, f we use experimental data of different authors, and also the theoretical relationships obtained ir Chapter V. Comparison of exponents a and b, obtained by different authors, shows that these indices change depending upon the range of values of W in which experiments were carried out. Thus, on Fig. 117 are represented the dependences of the relative radius of a drop $\frac{r_a}{a}$ on W (in the range from 10 to 100) for different values of Lp accord ; to experiments of D. Li and R. Spencer [11]. It turns out that in the shown range of W the influence of Lp is small, and a is close to -(1/3) (straight line on Fig. 117 corresponds to this value).
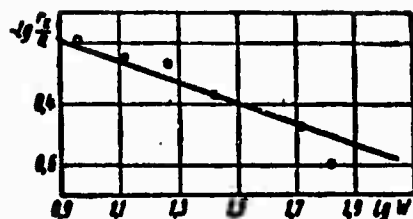
A. S. Lyshevskiy [10] for a range of change of W close to the above obtained the criterial formula:

$$\frac{r_{cp}}{a} = C_1 W^{-0.266} Lp^{-0.0733}.$$

Index a is close to $-(1/3)$, and b is very small, which also will agree with data of Li's experiments [11].

At higher values of W (>500) according to experiments of Weiss and Worsham [32], which were conducted with jets streamlined by coaxial (accompanying or impinging) flows of air, the obtained results can be represented in the form of the following formula:

$$\frac{r_{cp}}{a} = 0.63 W^{-\frac{2}{3}} Lp^{-\frac{1}{4}} M^{-\frac{5}{15}} (1 + 10^3 M) N^{\frac{1}{6}}. \qquad (425)$$

Increase of W leads to a growth of the absolute values of indices a and b, which is apparently connected with a change of the character of disintegration.

To explain the change of exponents a and b we use the theory of disintegration of a jet set forth in Chapter V.

At moderate values of W (<100) a cylindrical jet loses stability and disintegrates into pieces as a result of axisymmetrical disturbances, since the increment of oscillations in this case is the biggest as compared to other forms of disturbances. This means that axisymmetrical disturbances develop faster, and they determine the drop size.

258

Then the wavelength of the most unstable disturbances in accordance with formula (271) will be equal to

$$\lambda_{opt} = \frac{3\pi a}{W}.$$

To establish the connection between drop diameter and wavelength λ_{opt}, we will use Rayleigh's hypothesis that the jet breaks up into drops whose volumes equal the volumes of a cylinder of radius a and length λ_{opt}. Equating cylinder volume to the volume of a spherical drop of radius r, we obtain

$$\frac{r}{a} = \sqrt[3]{4\pi} W^{-\frac{1}{3}}. \tag{426}$$

Thus, the value a = -(1/3) is characteristic for moderate values of W.

With an increase of W wavelengths decrease and become small as compared to the jet radius. In this case disintegration of the stream occurs according to the pattern connected with breakaway of drops from the surface of the stream without preliminary disturbance of its integrity. The size of these drops is of the order of a wavelength. Cylindricity of the stream here ceases to affect disintegration, and the characteristic dimension will be no longer the stream radius but thickness of the boundary layer in the liquid or in the gas on interface between the liquid and gaseous medium.

If we take into account one boundary layer in the liquid, then for large values of Weber number (W > 0.1), calculated with respect to the thickness of the boundary layer, the wavelength of the most unstable disturbance is proportional to the thickness of the boundary layer. If we assume that the boundary layer is laminar, for which the relationship

$$\frac{h}{a} \approx Re^{-0.5} \tag{427}$$

is valid, where Re is the Reynolds number, calculated according to the radius of the nozzle hole a, then

$$\frac{\lambda_{opt}}{a} \approx W^{-0.25} M^{0.25} L_p^{-0.25}. \tag{428}$$

In the case of a turbulent boundary layer $\frac{\delta}{a} \sim Re^{-0.2}$ and

$$\frac{\lambda_{opt}}{a} \approx W^{-0.1} M^{0.1} L_p^{-0.1}. \tag{429}$$

If the turbulent boundary layer in the nozzle hole was closed, the ratio of the thickness of displacement to the radius can be expressed through the exponent n in the equation of the profile of velocity $w = \left(\frac{y}{a}\right)^{\frac{1}{n}}$:

$$\frac{\delta^*}{a} = \frac{1}{2+n}.$$

Using the empirical dependence of n on Reynolds number Re [17], we obtain

$$\frac{\delta^*}{a} \approx Re^{-\frac{1}{24}}. \tag{430}$$

This means that the thickness of boundary layer almost does not depend on the Reynolds number, and in the case of a closed turbulent boundary layer we obtain $\frac{\lambda_{opt}}{a} \approx \text{const}$.

Let us examine further the results of treatment in dimensionless criteria of the data of measurements of the size of drops forming upon disintegration of a jet streamlined by a transverse gas flow. For this the experiments of Bitron [18], M. S. Volysnkiy [5] and the authors were used. For the experiments W was calculated by flow parameters behind a normal shock. Treatment with respect to other criteria (Lp, M, N) was not carried out in view of the absence of data about corresponding physical constants under experimental conditions.

On Fig. 118 is represented the dependence of $\frac{r_x}{a}$ on W, obtained on the basis of results of experiments by the above researchers for different values of Lp (from 2×10^3 to 35×10^3). The line on Fig. 118 has slope $-(1/2)$. Experimental points with a certain scattering are clustered on this line to which corresponds the equation

$$\frac{r_{cp}}{s} = CW^{-\frac{1}{3}}.$$ (431)

where C = 1.585 is a function of Lp, M, N.

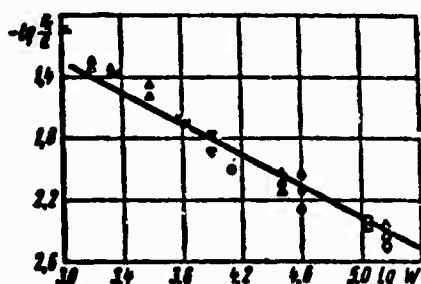Fig. 118. Dependence of $\frac{r_s}{s}$ on W: × — experiments of Bitron [18]: ●, ○, □, ◊, ▼ — experiments of M. S. Volynskiy; Δ — experiments of the authors.

In experiments M was changed within limits from 1.5×10^{-3} to 4.5×10^{-3}, and N was changed from 0.9×10^{-2} to 1.3×10^{-2}.

Let us now turn to treatment in dimensionless criteria of the results of investigation of the characteristics of atomization of liquids by swirlers. A feature of this treatment is that the film thickness δ, present in W and Lp, depends on flow velocity, density of the gaseous medium, constants of the liquid, i.e., also on W, Lp, M, N. Consequently, criterial formulas for a swirler can be written in the form

$$\frac{d_{cp}}{\delta} = CW^{\bullet},$$ (432)

where $\frac{\delta}{r_c} = F(W_b, Lp_b, M, N)$, while W_b and Lp_b are calculated with respect to the film thickness on leaving the nozzle hole of the injector δ_0 (r_c — radius of nozzle hole). At present there are no known empirical dependences of δ on W_b, Lp_b, M, N. Therefore criterial formula (432) can be sought only for a case of liquid flow into the atmosphere or into air of increased density and W, Lp can be calculated with respect to the thickness of the film on leaving the nozzle hole δ_0:

$$\frac{d_{cp}}{\delta_0} = C(WM^{-1})^r Lp^s.$$ (433)

where

$$W = \frac{\rho_2 \delta_0 V^2}{\sigma}; \quad Lp = \frac{\rho_1 \delta_0 \sigma}{\mu_1^2}.$$

It is assumed that the influence of N is not essential and, as experiments with jet injectors show, the influence of N is apparently small.

There have been many experimental investigations of the fireness of atomization of liquids by swirlers. Results of these investigations have been published in the form of empirical dimensional and criterial formulas, tabular and graphic data. A survey of empirical formulas can be found in a monograph by L. A. Vitman and others [4].

It is necessary to consider that each of the empirical formulas is obtained for a defined range of change of variables and cannot be extended beyond the limits of this range.

Table 7

No. points on Figures 119 & 120	Liquid	Method of measurement	Researchers
1	Kerosene	Catching on layer of soot	Dzhiffern and Murashev
2	Water	The same	The same
3	Water and aqueous solutions of glycerine	Catching on layer of oil and vaseline	Bloch and Kichkina
4	Water	Catching on layer of soot	Authors
5	Liquified paraffin	Screening on sieves	Longwell
6	The same	The same	Authors
7	Water	Catching on layer of oil	Weinberg
8	Kerosene	Catching on layer of soot	Fraser
9	Water, Kerosene, ethylene-glycol	Optical-sedimentation method	Konsil'o and Sliptsevich
10	Water	Catching on layer of soot	Pickford and Payl
[Editor's Note: spelling of Non-Soviet names not verified]			

Results of the authors' measurements were selected for treatment of experiments in criteria. Table 7 enumerates liquid, and methods of measuring drop size. The measured average drop sizes when necessary were converted into median diameter d_M, which was also used to calculate $\frac{d_M}{\delta}$. Film thickness on exit from the nozzle was calculated by the rough formula

$$\frac{\delta_0}{r_c} = \frac{1 - \sqrt{1 - \mu \cos \alpha}}{\cos \alpha},$$ (434)

where r_c — radius of nozzle.

This formula is obtained for a conical film with angle 2α at the vertex by equating the flow rates of the liquid, expressed, on the one hand, through area of cross section, equal to lateral surface of frustum of a cone, and on the other — through discharge coefficient μ. Formula (434) is especially convenient when μ and 2α can be taken from experiment.

From Table 7 it follows that empirical data basically belong to two groups: atomization of kerosene or of liquified paraffin, atomization of water and aqueous solutions of other substances (for example, glycerine). The drop size was measured by catching drops of a layer of soot and oil or by screening the hardening drops of paraffin. The only exception is experimental data from Konsil'no and Sliptsevich, which were obtained by the optical-sedimentational method.

On Figures 119 and 120 in logarithmic coordinates are constructed empirical data of the above authors for two types of liquids: kerosene (liquified paraffin) and water (aqueous solutions of glycerine) accordingly. As we see, the lines have identical slope; however, the lines for kerosene (liquified paraffin) pass below these for water (solutions of glycerine). It is possible to assume that the cause of this is the different N and unequalness of the index d for the M.

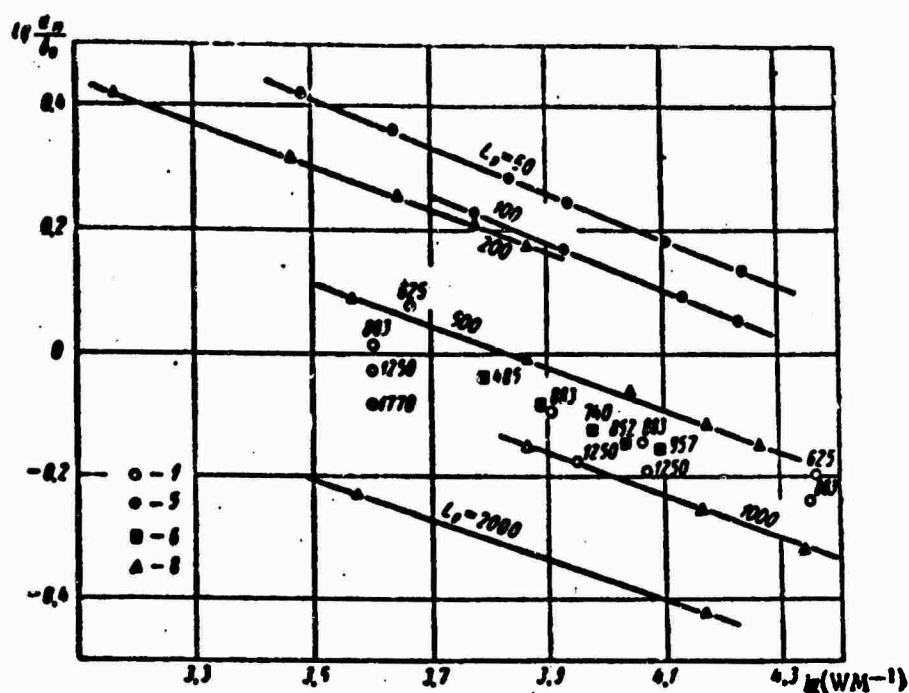The fact that a cause of the deviation is the method of measuring the drop size also is not excluded.

Fig. 119. Dependence of $\frac{d_n}{d_0}$ on WM^{-1} at differ-
ent values of Lp. Treatment of results of
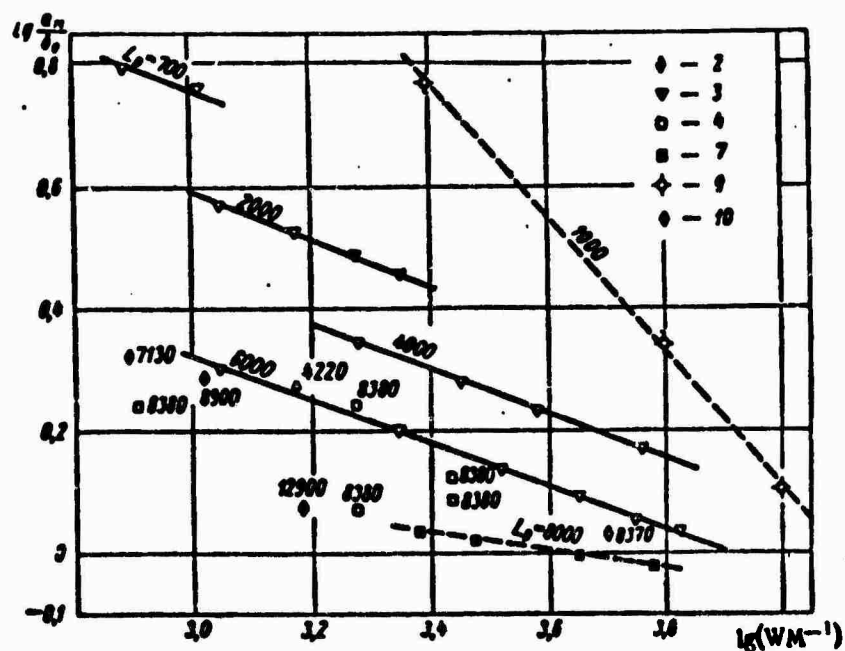measuring the drop size of kerosene (liquified
paraffin).

Fig. 120. Dependence of $\frac{d_n}{d_0}$ on WM^{-1} for dif-
ferent values of Lp. Treatment of results of
measured drop size for water and aqueous solu-
tions of glycerine.

264

The broken lines, obtained by Weinberg and Konsil'o and Sliptsevich, differ from data of the remaining researchers.

In the first case the distinction is apparently caused by the fact that the optical-sedimentational method of measuring drop size used in this work is useful, as the authors show, for drops with diameters not exceeding 40 microns. In the second case, the distinction is explained by the fact that experiments were conducted at very low pressure drops (0.15-1.75 kgf/cm^2), when the character of the dependence of drop diameter on exit velocity of the liquid somewhat differs from its character at a higher exit velocity.

Thus, in order to obtain a single criterial formula, further experiments are necessary with a variation of M and N in wider limits.

Treatment of experimental data for water and aqueous solutions of glycerine gave the following criterial formula:

$$\frac{d_\pi}{d_0} = 1415 L p^{-0.463} (WM^{-1})^{-0.25}. \tag{435}$$

and for kerosene (liquified paraffin)

$$\frac{d_\pi}{d_0} = 269 L p^{-0.423} (WM^{-1})^{-0.35}. \tag{436}$$

Application of these formulas is limited by the range of WM^{-1}, shown on the graphs on Figs. 119 and 120, where for formula (425) $M = 1.2 \times 10^{-3}$ and $N = 1.8 \times 10^{-2}$, and for formula (426) $M = 1.5 \times 10^{-3}$ and $N = 10^{-2}$.

By these empirical formulas one can determine median diameters of drops of kerosene and water (aqueous solutions of glycerine) in air at atmospheric density, if the dimensions of the swirler and the operating regime are given.

At present there are no empirical formulas connecting the constant of distribution with dimensionless criteria. An attempt to establish such a connection has been made by B. V. Raushenbakh and others

[16]; however, this work uses a criterion which does not consider the effects of the viscosity of the liquid.

In formulas (425) and (426) we note the large b for L_p as compared to b in case of jet injectors in formula (425). The large b apparently is connected with rotation of liquid in the nozzle hole of the injector.

The results of measuring drop size during atomization of liquids by revolving disks can be treated on the basis of data in a monograph by Marshall and in works of A. M. Lastovtsev. Lastovtsev [9] investigated atomization of different liquids (water, organic liquids, solutions of organic liquids, solutions of mineral layers) in a wide range of change of parameters. Treatment of results of experiments in dimensionless criteria can be represented in the form of the following dependence:

$$\frac{d_{cp}}{\delta} = CW^{-0.5}L_p^{-0.04}M^{0.5},\qquad (437)$$

where δ — thickness of layer of liquid on periphery of disk; criterion W is calculated with respect to the absolute velocity of the liquid at breakaway from the disk.

If d_{cp} — is the mean surface diameter, then C = 81.5; if d_{cp} — is the mean mass diameter, then C = 8.5.

In the treatment of results of the measurements of drop size for electrical atomization of liquids criterion W no longer can be used.

From analysis of the stability of a liquid jet under the influence of a longitudinal electrical field [13] it follows that for inviscid liquids, determining disintegration in air, we must have criterion $\Pi = \frac{\sigma}{(1-s^2)E^2D}$, where ε — dielectric constant of liquid in V/s; E — electric field strength; D — diameter of stream.

In the same work experiments were performed on the electrical atomization of amyl alcohol, results of which are represented on Fig. 121 in the form of the dependence of $\frac{d_x}{D}$ on criterion Π
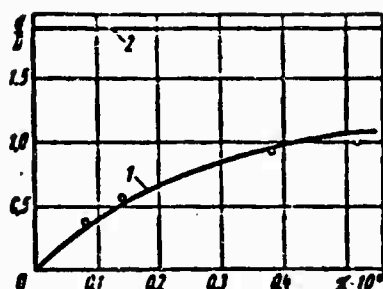
266

Fig. 121. Dependence of $\frac{d_\kappa}{D}$ on criterion π [13]: 1 — experimental curve; 2 — asymptote.

(d_κ — diameter of drop). The curve drawn through the experimental points should have asymptote $\frac{d_\kappa}{D}$ = 1.89 when $\Pi \to \infty$, corresponding to the case of disintegration of a jet in the absence of an electrical field (E = 0), when the wavelength of the maximally unstable disturbances λ = 4.508 D (see § 1 Chapter V).

Literature

1. Astakhov I. V. Vliyaniye vyazkosti topliva i drugikh faktorov na melkost' raspyla (The effect of fuel viscosity and other factors on the fineness of atomization). "Dizelestroyeniye", 1937, No 2.

2. Blokh A. G. i Kichkina Ye. S. Sredniy razmer kapel' pri raspylivanii zhidkogo topliva tsentrobezhnymi forsunkami (Average drop size in the atomization of liquid fuel by swirlers). "Teploenergetika", 1955, No 9.

3. Bukhman S. V. Eksperimental'noye issledovaniye raspada kapel' (Experimental investigation of the disintegration of drops). "Vestnik AN Kazakhskoy SSR", 1954, No 11.

4. Vitman L. A., Katsnel'son B. D. i Paleyev I. I. Raspylivaniye zhidkosti forsunkami (Atomization of liquid by injectors). M.-L., Gosenergoizdat, 1962.

5. Volynskiy M. S. Raspylivaniye zhidkosti v sverkhzvukovom potoke (Atomization of liquid in supersonic flow). "Izvestiya AN SSSR. Otd. tekhn. nauk. Mekhanika i mashinostroyeniye", 1963, No 2.

6. Volynskiy M. S. O droblenii kapel' zhidkosti v potoke vozdukha (The breaking up of liquid drops in an airflow). DAN SSSR. T. 62, 1948, No 3.

7. Glonti G. A. K teorii ustoychivosti zhidkikh struy v elektricheskom pole (The theory of stability of liquid jets in an electrical field). "Zhurnal eksperimental'noy teoreticheskoy fiziki". T. 34, 1958, No 5.

8. Lamekin N. S. Metod rascheta zazora generatora forsunki zhidkogo topliva (Method of calculating the clearance in the generator of a liquid-fuel injector). "Izvestiya vuzov. Mashinostroyeniye", 1961, No 10.

9. Lastovtsev A. M. Uravneniye drobleniya zhidkosti vrashchayushchimisya raspylitelyami (Equation for breaking up of a liquid by revolving atomizers). M., 1957 (Trudy MIKhM. T. 13).

10. Lyshevskiy A. S. Zakonomernosti drobleniya zhidkostey mekhanicheskimi forsunkami davleniya (Regularities of the breaking up of liquids by mechanical pressure injectors). Novocherkassk, 1961 (Trudy Novocherkasskogo politekhnicheskogo instituta).

11. Li. D. i Spenser R. Issledovaniye toplivnykh struy po mikrofotografiyam (Investigation of fuel jets by microphotography). In collection "Dvigateli vnutrennogo sgoraniya", T. 1. M., ONTI, 1936.

12. Manson i dr. Mikrofotograficheskoye issledovaniye raspylivaniya zhidkikh topliv (Using microphotography in the investigation of atomization of liquid fuels). "Voprosy raketnoy tekhniki", 1956, No 4.

13. Peskin R. i Rako R. Razmer kapel' v struye zhidkosti, raspadayushcheysya v prodol'nom ele tricheskom pole (Drop size in a liquid jet, disintegrated in a longitudinal electrical field) "Raketnaya tekhnika i kosmonavtika", 1964, No 4.

14. Prandtl' L. Gidroaeromekhanika (Hydroaeromechanics). M., Izd-vo inostr. lit., 1949.

15. Protsessy goreniya. Pod red. L'yuisa, Piz i Teylora (Burning processes. Edited by Lewis, Pease and Taylor). M., Fizmatgiz, 1961.

16. Raushenbakh B. V. i dr. Fizicheskiye osnovy rabochego protsessa v kamerakh sgoraniya vozdushno-reaktivnykh dvigateley (Physical bases of the working process in combustion chambers of air-breathing jet engines). M., Izd-vo, "Mashinostroyeniye",1964.

17. Shlikhting G. Teoriya pogranichnogo sloya (Boundary layer theory). M., Izd-vo inostr. lit., 1956.

18. B i t r o n M. Atomization of liquids by supersonic air jets. Industrial and Engineering Chemistry, V. 47, No. 1—2, 1955.

19. C h e n T s u—F a n g, D a v i s J. Disintegration of a turbulent water jet. Journal Hydraulics Division Proceedings American Society of Civil Engineers, V. 90, No. 1, Pt. 1, 1964.

20. De C o r s o S. Effect of ambient and fuel pressure on sprays drop size Transactions of the ASME, Ser. A, V. 82, No. 1, 1960.

21. F r y F., T o m a s P. The production of firefighting sprays by impinging jets. Enigneering, V.179, No. 7, 1953.

22. H a a s F. Stability of droplet suddenly exposed to high velocity gas stream. American Institute Chemical Engineering Journal, V. 10, No. 6, 1964.

23. H a n s o n A., D o m i c h E., A d a m s H. Shock tube investigation of the breakup of drops by air blasts. The Physics of Fluids, V. 6, No. 8, 1963.

24. L a n e W. Shatter of drops in streams of air. Industrial and Engineering Chemistry, V. 43, No. 6, 1951.

25. L i t t a y e G. Sur une théorie de la pulverisation des jets liquid. Comptes Rendus hebdomdaires des séances de l'Académie des sciences, V. 217, No. 4, 1943.

26. L i t t a y e G. Sur les modes de resolution d'un jet liquid en gouttes. Comptes Rendus hebdomadaires des séances de l'Académie des sciences, V. 208, No. 3, 1939.

27. O h n e s o r g e W. The formation of drops at nozzle and disintegration of fluid jets. Zeitschrift des Vereines Deutscher ingenieure, V. 81, 1937.

28. O s c h a t z W. Versuche zur Frage der Kraftstoffaufbereitung durch die Einspritzdüse. Deutsche Kraftfahrforschung, Heft 57, Berlin, 1941.

29. P i g f o r d R., P y l e C. Performance characteristics of spray—type absorption equipment. Industrial and Engineering Chemistry, V. 43, No. 7, 1951.

30. P o p o v M. Incercări pe modele cu pulverizarea fluidelor. Studii si cercetări de mecanica aplicata Academia Repiblicii Populare Romane, V. 7, No. 1, 1956.

31. W e i n b e r g S. Heat transfer to low pressure sprays in steam atmosphere. Part I. The mechanics of sprays. Heat and Air Treatment Engineering, No. 1, 1953.

32. W e i s M., W o r s h a m C. Atomization in high velocity air—streams, American Rocket Society Journal, V. 16, No. 1—2, 1961.

33. W i l c o x R., T a t e R. Liquid atomization in high intensity sound field. American institute Chemical Engineering Journal, V. 11, No. 1, 1965.

Footnotes

[1]Exit velocity was determined by the formula $\omega = \varphi_v \sqrt{\frac{2}{\rho} \Delta p}$,

where Δp — pressure drop on injector; $\varphi_v = \frac{\mu}{\phi} \cos\alpha$ — velocity

factor; μ — discharge coefficient; ϕ — space factor of nozzle; 2α — root angle of spray from swirler.

[2]The Re and Lp were calculated with respect to the thickness of the film in the nozzle exit section.

C H A P T E R   VII

DISTRIBUTION OF ATOMIZED LIQUID IN THE SPRAY

§ 1.   Characteristics of Distribution of Atomized Liquid

The distribution of atomized liquid in the spray created by an
injector is an essential characteristic on which depends perfection
of the process (technological or the burning process of a liquid
combustible in the combustion chamber of an engine) realized using
a given injector.

Distribution of atomized liquid in a spray is most fully charac-
terized by a field of specific fluid flow in different points of the
spray. Specific fluid flow is equal to the ratio of its flow rate
per second through an area perpendicular to the direction of motion
of the drops, to the magnitude of this area:

$$q_a = \frac{\Delta G}{\Delta f_a}.$$

Since due to the suction of gas the trajectories of the drops
are distorted, it is difficult to find the true course of direction
of the flying drops. Therefore usually a somewhat different determina-
tion is introduced. The specific flow is the ratio of the flow rate
per second of liquid through an area perpendicular to the axis of
the injector nozzle to the magnitude of this area:

$$q = \frac{\Delta G}{\Delta f_0}.$$

With such a definition measurement of specific flow is not
difficult; it is necessary only to have receivers in a plane
perpendicular to the axis of the injector nozzle.
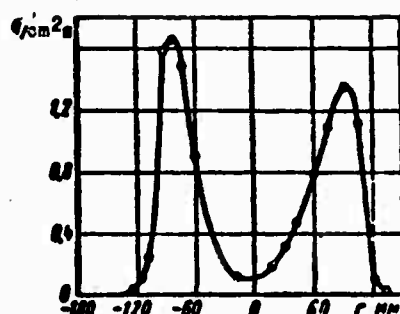
Fig. 122. Field of specific flows for a swirler.

On Fig. 122 is shown the field of specific flows of a swirler. This field was measured with help of a test tube. During the study of distribution of atomized liquid with respect to the radius of the spray, annular collection is also used. Totalling the volumes of liquid entering the collection cells, consecutively located from the center to the periphery, and referring the obtained values of volumes to the overall volume of liquid entering the catcher, we find
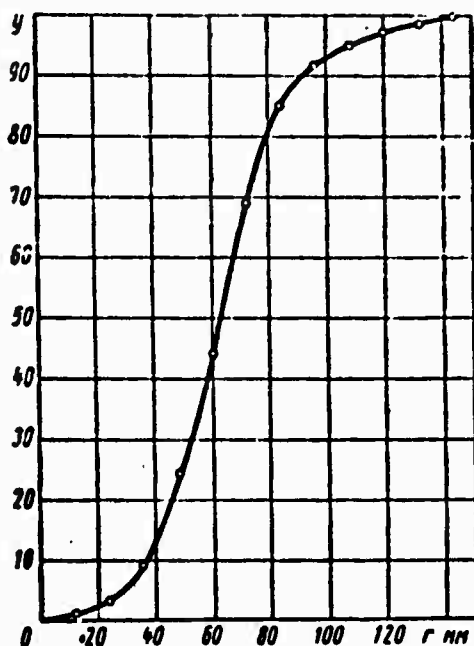
Fig. 123. Total distribution curve for a swirler.

a total distribution curve analogous to the total distribution curve of drops with respect to diameters (see § 1 Chapter VI). On Fig. 123 is the total distribution curve for a swirler. This curve can be approximated by the equation

$$y = 1 - e^{-ar^2}.$$ (438)

where

$$y = \frac{\sum\limits_{i=N}^{i} q_i}{\sum\limits_{i=1}^{N} q_i} ; \quad x = \frac{r}{\bar{r}} .$$

N — number of annular cells in collection; $\bar{r}$ — constant of dimension; r — radial coordinate; n — constant of distribution.

As constant $\bar{r}$ we can use the radius of the circumference for which 50% of the liquid discharge on a given distance from the injector nozzle passes inside, and 50% outside it. In this case a = 0.693.

The meaning of the constant of distribution is simple to clarify if we differentiate the left and right side of equation (438) with respect to x and assume that x = 1. Then $\frac{dy}{dx_1} = 0.3465n$. Consequently, the constant of distribution is directly proportional to the tangent of the angle of inclination of the tangent to the curve at point $x = 1$, $y = 0.5$. The greater n, the steeper the total curve at this point.

Distribution of atomized liquid around the axis of the spray is measured with the help of a sector catcher located under the injector and moved various distances from the nozzle so that its axis coincides with the axis of the injector. The factor of nonuniformity of distribution of atomized liquid around the axis of the spray is defined as the ratio between maximum and minimum volumes of liquid entering the separate sectors to the average volume:

$$k = \frac{(Q_{max} - Q_{min}) N}{\sum\limits_{i=1}^{N} Q_i} , \tag{439}$$

where N is the number of collector sectors.

The totality of three quantities (constant of dimension $\bar{r}$, constant of distribution n, and variation factor k) characterizes with sufficient fullness distribution of liquid in the spray.

272

§ 2. Root Angle of Spray and Distribution of Atomized Liquid in the Spray of a Jet Injector

Expansion of the spray of liquid from an atomized jet injector is determined by the value of root spray angle and distribution of liquid with respect to the radius of the spray.

Dependence of root spray angle on geometric dimensions of the nozzle, exit velocity and counterpressure was investigated experimentally by Gol'fel'der, P. I. Pobyarzhin [3], A. Kh. Rakhmanovich [4], A. S. Lyshevskiy [2] and others.

We can assume that the root spray angle during continuous outflow of liquid depends on criteria characterizing atomization W, Lp, M, and also on the parameter depending on initial disturbances on the fluid flow.

A. S. Lyshevskiy [2] proposed a dependence of the tangent of half the root spray angle on criteria in the following form:

$$\text{tg}\frac{a}{2} = CW^k Lp^l M^m, \tag{440}$$

where C, k, l, m are numbers determined during treatment of experimental data.

In experiments with cylindrical nozzles (diameters from 0.23 to 1.04 mm) A. S. Lyshevskiy obtained in the range of change of criteria $W = 1.33 \cdot 10^2 - 2 \cdot 10^4$; $Lp = 0.135 \cdot 10^4 - 3 \cdot 10^2$; $M = 0.95 \cdot 10^{-2}$ to $2.8 \cdot 10^{-2}$ the following values of constants: $C = 0.0112$; $k = 0.32$; $l = 0.07$; $m = 0.18$. At small counterpressures, when M changed in the range $1.4 \cdot 10^{-3} - 9 \cdot 10^{-3}$, these coefficients turned out to be: $C = 0.00364$; $k = 0.32$; $l = 0.07$; $m = 0$. [1]

---

[1]Criterion W is calculated with respect to the exit velocity of the liquid (on nozzle section).

273

Comparison of results of these experiments with experiments of other authors shows that coefficient C changes depending upon the top of the nozzle hole and range of change of criterion M.

Let us consider further the distribution of liquid with respect to the spray radius. The corresponding measurements have been made by Yugas [Editor's Note: spelling of name not verified] and others.
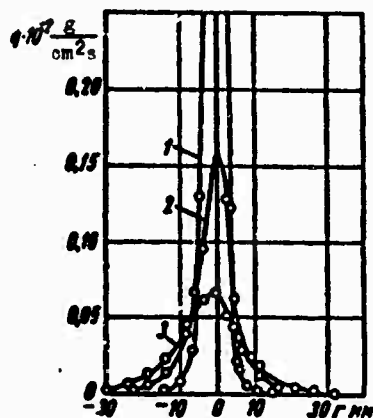

Fig. 124. Fields of specific flows of atomized liquid for a jet injector at different distances l from the nozzle hole. Diameter of nozzle D = 0.75 mm, kerosene, pressure drop Δp = 97 kgf/cm^2: 1 — l = 80 mm; 2 — l = 180 mm; 3 — l = 280 mm.

On Fig. 124 is shown the distribution of specific fluid flow at different distances from nozzle hole (measurement of K. N. Yeraston). Maximum specific flow is on the spray axis, and with distance from the axis the specific flows decrease. As distance from the nozzle hole increases, the fields of specific flows in the cross section of the spray level off.

As gas counterpressures increase, the fields of specific flows also become more uniform (Fig. 125) [4]. If exit velocity increases (pressure drop) from the injector, this also leads to a levelling off of the fields of specific flows (Fig. 126). An increase in diameter of the nozzle hole (other conditions of outflow being constant) results in an increase of specific flows and expansion of the spray boundary (Fig. 127).

On the basis of his own experiments A. S. Lyshevskiy [2] proposed criterial formulas for calculating the specific flows of jet injectors for the primary section of a spray of atomized liquid.
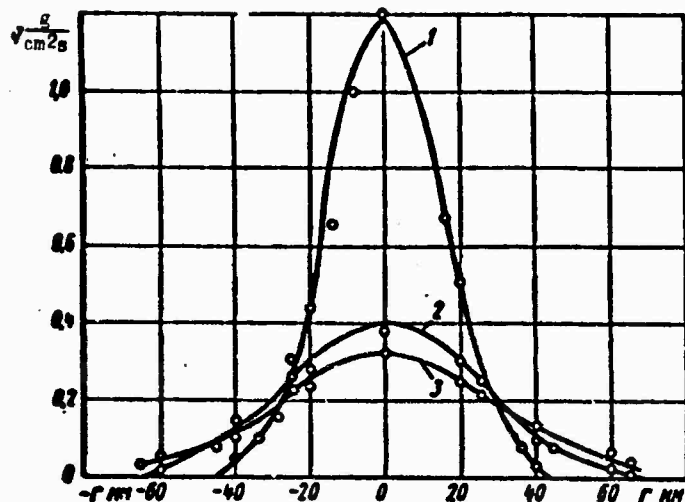
Fig. 125. Field of specific flows of atomized liquid for a jet injector under different counterpressures of air [2]. Diameter of nozzle D = 0.38 mm, diesel fuel, distance from nozzle hole 350 mm, pressure drop Δp = 250 kgf/cm^2; 1 — p = 7 at; 2 — p = 13 at; 3 — p = 16 at.
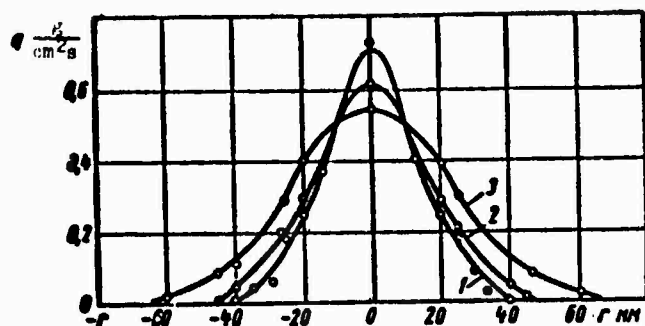

Fig. 126. Fields of specific flows of atomized liquid for a jet injector at different pressure drops [2]. Nozzle diameter D = 0.38 mm, diesel fuel, distance from nozzle hole 350 mm, counterpressure p = 10 at: 1 — Δp = 85 kgf/cm^2; 2 — Δp = 220 kgf/cm^2; 3 — Δp = 330 kgf/cm^2.
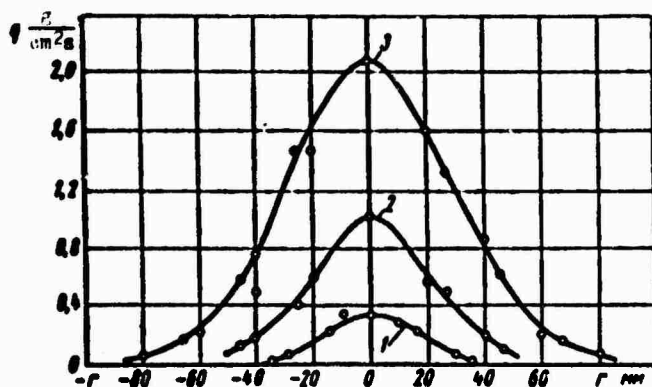
Fig. 127. Fields of specific flows of atomized liquid for jet injectors at different diameters D of nozzle hole [2]. Pressure drop Δp = 250 kgf/cm^2, counterpressure p = 10 at, distance from nozzle hole 350 mm: 1 — D = 0.23 mm; 2 — D = 0.54 mm; 3 — D = 1.04 mm.

275

When criterial change within the limits W = 1330-20,300;
Lp = $0.03 \cdot 10^4$-$0.135 \cdot 10^4$; M = $9.5 \cdot 10^{-3}$-$28 \cdot 10^{-3}$ (large counterpressures)
the relation of specific flows is expressed by the following formula:

$$\frac{q}{q_0} = 347 \left(\frac{d_c}{x}\right)^2 Lp^{-0.2}W^{-0.6}M^{-1} \times$$
$$\times \exp\left[-1390\left(\frac{r}{x}\right)^2 Lp^{-0.2}W^{-0.6}M^{-1}\right]. \qquad (441)$$

where q_0 — specific fluid flow in initial section of spray; d_c — diameter of nozzle; x — distance of examined section of spray from cut of nozzle; r — radial coordinate.

When criteria change within the limits W = 1330-20,300;
Lp = $0.03 \cdot 10^4$-$0.135 \cdot 10^4$; M = $1.4 \cdot 10^{-3}$-$9.5 \cdot 10^{-3}$ (low counterpressure)
this relation will be

$$\frac{q}{q_0} = 1380 \left(\frac{d_c}{x}\right)^2 Lp^{-0.2}W^{-0.6}M^{-0.2} \times$$
$$\times \exp\left[-55.5 \cdot 10^3\left(\frac{r}{x}\right)^2 Lp^{-0.2}W^{-0.6}M^{-0.2}\right]. \qquad (442)$$

As earlier, criterion W is calculated with respect to the velocity of liquid on the nozzle cross section.

Comparison of results of calculation by these formulas with experimental data of P. I. Pobyarzhin [3], A. Kh. Rakhmanovich [4] and Yugas [5] showed satisfactory agreement.

The distribution of atomized liquid in the spray of an injector with impinging jets has been measured by I. G. Panevin.

On Fig. 128 are the results of measurement of the relative specific flow in different radial sections of the spray. By relative specific flow is understood the ratio of specific flow through the total area of the intakes in some radial section of the spray to the corresponding specific flow in the central radial section ($\varphi = 0$). Curves on Fig. 128 correspond to different diameters and
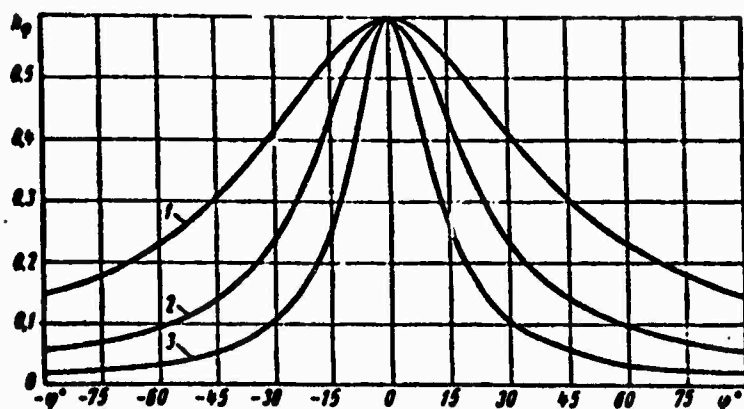
Fig. 128. Change of relative specific flow in principal plane of the spray of an injector with impinging jets (experiments of I. G. Panevin): 1 — $2\alpha_1 = 120°$; 2 — $2\alpha_1 = 90°$; 3 — $2\alpha_1 = 60°$.

lengths of streams (d = 1-2 mm; l = 3-7 mm) at different pressure drops on injector (Δp = 2-5 kgf/cm^2). Change of exit velocity, diameter and length of streams does not affect distribution of liquid in the principal plane of the spray of an injector with impinging jets.
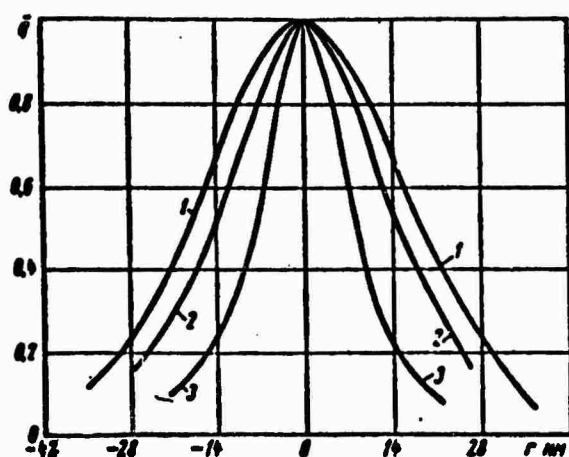

Fig. 129. Change of relative specific flow in central radial section of the spray of an injector with impinging jets depending upon radius at different angles of collision of streams. Diameter of nozzle 1.5 m, pressure drop on injector Δp = 5 kgf/cm^2, distance of intake from point of collision of streams 130 mm: 1 — $2\alpha_1 = 120°$; 2 — $2\alpha_1 = 90°$; 3 — $2\alpha_1 = 60°$.

Investigation of the distribution of atomized liquid in the radial direction (Fig. 129) showed that relative specific flow is influenced only by the angle of collision of the streams. Along the x-axis on Fig. 129 are plotted distances relative to the principal plane, and along the y-axis is the relative specific flow. Experiments also showed that an increase of exit velocity and diameter of streams leads to a small decrease of the scattering of liquid in the radial section of the spray. With distance from the injector uniformity of the distribution of liquid is increased.

§ 3. Distribution of Atomized Liquid in the Spray of a Centrifugal Injector (Swirler)

Figure 130 shows the fields of specific fluid flow for a swirler at different pressure drops (Fig. 130a) and at different distances from the nozzle (Fig. 130b). Distribution of liquid with respect
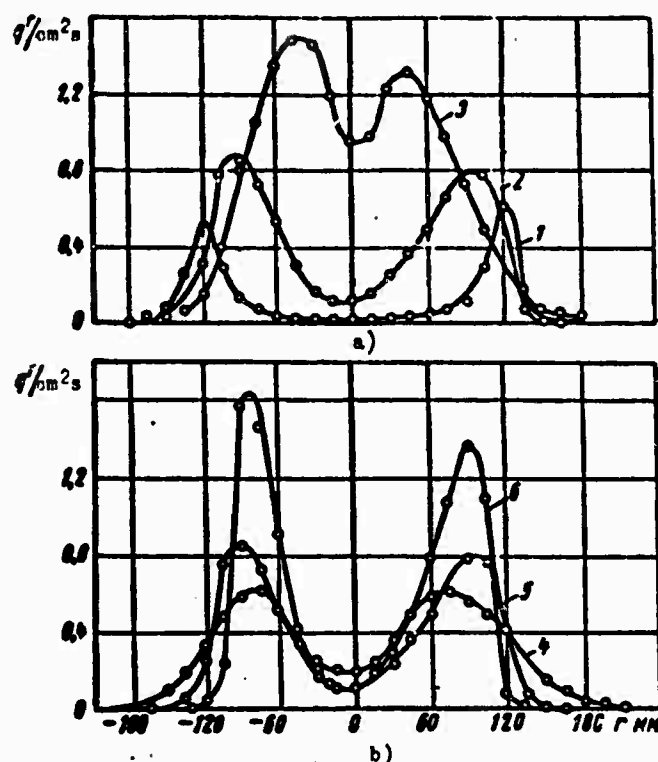

Fig. 130. Fields of specific flows of atomized liquid for a swirler: a) at different pressure drops on injector H = 150 mm; b) at different distances from nozzle ($\Delta p = 40$ kgf/cm^2); 1 — $\Delta p = 5$ kgf/cm^2; 2 — $\Delta p = 20$ kgf/cm^2; 3 — $\Delta p = 40$ kgf/cm^2; 4 — H = 200 mm; 5 — H = 150 mm; 6 — H = 120 mm.

to radius of spray is nonuniform. With an increase of pressure drop or distance from nozzle the central part of the spray is filled with liquid, and irregularity of distribution drops off. In contrast to a jet injector, for which the maximum specific flow is attained on the axis of the spray and with distance from the axis the specific flow instantly decreases, in the spray of a swirler the specific flow on the axis is close to zero and with increased distance from the axis at first it increases, and then, attaining maximum, gradually decreases.

For low exit velocities (small pressure drops) the shape of the spray is close to conic. As exit velocity increases, even at comparatively short distances from the nozzle the spray begins to

278
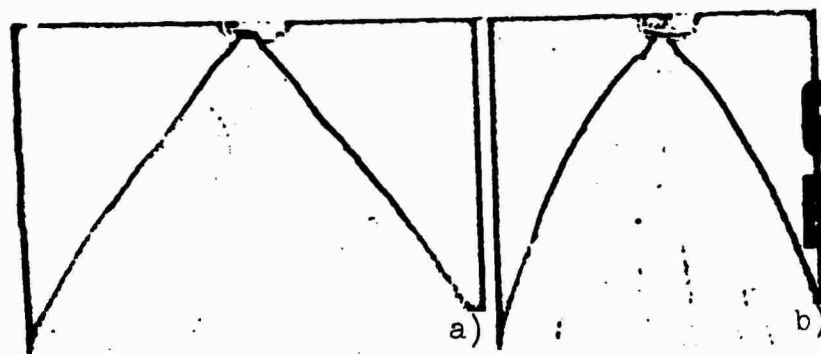
Fig. 131. Shape of atomized liquid spray:
a) $\Delta p = 4$ kgf/cm^2; b) $\Delta p = 40$ kgf/cm^2.

be compressed, and its shape approaches cylindrical (Figs. 130a and 131). The spray is compressed because from the space surrounding the spray gas is ejected, so that its velocity has a component directed inside the spray, consequence of which drops are deflected from their initial direction (to the axis of the spray) and inside the spray rarefaction develops. However, compression of the spray does not occur for all values of the root angle. As the root angle increases, compression of the spray drops off, and, as experiment shows, values of the root angle exceeding 100-110°C, it ceases.

Development of a spray thus essentially depends on conditions of ejecting the gas surrounding the spray. By changing artificially these conditions, it is possible to modify the shape of the spray. Thus, for example, if one were to place the spray inside a solid conical shell whose vertex angle is close to the root spray angle, and preventing access of gas from surrounding space, the spray not only will not be compressed, on the contrary, will be pressed to the internal surface of the shell.

Let us examine the influence of different factors on distribution of atomized liquid with respect to radius of the spray.

Figure 132 shows the change of radius $\overline{r}$ depending upon distance of examined section from nozzle for injectors with different root spray angles. At low exit velocities the trajectories of the drops are close to linear for all investigated values of the root spray
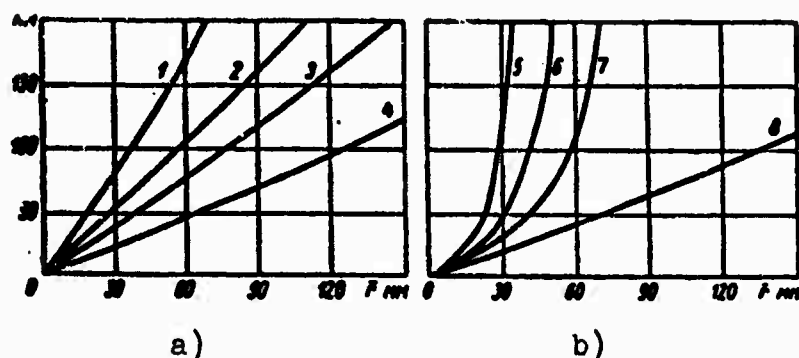
a)   b)

Fig. 132. Change of radius $\bar{r}$ depending upon
distance of examined section from nozzle of
injector: a) $\Delta p = 5$ kgf/cm^2; b) $\Delta p = 30$
kgf/cm^2; $1 - \alpha = 63^{\circ}$; $2 - \alpha = 74^{\circ}$; $3 -$
$\alpha = 88^{\circ}$; $4 - \alpha = 110^{\circ}$; $5 - \alpha = 63^{\circ}$; $6 -$
$\alpha = 80^{\circ}$; $7 - \alpha = 88^{\circ}$; $8 - \alpha = 116^{\circ}$.

angle. As exit velocity increases, the spray is compressed if the
root angle is less than 100-110°. For large root angles compression
of the spray is not observed.

Figure 133 shows the total distribution curves at different
pressure drops on the injector. These curves are represented in
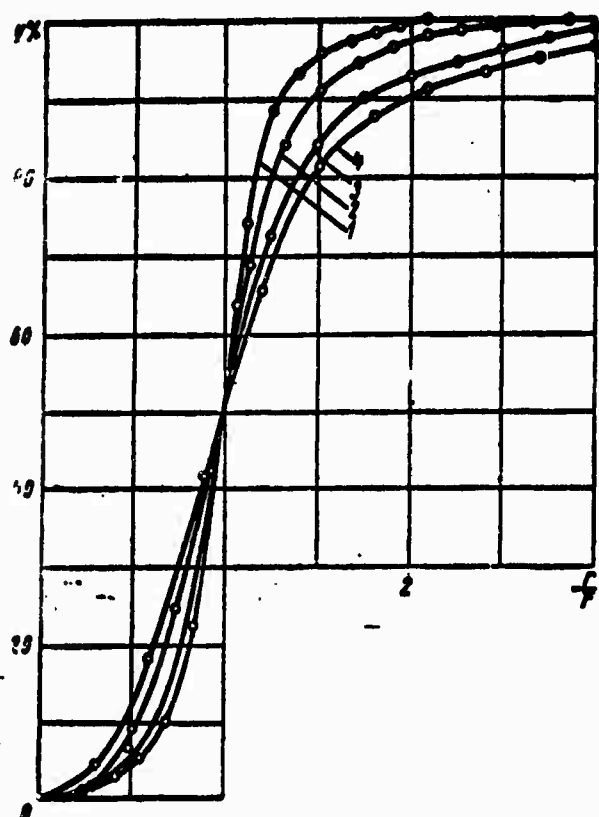
Fig. 133. Total distribution
curves at different pressure
drops for a swirler. Spray
root angle $\alpha = 78^{\circ}$, distance
from nozzle H = 150 mm: $1 -$
$\Delta p = 5$ kgf/cm^2; $2 - \Delta p = 20$
kgf/cm^2; $3 - \Delta p = 30$ kgf/cm^2;
$4 - \Delta p = 40$ kgf/cm^2.

dimensionless form; $r/\bar{r}$ is used as the abscissa. As the pressure
drop increases, distribution of liquid with respect to the radius
becomes more uniform, since the growth of pressure drop strengthens
erosion of the spray due to turbulent pulsations of the gas ejection.
The spray also erodes with distance from the injector nozzle. In
the case of injectors having different root spray angles, but smaller
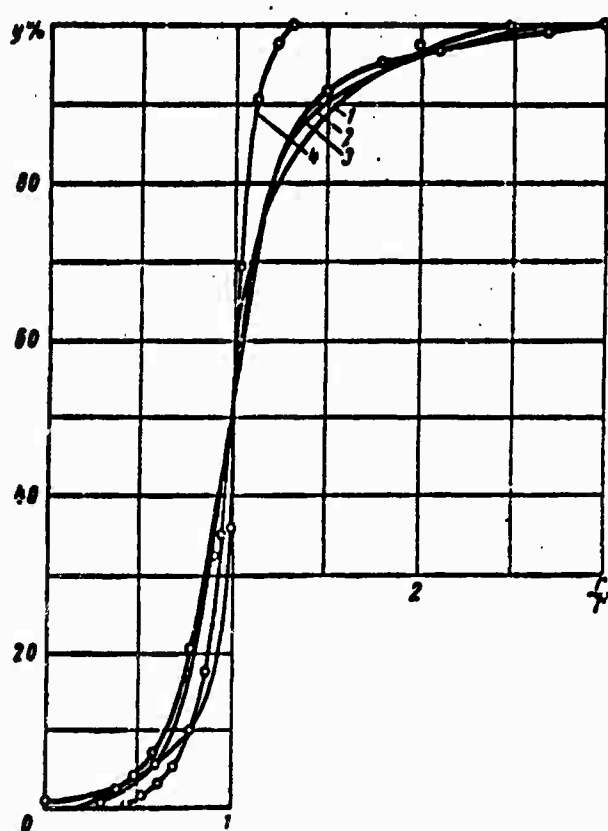than 100-110°, the total distribution curves are located close to
one another (Fig. 134).

Fig. 134. Total distribution
curves for injectors with
different spray root angles.
Pressure drop Δp = 30 kgf/cm^2,
distance from nozzle H = 150
mm; 1 — α = 63°; 2 — α = 88°;
3 — α = 80°; 4 — α = 116°.

A change of the distribution curve depends on conditions of
gas ejection, which determines the spray compression. At a given
distance from the injector nozzle H compression of the spray can
be characterized by the ratio of the spray angle $\bar{\alpha}$ to the root
spray angle, while $\bar{\alpha}$ is determined from the relationship

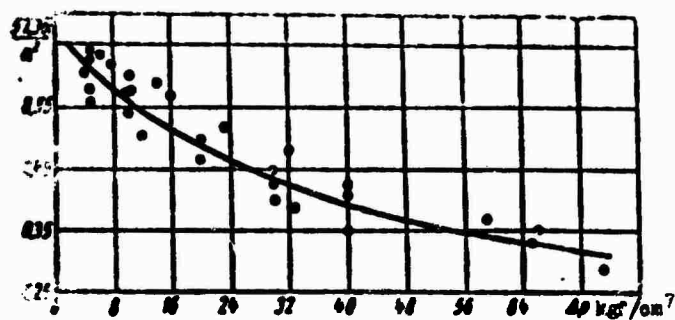$$\operatorname{tg}\frac{\bar{a}}{2} = \frac{\bar{r}}{H}.$$

(443)

Fig. 135. Change of $\frac{57.3\bar{\alpha}}{\alpha^2}$ depending upon pressure drop.

Figure 135 is the generalized dependence of the ratio $57.3\bar{\alpha}/\alpha^2$ on pressure drop for injectors whose root spray angle torch is in the interval from 60° to 90° (for liquid flow rates from 10 to 80 g/s). The ratio decreases as pressure drop increases, and increases as the root spray angle increases, independently of the flow rate of liquid through the injector:

$$\frac{\bar{\alpha}}{\alpha} = \frac{\alpha}{57,3} f(\Delta p). \qquad (444)$$

Function $f(\Delta p)$ is depicted on Fig. 135.

Thus, distribution of rigidity with respect to the spray radius of a swirler depends on three parameters: pressure drop on injector, root spray angle and distance between examined section of spray and injector nozzle. At present there still are no formulas for swirlers connecting specific flows of atomized liquid with criteria W, Lp, M, as has been done for jet injectors in formulas (441) and (442).

In a number of cases (atomization of liquid in an axisymmetrical gas flow) it is worthwhile to detect irregularity of the distribution of atomized liquid around the spray axis. First of all it is necessary to clarify the causes of this irregularity and to find ways to decrease it.

Causes of irregular distribution of liquid around the spray axis are different asymmetries, connected with the atomizer design (final number of entrance channels) and technology of manufacture (eccentricity of nozzle with respect to swirl chamber, difference in size of separate entrance channels or size of swirl arm, misalignment of nozzle hole, roughness on moistened surfaces of swirl chamber and nozzle, etc.).

The strongest influence on uniformity of distribution comes
from the number of entrance channels, eccentricity of nozzle with
respect to swirl chamber and cleanness of nozzle hole and channels
along which liquid flows to it. These deviations result in asymmetry
of fluid flow in the nozzle.

Interaction of the spray of atomized liquid with the surrounding
gaseous medium is a secondary factor, only increasing the conse-
quences of irregularity in the injector.

Below are certain results of experimental investigations of ·
the uniformity of distribution of atomized liquid around the spray
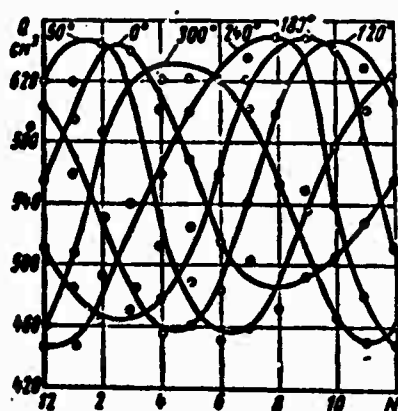angle, conducted by S. A. Kosberg.

Fig. 136. Distribution
of liquid with respect
to collectors as the
injector turns on its
axis.

Figure 136 gives results of experiment, showing that irregularity
of the distribution of liquid is determined first of all by the
properties of the injector itself. If we turn the injector around
the axis of the nozzle, giving a nonuniform distribution of liquid,
then its distribution with respect to the collectors shifts by the
angle of rotation of the injector.

Increase of the number of entrance channels promotes a more
symmetric flow of liquid in the swirl chamber and reduces irregu-
larity of distribution of liquid in the spray.

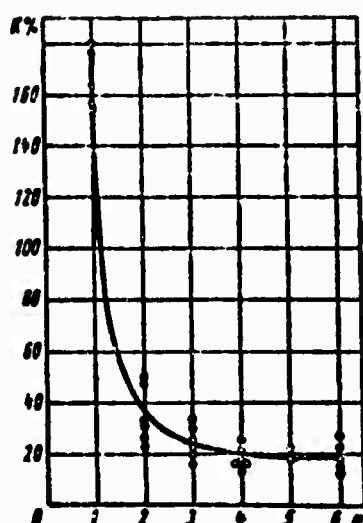Change of variation factor k depending upon number of entrance

Fig. 137. Change in the variation factor depending upon the number of entrance channels.

·····els n is shown on Fig. 137. Investigated injectors differed ···· by the number of entrance channels, while the total area of ····· channels remained constant. A transition from one channel to ···· sharply improves the uniformness of distribution, whereas at · ? 3 quantity k practically does not depend on n. Thus, in designir·· ·wirlers the number of entrance channels should be from 3-4.
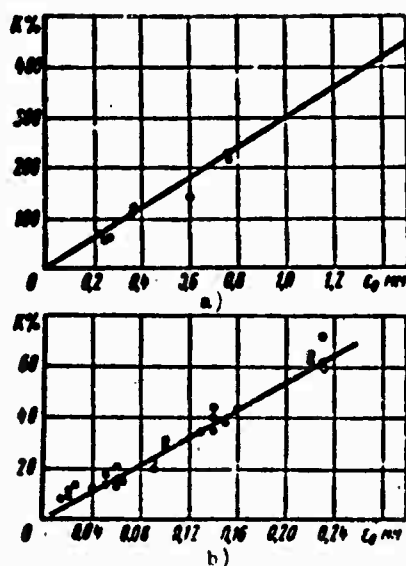

Fig. 138. Change in the variation factor, depending upon the magnitude of nozzle eccentricity in relation to the swirl chamber: a) $0 < \varepsilon < 1.6$ mm; b) $0 < \varepsilon < 0.25$ mm.

On Fig. 138 is shown the change of variation factor k depending upon eccentricity of the nozzle with respect to the swirl chamber. As we see, it grows in direct proportion to eccentricity and even

284

at comparatively small values of the latter (ε_0 = 0.1-0.15 mm)
goes beyond permissible (according to technical conditions) limits.

Consequently, for sufficiently equal distribution of liquid
around the spray axis it is necessary to ensure an injector design
(structural and technological) in which relative eccentricity of
the nozzle hole $\left(\varepsilon = \dfrac{\varepsilon_0}{d_c}\right)$ does not exceed 0.075. Experiments also
show that as the geometric characteristic of the injector A increases,
the irregularity of distribution increases. Consequently, the less
the discharge coefficient of the injector and the greater the root
spray angle, the more difficult it is to obtain equal distribution
of liquid around the spray axis and the more exact must the coaxiality
of nozzle and swirl chamber be maintained. To prevent a shift of
the nozzle with respect to the swirl chamber, it is advisable to
make the atomizer in the form of a nondetachable part (Fig. 139),
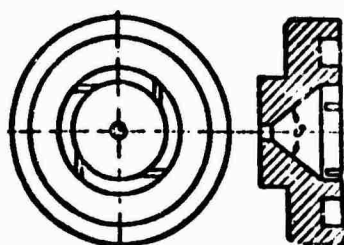which will allow minimization of the eccentricity of the nozzle.

Fig. 139. Nondetachable
injector atomizer.

Angle $ when the flow enters the nozzle (Fig. 140) also affects
variation factor k. Nozzles with small angle $ are very long, which
increases the path covered by liquid particles from swirl chamber
to the cut of the nozzle. Besides, due to the influence of forces
of viscosity, the initial irregularity appearing in the swirl chamber
is weakened and eccentricity of the air vortex with respect to the
nozzle axis decreases. This circumstance leads to an increase of
uniformity of distribution of liquid in the spray. However a nozzle
with angle $ less than 60° is difficult to construct.

Figure 141 illustrates the influence on k of a pressure drop
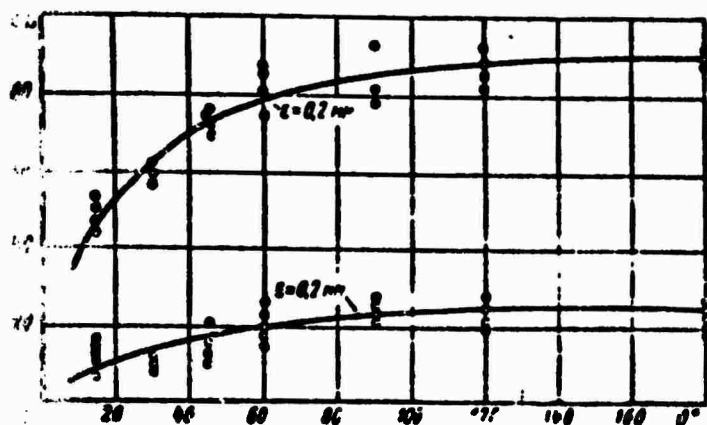on injectors. At short distances from nozzle (35 and 50 mm)

Fig. 140. Dependence of variation factor on cone angle on nozzle entrance.

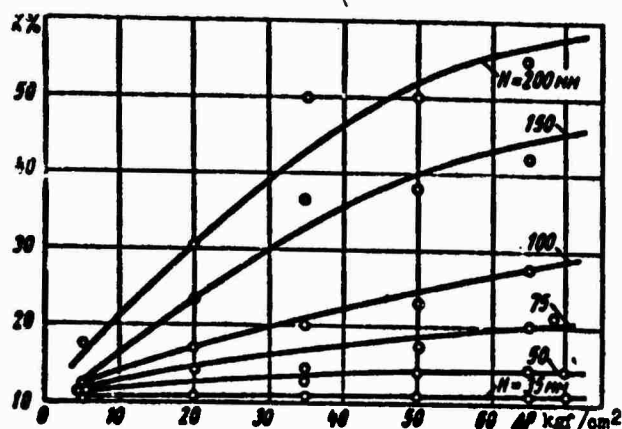Pressure drop $\Delta p = 40$ kgf/cm², distance from nozzle H = 100 m.

Fig. 141. Dependence of variation factor on pressure drop at different distances from the nozzle.

quantity k has almost no dependence on pressure drop and is determined by the flow conditions in the nozzle. When distance from the nozzle increases, the gas flow ejected by the drops causes a distribution of liquid in the spray and increases the irregularity of its distribution. As the pressure drop on the injector drops off, the velocity of the ejected gas flow increases, leading to a more intense increase of drops from some sections of the spray to another, and, consequently, to an increase of the variation factor. At short distances from the nozzle drops still do not lose their intrinsic velocity, and in spite of the influence of the gas flow, in this part of the spray a distribution close to the initial is maintained.

Quality of finishing the nozzle hole strongly affects uniformity of distribution of liquid. Therefore thorough treatment of nozzle

286

hole (grinding with abrasive paste) and channels feeding the liquid
to the swirl chamber is required.

§ 4. Distribution of Atomized Liquid in the Spray Created by a Revolving Atomizer

Experimental investigations of the distribution of atomized
liquid in the spray created by a revolving atomizer have been con-
ducted by a number of authors. The most detailed was carried out
recently by A. M. Lastovtsev and N. I. Deryabin [1]. The basic
characteristic of distribution was radius r_{99}, including 99% of the
atomized liquid. Total distribution curves similar to those on
Fig. 123 were experimentally obtained, and by these curves the r_{99}
were determined. As a result of treatment of the experimental data
with the help of dimensionless criteria empirical formulas connecting
$\dfrac{r_{99}}{d_{cp}}$ with Reynolds criteria

$$Re = \frac{u_A d_{cp} \rho_1}{\mu_1},$$

and Froude criteria

$$Fr = \frac{u_A^2}{d_{cp} g} \quad \text{and} \quad M = \frac{\rho_2}{\rho_1}$$

were obtained, where u_A — absolute velocity of liquid from edge of
revolving disk; d_{cp} — average diameter of drop.

Since $Re \gtrsim 500$ three formulas are obtained distinguished by
the range of change of absolute velocity:

at u_A = 37-60 m/s

$$\frac{r_{99}}{d_{cp}} = 0.25 \cdot 10^5 Re^{-0.83} Fr^{-0.033} M^{-0.8};$$

at u_A = 60-68 m/s

$$\frac{r_{99}}{d_{cp}} = 25 Re^{-0.53} Fr^{0.43} M^{-0.3}; \qquad (445)$$

at u_A = 68-105 m/s

$$\frac{r_{99}}{d_{cp}} = 0.37 Re^{-0.51} Fr^{0.7} M^{-0.8}.$$

Since the mean drop diameter depends on criteria W, Lp, M, it is obvious that radius r_{99} can be represented in the following way:

$$\frac{r_{99}}{D_0} = F(W, Lp, M, Fr).$$

where D_0 — diameter of revolving disk.

Literature

1. Lastovtsev A. M. i Deryabin N. I. Eksperimental'noye opredeleniye razmerov fakelov vrashchayushchikhsya raspyliteley v spokoynom i dvizhushchemsya gaze (Experimental determination of the dimensions of sprays of revolving atomizers in still and moving gas). M., 1964 (Trudy MIKhM. T. 26).

2. Lyshevskiy A. S. Protsessy raspylivaniya topliva dizel'nymi forsunkami (Fuel atomization by diesel injectors). M., Mashgiz, 1963.

3. Pobyarzhin P. I. Issledovaniye vliyaniya vnutrennego vikhreobrazo vaniya v forsunke na kachestvo raspyli aniya i fakel raspylennogo topliva (Investigation of the influence of internal eddy formation in an injector on quality of atomization and the spray of atomized fuel), M., 1958 (Trudy VMTU No. 76).

4. Rakhmanovich A. Kh. i dr. Issledovaniye razvitiya strui topliva metodom vysokochastotnoy kinematografii (Investigation of the development of a stream of fuel by the method of high-frequency cinematography). "Dizelestroyeniye", 1937, No. 11.

5. Yugas i dr. Obrazovaniye i rasseivaniye toplivnykh struy (Formation and dispersion of fuel streams). Collection "Dvigateli vnutrennego sgoraniya". T. 1, M., ONTI, 1936.

C H A P T E R   VIII

EXPERIMENTAL INVESTIGATION OF THE WORK OF INJECTORS

During an experimental investigation of the work of injectors
and other liquid atomizing devices, usually the following quantities
characterizing the hydraulic properties of these devices and quality
of liquid atomization are determined:

1) discharge coefficient of injector;

2) root spray angle of atomized liquid;

3) distribution of atomized liquid across cross section of
spray;

4) distribution of drops with respect to size and average
diameter.

§ 1. Hydraulic Investigations of Injectors

Hydraulic investigations of injectors usually determine the
discharge coefficients of injectors and root spray angles of the
atomized liquid.

There exist several methods of determining discharge coeffi-
cients (or flow rate characteristics). Most frequently encountered
are two methods — the volume method and a method using throttle
instruments.

The setup for removing flow rate characteristics is shown on
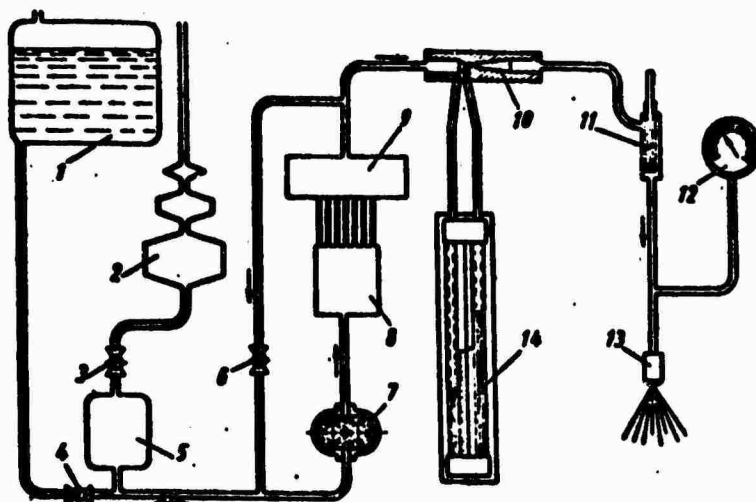Fig. 142. From tank 1 liquid proceeds through stopcock 1 to

289

Fig. 142. Setup for removing flow rate
characteristics of injectors: 1 — tank;
2 — probe tester; 3, 4, and 6 — cocks;
5 — tank; 7 — booster pump; 8 — high
pressure pump; 9 — container; 10 —
Venturi tube; 11 — thermometer; 12 —
manometer; 13 — injector; 14 — differen-
tial manometer.

booster pump 7 and further to high pressure pump 8, from which it
moves into container 9 for damping pulsations. The liquid flow
rate is changed by partially bypassing it into the suction tube of
the booster pump through control cock 6. Between cock 4 and line of
bypass is probe tester 2 with cock 3 and tank 5. The probe tester
has measuring capacities of different volume. A stopwatch determines
the support time of one of the measuring capacities and thus the
volumetric flow rate of liquid through injector is found.

Tank 5 prevents air from entering the system.

From damping container 9 liquid enters Venturi tube 10, pressure
drop on which is measured with differential mercury manometer 14.
Further liquid washes the small container with thermometer 11 and
heads to injector 13. In front of the injector liquid pressure
is measured by spring manometer 12. If the Venturi tube is calibrated
beforehand by the probe tester, then, by measuring pressure drop
one can determine the instantaneous liquid flow rate.

An essential value in removing the flow rate characteristics belongs to a constancy of pressure before the injector while measuring the support time of the measuring capacity. If this pressure is not constant, an increase of the time of measurement will not lead to a reduction of error in the flow rate measurement.

The discharge coefficients of injectors during the outflow of liquid into a gaseous medium whose pressure exceeds atmospheric are determined by special flowmeters; a description of one of such flowmeters can be found in a work by Kling and others [9].

The root spray angle of atomized liquid is determined by photographing the spray, which is illuminated by strong lateral light, against the background of a screen of black velvet. The angle is determined by the photograph. Photographing can be replaced by projecting the spray onto a transparent screen.

§ 2. Measurement of Distribution of Atomized Liquid in Spray

The field of specific flows of atomized liquid in a spray is determined with the help of measuring glasses placed along the diameter of the spray. Intake openings of measuring glasses must have pointed edges to avoid reflection of drops from their edges.

In order to establish the distribution of atomized liquid around the spray axis, sector collection is used; a diagram is shown on Fig. 143. Liquid going from injector 1 into separate sectors of catcher 2 flows along tubes into rocking funnels 3, which can be set in two positions — measurement and overflow. In the first position liquid flows into measuring glasses 6, and in the second into collector 7 and further into the overflow tube. When funnels shift from one position into the other, stopwatch 5 is started or stopped by cam 4. By measuring the quantity of liquid in every measuring glass one can determine by formula (439) the variation factor of the distribution of liquid in the spray.

It is necessary to consider that the variation factor depends on the number of collection sectors and increases as they increase,
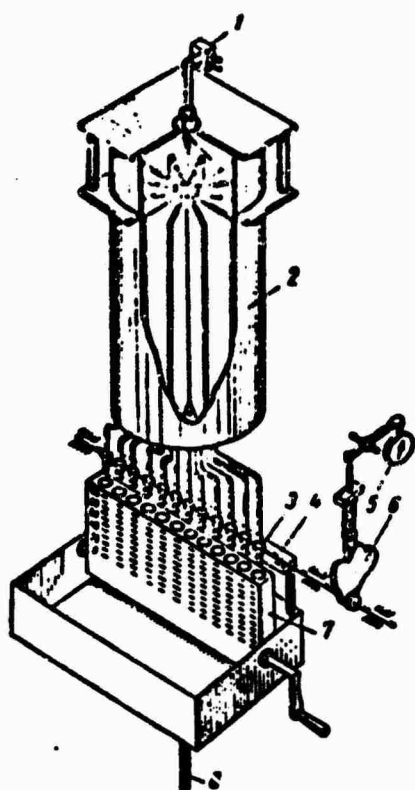
291

Fig. 143. Sector
collection: 1 —
injector; 2 and 4 —
collector; 3 — funnel;
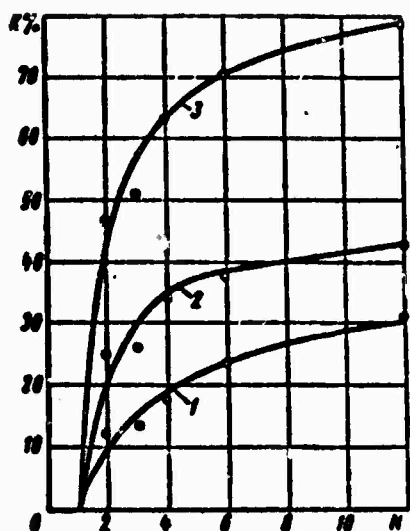5 — stopwatch; 6 — cam;
7 — measuring glass;
8 — overflow.

Fig. 144. Dependence
of variation factor on
number of collection
sectors: 1, 2, 3 —
dependence for injectors
with different degree
of variation.

as can be seen on Fig. 144 for injectors with different degree of
irregularity. Therefore for comparable results it is necessary to
use collectors with an identical number of sectors, for example,
twelve. Also it is necessary that the distance of the injector
nozzle from the plane not be changed and that pressure drops on
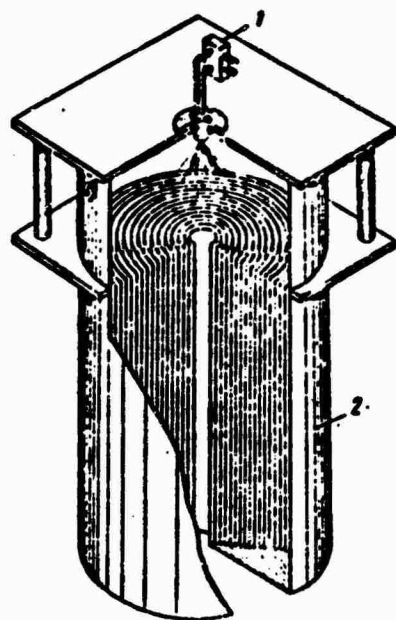injectors remain constant.

292

Fig. 145. Circular
collector: 1 — injector;
2 — collection.

Distribution of atomized liquid with respect to radius of spray
s determined with the circular collector shown on Fig. 145. Liquid
atering separate ring-shaped cells, is removed into measuring glasse.,
whose setup is similar to Fig. 143 for sector collection. By measuring
the quantity of liquid in every measuring glass, it is possible to
construct the total distribution curve of the liquid (see § 1
Chapter VII).

§ 3. Measurement of Fineness of the Atomization of Liquids

The fineness of atomization of liquids (or dispersion analysis)
is primarily measured to clarify the performance quality of different
types of injectors or when establishing the influence of different
parameters of injectors and physical properties of liquid on drop
size, and to determine the influence of parameters of the gaseous
medium (velocity, density, etc.) on drop size.

The solution of similar problems is connected first of all
with measurement of a huge number of drops. The measurements are
very laborious and tedious. Frequently it turns out that the results
of measurements which are not thorough give a distorted idea of drop
size. This partly explains the large variety of methods to measure
drops.

293

Below we will examine only methods either having practical application or having promise of application.

Existing methods can be divided into three groups:

1) direct methods of measurement, when the radiated liquid is atomized;

2) methods based on replacement of the investigated liquid by a substance with low melting point, which when heated has the physical properties of the radiated liquid with subsequent solidification of drops in flight;

3) indirect methods of measurement (optical, sedimentometric, other).

Let us consider direct methods of measurement.

Measurement based on catching drops by an immersion medium is one of the simplest and therefore one of the most widespread.

Into the flow of liquid drops is introduced a plate covered by immersion material (viscous oil, soot, etc.). Flying drops, hitting the catching layer, are held back in it, or leave imprints (craters). The plate with drops or its photographs is investigated under a microscope using an automatic meter to produce a distribution curve of drops with respect to size.

In the atomization of water and aqueous solutions a mixture of vaseline with transformer oil, castor oil, silicone, etc., is used to catch drops. Thickness of the layer should exceed the maximum diameter of the drops. It is necessary that drops in the layer not merge with each other and not lose their spherical shape.

To catch drops of liquid hydrocarbons (petroleum fuels), plates, covered by a layer of soot obtained when kerosene is burned

~re used. The surface of the soot usually is covered by a thin layer
of white magnesium oxide, which increases the clearness of the drop
imprints.

It is necessary to note that results of the measurements of
drop size using this method frequently were not trusted because when
drops strike the catching layer they undergo considerable deformation
and therefore imprints on the layer characterize not the diameter of
~ spherical drop, but the diameter of a deformed drop;· the true
·'rop dimensions remains unknown.

Studying the relationship between diameter of drop d and imprint
d' on the layer of soot under conditions when the drop hits against
layer of soot, Stoker [11] obtained the following empirical formula:

$$\frac{d'}{d} = 0.77 W^{\frac{1}{4}},$$

·:here $W = \cdot \frac{\rho d V^2}{\sigma}$ — Weber criterion (ρ — density of liquid of the
drop; σ — coefficient of surface tension of liquid of the drop with
respect to air; V — velocity of drop before collision).

It is necessary to note that in experiments of Stoker thickness
of the layer was not even measured and was not considered.

M. S. Volynskiy, investigating the collision of drops with a
layer of soot, established (qualitatively) the influence of thickness
of the layer of soot on d'/d, but did not obtain numerical relation-
ships. Figure 146 gives the results of experiments which established
the influence of relative thickness of layer of soot h/d on d'/d.
As the thickness of the layer increases, the slope of the line
decreases. When h/d = 1.5, 3.5, 4.5 then d'/d is close to one.
Thus, at h/d = 1.5 without great error, in the examined range of
Weber numbers (to W = 1500), the diameter of the imprint can be
taken equal to the diameter of the drop.

G. D. Salamandra and I. M. Naboko [2] carried out high-speed
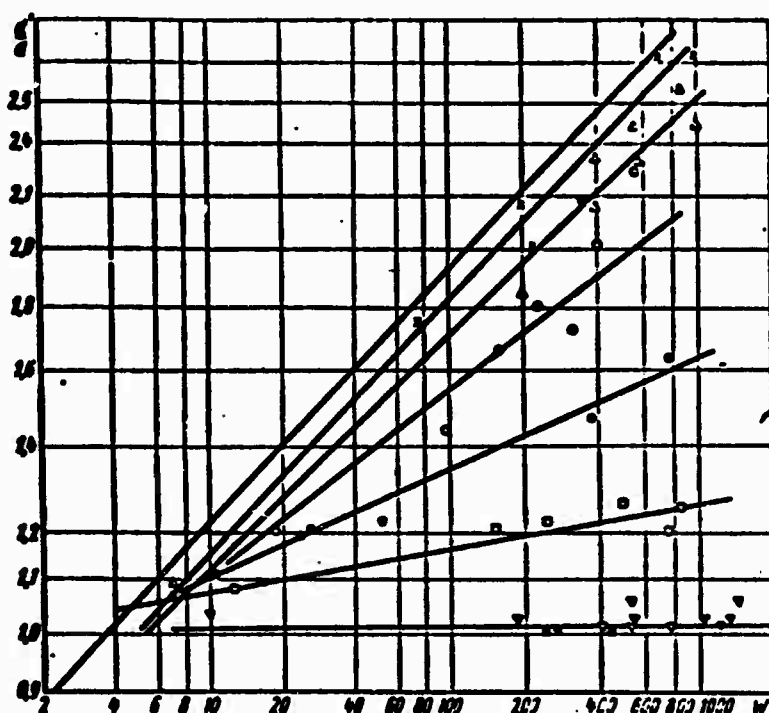filming of the collision of a drop with a layer of soot. It turned

295

Fig. 146. Change of the ratio of diameter of the imprint to diameter of the drop depending upon criterion W and relative thickness of layer of soot h/d: $x - \frac{h}{d} - 0.16$; $\triangle - \frac{h}{d} - 0.3$; $o - \frac{h}{d} - 0.6$; $\bullet - \frac{h}{d} - 0.75$; $\square - \frac{h}{d} - 0.9$; $\triangledown - \frac{h}{d} - 1.5$; $\blacktriangledown - \frac{h}{d} - 3.0$; $\blacksquare - \frac{h}{d} - 4.5$

out that a drop in a number of cases can be split up upon collision. It was shown that the method of catching can be used only when during investigation under a microscope all imprints will appear unary, deep, with even edges. In these conditions with sufficient thickness of the layer of soot the diameter of the imprint will equal the diameter of the drop.

The method of catching on soot becomes inapplicable when drops are very large, or, conversely, are very small.

In coarse atomization, when in the spray are drops whose diameter exceeds 500 μm, it is necessary that the thickness of the layer exceed 0.7-0.75 mm. When thickness exceeds 0.7 mm, the layer of soot is not strong enough and under the impact of drops is easily broken up.

During atomization into very small drops, for example, when the maximum diameter does not exceed 25-30 μm, a considerable part of drops with diameter less than 10 μm cannot be considered, since due to the resistance of air they lose velocity near the nozzle. Breakthrough ability of these drops is lost, they do not strike the layer and form no imprint. As a result small drops are not considered and the distribution curve of drops with respect to size is incomplete.

Besides the above possible measurement errors, inaccuracy of the method of catching drops on immersion media also involves the fact that drops for investigation are not sampled from the whole torch. Consequently, the real distribution of drops in the investigated section of the spray cannot be considered. Further, the number of investigated drops cannot be made sufficiently large enough for objective data. Furthermore, sources of inaccuracies are errors in measuring the imprints of drops on microphotographs. All these errors can compose up to +30%. Nonetheless the method of catching drops is widely used both when measuring drop size under conditions of a motionless surrounding gaseous medium and under conditions of gas flow.
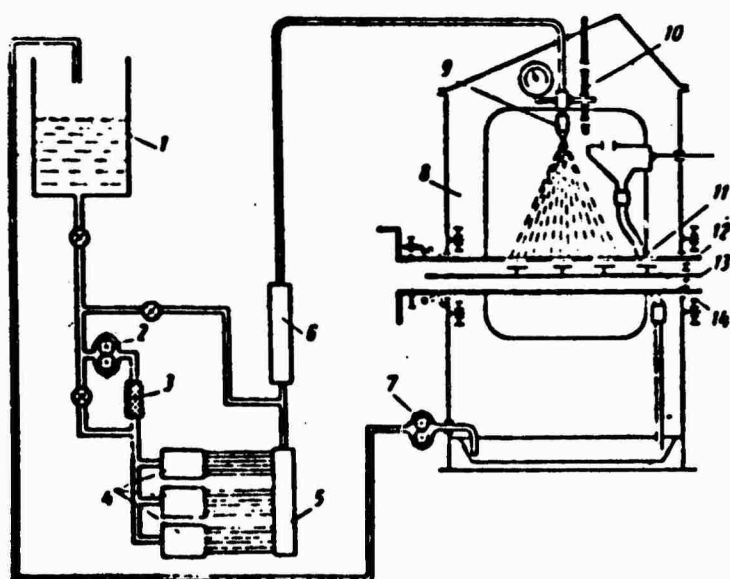

Fig. 147. Setup for measuring fineness of the atomization of liquids by the method of catching drops: 1 — tank for liquid; 2 — booster pump; 3 — filter; 4 — high pressure pumps; 5 — collector; 6 — accumulator; 7 — scavenge pump; 8 — chamber; 9 — injector; 10 — bracket; 11 — cuts in pipe; 12 — pipe; 13 — rod of drop catcher; 14 — plates, covered by layer of soot.

1. Measurement of the fineness of atomization under conditions of motionless surrounding gaseous medium. Figure 147 shows the setup for measuring the fineness of atomized liquid with the method of catching drops.

Drops are sampled in the following way. Liquid under a given pressure moves to injector 9, which injects it vertically downwards. The injector is fastened on mobile bracket 10, which can be moved up and down.

Perpendicularly to the spray of atomized liquid in chamber 8 is a turning dropcatcher in the shape of rod 13 with plates 14, covered by a layer of soot and magnesium oxide. The rod with plates is in pipe 12, having a series of longitudinal cuts 11, separated from each other by narrow crosspieces. The plates always are turned upwards against the spray; the pipe, resting on ballbearings in the chamber wall, prior to the moment when the regime is reached is turned by its notches downwards.

After establishing the flow regime of liquid in the p pe, a special mechanism is used to make one turn. When the notches of the pipe match the rod, drops have access to the inside of the pipe and get on the plates with the catching layer. Rotation rates of the pipe can be modified in accordance with the necessary exposure of the preliminary tightening of the spring on the turning mechanism. After sampling the drops, the rod and plates are drawn from the pipe. Specific sections of the plates are photographed with magnification (usually 50-100 times).

2. Measurement of fineness of atomization under conditions of gas flow. These measurements are considerably more complex than under conditions of a fixed gaseous medium. For measurements under conditions of high velocities of gas flow and high gas pressures not one of the existing methods of measuring drop size has been adopted, with the exception, apparently, of the method of catching on a layer of soot. However, the layer is not strong, and at very strong concussions it is destroyed; furthermore, it is blown off

..der the counter gas flow. Therefore it is necessary to take
measures to protect the layer from destruction. For a great con-
centration of drops the layer of soot can be eroded by the flow of
drops.

In a number of cases (not very high gas velocities and low con-
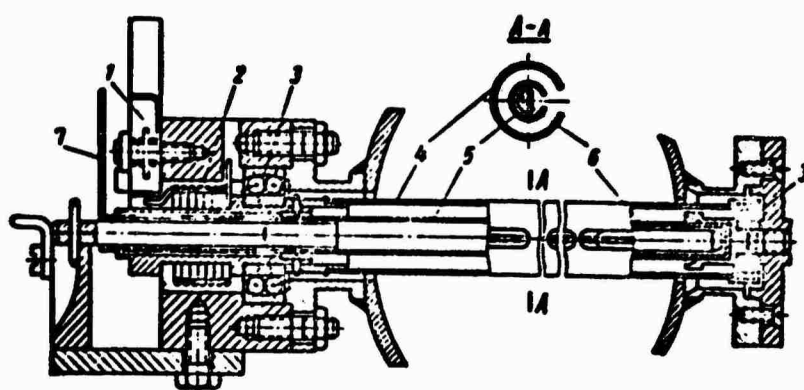centration of liquid) the dropcatcher on Fig. 148 can be used.

Fig. 148. Attachments for catching drops in
a gas flow: 1 — ratchet; 2 — spring; 3 —
bearings; 4 — pipe with notches; 5 — housing;
6 — rod; 7 — handle.

On bearings 3, fastened in bosses of the chamber, is pipe 4
with notches along its generatrix. On one end of the pipe is
fastened ratchet 1, which is used to start spring 2, connected with
the pipe. Inside the pipe is introduced rod 6, fastened in housing
5, with a flat covered by a layer of soot beforehand.

Along the whole length of housing 5 is a narrow slot. To protect
the layer of soot from the gas flow and drops of liquid the slot of
the housing and notches of the turning pipe are directed along the
flow. To catch the drops, the housing with the help of handle 7
turns 180° against the flow and simultaneously the safety device of
ratchet 1 is pressed, which holds the spring in a raised state.
The liberated spring turns the pipe one full turn. When the notches
of the pipe meet the slot of the case, and consequently also the rod,
drops get on the catching layer. Then the case returns to its initial
position, i.e., its slot is again along the flow, and the rod is
extracted from the pipe.

299

Such a dropcatcher permits avoiding damage to the layer and obtaining satisfactory imprints of the drops at moderate gas flow velocities (to 70 m/s).

Counting the number of drops and measuring the diameters on microphotographs can be automated with the help of electronic readers [4]. These devices permit essentially accelerating the treatment of microphotographs of the drops and obtaining distribution curves of drops with respect to size.

Let us consider another direct method — microphotographing the spray of atomized liquid under illumination by spark discharge.

During atomization of liquid drops move at up to 100-200 m/s. In order to photograph, it is necessary to have a source of sufficiently bright light, which could illuminate the moving drops through a very short interval of time. This is attained with the help of a spark discharge 10^{-6}-10^{-7} s long.

In opaque chamber 4 (Fig. 149) is located injector 2 and the illuminator. On the wall of the chamber is attached camera 3.
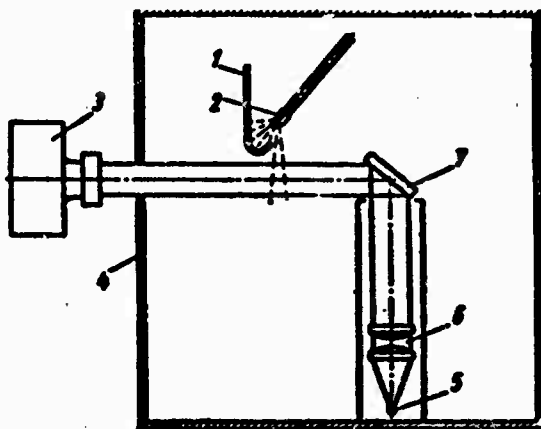

Fig. 1.49. Device for macrophotographing the spray using a spark discharge: 1 — jet cutoff; 2 — injector; 3 — camera; 4 — opaque chamber; 5 — electrodes of discharger; 6 — condenser; 7 — prism.

Between electrodes of discharger 5 skips a spark, the light from which enters condenser 6 and in the form of a parallel beam — prism 7. Being reflected in the prism, horizontal bundle of light enters the field of sight of the camera objective.

Part of the liquid atomized by the injector with the help of cutoff 1, is removed into the overflow pipe. The bundle of light before getting into the objective, intersects the spray of atomized liquid.

Another way of microphotographing the spray can be found in a work by G. D. Salamandra and I. M. Naboko [3] and in a survey of articles of Clare and Corbeau [5, 6].

Usually for more convenient treatment of the photographs results are enlarged (10× and more). Treatment of the photographs reduces to measuring drop size, grouping them with respect to size and constructing the distribution curve. The number of photographed drops by which the distribution curve is constructed is very small, and in this respect microphotographing the drops has no advantages over the method of catching them on a layer of soot.

The advantage of the method of microphotographing over the method of catching is only that it gives a more correct idea of the mutual location of drops in the spray and partly about the form of the drops. However, if we consider that the photograph fixes only drops in the focus, and that many drops remain outside the focus, then these advantages become doubtful during a measurement only in one plane of focusing.

Let us now turn to consideration of methods of measuring drop size based on the replacement of the liquid by a substance with a low melting point, which upon being heated obtains the physical properties of the studied liquid with subsequent solidification of drops in flight. These methods make it possible to obtain detailed characteristics of the fineness of atomized liquid, since they satisfy more or less fully the following basic requirements:

1) in the investigated mass of drops must be drops of all the available sizes in the spray;

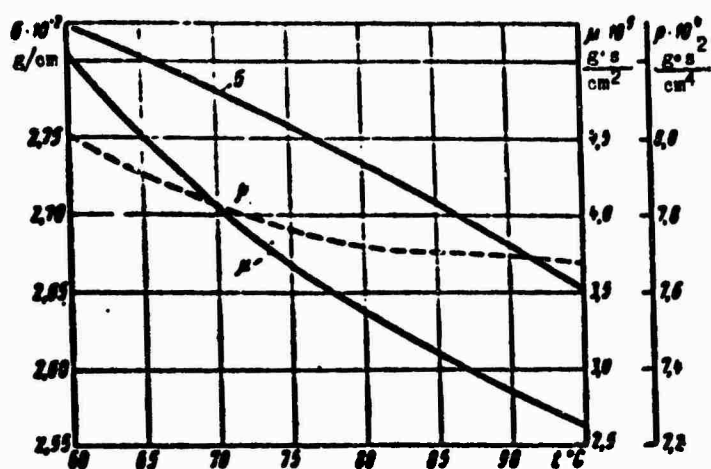2) the number of drops with respect to which the fineness of

Fig. 1.50. Change of coefficient of surface tension, viscosity and density of paraffin depending upon temperature of heating.

atomization is determined should be sufficiently large.

Solidified drops are collected, shifted through a set of screens, and the drops which settle on the screens are weighed.

As the modelling substance paraffin, cerezine, wax and others are usually selected. On Fig. 150 are given curves of the measurement of coefficient of surface tension, viscosity and density with respect to temperature. At a paraffin temperature of 90°C, values of the above quantities, with the exception of density, are close to values corresponding to those quantities for kerosene at $15-20^{\circ}$C. In a work by Moroshkin and Heller [1] can be found data about certain substances capable of being used as modelling substances.
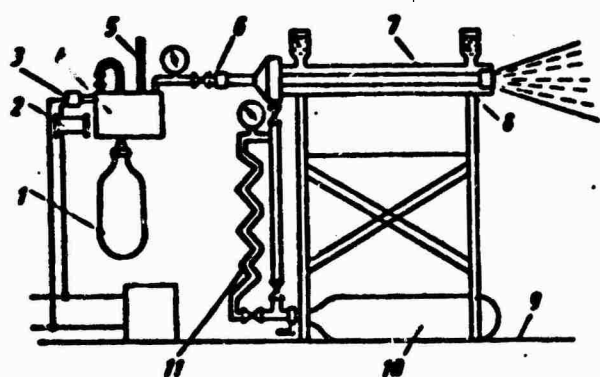

Fig. 151. Setup for measuring fineness of atomization according to Joys [7]: 1 — tank with nitrogen; 2 — heater; 3 — thermostat; 4 — tank for paraffin; 5 — thermometer; 6 — washer; 7 — injector; 8 — free jacket; 9 — sheets of paper for collecting drops; 10 — air container; 11 — air heater.

On Fig. 151 is one of the first installations for investigating the fineness of liquid paraffin atomized by injectors [8]. An improved setup is shown on Fig. 152.
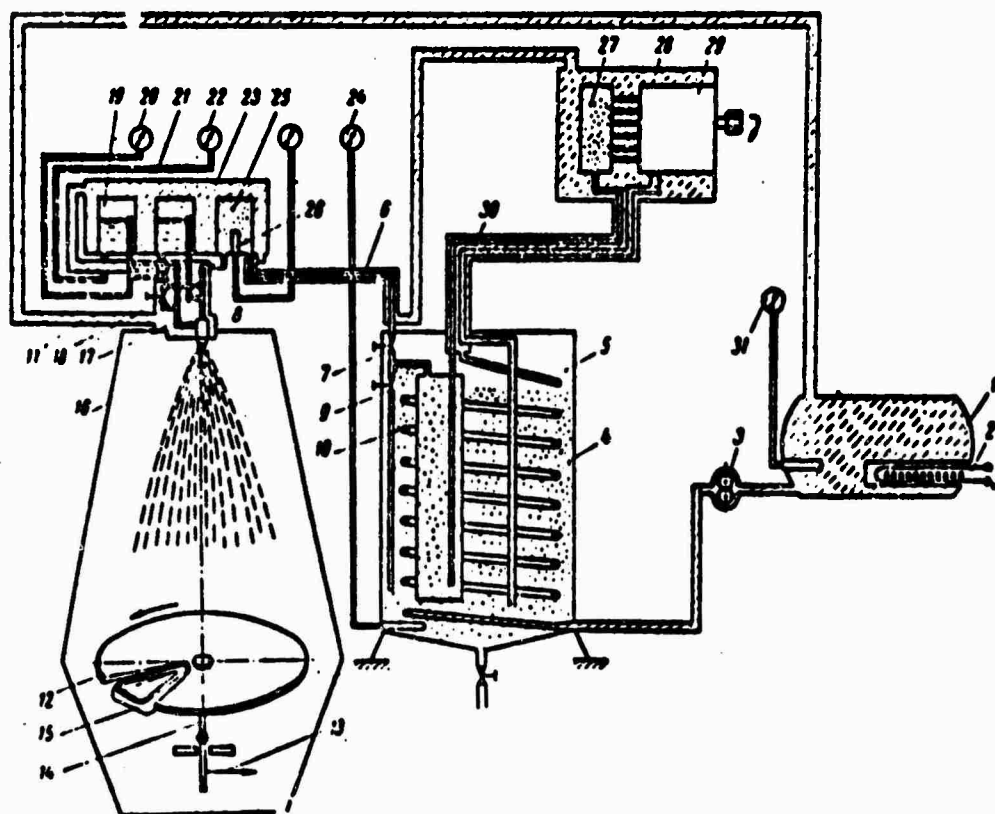
302

Fig. 152. Setup for measuring fineness of atomization using melted paraffin: 1 — tank for oil; 2 — electric heater for oil; 3 — oil pump; 4 — coil for oil; 5 — paraffin heater; 6 — charging pipeline; 7 and 9 — cock; 8 — pipeline; 10 — collector; 11 — injector; 12 — disk; 13 — cable for turning dropcatcher; 14 — axis; 15 — bath with alcohol; 16 — chamber; 17 — pipeline for second stage of injector; 18 — cock; 19 — chamber for measuring pressure; 20, 22, 24 and 31 — manometers; 21 — pipeline to manometer; 23 — jacket; 25 — chamber for aerothermometer; 26 — aerothermometer with alcohol; 27 — accumulator; 28 — chamber for heating oil pump; 29 — pump to supply paraffin; 30 — pipeline with preheating.

To sample drops of paraffin hardening in flight, a dropcatcher s used, constituting bath 15 filled with ethyl alcohol. Prior to he establishment of operating conditions of the injector the bath is under disk 12, having a cut in the form of a sector. At the beginning of measurements the bath combines with the cut and together with the disk revolves around axis 14. After one turn the disk stops, and the bath is removed under the disk. The sampling of drops in the bath is thus from the whole section of the spray. The removed mass of drops contains drops of all those sizes available in the spray, i.e., the test is very representative.

303

To separate drops by size the solidified drops of paraffin are sifted through a series of screens with different size holes.

Ethyl alcohol prevents adhesion of the drops of paraffin during catching and sifting. In view of the small difference in specific gravity of alcohol and paraffin, drops getting into the alcohol at first are in suspension and then slowly settle on the bottom of the bath. Adhesion of drops is prevented by the thin film of alcohol between them. Paraffin somewhat goes into solution in alcohol (0.071 g in 100 g alcohol), which promotes disconnection of the stuck drops.

The screening attachment is shown on Fig. 153. From the dropcatcher bath upper glass 2 is filled with the alcohol and suspended
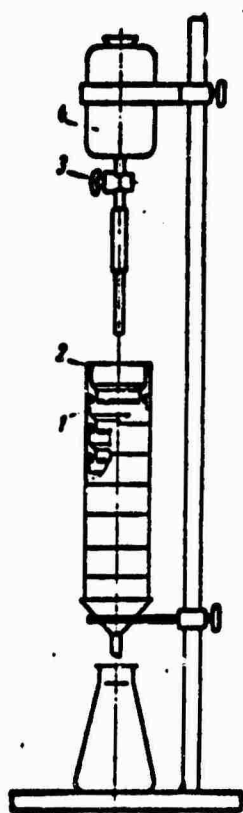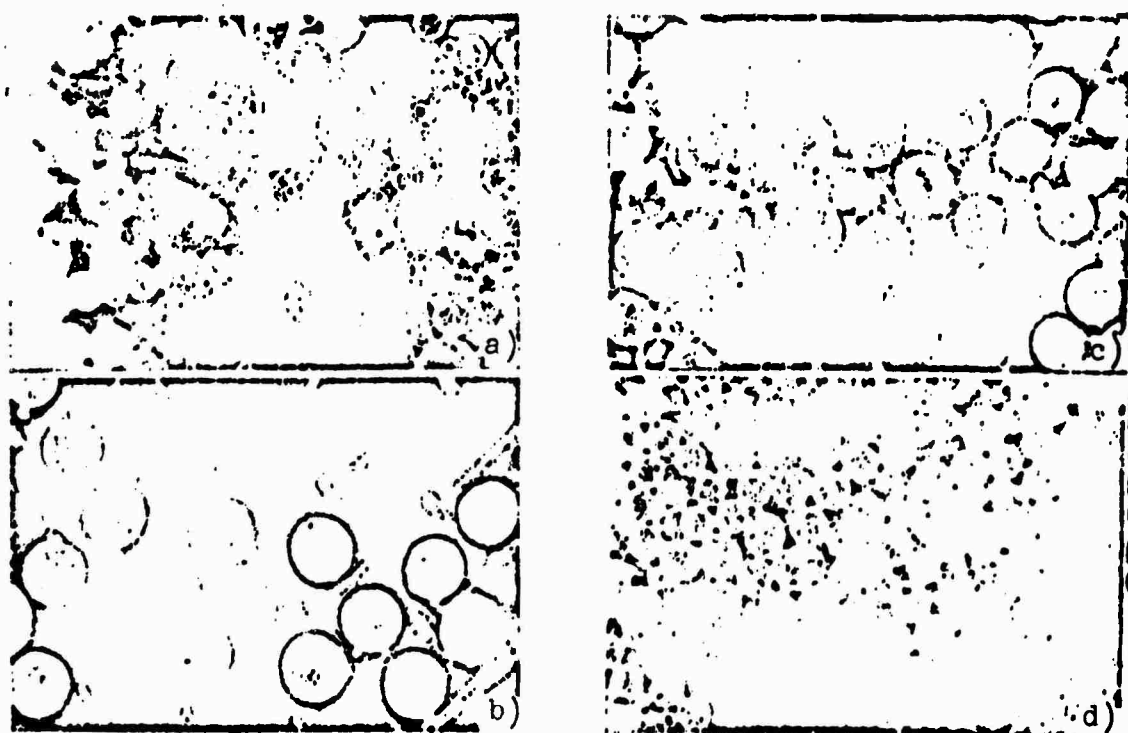
Fig. 153. Attachment for screening drops of paraffin: 1 — sieve; 2 — glass; 3 — cock; 4 — tank with alcohol.

paraffin drops, then cocks of the vessel with alcohol is opened. Flowing through the screens, alcohol attracts the drops. The size of drops in each group is determined by the size of the holes in two neighboring screens. The screens with drops are then dried and weighed.

Fig. 154. Microphotographs of paraffin drops: a) prior to sifting; b), c), and d) after sifting.

On Fig. 154a are shown drops prior to screening, and on Fig. 154b, c, and d — drops on screens after screening.

The number of strongly cohering drops remaining unseparated is small and is at maximum 1% by weight, which cannot essentially distort the results of measurements.

Use of this method of measurements involves several millions of drops (at a total weight of 5-7 g). The fineness of atomized liquid is determined in a time approximately 10 times less than in the case of catching drops on a layer of soot.

Experiments show that duplication of measurement results is sufficiently high. Thus, for example, the deviations of median diameters for one value of pressure drop on the injector do not exceed 5-7%.

Comparison of results for kerosene and liquid paraffin obtained

in identical conditions of atomization by the same swirler showed
that drops of paraffin are finer than drops of kerosene. A possible
explanation of this difference is that directly after the zone of
jet disintegration is a zone of merging drops, in which collisions
force drops to increase in size. When a stream of liquid paraffin
disintegrates, due to the rapid hardening of drops merging, and
consequently enlargement, do not occur. Therefore the sizes of
paraffin drops will be somewhat less than the sizes of kerosene
drops. This circumstance must be considered in comparing measurement
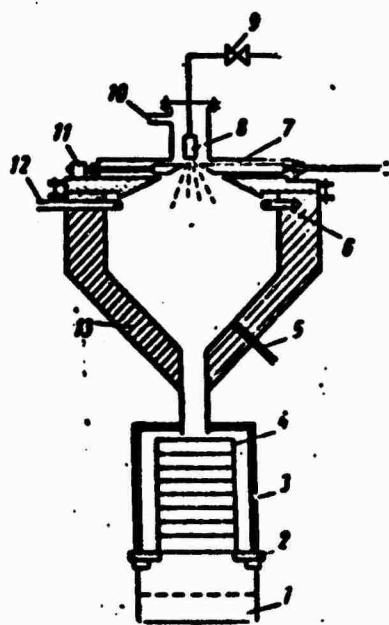results for kerosene and paraffin.

Fig. 155. Setup for sampling and freezing
drops of liquid [10]: 1 — overflow of
liquid nitrogen; 2 — flange of set of
screens; 3 — insulated housing of set of
screens; 4 — screen; 5 — thermocouple;
6 — collector for liquid nitrogen; 7 —
spray cutoff; 8 — injector; 9 — solenoid
valve; 10 — gas inlet; 11 — relay; 12 —
liquid nitrogen inlet; 13 — silica gel
thermoinsulation.

One modification of the examined method is a method based on
freezing drops of the investigated liquid in liquid nitrogen.
Figure 155 shows the setup for sampling and freezing drops of liquid
[10]. Liquid nitrogen moves into the upper part of the chamber and
cools the air in it. Liquid drops freeze and rest on screens, a
set of which is in the lower part of the chamber. Thus, the screening
occurs in the presence of a flow liquid nitrogen, which accumulates
in the lower collector. Drops held on the screen are weighed in
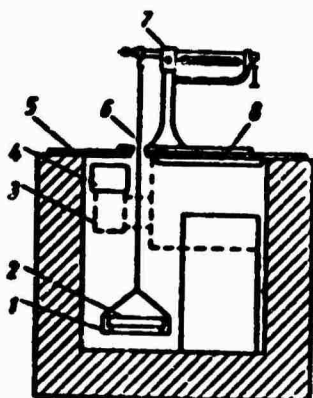the cooling chamber (Fig. 156).

Fig. 156. Cooling chamber for weighting of screens [10]: 1 — cup; 2 — screen; 3 — fan; 4 — cold air entrance; 5 — plastic cover; 6 — string; 7 — scales; 8 — warm air outlet.

Let us consider, finally, indirect methods of measuring the size of drops of liquid. The sedimentometric method proposed for measuring the size of drops of liquids uses Stokes' law. In accordance with this law the resisting force in the free fall of a drop of radius r in a medium of viscosity μ, is equal to R = $6\pi\mu rV$. This force balances the force $F = \frac{4}{3}\pi r^3(\rho_1 - \rho_2)g$, under the impact of which a drop falls. The fall rate is V = $\frac{H}{t}$, where H — height of fall, t — time of settling.

Equating these forces, we obtain $r = \frac{k}{\sqrt{t}}$, where k is constant. Tests showed very great limitations of this method.

Of optical methods we should note the photometric method and a method based on use of the rainbow phenomenon. However, these methods do not permit obtaining the distribution of drops with respect to size.

Literature

1. Moroshkin M. Ya. i Geller Z. I. K voprosu o vybore veshchestva dlya modelirovaniya protsessa raspylivaniya vysokovyazkikh ostatkov (The question of selecting the substance for modelling the atomization of high-viscosity residues). "Izvestiya vuzov. Neft' i gaz". 1960, No. 5.

2. Salamandra G. D. i Naboko I. M. Ulavlivaniye na plastinku, pokrytuyu sloyem sazhi, kak metod opredeleniya krupnosti raspylivaniya (Catching on a plate covered by a layer of soot as a method for determining the coarseness of atomization). "Zhurnal tekhnicheskoy fiziki". T. 27, 1957.

3. Salamandra G. D. i Naboko I. M. Skorostnoye mikrofotografi-rovaniye kalel' raspylennoy zhidkosti v polete (High-speed micro-photographing drops of atomized liquid in flight). "Zhurnal tekhnicheskoy fiziki". T. 27, 1957.

4. Adler C. A. scanning device for determining the size distribution of sprays droplet images. Chemical Engineering Progress, V. 50, No. 1, 1954.

5. Clare H., Gardiner J., Neale M. Study of fuel injection in air breating combustion chambers. Experimental Methods in Combustion research. AGARD, London, 1963.

6. Corbeau J. Etude de l'injection dans les foyers de moteurs—fusées a propergol liquide. Experimental Methods in Combustion research. AGARD, London, 1963.

7. Hasson D., Mizrahy J. The drop size of fan spray nozzles measurements by the solidifying wax method compared with those obtained by other sizing techniques. Transactions of the Institution of Chemical Engineering. V. 39, No. 6, 1961.

8. Joys J. Droplet size measurement of various steel furnace oil burners. Journal of the Institute of Fuel, V. 26, No. 153, 1953.

9. Kling R., Leboeuf R. L'ecoulement dans les orifices d'injection. Application aux moteur—fusees. La Recherche Aeronautique, No. 35, 1953.

10. Nelson P., Stevens W. Size distribution of droplets from centiguḡal spray nozzles. American Institute Chemical Engineering Journal, V. 7, No. 1, 1961.

11. Stocker A. A method of determining the size of droplets dispersed in a gas. Journal of Applied Physics, V. 17, No. 4, 1946.

U. S. BOARD ON GEOGRAPHIC NAMES TRANSLITERATION SYSTEM

Block	Italic	Transliteration	Block	Italic	Transliteration
А а	*А а*	A, a	Р р	*Р р*	R, r
Б б	*Б б*	B, b	С с	*С с*	S, s
В в	*В в*	V, v	Т т	*Т т*	T, t
Г г	*Г г*	G, g	У у	*У у*	U, u
Д д	*Д д*	D, d	Ф ф	*Ф ф*	F, f
Е е	*Е е*	Ye, ye; E, e*	Х х	*Х х*	Kh, kh
Ж ж	*Ж ж*	Zh, zh	Ц ц	*Ц ц*	Ts, ts
З з	*З з*	Z, z	Ч ч	*Ч ч*	Ch, ch
И и	*И и*	I, i	Ш ш	*Ш ш*	Sh, sh
Й й	*Й й*	Y, y	Щ щ	*Щ щ*	Shch, shch
К к	*К к*	K, k	Ъ ъ	*Ъ ъ*	"
Л л	*Л л*	L, l	Ы ы	*Ы ы*	Y, y
М м	*М м*	M, m	Ь ь	*Ь ь*	'
Н н	*Н н*	N, n	Э э	*Э э*	E, e
О о	*О о*	O, o	Ю ю	*Ю ю*	Yu, yu
П п	*П п*	P, p	Я я	*Я я*	Ya, ya

* ye initially, after vowels, and after ъ, ь; e elsewhere.
When written as ё in Russian, transliterate as yё or ё.
The use of diacritical marks is preferred, but such marks
may be omitted when expediency dictates.

FOLLOWING ARE THE CORRESPONDING RUSSIAN AND ENGLISH

DESIGNATIONS OF THE TRIGONOMETRIC FUNCTIONS

Russian	English
sin	sin
cos	cos
tg	tan
ctg	cot
sec	sec
cosec	csc
sh	sinh
ch	cosh
th	tanh
cth	coth
sch	sech
csch	csch
arc sin	$\sin^{-1}$
arc cos	$\cos^{-1}$
arc tg	$\tan^{-1}$
arc ctg	$\cot^{-1}$
arc sec	$\sec^{-1}$
arc cosec	$\csc^{-1}$
arc sh	$\sinh^{-1}$
arc ch	$\cosh^{-1}$
arc th	$\tanh^{-1}$
arc cth	$\coth^{-1}$
arc sch	$\sech^{-1}$
arc csch	$\csch^{-1}$

—

rot	curl
lg	log